63-3.

THE UNIVERSITY OF MICHIG

EFFICIENCY AND START-OSCILLATION CONDITIONS IN NONUNIFORM BACKWARD-WAVE OSCILLATORS

TECHNICAL REPORT NO. 61

ELECTRON PHYSICS LABORATORY

Department of Electrical Engineering

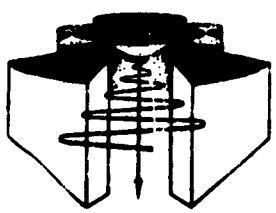

By: George I. Haddad

Approved By: J. E.

March, 1963

CONTRACT WITH:

HARRY DIAMOND LABORATORIES, UNITED STATES ARMY MATERIAL COMMAND WASHINGTON, D. C. HARRY DIAMOND LABORATORIES PROJECT NO.96393, CONTRACT NO. DA-49-186-AMC-68(X).

THE UNIVERSITY OF MICHIGAN
ANN ARBOR, MICHIGAN

EFFICIENCY AND START-OSCILLATION CONDITIONS IN NONUNIFORM BACKWARD-WAVE OSCILLATORS

TECHNICAL REPORT NO. 61

Electron Physics Laboratory
Department of Electrical Engineering

By

George I. Haddad

Approved by: J. E. Rowe

J. E. Rowe, Director
Electron Physics Laboratory

Project 05670

CONTRACT NO. DA-49-186-AMC-68(X)
HARRY DIAMOND LABORATORIES PROJECT NO. 96393
HARRY DIAMOND LABORATORIES
UNITED STATES ARMY MATERIAL COMMAND
WASHINGTON, D. C.

March, 1963

This report has also been submitted as a dissertation in partial fulfillment of the requirements for the degree of Doctor of Philosophy in The University of Michigan, 1963.

ABSTRACT

The purpose of this study is to investigate various means for improving the efficiency of O-type backward-wave oscillators. Several means are considered here namely, circuit phase velocity tapers, voltage gradients, prebunched beams and depressed collectors.

The effect of nonuniformities in the circuit phase velocity and beam potential on the efficiency and start-oscillation conditions of O-type backward-wave oscillators is investigated. These nonuniformities include linear, quadratic and exponential circuit phase velocity tapers and linear, quadratic, exponential and sinusoidal beam potential variations. The start-oscillation conditions were obtained by solving the characteristic equations on an analog computer. This method was found to be very convenient since the nonuniformity could be easily applied at any point along the length of the tube. A coupled-mode theory is also employed to study the effect of weak circuit phase velocity tapers on the start-oscillation conditions. It is shown that for very weak tapers a closed form solution can be obtained through a WKBJ approximation. The results of this theory are in good agreement with those obtained by the analog computer method.

It is shown that under certain conditions the start-oscillation current in a nonuniform backward-wave oscillator could be lower than that of a uniform one. It is also shown that under certain conditions no oscillation can take place. This characteristic can be exploited as a means of suppressing backward-wave oscillations in forward-wave traveling-wave amplifiers.

The effect of a sinusoidal-beam potential variation which is inherent in electrostatically focused backward-wave oscillators is investigated. It is shown that a slight increase in the start-oscillation current results. The increase depends on the focusing lens strength and on the d-c focusing period.

The effect of circuit phase velocity tapers on the efficiency of backward-wave oscillators is investigated through a nonlinear analysis and the resulting set of partial integro-differential equations are solved on an IBM 7090 digital computer. A set of circuit phase velocity tapers through which phase focusing can be achieved are derived for ideal conditions. The application of these tapers to actual situations is shown to yield higher efficiencies in the device. The efficiency enhancement due to tapering is found to depend on the operation conditions of the untapered oscillator.

The nonlinear analysis is also employed to determine the effect of a sinusoidally varying beam potential on the efficiency. It was found that for certain values of lens strength and d-c focusing period the efficiency is higher in the sinusoidally varying beam potential tube than that of a uniform tube whose beam potential is equal to the average

potential of the former one. However, for certain values of lens strength and d-c focusing period no oscillation condition could be determined.

Since in the nonlinear calculations the energy state of the spent beam is easily obtainable, the effect of depressed collectors on the efficiency of the device can be calculated. This is done in this study and it is shown that high efficiency improvement factors can be achieved. These improvement factors depend on the operating conditions of the oscillator. The optimum potentials of the depressed-collector segments are found for different operating conditions.

The effect of prebunched beams on the start-oscillation conditions and efficiency is also investigated. It is shown that the start-oscillation length can be considerably decreased by using a prebunched beam. The efficiency can be considerably improved by employing a prebunched beam in connection with a tapered circuit; the degree of improvement depending on how well an electron beam can be bunched.

An S-band experimental BWO was built where a linear velocity taper was incorporated into the tape helix slow-wave structure. The results from this oscillator agree qualitatively with the theoretical predictions. Interaction efficiency improvement factors of approximately 1.2 to 2 to 1 over the frequency band of 2.0 to 4.0 Gc have been obtained.

ACKNOWLEDGMENTS

The author wishes to express his gratitude to Professor Joseph E. Rowe, the chairman of his doctoral committee, for his guidance and helpful suggestions during the course of the work. He would also like to thank the other members of his committee for their suggestions in preparing the final manuscript. Special thanks should go to Mr. R. Martin, for his help in programming the analog computer, to T. DeMassa, for his assistance in taking some of the analog computer data, to Mr. A. Pajas, for programming the digital computer, to Messrs. J. Johnson and G. Beauchamp, for their work in drawing the figures, and to Messrs. J. Murphy, E. Kayser, and H. Krage, for their work on the assembly of the experimental tube. Finally the author wishes to express his appreciation to the secretarial staff of the laboratory for their hard and excellent work in the preparation of the text.

This work was made possible through the sponsorship of the Harry Diamond Laboratories under Contract No. DA-49-186-AMC-68(X).

TABLE OF CONTENTS

LIST OF ILLUSTRATIONS

LIST OF TABLES

CHAPTER I. STATEMENT OF THE PROBLEM AND LITERATURE SURVEY

1.1 Introduction

The O-type backward-wave oscillator[1], or as called by the French[2] "O-type Carcinotron" is a very important and widely used device in the generation of r-f power from uhf up to and including millimeter wave frequencies. It can be continuously frequency tuned or modulated at fast rates over a very wide band of frequencies by electronic methods. The operation of the oscillator depends on the interaction of an electron beam with an electromagnetic wave whose phase velocity is in the direction of electron flow and whose group velocity is in the opposite direction. Such an electromagnetic wave is called a "backward wave". All periodic structures such as the helix, interdigital line, ladder structures and others do support such backward waves. A schematic diagram of a backward-wave oscillator is shown in Fig. 1.1.

The buildup of oscillation can be briefly described as follows. If a pulse of noise at a certain frequency f develops on the slow-wave structure at the collector end of the tube, some of this energy will propagate toward the gun end of the structure or the output end. If an electron beam is present whose velocity is slightly greater than the phase velocity of the circuit and flows in the same direction as that of the phase velocity some of the kinetic energy of the beam will be converted into r-f energy and thus the energy at the output end will be increased. The energy at the output end produces velocity modulation of the incoming electron beam; this velocity modulation is converted into current modulation at the collector end of the tube. The current modulation induces energy on the circuit which travels back toward the output

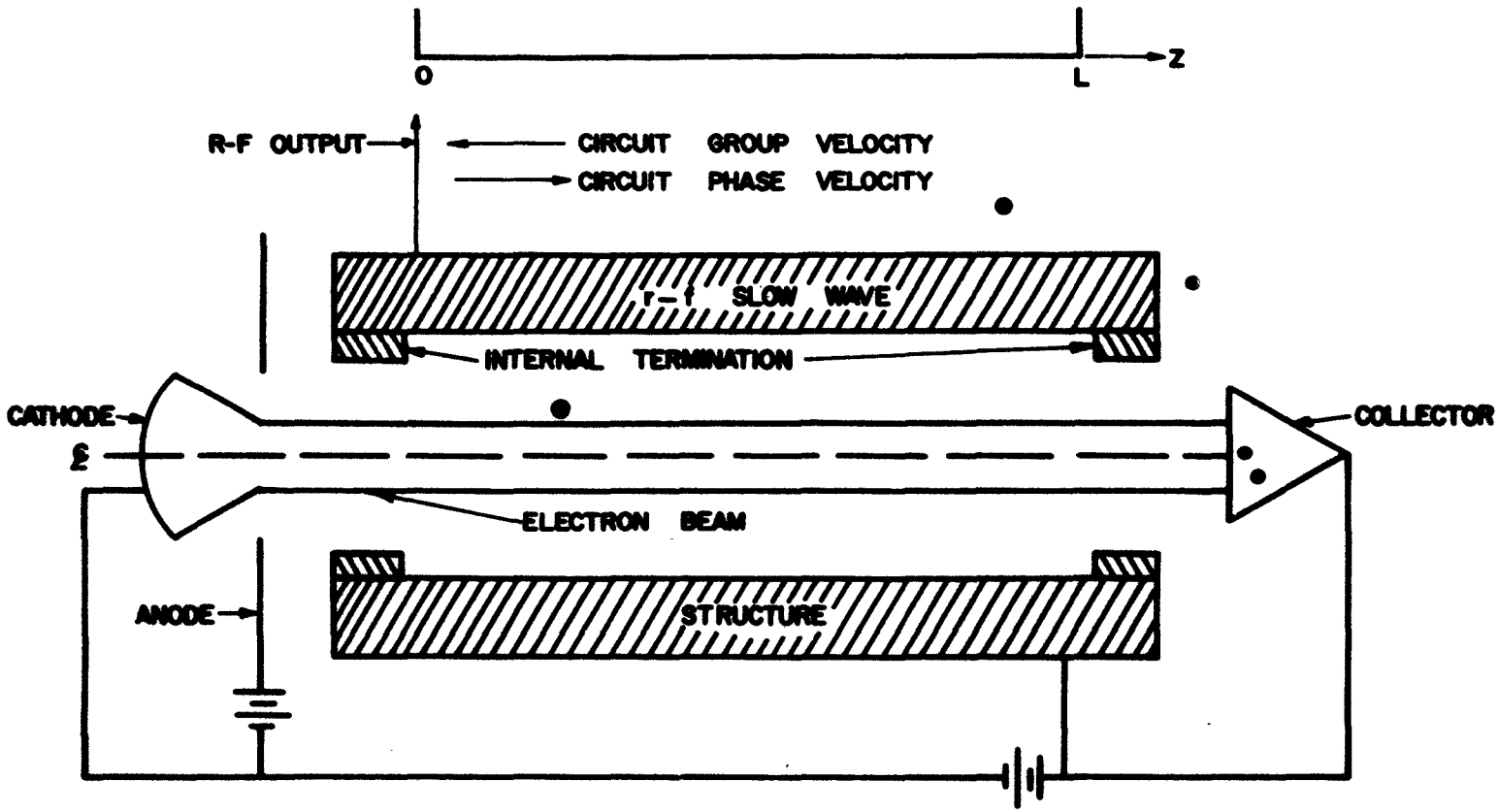

FIG. 1.1 SCHEMATIC DIAGRAM OF AN O-TYPE BACKWARD-WAVE OSCILLATOR.

end. The increased energy at the output end produces further bunching and so this cycle is repeated. It is obvious that this device is inherently regenerative even when the circuit is perfectly matched at both ends (i.e., the regeneration does not depend on reflections from the ends of the structure). It is now fairly obvious that for low beam currents regenerative amplification occurs. This amplification is very narrow band but the center frequency can be tuned over a wide frequency range by merely changing the beam voltage. This is due to the fact that backward waves are dispersive and thus changing the beam voltage will maintain the electron velocity approximately synchronous with the phase velocity at different frequencies. If the beam current is increased above a certain value then the tube will oscillate. The oscillation frequency can in turn be controlled by changing the beam voltage.

The operation of the backward-wave oscillator is similar in many respects to that of the forward-wave amplifier[3]. However, the forward-wave amplifier is a growing-wave device while the backward-wave amplifier and oscillator are beating-wave devices. A forward-wave amplifier can be made to oscillate by using appropriate feedback circuits, although this results in discrete modes and thus in a discontinuous tuning curve. In order for an oscillator to stay in the same mode, it must have an integral number of wavelengths around any feedback loop. This condition is automatically satisfied in the backward-wave oscillator but is difficult to satisfy in forward-wave oscillators. The condition for gain is that the electron beam velocity must be approximately equal to the phase velocity in the circuit and this fortunately makes the net length of any loop in the backward-wave oscillator zero wavelengths which results in an automatic mode selection mechanism.

Forward-wave amplifiers are more efficient than backward-wave devices, both oscillators and amplifiers. This is because in the forward-wave amplifier the circuit field is strongest when the beam modulation is strongest while in backward-wave devices the field is weak where the density modulation is strong and vice versa. This results in a smaller interaction efficiency in a backward-wave device than that in a forward-wave device.

1.2 Literature Survey

The start-oscillation conditions in uniform* backward-wave oscillators have been analyzed extensively both theoretically and experimentally by several authors[1,2,4,5,6,7,8,9,10]. In these analyses, small-signal conditions were assumed and so the equations describing the behavior of the oscillator can be linearized. These conditions do apply at the onset of oscillation. Grow and Watkins[9] and Johnson[5] have made estimates of the efficiency by using the linear theory and assuming certain values for the ratio of fundamental r-f current to the d-c current in the beam. The characteristics of the operating** backward-wave oscillator can only be determined from a nonlinear analysis of the device since it is the nonlinearities that ultimately determine the output levels and frequency. Due to the severe bunching effects shown theoretically by Sedin[12] and experimentally by Gewartowski[13], a hydrodynamical approach using nonlinear equations would not be valid. Rowe[20] and Sedin[12] have

---

* A uniform tube is one in which the beam potential and circuit phase velocity are constant along the length of the tube.

** An operating backward-wave oscillator is one which is operating at currents well above the start-oscillation current.

employed a Lagrangian formulation to study the characteristics of the operating backward-wave oscillator.

As to nonuniform tubes the forward-wave amplifier has received a great deal of attention. Theoretical and experimental work on circuit phase velocity tapered and voltage gradient amplifiers has been reported by several authors[14,15,16,17]. Efficiency improvement and higher saturation power outputs have been obtained in such forward-wave amplifier tubes. As to nonuniform backward-wave oscillators, nothing has been reported on the efficiency. D. V. Geppert[18] has briefly considered circuit velocity tapers neglecting space charge. He predicted that for "one direction of taper the start oscillation CN is reduced for backward-wave oscillators". He, however, did not say what direction or form the taper must have for this to be true. He also considered the possibility of backward-wave oscillation suppression through a velocity taper. Bevensee[19] recently investigated the effect of weak linear tapers on the start-oscillation conditions. He employed coupled-mode theory and neglected the fast space-charge wave. This will be discussed further in Chapter II, where this author has also investigated the start-oscillation conditions of a tapered backward-wave oscillator in a similar manner.

1.3 Statement of the Problem

The interaction mechanism and thus the mechanism of energy conversion from kinetic energy of the electrons to r-f energy of the wave is very similar in the forward-wave amplifier to that in the backward-wave oscillator. The ideal condition for this energy conversion is when the beam velocity is approximately synchronous with the phase velocity on the circuit. For a uniform circuit the phase velocity is constant along the length of the circuit, and thus when some of the beam energy is

converted into r-f power, the electrons must slow down and thus "fall out of phase" with the electromagnetic wave. This leads to saturation, for now no more kinetic energy can be extracted from the electrons. This situation can be remedied by either tapering the circuit phase velocity or introducing a voltage gradient at an appropriate position along the length of the tube. As mentioned above this was applied successfully[14] to the forward-wave amplifier to enhance the efficiency and the saturation power output. This same problem also occurs in the backward-wave oscillator. The purpose of this dissertation is then to study in detail, theoretically and experimentally, the effect of nonuniform circuit phase velocities and nonuniform beam potentials on the efficiency and start-oscillation conditions of O-type backward-wave oscillators.

CHAPTER II. COUPLED-MODE DESCRIPTION OF THE INTERACTION BETWEEN NONUNIFORM CIRCUITS AND BEAMS

2.1 Introduction

Coupled-Mode Theory was first introduced by Pierce[21] and has been widely used since to describe the interaction between waves propagating on circuits and electron beams[22,23,24]. This subject has also been treated extensively by Louisell[25]. These trestises, however, have always assumed the circuit and the beam to be uniform. This treatment takes into account a voltage gradient along the beam and a phase velocity taper along the circuit. First, coupled-mode equations are derived for the nonuniform beam and circuit separately and then the two are combined to study the effect of circuit phase velocity tapers on the start-oscillation conditions of an O-type backward-wave oscillator.

2.2 Coupled Modes in Transmission Lines with Variable Parameters

In this development which is similar to that of Louisell's[25] for uniform circuits, the transmission-line parameters are assumed to be functions of distance along the line. The differential equations for such a transmission line which is considered to be lossless can then be written as follows.

$$\frac{\partial V_c(z,t)}{\partial z} = - L(z) \frac{\partial I_c(z,t)}{\partial t} , \qquad (2.1)$$

$$\frac{\partial I_c(z,t)}{\partial z} = - C(z) \frac{\partial V_c(z,t)}{\partial t} , \qquad (2.2)$$

where $L(z)$ = inductance per unit length, henrys/m,

$C(z)$ = capacitance per unit length, farads/m,

$V_c(z,t)$, $I_c(z,t)$ = the voltage and current on the line respectively and are taken as real quantities.

Now in order to put Eqs. 2.1 and 2.2 in a form similar to that of the "normal modes"† on a uniform transmission line, let us define the following,

$$b_{\pm}(z,t) = \frac{1}{2} \frac{1}{\sqrt{Z_o(z)}} [V_c(z,t) \pm Z_o(z)\, I_c(z,t)] \quad , \tag{2.3}$$

where

$$Z_o(z) = \sqrt{L(z)/C(z)} \quad . \tag{2.4}$$

Differentiating Eq. 2.3 with respect to z and utilizing Eqs. 2.1, 2.2, 2.3 and 2.4, it is easily shown that,

$$\frac{\partial b_{\pm}(z,t)}{\partial z} = \mp \sqrt{L(z)C(z)} \frac{\partial b_{\pm}(z,t)}{\partial t} - \frac{1}{2} \frac{d\ell n Z_o(z)}{dz} b_{\mp} \quad . \tag{2.5}$$

Now introduce the complex notation and express $b_{\pm}(z,t)$ as,

$$b_{\pm}(z,t) = a_{\pm}(z)\, e^{j\omega t} + a_{\pm}^{*}(z) e^{-j\omega t} \quad , \tag{2.6}$$

$V_c(z,t)$ as,

$$V_c(z,t) = \text{Re}\, V(z) e^{-j\omega t} \quad , \tag{2.7}$$

and $I_c(z,t)$ as,

---

† The modes are called "normal modes" when they are decoupled.

* Indicates the complex conjugate.

$$I_c(z,t) = \text{Re } I(z)\, e^{j\omega t} \quad , \tag{2.8}$$

where

$$a_{\pm}(z) = \frac{1}{4\sqrt{Z_o(z)}} [V(z) \pm Z_o(z)I(z)] \quad . \tag{2.9}$$

Equations 2.1 and 2.2 can be written in terms of V(z) and I(z) as follows:

$$\frac{dV(z)}{dz} = - j\omega L(z)I(z) \quad , \tag{2.10}$$

$$\frac{dI(z)}{dz} = - j\omega C(z)V(z) \quad . \tag{2.11}$$

The modes $a_{\pm}(z)$ have been chosen so that the average power carried in the modes is

$$P = \frac{1}{2} \text{Re} V(z)I^*(z) = 2 [|a_+(z)|^2 - |a_-(z)|]^2 \quad . \tag{2.12}$$

Defining $\beta(z)$ as

$$\beta(z) \triangleq \omega\sqrt{L(z)C(z)} \tag{2.13}$$

and employing Eqs. 2.9, 2.10, and 2.11, the following equation and its conjugate can be easily obtained,

$$\frac{da_{\pm}(z)}{dz} = \mp j\beta(z)a_{\pm}(z) - \frac{1}{2} \frac{d\ell nZ_o(z)}{dz} a_{\mp}(z) \quad . \tag{2.14}$$

The $a_+(z)$ mode can be identified with the forward mode on a transmission line and the $a_-(z)$ with the backward mode. It can be seen from Eq. 2.14 that if L(z) and C(z) are constant, the two modes become decoupled and these would represent the forward and backward "normal modes" of a uniform

transmission line. These two decoupled modes then represent two independent solutions of the transmission-line equations; namely,

$$a_+(z) = a_+(0)\, e^{-j\beta z} \tag{2.15}$$

and

$$a_-(z) = a_-(0)\, e^{j\beta z} \quad . \tag{2.16}$$

These two modes can be excited separately on a uniform transmission line if so desired.

It can also be seen from Eq. 2.14 that in a nonuniform transmission line the forward and backward modes are coupled and one cannot be excited without the other. This is true of course because any change in the characteristic impedance will introduce reflections on the line and in Eq. 2.14 the coupling term depends on the change of Z_o. Here the characteristic impedance will be assumed to vary slowly with distance (i.e., the change is very small within a wavelength) which will make the coupling term $(1/2)[d\ln Z_o(z)/dz]$ very small and thus negligible. The two modes are now decoupled and Eq. 2.14 reduces to,

$$\frac{da_\pm(z)}{dz} = \mp j\beta(z)\, a_\pm(z) \quad , \tag{2.17}$$

where $a_\pm(z)$ here are the forward and backward normal modes on a nonuniform transmission line, and they represent two independent solutions of the transmission-line equations; namely,

$$a_+(z) = a_+(0)\, e^{-j\int_0^z \beta(z')\, dz'} \quad , \tag{2.18}$$

$$a_-(z) = a_-(0)\, e^{j \int_0^z \beta(z')\, dz'} \quad . \tag{2.19}$$

The phase velocity is now a function of z and is

$$v_p(z) = \frac{\omega}{\beta(z)} \quad . \tag{2.20}$$

2.3 Space-Charge Modes in a One-Dimensional Electron Beam in a Drift Region with a Nonuniform Potential

2.3.1 General Introduction. The basic equations which govern wave propagation on electron beams are the following. (All equations are given in mks rationalized units.)

Maxwell's equations,

$$\nabla \times \vec{H} = \vec{J} + \epsilon_o \frac{\partial \vec{E}}{\partial t} \quad , \tag{2.21}$$

$$\nabla \times \vec{E} = - \mu_o \frac{\partial \vec{H}}{\partial t} \quad , \tag{2.22}$$

$$\nabla \cdot \vec{E} = \frac{\rho}{\epsilon_o} \quad , \tag{2.23}$$

$$\nabla \cdot \vec{H} = 0 \quad . \tag{2.24}$$

The continuity equation, which can be derived from the above equations, is given by,

$$\nabla \cdot \vec{J} + \frac{\partial \rho}{\partial t} = 0 \quad . \tag{2.25}$$

The equation of motion is expressed by

$$\frac{d\vec{u}}{dt} = \frac{\partial \vec{u}}{\partial t} + (\vec{u} \cdot \nabla)\, \vec{u} = - \frac{|e|}{m} (\vec{E} + \vec{u} \times \mu_o \vec{H}) \quad . \tag{2.26}$$

The relationship between current density, space-charge density and velocity, which is applicable when the spread in electron velocities is small compared with the average velocity so that all electrons passing a given point can be assumed to have the same velocity, is given by

$$\vec{J} = \rho\vec{u} \quad . \tag{2.27}$$

In the above equations all quantities are functions of (r,t) and they are defined below.

$\vec{H}$ = the magnetic field intensity in (amperes/m),

$\vec{E}$ = the electric field intensity in (volts/m),

ρ = the space-charge density in (coulombs/m^3),

$\vec{u}$ = the velocity of the electrons in (meters/sec.),

$\vec{J}$ = the current density in (amperes/m^2),

μ_o, ϵ_o = the permeability and dielectric constant of free space respectively.

It is seen that the equation of motion is nonlinear in u and the current density equation is nonlinear in ρ and u. These equations will be linearized here by making a small-signal approximation. It is then assumed that any of the quantities in the above equations can be written as a sum of a time average term (d-c term) and an a-c term as follows:

$$F(r,t) = F_o(r) + F_1(r)\, e^{j\omega t} \quad . \tag{2.28}$$

where r is a generalized position coordinate. Under a small-signal approximation the a-c term will be assumed small compared with the d-c term and all products of a-c terms will be neglected.

The following additional assumptions will now be introduced.

1. The beam is confined by a homogeneous d-c magnetic field in the z-direction and thus only z-components of velocity and current density will be present.

2. The beam is infinite in the transverse plane and thus all quantities are independent of the transverse dimensions.

3. The beam is neutralized by the presence of ions which cancel the d-c space-charge forces.

4. A voltage gradient exists along the beam so that the d-c beam velocity is now a function of distance.

With these assumptions the fundamental equations (Eqs. 2.1 - 2.7) reduce to a d-c part which is given by ($\vec{k}$ is a unit vector in the z-direction)

$$\nabla \times \vec{H}_o = J_o \vec{k} \ , \tag{2.29}$$

$$\nabla \times \vec{E}_o = 0 \ , \tag{2.30}$$

$$\frac{\partial J_o}{\partial z} = 0 \ , \tag{2.31}$$

$$u_o(z) \frac{du_o(z)}{dz} = - \frac{|e|}{m} E_{oz}$$

or

$$\frac{1}{2} m (u_{o2}^2 - u_{o1}^2) = \frac{|e|}{m} (V_{o2} - V_{o1}) \ , \tag{2.32}$$

$$J_o = \rho_o(z) \, u_o(z) \tag{2.33}$$

and an a-c part which is given by,

$$\nabla \times \vec{H}_1 = J_1 \vec{k} + j\omega\varepsilon_o \vec{E}_1 \quad , \tag{2.34}$$

$$\nabla \times \vec{E}_1 = - j\omega\mu_o \vec{H}_1 \quad , \tag{2.35}$$

$$\frac{\partial J_1}{\partial z} = - j\omega\rho_1 \quad , \tag{2.36}$$

$$j\omega u_1 + \frac{\partial}{\partial z}(u_o u_1) = - \frac{|e|}{m} E_{1z} \quad , \tag{2.37}$$

$$J_1 = \rho_o u_1 + \rho_1 u_o \quad . \tag{2.38}$$

2.3.2 Space-Charge-Wave Equations on an Electron Beam with a D-c Voltage Gradient. If we now consider the z-component of Eq. 2.34, we obtain,

$$J_1 + j\omega\varepsilon_o E_{1z} = 0 \quad . \tag{2.39}$$

Substituting for E_{1z} from Eq. 2.39 into Eq. 2.37 yields,

$$j\omega u_1 + \frac{\partial}{\partial z}(u_o u_1) = - j \frac{|e|}{m\omega\varepsilon_o} J_1 \quad . \tag{2.40}$$

Also by utilizing Eq. 2.38 and substituting into Eq. 2.36 the following is obtained,

$$\left[\frac{\partial}{\partial z} + j \frac{\omega}{u_o(z)} \right] J_1 = j\omega \frac{\rho_o(z)}{u_o(z)} u_1 \quad . \tag{2.41}$$

Equations 2.40 and 2.41 are the fundamental equations which describe wave propagation in an infinite beam which is confined to flow in the z-direction and whose velocity is a function of distance along the z-direction.

In order to put these equations in a coupled-mode form similar to those for a nonuniform transmission line, the following quantities are defined.

$$V_1(z) \triangleq \frac{m}{|e|} u_o(z)\, u_1 \quad , \tag{2.42}$$

which is the beam kinetic voltage,

$$\omega_p^2(z) \triangleq \frac{|e|\rho_o(z)}{\epsilon_o m} \quad , \tag{2.43}$$

where $\omega_p(z)$ is the plasma frequency.

$$\beta_p(z) \triangleq \frac{\omega_p(z)}{u_o(z)} \quad , \tag{2.44}$$

$$\beta_e(z) \triangleq \frac{\omega}{u_o(z)} \quad , \tag{2.45}$$

$$\frac{1}{2} m\, [u_o(z)]^2 \triangleq |e|\, V_o(z) \quad , \tag{2.46}$$

$$V_1(z) \triangleq V_1'(z)\, e^{-j \int_o^z \beta_e(z')\, dz'} \quad , \tag{2.47}$$

$$J_1(z) \triangleq J_1'(z)\, e^{-j \int_o^z \beta_e(z')\, dz'} \quad . \tag{2.48}$$

Substituting Eqs. 2.42 - 2.48 into Eqs. 2.40 and 2.41, the following equations are obtained,

$$\frac{dV_1'(z)}{dz} = -j \frac{\beta_p^2(z)}{\beta_e(z)} \frac{2V_o(z)}{|J_o|} J_1'(z) \quad , \tag{2.49}$$

$$\frac{dJ_1'(z)}{dz} = -j\frac{\beta_e(z)|J_o|}{2V_o(z)} V_1'(z) \quad . \tag{2.50}$$

Equations 2.49 and 2.50, which describe space-charge-wave propagation, are essentially the same as the nonuniform transmission-line equations. If the line voltage V(z) is identified with the beam kinetic voltage $V_1'(z)$, and the line current I(z) with the beam current density $J_1'(z)$, then Eqs. 2.49 and 2.50 will describe wave propagation along a nonuniform transmission line whose inductance per unit length is

$$L(z) = \frac{\beta_p^2(z) 2V_o(z)}{\beta_e(z)\ \omega|J_o|} \tag{2.51}$$

and whose capacitance per unit length is

$$C(z) = \frac{\beta_e(z)|J_o|}{2V_o(z)\omega} \quad . \tag{2.52}$$

Now let us define the mode amplitudes as follows:

$$a_\pm'(z) \triangleq \frac{1}{4\sqrt{Z_b(z)}} [V_1'(z) \pm Z_b(z)(-J_1'(z))] \quad , \tag{2.53}$$

where

$$Z_b(z) \triangleq \frac{2V_o(z)\ \omega_p(z)}{|J_o|\ \omega} \quad . \tag{2.54}$$

Substituting Eq. 2.53 into Eqs. 2.49 and 2.50, gives

$$\frac{da_\pm'(z)}{dz} = \pm j\beta_p(z)\ a_\pm' - \frac{1}{2}\frac{d\ln Z_b(z)}{dz} a_\pm'(z) \tag{2.55}$$

and defining

$$a_{\pm}(z) \triangleq a'_{\pm}(z)\, e^{-j \int_0^z \beta_e(z')\, dz'}$$

$$\triangleq \frac{1}{4\sqrt{Z_b(z)}} \left[V_1(z) \pm Z_b(z)(-J_1(z)) \right] , \qquad (2.56)$$

Eq. 2.55 then becomes

$$\left\{ \frac{d}{dz} + j \left[\beta_e(z) \mp \beta_p(z) \right] \right\} a_{\pm}(z) = -\frac{1}{2} \frac{d\ell n Z_b(z)}{dz} a_{\mp}(z) . \qquad (2.57)$$

Equation 2.57 and its conjugate describe the coupled space-charge modes on an electron beam with a voltage gradient along its length. It is seen that when no voltage gradient is present, Z_b, β_e and β_p are constant, and we obtain the normal space-charge modes, namely

$$\left[\frac{d}{dz} + j(\beta_e \mp \beta_p) \right] a_{\pm}(z) = 0 \qquad (2.58)$$

and the solution can be written in the following form,

$$a_{\pm}(z) = a_{\pm}(0)\, e^{-j(\beta_e \mp \beta_p) z} . \qquad (2.59)$$

The $a_+(z)$ mode is the fast space-charge mode since its phase velocity $v_{p_+} = u_o/[1 - (\omega_p/\omega)]$ is slightly greater than the d-c beam velocity, and the $a_-(z)$ mode is the slow space-charge mode since its phase velocity $v_{p_-} = u_o/[1 + (\omega_p/\omega)]$ is slightly less than the d-c beam velocity.

It is seen from Eq. 2.57 that when a voltage gradient is present, the modes are coupled, which implies a transfer of power between the two

modes. This is similar to the nonuniform transmission line where the forward and backward modes are coupled, and thus one cannot excite one without the other. The first point that comes to mind here is that, since noise excitation on an electron beam can be described in terms of the space-charge waves and since introducing a voltage gradient introduces coupling between the slow and fast space-charge waves, then it might be possible to introduce a certain voltage gradient which affects a noise power transfer from the slow space-charge wave to the fast space-charge wave and thus the noise can be removed. This of course would lead to very low-noise traveling-wave amplifiers. This is a subject in itself and will not be pursued here any further. If we assume that the voltage gradient is small, the coupling term $1/2\ (d/dz) \ln Z_b(z)$ will then be very small and may be neglected, the modes in Eq. 2.57 reduce to the normal modes on an electron beam with a voltage gradient and are written below as,

$$\frac{da_{\pm}(z)}{dz} + j\left[\beta_e(z) \mp \beta_p(z)\right] a_{\pm}(z) = 0 \ , \qquad (2.60)$$

where $a_{\pm}(z)$ are the fast and slow space-charge modes on the electron beam and they represent two independent solutions which can be written as follows:

$$a_{\pm}(z) = a_{\pm}(0)\, e^{j \int_0^z [\beta_e(z') \mp \beta_p(z')]\, dz'} \ . \qquad (2.61)$$

The phase and group velocities of the modes are now a function of distance and can be represented as,

$$v_{p_\pm}(z) = \frac{u_o(z)}{1 \mp \frac{\omega_p(z)}{\omega}} \tag{2.62}$$

and

$$v_{g_\pm}(z) = u_o(z) \quad . \tag{2.63}$$

In order to account for a finite beam in a drift region ω_p will be reduced by a certain factor, called a reduction factor R, which has been computed by Branch and Mihran[26] for several geometries and a reduced plasma frequency will then be used in the previous equations which is defined as follows:

$$\omega_q \triangleq R\omega_p \tag{2.64}$$

and

$$\beta_q \triangleq R\beta_p \quad . \tag{2.65}$$

2.4 Coupled-Mode Description of Interaction Between Nonuniform Circuits and Beams

In the last two paragraphs the normal modes on nonuniform circuits and beams were formulated separately. In this paragraph it will be assumed that a weak interaction between the circuit and the beam exists and this interaction will be described in terms of mode coupling in the two systems.

An equivalent lumped parameter transmission-line circuit, as used by Pierce[3], whose phase velocity can be chosen to be the same as that of

the actual slow-wave circuit phase velocity and whose parameters can be so chosen that for unit power flow the longitudinal field acting on the electrons is $-(\partial V/\partial z)$ which is equal to the true field in a particular circuit. This, as shown by Pierce[3], is a good approximation for phase velocities which are small compared to the velocity of light. The beam with convection current $i_1(z)$ will be assumed to flow very close to the circuit and is capacitively coupled to it. The beam then will induce a current per unit length in the circuit which is given by $-\partial i_1/\partial z$.

With the above assumptions the transmission-line equation can then be written as,

$$\frac{dV_c(z)}{dz} = - j\omega L(z)\, I_c(z) \quad , \tag{2.66}$$

$$\frac{dI_c(z)}{dz} = - j\omega C(z)\, V_c(z) - \frac{di_1(z)}{dz} \quad , \tag{2.67}$$

where di_1/dz is the current induced in the circuit due to the beam and all other quantities have been defined previously.

The beam, in addition to the space-charge field, will now experience a force due to the field of the circuit and so the beam equations now become,

$$\left[\frac{d}{dz} + j\beta_e(z)\right] V_1(z) = - j \frac{[\beta_q(z)]^2}{\beta_e(z)} \frac{2V_o(z)}{|I_o|} i_1 + \frac{dV_c(z)}{dz} \quad , \tag{2.68}$$

$$\left[\frac{d}{dz} + j\beta_e(z)\right] i_1(z) = - j\beta_e(z) \frac{|I_o|}{2V_o(z)} V_1(z) \quad , \tag{2.69}$$

where all these quantities have been defined in the previous paragraphs.

Now, following the same procedure as that for the separate transmission line and beam, we define the mode amplitudes as follows*.

$$a_{c_\pm}(z) \triangleq \frac{1}{4\sqrt{Z_c(z)}} \left[V_c(z) \pm Z_c(z)\, I_c(z)\right] , \tag{2.70}$$

$$a_{b_\pm}(z) \triangleq \frac{1}{4\sqrt{Z_b(z)}} \left[V_1(z) \pm Z_b(z)(-i_1(z))\right] , \tag{2.71}$$

where all the quantities in the above equations have been defined, and the total average power on the beam and the circuit can be expressed as,

$$P_t = 2\left[|a_{c_+}|^2 + |a_{b_+}|^2 - |a_{c_-}|^2 - |a_{b_-}|^2\right] . \tag{2.72}$$

Employing Eqs. 2.70 and 2.71, and substituting in Eqs. 2.66 - 2.69, yields the following coupled-mode equations which describe the interaction between a nonuniform circuit and an electron beam with a voltage gradient,

$$\left[\frac{d}{dz} \pm j\beta_c(z)\right] a_{c_\pm}(z) = -\frac{1}{2}\frac{d}{dz} \ln Z_c(z)\, a_{c_\mp}(z)$$

$$\pm \frac{1}{2}\sqrt{\frac{Z_c(z)}{Z_b(z)}}\, \frac{d}{dz}\left(a_{b_+}(z) - a_{b_-}(z)\right) \tag{2.73}$$

and

---

* The subscript "c" refers to the circuit and the "b" refers to the beam.

$$\left[\frac{d}{dz} + j\left(\beta_e(z) \mp \beta_q(z)\right)\right] a_{b_\mp}(z) = -\frac{1}{2}\frac{d}{dz} \ln Z_b(z)\, a_{b_\mp}(z)$$

$$+ \frac{1}{2}\sqrt{\frac{Z_c(z)}{Z_b(z)}}\,\frac{d}{dz}\left(a_{c_+}(z) + a_{c_-}(z)\right) . \quad (2.74)$$

It will now be assumed that the impedance variation along the circuit and beam is small, so that (d/dz) ln Z becomes very small, which in essence decouples the forward and backward modes on the transmission line and also the space-charge modes on the beam. With this assumption, Eqs. 2.73 and 2.74 now reduce to,

$$\left[\frac{d}{dz} \pm j\beta_c(z)\right] a_{c_\pm}(z) = \frac{1}{2}\sqrt{\frac{Z_c(z)}{Z_b(z)}}\,\frac{d}{dz}\left[a_{b_+}(z) - a_{b_-}(z)\right] \quad (2.75)$$

and

$$\left[\frac{d}{dz} + j\left(\beta_e(z) \mp \beta_q(z)\right)\right] a_{b_\pm}(z) = \frac{1}{2}\sqrt{\frac{Z_c(z)}{Z_b(z)}}\,\frac{d}{dz}\left[a_{c_+}(z) + a_{c_-}(z)\right] .$$

(2.76)

If we now assume that the interaction between the beam and the circuit is weak, and that $\beta_e(z)$ and $\beta_c(z)$ vary in the same manner and are approximately equal at each value of z, then we can replace the derivative on the right-hand sides of Eqs. 2.75 and 2.76 approximately by $-j\beta_e(z)$. With these assumptions, the coupled-mode equations, Eqs. 2.75 and 2.76, become:

$$\left[\frac{d}{dz} \pm j\beta_c(z)\right] a_{c_\pm}(z) = \mp C_{12}(z)\left[a_{b_+}(z) - a_{b_-}(z)\right] , \qquad (2.77)$$

$$\left[\frac{d}{dz} + j\left(\beta_e(z) \mp \beta_q(z)\right)\right] a_{b_\pm}(z) = - C_{12}(z)\left[a_{c_+}(z) + a_{c_-}(z)\right] , \qquad (2.78)$$

where

$$C_{12}(z) = \frac{j}{2}\sqrt{\frac{Z_c(z)}{Z_b(z)}}\,\beta_e(z) . \qquad (2.79)$$

Equations 2.77 and 2.78 are the coupled-mode equations which describe the interaction between a nonuniform circuit and an electron beam with a nonuniform voltage. These equations will be applied next to study the effect of a tapered circuit on the start-oscillation conditions of an O-type backward-wave oscillator.

2.5 Coupled-Mode Description of an O-Type Backward-Wave Oscillator with a Tapered Circuit

A general description of O-type backward-wave oscillators and their principles of operation have already been discussed in Chapter I, and will not be repeated here. Under high space-charge conditions the coupling between the circuit wave and the fast space-charge wave becomes negligible. Thus the start-oscillation conditions can be determined by considering the coupling between the circuit wave, whose phase velocity is in the +z direction and whose energy propagates in the -z direction, and the slow space-charge wave which carries negative energy[27] in the +z direction. Gould[23] applied the coupled-mode theory to determine the start-oscillation conditions in a uniform backward-wave oscillator. He

also assumed a high space-charge condition and thus neglected the coupling to the fast space-charge wave. Here this approach will be employed to study the start-oscillation conditions in a tapered circuit backward-wave oscillator. This latter problem has been recently investigated by R. M. Bevensee[19]. The method employed here is very similar to that employed by Bevensee, and the results are in agreement. However, this author feels that Bevensee did not take into consideration a certain situation in which the start-oscillation current in a tapered tube could be lower than that in a uniform one. This will be discussed later.

In this treatment, the circuit phase velocity is assumed to be a function of distance, and also that it varies very slightly over the length of the circuit. A varying phase velocity can be easily achieved by either tapering the pitch on the slow-wave structure or dielectrically loading the structure in a nonuniform manner. Either of these will have an effect on the interaction impedance, that is, the interaction impedance now becomes a function of distance. However, it will be assumed here that the beam flows very close to the circuit, and the interaction impedance remains approximately constant over the length of the tube. This is not a bad approximation since a helix backward-wave oscillator usually employs a hollow beam which flows close to the circuit. Of course this approximation gets worse when the beam flows farther away from the circuit. The impedance variation will be proportional to the phase velocity variation and can be included in the equations as such. This is done in a later chapter on efficiency studies. For now, however, the interaction impedance is assumed to be constant. It is also assumed that the voltage and thus the beam velocity is also constant, and that

a high space-charge condition exists so that the coupling between the circuit wave and the fast space-charge wave can be neglected.

Under these assumptions the coupled-mode equations for an O-type backward-wave oscillator can be written as follows:

$$\left[\frac{d}{dz} + j\beta_c(z)\right] a_c = - C_{12}\, a_b \quad , \tag{2.80}$$

$$\left[\frac{d}{dz} + j\beta_b\right] a_b = - C_{12}\, a_c \quad , \tag{2.81}$$

where a_c = the circuit mode amplitude,

a_b = the beam mode amplitude, and

$\beta_b = \beta_e + \beta_q$.

Let us now define the following parameters which were introduced by Pierce[3] and are commonly used.

$$C_o^3 = \frac{I_o Z_c}{4 V_o} \tag{2.82}$$

and

$$\frac{\omega_q}{\omega} \cong C_o \sqrt{4QC} \quad . \tag{2.83}$$

Recalling that $Z_b = 2V_o\omega_q/I_o\omega$ and from the above definitions the coupling coefficient in Eqs. 2.80 and 2.81 can then be written as

$$C_{12} = \frac{j}{2}\left(\frac{Z_c}{Z_b}\right)^{1/2} \beta_e = \frac{j\beta_e C}{\sqrt{2}\,(4QC)^{1/4}} \quad . \tag{2.84}$$

Next let us define a normalized coordinate y as follows:

$$y = \beta_e C_o z \quad . \tag{2.85}$$

Introducing the following commonly used parameter,

$$b = \frac{1}{C_o}\left[\frac{u_o - v_o}{v_o}\right] \quad , \tag{2.86}$$

where u_o = the d-c beam velocity, and

v_o = the cold circuit phase velocity at z = 0,

and defining

$$v_c(z) \triangleq v_o/\xi(z) \tag{2.87}$$

or

$$\beta_c(z) = \beta_{c_o}\xi(z) \quad , \tag{2.88}$$

Eqs. 2.80 and 2.81 become,

$$\left[\frac{d}{dy} + j\beta_{c_n}(y)\right] a_c(y) = - k\, a_b(y) \tag{2.89}$$

and

$$\left[\frac{d}{dy} + j\beta_{b_n}\right] a_b(y) = - k\, a_c(y) \quad , \tag{2.90}$$

where

$\beta_{c_n}(y)$ = normalized circuit phase parameter

$$= \beta_{c_{on}}\xi(y) = \left(\frac{1 + C_o b}{C_o}\right)\xi(y) \quad ,$$

β_{b_n} = normalized beam phase constant

$$= \frac{1}{C_o}\left[1 + C_o\sqrt{4QC}\right] ,$$

k = normalized coupling coefficient

$$= \frac{-j}{\sqrt{2}\,(4QC)^{1/4}} .$$

It should be noted here that Eqs. 2.89 and 2.90 apply for very weak tapers, since this assumption was originally made in order to put the equations in coupled-mode form as they stand.

Now the standard WKBJ[28] method will be employed to get an approximate solution for very weak tapers. This is carried out in Appendix A and the results are given below.

The beam and circuit mode amplitudes can be expressed as follows:

$$a_b(y) = \frac{C_1}{\sqrt{r(y)}}\left[e^{j\int_o^y r(y')dy'} - e^{-j\int_o^y r(y')dy'}\right] e^{-j\int_o^y \frac{\beta_{c_n}(y')+\beta_{b_n}}{2}dy'} \tag{2.91}$$

and

$$a_c(y) = \frac{-C_1}{k}\left\{j2r^{1/2}\cos\int_0^y r(y')\,dy' + \left[\left(\beta_{c_n}(y) - \beta_{b_n}\right)r^{-1/2} - jr^{-3/2}\,r'\right]\sin\int_0^y r(y')\,dy'\right\} e^{-j\int_o^y \frac{\beta_{c_n}(y')+\beta_{b_n}}{2}dy'} , \tag{2.92}$$

where

$$[r(y)]^2 = \left[|k|^2 - j \frac{\beta_{c_n}'(y)}{2} + \left(\frac{\beta_{c_n}(y) - \beta_{b_n}}{2} \right)^2 \right] . \qquad (2.93)$$

where ' denotes differentiation with respect to y.

Applying the boundary condition that, at $y = y_1$, $a_c(y) = 0$, assuming that $\xi(y) = (1+\alpha y)$, $|\alpha\beta_{c_{on}}/2|k|^2| \ll 1$ and $1/4|k|^2 [\beta_{c_{on}}(1+\alpha y) - \beta_{b_n}]^2 \ll 1$, gives the following very approximate start-oscillation conditions:

$$\frac{\alpha\beta_{c_{on}}}{2} y_1 \cong \left[\beta_{c_{on}}(1+\alpha y_1) - \beta_{b_n} \right] \qquad (2.94)$$

and

$$\cot |k|y_1 \cong \frac{1}{24} \left(\frac{\alpha\beta_{c_{on}}}{2|k|^2} \right)^2 \left[(|k|y_1)^2 - 6 \right] |k|y_1 , \qquad (2.95)$$

where y_1 is the normalized start-oscillation length of the tapered tube.

It can be easily seen from Eq. 2.94 that when $\alpha = 0$, i.e., for a uniform circuit tube,

$$\beta_{c_{on}} = \beta_{bn} ,$$

or

$$\frac{1+C_o b_o}{C_o} = \left(\frac{1}{C_o} + \sqrt{4QC} \right) ,$$

or

$$b_o = \sqrt{4QC} , \qquad (2.96)$$

where b_o here refers to the uniform tube.

From the definition of b (Eq. 2.86), we have for a uniform tube

$$\frac{u_o}{v_o} = 1 + C_o b_o \quad . \tag{2.97}$$

For a nonuniform circuit, however, we have from Eq. 2.94,

$$\frac{\beta_{c_{on}}}{\beta_{b_n}} = \frac{1}{1 + \frac{\alpha y_1}{2}} \quad , \tag{2.98}$$

or

$$\frac{\beta_{c_n}}{\beta_{b_n}} = \frac{1+\alpha y}{1 + \frac{\alpha y_1}{2}} \tag{2.99}$$

and $\beta_{c_n} = \beta_{b_n}$ at $y = y_1/2$ or the two waves are synchronous midway along the tube.

The start-oscillation current in a tapered tube can now be compared to that of a uniform one under several conditions. In comparing the start-oscillation currents it is <u>assumed</u> that the frequency of oscillation and the physical lengths of the two tubes are equal. It is believed that this basis for comparison is meaningful and eliminates any variation in the interaction impedance due to a frequency change, in which case the impedance variation of the slow-wave structure with frequency must be specified.

With the above basis for comparison, the following situations can exist where the start-oscillation conditions are satisfied.

1. If one starts with a uniform tube, and this uniform tube is tapered, then one can compare the start-oscillation current in the tapered tube to that in the uniform one (i.e., the phase velocity of the tapered tube at $z = 0$ is equal to the phase velocity in the uniform

tube). For this case, the beam velocity has to be different in the tapered tube than that in the uniform one.

This difference in beam velocity is proportional to the taper and can be expressed as*

$$\frac{u_1}{u_o} = \frac{1 + C_1 b_1}{1 + C_o b_o} = \frac{1}{1 + \frac{\alpha y_1}{2}} , \qquad (2.100)$$

where the subscript "1" refers to the tapered tube and the subscript "0" to the uniform tube and b_1 can be expressed as

$$b_1 = \frac{1}{C_1}\left[\frac{1 + C_o b_o}{1 + \frac{\alpha y_1}{2}} - 1\right] . \qquad (2.101)$$

It can be seen from Eq. 2.101 that, at a constant frequency, when α is positive (decreasing phase velocity) b_1 is less than b_o and the nonuniform tube will oscillate at a lower beam velocity (lower voltage) than the uniform tube. However, when α is negative (increasing phase velocity) the nonuniform tube will oscillate at a higher voltage than the uniform one.

Now, from Eq. 2.95 it is apparent that when $\alpha = 0$, $\cot |k| y_o = 0$, and $|k| y_o = \pi/2$ for the lowest order oscillation condition. When α is not zero y_1 must increase in order to satisfy the equation regardless of the sign of α, i.e., regardless of the direction of taper. This does not necessarily mean an increase in the start-oscillation current[19], and

---

* The subscript "1" refers to uniform tube and "o" refers to the tapered tube.

as shown below the direction of taper does make a difference in the start-oscillation current.

The start-oscillation currents for this case can then be compared as follows,

$$y_o \triangleq 2\pi(CN)_o = \frac{\omega}{u_o} C_o L_o \qquad (2.102)$$

where N is the number of beam wavelengths, and

$$y_1 = 2\pi(CN)_1 = \frac{\omega}{u_1} C_1 L \quad , \qquad (2.103)$$

where L_o and L_1 are the physical lengths of the two oscillators. Also

$$I_o = \frac{4V_o(C_o)^3}{Z_o} \quad , \qquad (2.104)$$

$$I_1 = \frac{4V_1(C_1)^3}{Z_1} \quad . \qquad (2.105)$$

Therefore,

$$\frac{I_1}{I_o} = \left(\frac{u_1}{u_o}\right)^2 \left(\frac{C_1}{C_o}\right)^3 \quad , \qquad (2.106)$$

where it has been assumed that $Z_1 = Z_o$.

Assuming that the physical lengths of the two tubes are equal, $(L_1 = L_o)$, then from Eq. 2.102 and 2.103 we have

$$\left(\frac{C_1}{C_o}\right) = \left(\frac{u_1}{u_o}\right)\left(\frac{y_1}{y_o}\right) \quad . \qquad (2.107)$$

Substituting Eq. 2.107 into Eq. 2.106 gives

$$\frac{I_1}{I_o} = \left(\frac{u_1}{u_o}\right)^5 \left(\frac{y_1}{y_o}\right)^3 = \left(\frac{1+C_1 b_1}{1+C_o b_o}\right)^5 \left(\frac{y_1}{y_o}\right)^3 = \left(\frac{1}{1+\frac{Qy_1}{2}}\right)^5 \left(\frac{y_1}{y_o}\right)^3 \quad . \qquad (2.108)$$

It is seen from Eq. 2.108 that since (y_1/y_o) is always greater than unity irrespective of the direction of taper, i.e., irrespective of the sign of α, the start-oscillation current will always increase for α negative, i.e., for an increasing phase velocity. However, it is possible for the start-oscillation current to decrease when α is positive, i.e., for a decreasing phase velocity. This, of course, depends on the actual operating parameters of the tube.

The $|k|y_1/|k|y_o$ is plotted in Fig. 2.1 as a function of $\alpha\beta_{c_{on}}/2|k|^2$. In order to compare the oscillation currents in the two tubes, one must choose particular operating parameters. Let us choose QC = 0.25, and investigate the start-oscillation currents when $\beta_{c_{on}}$ and α are varied. It should be recalled here that $\beta_{c_{on}} = 1/C(1+Cb)$, so that a variation in C will be actually a variation in $\beta_{c_{on}}$. Employing Eq. 2.108 and assuming that the coupling parameter is the same in the two tubes, I_1/I_o can be computed as a function of α for different values of C_1 or C_o. Actually for the cases considered C_1 is approximately equal to C_o as can be easily seen from Eq. 2.107. However, C_1^3 will be quite different from C_o^3. This is plotted in Fig. 2.2 and it is seen that, for some of the cases considered, the start-oscillation current is smaller in a tapered tube than that in a uniform tube. The assumption that the coupling parameter is the same in both tubes, or $|k_1| \cong |k_o|$ is a reasonable assumption, since $|k|$ varies as $1/(Iu)^{1/12}$ and thus any change in the current or the beam velocity will have a negligible effect on $|k|$, and thus assuming QC the same in both tubes will have a negligible effect on the results. A comparison of the start-oscillation current for QC = 0.5 is also shown in Fig. 2.3.

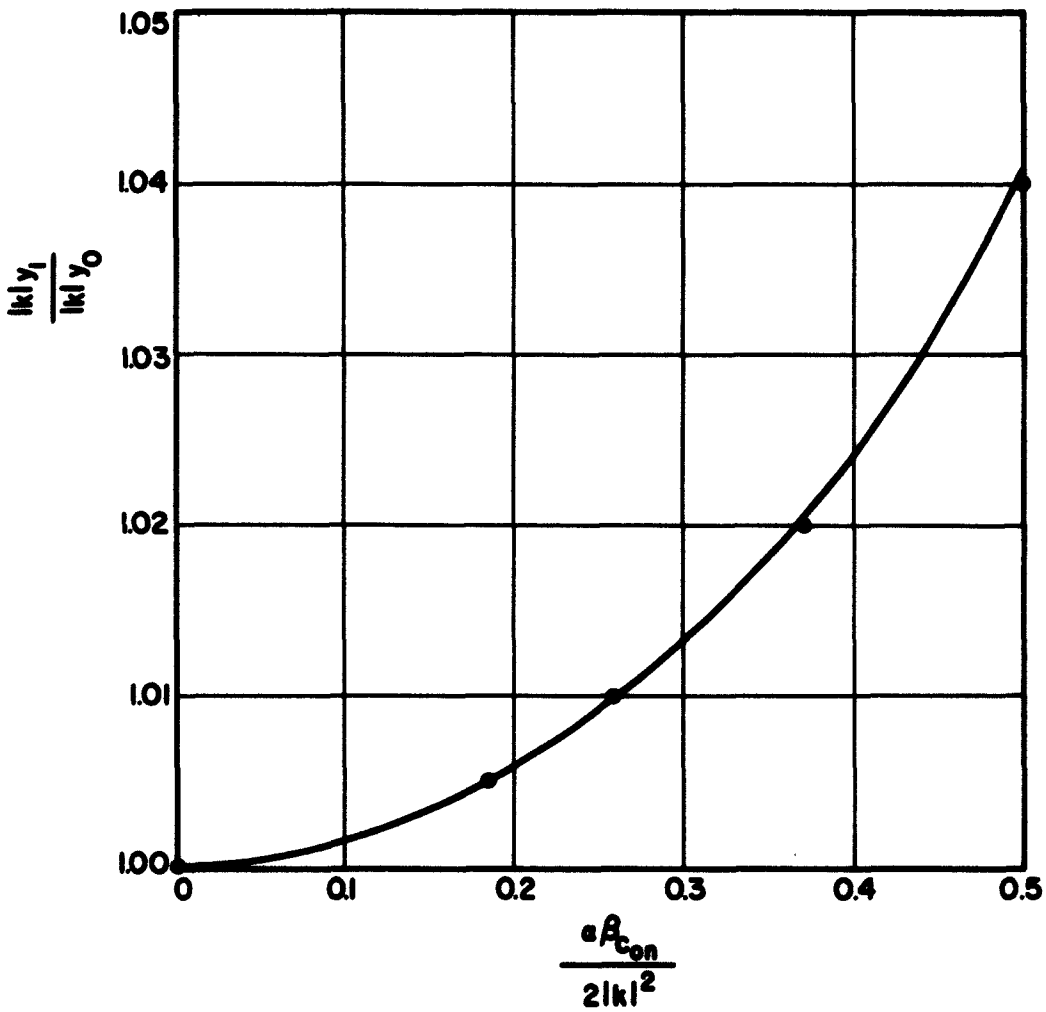

FIG. 2.1 START-OSCILLATION CONDITIONS IN A TAPERED BWO FROM WKBJ APPROXIMATION.

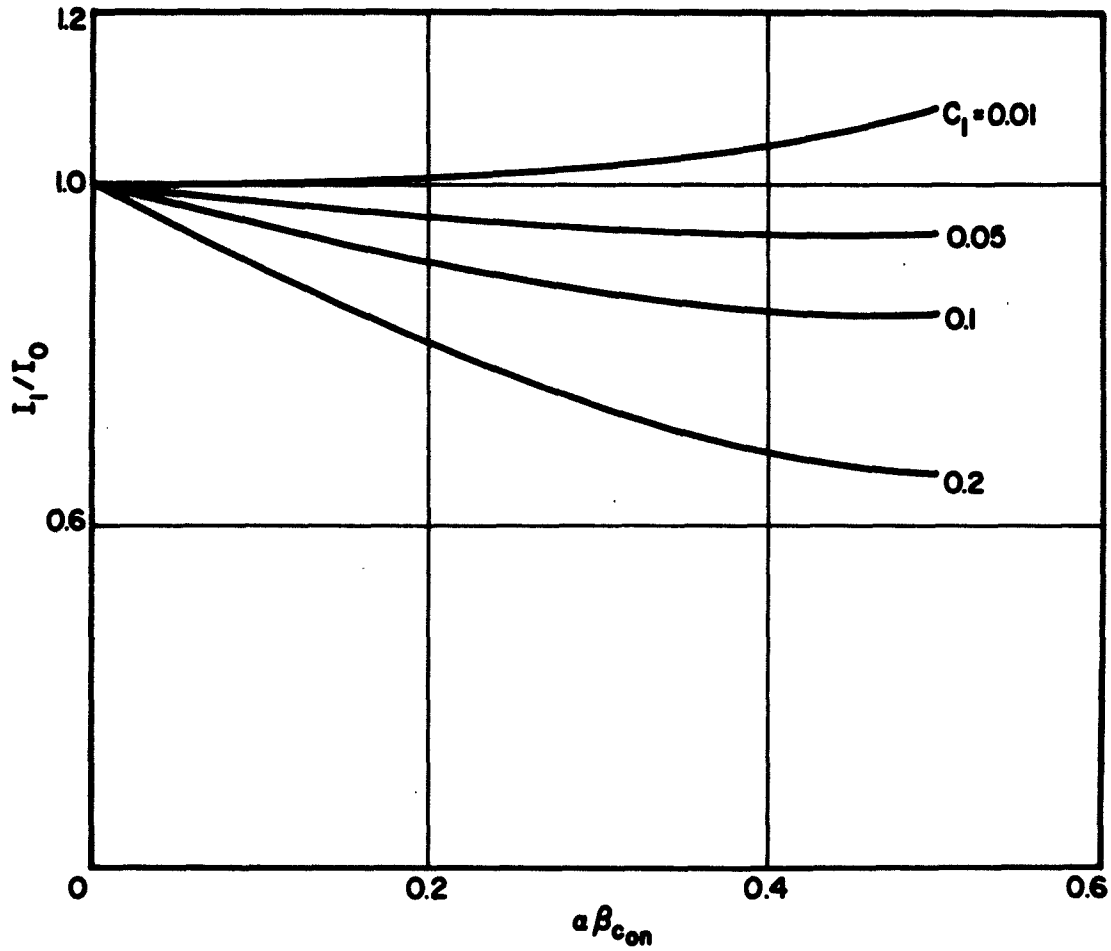

$\frac{I_1}{I_o}$ = Ratio of Oscillation Current in the Tapered Tube to that in the Uniform Tube.

$\alpha\beta_{c_{on}}$ = Taper Parameter.

FIG. 2.2 COMPARISON OF START-OSCILLATION CURRENTS IN UNIFORM AND TAPERED BACKWARD-WAVE OSCILLATORS. ($QC = 0.25$)

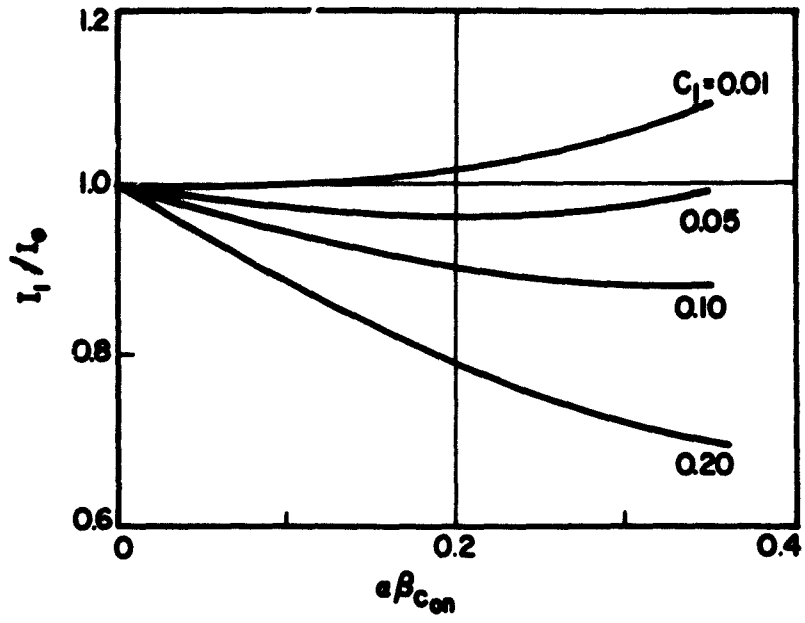

$\frac{I_1}{I_o}$ = Ratio of Oscillation Current in the Tapered Tube to that in the Uniform Tube.

$\alpha\beta_{c_{on}}$ = Taper Parameter.

FIG. 2.3 COMPARISON OF START-OSCILLATION CURRENTS IN UNIFORM AND TAPERED BACKWARD-WAVE OSCILLATORS. (QC = 0.5)

It is thus seen that it is possible for the start-oscillation current to decrease in a tapered tube whose phase velocity decreases along the tube. This case was not considered by Bevensee[19]. He states that the current will increase irrespective of the direction of the taper. It is believed that Bevensee did not take into account the fact that in order for the two tubes to oscillate at the same frequency the operating voltages in the two tubes will be different in this case.

2. The start-oscillation currents of a uniform and tapered tube can be also compared at the same voltage. In this case, in order for the two tubes to oscillate at the same frequency, the phase velocity in the uniform tube has to be lower than the phase velocity of the tapered tube at $z = 0$. It can be easily shown from the above analysis that the start-oscillation current in a uniform tube is proportional to u^7. Thus the ratio of the start-oscillation current of a uniform tube operating at u_1 to that of a uniform tube operating at u_o can be expressed as

$$\frac{I_{u_1}}{I_{u_o}} = \left(\frac{u_1}{u_o}\right)^7 . \qquad (2.109)$$

It is then seen by comparison with Eq. 2.108 that in this case the decrease in the start-oscillation current is greater than that of the first case.

It can then be concluded* that the only way the start-oscillation current can decrease in a tapered tube operating at the same frequency, length and interaction impedance as that of a uniform one is to operate

---

* The author has corresponded with Professor Bevensee, and we are in agreement about the above conclusion.

the tapered tube at a lower beam potential. However, if a uniform tube is operated at this lower potential, and its length, frequency and interaction impedance remain the same (i.e., the phase velocity of the uniform tube will now be lower than that of the tapered one at $z = 0$), then the start-oscillation current in this uniform tube will be lower than that of the tapered one.

Since it has been concluded that a tapered tube will oscillate at a lower voltage than the uniform tube at the same frequency, we can then say that the tuning rate for a tapered tube will be faster than that of a uniform one. From Eq. 2.100 it is obvious that the ratio of the voltage in the tapered tube V_1 to that in the uniform tube V_o can be expressed as follows:

$$\frac{V_1}{V_o} = \left(\frac{u_1}{u_o}\right)^2 = \left(\frac{1}{1 + \frac{\alpha y_1}{2}}\right)^2 . \qquad (2.110)$$

For a typical uniform S-band backward-wave oscillator, covering the frequency range from 2.0 to 4.0 Gc, the power supply must be swept from approximately 200 - 3000 volts. If the phase velocity of this oscillator were tapered to say 90 percent from the beginning to the end of the tube this will correspond roughly to $V_1/V_o = 0.8$, and now the power supply will only have to vary from 160 to 2400 volts to cover the same range of frequencies.

This has been a very approximate analysis which applies for very weak tapers. In the next chapter this problem is solved employing an analog computer where no restriction is placed on the strength of taper and the coupling to the fast space-charge wave is not neglected as was done here.

CHAPTER III. START-OSCILLATION CONDITIONS OF NONUNIFORM BACKWARD-WAVE OSCILLATORS

3.1 Introduction

In Chapter II, coupled-mode theory was employed to determine the start-oscillation conditions of backward-wave oscillators with a tapered velocity extending over the entire length of the circuit. It was seen there that in order to obtain an analytical solution a very weak taper was assumed and the interaction with the fast space-charge wave was neglected. It was concluded there that under certain conditions the start-oscillation current can be lowered in a tapered tube. It was therefore decided to undertake a general study of the effect of circuit velocity tapers and voltage gradients on the start-oscillation conditions without any restriction on the strength of the tapers or the gradients and without neglecting the coupling to the fast space-charge wave.

In this chapter a general set of small-signal equations describing the behavior of nonuniform backward-wave oscillators is derived. These equations are then programmed on an analog computer and a trial and error procedure is employed to determine the oscillation conditions for several nonuniformities in the circuit and the beam.

The advantage of using an analog computer is that one can easily vary parameters by merely changing a potentiometer setting and the nonuniformity in the circuit or the beam can be easily introduced at any point along the length of the tube. Several kinds of nonuniformities in the circuit phase velocity and the beam potential, namely, linear, quadratic and exponential were investigated. These nonuniformities were

introduced at different points along the length of the tube and their effect on the start-oscillation conditions was determined. Another kind of nonuniformity which is inherent in electrostatically-focused tubes[31,32] is an approximately sinusoidal variation of the beam potential. The effect of this nonuniformity on the start-oscillation conditions was also investigated. The analog method was also employed by Rowe and Sobol[29] and Grow[9] to determine the oscillation conditions of modulated and uniform backward-wave oscillators.

In this analysis the slow-wave structure is replaced by an equivalent transmission line whose inductance and capacitance per unit length are chosen so that its phase velocity and characteristic impedance are the same as the phase velocity and interaction impedance of the pertinent space-harmonic of the slow-wave structure. The backward-wave oscillator operates on a harmonic whose phase and group velocities are in opposite directions. Pierce[3] first employed this equivalent transmission-line approach in his analysis of the forward-wave amplifier. Johnson[5] and others[4,9] applied this to the backward-wave oscillator by merely changing the sign of the impedance to account for energy flow in the backward direction and also found it convenient to change the sign of the passive mode parameter Q[3,5]. The fundamental equations describing the interaction in nonuniform backward-wave oscillators are then derived here in a similar manner and with the following assumptions:

1. Small-signal conditions, i.e., the a-c terms are assumed to be small with respect to the d-c terms and all products of a-c terms are neglected. This is a realistic assumption at start oscillation.

2. The beam is confined by a homogeneous d-c magnetic field in the z-direction and thus only z-components of velocity and current will be present.

3. No variations in the transverse plane are present which essentially makes the problem one dimensional.

4. Relativistic effects are negligible.

5. Thermal velocity spread in the beam is neglected.

3.2 Small-Signal Equations of Nonuniform O-Type Backward-Wave Oscillators.

3.2.1 Development of the Circuit Equation. The differential equations for the voltage and current on a nonuniform transmission line in the presence of the beam can be written as

$$\frac{\partial I_c(z,t)}{\partial z} = - C(z) \frac{\partial V_c(z,t)}{\partial t} + \frac{\partial \rho(z,t)}{\partial t} , \qquad (3.1)$$

$$\frac{\partial V_c(z,t)}{\partial z} = - L(z) \frac{\partial I_c(z,t)}{\partial t} - I_c(z,t)\, R(z) , \qquad (3.2)$$

where $V_c(z,t)$ and $I_c(z,t)$ are the voltage and current on the transmission line respectively,

$L(z)$, $C(z)$ and $R(z)$ are the inductance, capacitance and resistance per unit length and

$\partial\rho(z,t)/\partial t$ is the current per unit length induced in the transmission line due to the presence of the beam.

In order to obtain an equation in V_c alone, we follow the standard procedure of differentiating Eq. 3.2 with respect to z and Eq. 3.1 with respect to t, thus obtaining,

$$\frac{\partial^2 V_c(z,t)}{\partial z^2} = - L(z) \frac{\partial^2 I_c(z,t)}{\partial z\, \partial t} - \frac{\partial I_c(z,t)}{\partial t} \frac{dL(z)}{dz} - I_c(z,t) \frac{dR(z)}{dz} - R(z) \frac{\partial I_c(z,t)}{\partial z} , \qquad (3.3)$$

$$\frac{\partial^2 I_c(z,t)}{\partial z\, \partial t} = - C(z) \frac{\partial^2 V_c(z,t)}{\partial t^2} + \frac{\partial^2 \rho(z,t)}{\partial t} \quad . \qquad (3.4)$$

Substituting for $\partial^2 I_c(z,t)/\partial z\, \partial t$, its value from Eq. 3.4 and for $\partial I_c(z,t)/\partial z$, its value from Eq. 3.1 into Eq. 3.3 and arranging terms yields

$$\frac{\partial^2 V_c(z,t)}{\partial z^2} - L(z)\, C(z) \frac{\partial^2 V_c(z,t)}{\partial t^2} - \frac{d\ \ell n\ L(z)}{dz} \frac{\partial V_c(z,t)}{\partial z}$$

$$- R(z)\, C(z) \frac{\partial V_c(z,t)}{\partial t} = - L(z) \frac{\partial^2 \rho(z,t)}{\partial t^2} - R(z) \frac{\partial \rho(z,t)}{\partial t}$$

$$+ R(z)\, I_c(z,t) \left[\frac{1}{L(z)} \frac{dL(z)}{dz} - \frac{1}{R(z)} \frac{dR(z)}{dz} \right] \quad . \qquad (3.5)$$

We see that Eq. 3.5 still contains a term in $I_c(z,t)$. For a lossless transmission line [$R(z) = 0$], this term will not be present and we get a differential equation in $V_c(z,t)$ and $\rho(z,t)$ alone. If one assumes, however, that $L(z)$ and $R(z)$ vary in the same manner, i.e., $L(z) = L_o f(z)$ and $R(z) = R_o f(z)$, then the last term on the right-hand side of Eq. 3.5 is identically zero. This is not an illogical choice for physical inductive elements and does not significantly restrict the applicability of the equations. With this assumption, the final second-order partial differential equation for the circuit voltage becomes,

$$\frac{\partial^2 V_c(z,t)}{\partial z^2} - L(z)\, C(z) \frac{\partial^2 V_c(z,t)}{\partial t^2} - \frac{d\ \ell n\ L(z)}{dz} \frac{\partial V_c(z,t)}{\partial t}$$

$$- R(z)\, C(z) \frac{\partial V_c(z,t)}{\partial t} = - L(z) \frac{\partial^2 \rho(z,t)}{\partial t^2} - R(z) \frac{\partial \rho(z,t)}{\partial t} \quad . \qquad (3.6)$$

Let us now define the following parameters:

$Z_o(z) \triangleq \sqrt{L(z)/C(z)}$ is the characteristic impedance of the transmission line for a low-loss structure, ohms,

$v_o(z) \triangleq 1/\sqrt{L(z)\ C(z)}$ is the characteristic phase velocity of the line, meters/sec,

$d(z) \triangleq R(z)/2\omega C_o(z)\ L(z)$, a loss parameter used in traveling-wave tube theory and first introduced by Pierce[3]. $d(z)$ can be expressed as $\ell(z)/20(2\pi)\log_e C_o(z)$, dimensionless,

$\ell(z) \triangleq$ the series loss in db per wavelength along the line,

$C_o(z) =$ the gain parameter and is defined by $C_o^3(z) = I_o Z_o(z)/4V_o$,

$I_o =$ the d-c beam current, amperes,

$V_o =$ the d-c beam voltage at the entrance to the slow-wave structure, volts,

$u_o =$ the d-c beam velocity at the entrance to the structure and is $= \sqrt{2\eta\ V_o}$, m/sec,

$\eta =$ q/m, the charge-to-mass ratio of an electron coulomb/kg,

$\omega =$ the angular frequency of the wave on the circuit, radians/sec.

Substituting the above definitions in Eq. 3.6 results in,

$$\frac{\partial^2 V_c(z,t)}{\partial z^2} - \frac{1}{v_o^2(z)}\ \frac{\partial^2 V_c(z,t)}{\partial t^2} - \left[\ \frac{1}{Z_o(z)}\ \frac{Z_o(z)}{dz} - \frac{1}{v_o(z)}\ \frac{dv_o(z)}{dz}\right]\frac{\partial V_c(z,t)}{\partial z}$$

$$- \frac{2\omega C_o(z)\ d(z)}{v_o^2(z)}\ \frac{\partial V_c(z,t)}{\partial t} = -\frac{Z_o(z)}{v_o(z)}\left[\ \frac{\partial^2 \rho(z,t)}{\partial t^2}\right.$$

$$\left. + 2\omega C_o(z)\ d(z)\ \frac{\partial \rho(z,t)}{\partial t}\ \right]\ . \quad (3.7)$$

The above circuit equation applies to the forward-wave amplifier. As mentioned earlier, we will merely change the impedance sign to account for a backward wave and thus the circuit equation for the backward-wave oscillator becomes,

$$\frac{\partial^2 V_c(z,t)}{\partial z^2} - \frac{1}{v_o^2(z)} \frac{\partial^2 V_c(z,t)}{\partial t^2} - \left[\frac{1}{Z_o(z)} \frac{dZ_o(z)}{dz} - \frac{1}{v_o(z)} \frac{dv_o(z)}{dz} \right] \frac{\partial V_c(z,t)}{\partial z}$$

$$- \frac{2\omega C_o(z)\, d(z)}{v_o^2(z)} \frac{\partial V_c(z,t)}{\partial t} = \frac{Z_o(z)}{v_o(z)} \left[\frac{\partial^2 \rho(z,t)}{\partial t^2} \right.$$

$$\left. + 2\omega C_o(z)\, d(z) \frac{\partial \rho(z,t)}{\partial t} \right] . \quad (3.8)$$

Assuming that V_c, I_c and ρ vary as $e^{j\omega t}$ and defining $\beta_c(z) \triangleq \omega / v_o(z)$, Eq. 3.8 becomes

$$\frac{d^2 V_c(z)}{dz^2} + \beta_c^2(z)\, V_c(z) - \left[\frac{1}{Z_o(z)} \frac{dZ_o(z)}{dz} - \frac{1}{v_o(z)} \frac{dv_o(z)}{dz} \right] \frac{dV_c(z)}{dz}$$

$$- j2\, \beta_c^2(z)\, C_o(z)\, d(z)\, V_c(z) = -\omega\, Z_o(z) \left[\beta_c(z) \right.$$

$$\left. -j2\, \beta_c(z)\, C_o(z)\, d(z) \right] \rho_1(z) . \quad (3.9)$$

3.2.2 The Continuity Equation. Here it is assumed that a variable d-c voltage is present on the slow-wave structure, so that the d-c beam velocity is now a function of distance. The continuity equation is written as

$$\nabla \cdot i + \frac{\partial \rho}{\partial t} = 0 , \quad (3.10)$$

where* $i = -I_o + i_1(z,t)$, is the total current in the beam, amperes,

$\rho = \rho_o(z) + \rho_1(z,t)$, is the total line charge in the beam, coulombs/m.

Substituting in Eq. 3.10 and remembering that no variations with transverse dimensions are present and that $\rho_1(z,t)$ and $i_1(z,t)$ vary as $e^{j\omega t}$ yields,

$$\frac{\partial}{\partial z}\left[-I_o + i_1(z,t)\right] = -j\omega\,\rho_1(z,t) \quad . \tag{3.11}$$

In the absence of a-c effects, $i_1(z,t)$ and $\rho_1(z,t)$ are zero, Eq. 3.11 reduces to

$$\frac{\partial}{\partial z}(-I_o) = 0 \tag{3.12}$$

and thus I_o is constant. The hydrodynamical equation of flow can be utilized here, since under small-signal conditions the spread in electron velocities is assumed to be small compared with the d-c average velocity so that all electrons passing a given point can be assumed to have essentially the same velocity. We can then write

$$i = \rho u \quad , \tag{3.13}$$

where $u = u_o(z) + u_1(z,t)$ = the total velocity of the electrons, m/sec. Substituting in Eq. 3.13, we obtain

$$\left[-I_o + i_1(z,t)\right] = \left[\rho_o(z) + \rho_1(z,t)\right]\left[u_o(z) + u_1(z,t)\right] \quad . \tag{3.14}$$

Equating the d-c terms, gives

$$-I_o = \rho_o(z)\,u_o(z) \tag{3.15}$$

---

* Subscript "1" designates d-c quantities and "o" a-c quantities.

which shows that $\rho_o(z)$ and $u_o(z)$ vary in an opposite manner so that their product at any point is constant. Equating the a-c terms in Eq. 3.14 and neglecting the product of a-c terms gives (u_1 also varies as $e^{j\omega t}$)

$$i_1(z) = u_o(z)\,\rho_1(z) + \rho_o(z)\,u_1(z) \quad . \tag{3.16}$$

From the a-c part of Eq. 3.11 we have,

$$\frac{di_1(z)}{dz} = -j\omega\,\rho_1(z) \quad . \tag{3.17}$$

$$\rho_o(z)\frac{du_1(z)}{dz} + u_1(z)\frac{d\rho_o(z)}{dz} + u_o(z)\frac{d\rho_1(z)}{dz} + \rho_1(z)\frac{du_o(z)}{dz} + j\omega\,\rho_1(z) = 0 \quad . \tag{3.18}$$

Equation 3.18 can be written in a slightly different form. From Eq. 3.15 we have

$$\frac{d\rho_o(z)}{dz} = -\frac{\rho_o(z)}{u_o(z)}\,\frac{du_o(z)}{dz} \quad . \tag{3.19}$$

Substituting for $d\rho_o(z)/dz$ from Eq. 3.19 into 3.18 gives

$$\rho_o(z)\frac{du_1(z)}{dz} - \frac{\rho_o(z)}{u_o(z)}\,\frac{du_o(z)}{dz}\,u_1(z) + u_o(z)\frac{d\rho_1(z)}{dz} + \rho_1(z)\frac{du_o(z)}{dz} + j\omega\,\rho_1(z) = 0 \quad . \tag{3.20}$$

3.2.3 The Force Equation. Since the analysis here is restricted to slow waves, the electrons also move with speeds that are much lower than the speed of light and thus the effect of their own magnetic field is negligible. The electron beam is also assumed to be neutralized by the presence of ions, whose mass is much larger than that of the electrons.

The ions, due to their much heavier mass, do not respond to r-f fields but can follow the time average or d-c fields and thus cancel the d-c electron charge. Newton's force law can then be written as

$$\frac{d\vec{u}(z,t)}{dt} = \frac{\partial \vec{u}}{\partial t} + (\vec{u}\cdot\nabla)\,\vec{u} = -|\eta|\left[\vec{E}_c(z,t) + \vec{E}_{sc_1}(z,t) + \vec{E}_{d\text{-}c}(z)\right], \tag{3.21}$$

where $\vec{E}_c(z,t)$ = the circuit field acting on the electrons,

$\vec{E}_{sc_1}(z,t)$ = the space-charge field due to r-f interaction,

$\vec{E}_{d\text{-}c}(z)$ = the d-c field due to variation of beam voltage along the length of the tube.

Here again a one-dimensional formulation is assumed. Equation 3.21 can then be written as,

$$\frac{\partial}{\partial t}\left[u_o(z) + u_1(z,t)\right] + \left(u_o(z) + u_1(z,t)\right)\frac{\partial}{\partial z}\left[u_o(z) + u_1(z,t)\right]$$

$$= |\eta|\left[\frac{\partial V_c(z,t)}{\partial z} - E_{sc_1}(z,t) + \frac{dV_o(z)}{dz}\right], \tag{3.22}$$

where $V_o(z)$ is the d-c beam voltage. Again assuming that quantities vary with time as $e^{j\omega t}$ and neglecting products of a-c terms we get the d-c part

$$u_o(z)\frac{du_o(z)}{dz} = |\eta|\frac{dV_o(z)}{dz} \tag{3.23}$$

or

$$u_o(z) = \sqrt{2\eta\, V_o(z)} \tag{3.24}$$

and the a-c part

$$j\omega u_1(z) + u_o(z)\frac{du_1(z)}{dz} + u_1(z)\frac{du_o(z)}{dz} = |\eta|\left[\frac{dV_c(z)}{dz} - E_{sc_1}(z)\right] . \tag{3.25}$$

It can be shown that for a beam of finite radius, the space-charge field can be expressed as[29,30]

$$E_{sc_1}(z) = \frac{j\omega u_o(z)}{|\eta| I_o}\left(\frac{v_o(z)}{u_o(z)}\right)\left(\frac{\omega_q}{\omega}\right)^2 \rho_1(z) , \tag{3.26}$$

where ω_q = the reduced plasma radian frequency.

This form for the space-charge field is amenable to analog computation and it was employed by Rowe and Sobol[29] in determining the start-oscillation conditions in uniform and modulated backward-wave oscillators. Equation 3.25 then becomes,

$$j\omega u_1(z) + u_o(z)\frac{du_1(z)}{dz} + u_1(z)\frac{du_o(z)}{dz}$$

$$= |\eta|\frac{dV_c(z)}{dz} - \frac{j\omega u_o^2(z)}{I_o}\left(\frac{v_o(z)}{u_o(z)}\right)\left(\frac{\omega_q}{\omega}\right)^2 \rho_1(z) . \tag{3.27}$$

Equations 3.9, 3.20 and 3.27 are then the fundamental equations describing the behavior of a backward-wave amplifier or oscillator up to start oscillation.

3.3 Normalization of the Equations

It is now convenient to introduce several normalization factors and introduce some new assumptions in order to put the equations in a more convenient form.

Since the structure loss in a backward-wave oscillator is usually kept quite low, it is assumed that the loss parameter d is constant along

the length of the tube. We will also assume that the interaction impedance of the circuit is constant along the length of the tube. This is a fairly reasonable assumption for a hollow beam flowing very close to the circuit. However, the farther the beam flows away from the circuit the worse this approximation becomes. For a known circuit a certain realistic impedance variation as a function of the phase velocity on the circuit can be determined and then very easily included in the equations.

The following quantities are now defined

$$y \triangleq \beta_{eo} C_o z = 2\pi C_o N \tag{3.28}$$

is the normalized distance along the tube, where N = the number of beam wavelengths,

$$\beta_{eo} \triangleq \frac{\omega}{u_o} \tag{3.29}$$

and u_o = the d-c beam velocity in the uniform section of the tube.

$$C_o^3 \triangleq \frac{I_o Z_o(z)}{4V_o} , \tag{3.30}$$

where Z_o = the Pierce interaction impedance and is assumed to be constant, ohms and

V_o = the beam potential in the uniform section of the tube, volts.

Let us now define the following quantities,

$$V_o(y) \triangleq V_{oo}\zeta(y) , \tag{3.31}$$

thus

$$u_o(y) = u_{oo}\zeta^{1/2}(y) \tag{3.32}$$

and

$$\rho_o(y) \triangleq \rho_{oo}\xi^{-1/2}(y) \quad . \tag{3.33}$$

$$v_o(y) \triangleq v_{oo}\,\xi(y) \quad , \tag{3.34}$$

where $v_{oo} \triangleq$ the circuit phase velocity in the uniform section of the structure.

$\beta_c(y)$ then becomes

$$\beta_c(y) = \frac{\omega}{v_{oo}\,\xi(y)} = \frac{\beta_{co}}{\xi(y)} \quad . \tag{3.35}$$

A measure of the difference in the beam and circuit velocities in the uniform section is characterized by the parameter b which is defined as follows:

$$b = \frac{1}{C_o}\left[\frac{u_{oo} - v_{oo}}{v_{oo}}\right] \quad . \tag{3.36}$$

The ratio of the d-c beam velocity to that of the cold circuit phase velocity in the uniform section can then be expressed as

$$\frac{\beta_{co}}{\beta_{eo}} = \frac{u_{oo}}{v_{oo}} = (1 + C_o b) \quad . \tag{3.37}$$

The space-charge parameter "QC" which is widely used in traveling-wave amplifier and backward-wave oscillator theories can be expressed as follows:

$$(QC) = \frac{1}{4C_o^2}\left(\frac{\omega_q/\omega}{1 + \omega_q/\omega}\right)^2 \quad . \tag{3.38}$$

The following normalized quantities are also defined,

$$V_{cn}(z) \triangleq \frac{V_c(z)}{V_{oo}} \quad , \tag{3.39}$$

$$u_{1n}(z) \triangleq \frac{u_1(z)}{u_{oo}} \quad , \tag{3.40}$$

$$\rho_{1n}(z) \triangleq \frac{\rho_1(z)}{\rho_{oo}} \quad . \tag{3.41}$$

Substituting the above normalized parameters and utilizing the definition of the above quantities in Eqs. 3.9, 3.20 and 3.27 results in the following set of differential equations,

$$\frac{d^2V_{cn}(y)}{dy^2} + \left(\frac{1 + C_o b}{C_o} \right)^2 \frac{1}{\xi^2(y)} V_{cn}(y) + \frac{1}{\xi(y)} \frac{d\xi(y)}{dy} \frac{dV_{cn}(y)}{dy}$$

$$- j2 \frac{d}{C_o} (1 + C_o b)^2 \frac{1}{\xi^2(y)} V_{cn}(y)$$

$$= \frac{4C_o(1 + C_o b)}{\xi(y)} \rho_{1n}(y) - \frac{j8C_o^2 d(1 + C_o b)}{\xi(y)} \rho_{1n}(y) \quad , \tag{3.42}$$

$$\frac{1}{\zeta^{1/2}(y)} \frac{du_{1n}(y)}{dy} - \frac{1}{\zeta(y)} \frac{d\zeta^{1/2}(y)}{dy} u_{1n}(y) + \zeta^{1/2}(y) \frac{d\rho_{1n}(y)}{dy}$$

$$+ \left[\frac{d\zeta^{1/2}(y)}{dy} + \frac{j}{C_o} \right] \rho_{1n}(y) = 0 \quad , \tag{3.43}$$

$$\frac{1}{2}\frac{dV_{cn}(y)}{dy} + j\frac{4C_o QC}{(1 - 2C_o\sqrt{QC})^2}\frac{1}{(1 + C_o b)}\xi(y)\,\rho_{1n}(y)$$

$$= \left[\frac{j}{C_o} + \frac{d\zeta^{1/2}(y)}{dy}\right] u_{1n}(y) + \zeta^{1/2}(y)\frac{du_{1n}(y)}{dy} \quad . \quad (3.44)$$

The above equations are the normalized equations representing a nonuniform backward-wave oscillator under the assumptions introduced above. The nonuniformity in the circuit phase velocity is introduced into the equations through $\xi(y)$ and the nonuniformity in the beam potential through $\zeta(y)$.

3.4 Solution of the Equations

Equations 3.42 through 3.44 were programmed on an analog computer and the start-oscillation conditions were determined for several kinds of nonuniformities. The different kinds of nonuniformities that were investigated are discussed in the following sections. A detailed discussion of the scaling and programming of these equations is given in Appendix B. A brief discussion is given here.

First the boundary conditions must be specified. These are the usual conditions; namely, the beam enters the slow-wave structure with no r-f modulation other than noise which is negligible, the r-f output is matched, and the r-f circuit wave at the entrance plane is arbitrary. These assumptions then lead to the following boundary conditions respectively,

$$u_{1n}(y) = \rho_{1n}(y) = 0 \quad , \quad (3.45)$$

$$\frac{V_c(0)}{I_c(0)} = -Z_o(0) \quad (3.46)$$

and

$$V_{cn}(0) \text{ is arbitrary} \quad . \tag{3.47}$$

Since Eq. 3.42 is of second order, $[dV_{cn}(y)/dy]_{y=0}$ must also be specified. This can be easily determined from Eq. 3.2. Normalizing Eq. 3.2 yields

$$\left(\frac{dV_{cn}(y)}{dy}\right)_{y=0} = - V_{cn}(0)\left[j\,\frac{1 + C_o b}{C_o} + 2d(1 + \iota_o b)\right] \quad . \tag{3.48}$$

Knowing the boundary conditions, the equations were then separated into real and imaginary parts by assuming the following forms for the dependent variables,

$$V_{cn} = V_R + j\,V_I \quad , \tag{3.49}$$

$$u_{in} = u_R + j\,u_I \quad , \tag{3.50}$$

$$\rho_{in} = \rho_R + j\,\rho_I \quad . \tag{3.51}$$

By using a standard analog computer resolver for converting from cartesian into polar coordinates the magnitude of any of the above quantities can be easily determined. The oscillation conditions can then be determined as follows: For a given set of values C_o, QC, and d the circuit voltage is plotted as a function of y for different values of b. The value of b that forces the r-f circuit voltage to zero represents a start-oscillation condition. The start-oscillation length can then be determined from the value of y at which the circuit voltage becomes zero. A nonuniformity in the tube can be easily introduced on the analog computer at any point along the length of the tube. This is accomplished by merely running the computer up to the point where the nonuniformity starts

employing the uniform-tube equations. The computer is then switched into a "hold" position and thus the initial conditions for the nonuniform section are now established. With the computer still in the "hold" position, a switch is now employed to introduce the equations for the nonuniform section. The computer is then switched into the "operate" position and the run is completed.

3.5 Start-Oscillation Conditions

In this section, the start-oscillation conditions for several kinds of nonuniformities introduced at different points along the length of the tube are presented. These conditions are presented in the form of graphs where the oscillation conditions in a tapered tube are compared to those of a uniform one. The following notation is used in all the graphs that follow.

$\frac{b_1}{b_o}$ = the ratio of b(defined by Eq. 3.36) in the tapered or nonuniform tube to that in the uniform one,

$\frac{CN_{s,1}}{CN_{s,o}} = \frac{y_{s,1}}{y_{s,o}}$ = the ratio of the normalized start-oscillation length of a nonuniform tube to that of a uniform one,

$\frac{y_{s,t}}{y_{s,o}}$ = the ratio of the normalized length at which the nonuniformity begins to the normalized oscillation length of a uniform tube,

$\frac{I_{s,1}}{I_{s,o}}$ = the ratio of the start-oscillation current of a nonuniform tube to that of a uniform one.

The start-oscillation currents were compared in the same manner here as that in Section 2.5, namely,

$$\frac{I_{s,1}}{I_{s,o}} = \left(\frac{1 + C_o b_1}{1 + C_o b_o}\right)^5 \left(\frac{y_{s,1}}{y_{s,o}}\right)^3 , \qquad (3.52)$$

where the physical length in the two tubes is assumed to be the same and the oscillation frequency is the same. C_o in the two tubes was also assumed to be the same. This is not quite true, since any change in the beam current or velocity will also change C. However, as discussed in Section 2.5 this change is negligible and has a negligible effect on the final results. A more exact comparison for constant C_o could be made by comparing both the start-oscillation current and the starting length as follows (i.e., in this case the physical length of the tubes, L, is not the same).

$$\frac{I_{s,1}}{I_{s,o}} = \left(\frac{1 + C_o b_1}{1 + C_o b_o}\right)^2 \qquad (3.53)$$

and

$$\frac{L_{s,1}}{L_{s,o}} = \left(\frac{1 + C_o b_1}{1 + C_o b_o}\right)\left(\frac{y_{s,1}}{y_{s,o}}\right) . \qquad (3.54)$$

This can be easily obtained from the graphs if so desired. It is felt, however, that the comparison of the start-oscillation current with length in the two tubes fixed is more meaningful. The space-charge parameter in the two tubes is also essentially the same, since $QC \sim (Iu)^{1/3}$ and the changes in u and I encountered here are small.

Since the graphs presented in the following sections are comparisons to a uniform tube with a certain set of parameters, the oscillation conditions for such parameters are given in Table 3.1. They are also compared to oscillation conditions obtained from a digital computer by Rowe and Sobol[30].

Table 3.1

Start-Oscillation Conditions for a Uniform BWO

C	QC	d	b_o at Start Oscillation		$CN_{s,o}$ for Oscillation	
			Analog	Digital	Analog	Digital
0.05	0	0	1.55	1.559	0.3023	0.3013
	0.2	0	1.60	1.593	0.3184	0.3202
	0.5	0	1.70	1.69	0.3821	0.3691

3.5.1 Linear Circuit Phase Velocity Tapers. Since it was concluded in Chapter II that for a constant beam potential the start-oscillation current will increase when the circuit phase velocity increases as a function of distance along the tube, only circuit velocity tapers decreasing with distance were investigated. The linear taper was assumed to have the following form,

$$v_o(y) = v_{oo}(1 - \alpha y) \quad , \tag{3.55}$$

where α is a measure of the strength of the taper. The beam velocity is assumed constant along the length of the tube. $\xi(y)$ and $\zeta(y)$ in the general set of Eqs. 3.42 through 3.44 will then assume the following form,

$$\xi(y) = (1 - \alpha y) \quad , \tag{3.56}$$

$$\zeta(y) = 1 \quad . \tag{3.57}$$

Substituting the above values of $\xi(y)$ and $\zeta(y)$ into Eqs. 3.42 through 3.44 yields,

$$\frac{d^2V_{cn}(y)}{dy^2} + \left(\frac{1 + C_o b}{C_o}\right)^2 \frac{1}{(1 - \alpha y)^2} V_{cn}(y) - \frac{\alpha}{(1 - \alpha y)} \frac{dV_{cn}(y)}{dy}$$

$$- j2 \frac{d}{C_o} (1 + C_o b)^2 \frac{1}{(1 - \alpha y)^2} V_{cn}(y) = \frac{4C_o(1 + C_o b)}{(1 - \alpha y)} \rho_{1n}(y)$$

$$- j \frac{8C_o^2 d(1 + C_o b)}{(1 - \alpha y)} \rho_{1n}(y) \quad , \quad (3.58)$$

$$\frac{du_{1n}(y)}{dy} + \frac{d\rho_{1n}(y)}{dy} + \frac{j}{C_o} \rho_{1n}(y) = 0 \quad , \quad (3.59)$$

$$\frac{1}{2} \frac{dV_{cn}(y)}{dy} + j \frac{4C_o QC}{[1 - 2C_o \sqrt{QC}]^2} \frac{1}{(1 + C_o b)} (1 - \alpha y) \rho_{1n}(y)$$

$$= \frac{j}{C_o} u_{1n}(y) + \frac{du_{1n}(y)}{dy} \quad . \quad (3.60)$$

The solution of these equations on an analog computer is discussed in detail in Appendix B.1. The results are presented in Figs. 3.1 through 3.9.

In these figures the start-oscillation conditions of a tapered tube are compared to a uniform one as a function of the strength of the taper. As can be seen from the figures the tapers were introduced at different points along the length of the tube. For the value of C_o investigated there is good agreement with the coupled-mode theory analysis of Chapter II for weak tapers, i.e., the start-oscillation current decreases in a tapered tube under the conditions that were assumed. It was found, however, that when the taper became stronger than a particular

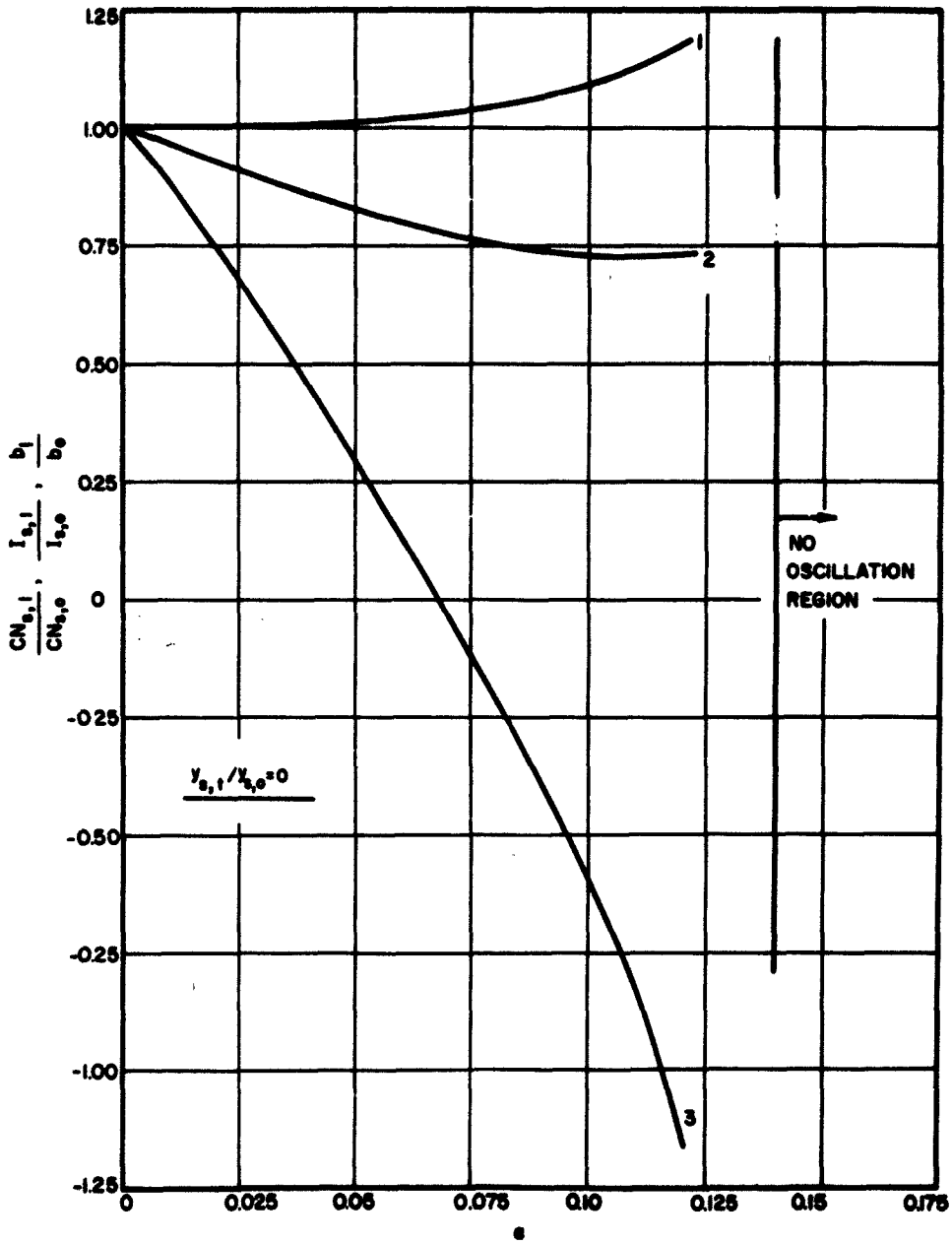

1. $\frac{CN_{s,1}}{CN_{s,o}}$ 2. $\frac{I_{s,1}}{I_{s,o}}$ 3. $\frac{b_1}{b_o}$

FIG. 3.1 $CN_{s,1}/CN_{s,o}$, $I_{s,1}/I_{s,o}$, b_1/b_o VS. α FOR A LINEAR CIRCUIT PHASE VELOCITY TAPER. (C = 0.05, QC = 0, d = 0)

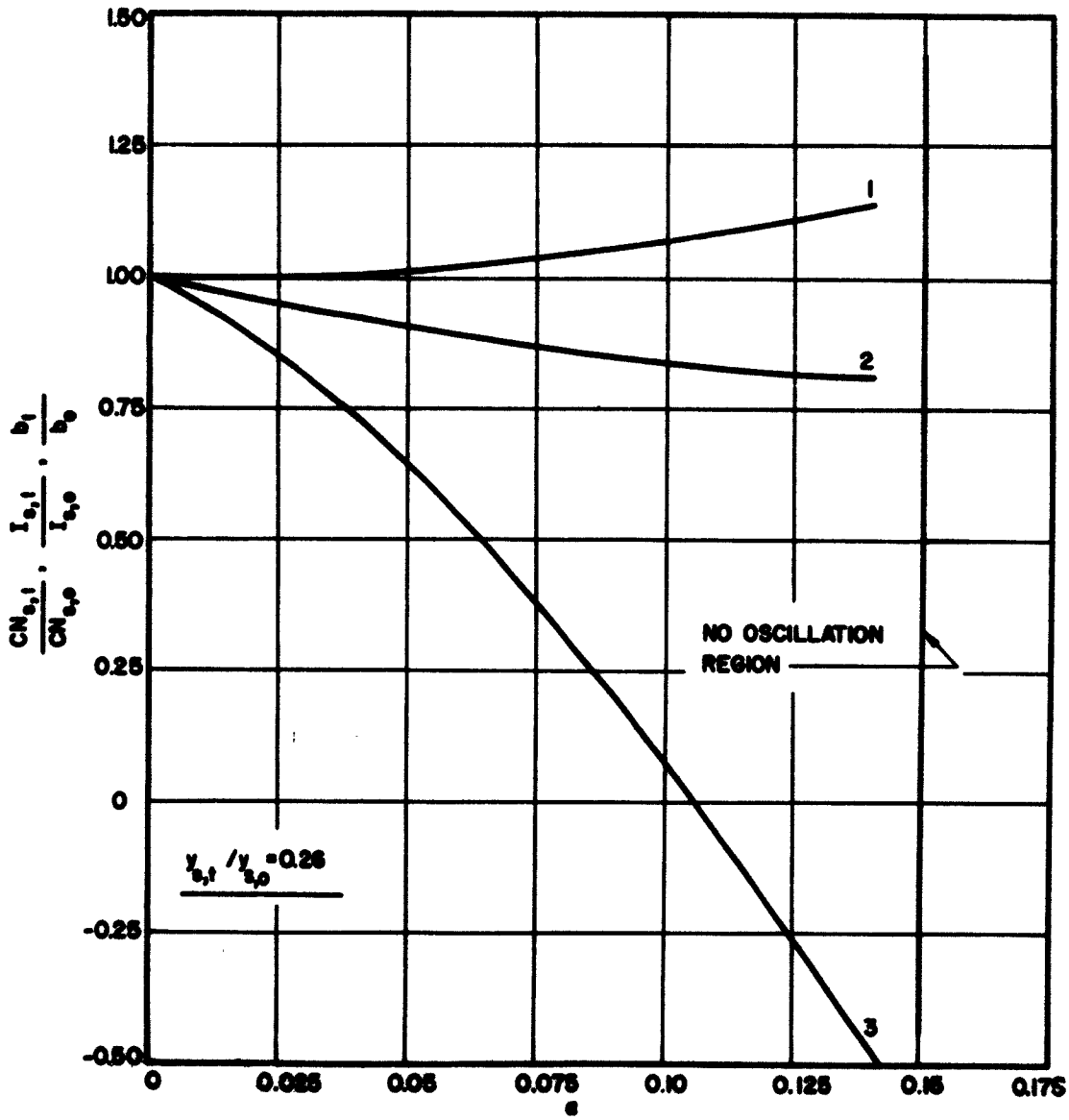

1. $\frac{CN_{s,1}}{CN_{s,0}}$ 2. $\frac{I_{s,1}}{I_{s,0}}$ 3. $\frac{b_1}{b_0}$

FIG. 3.2 $CN_{s,1}/CN_{s,0}$, $I_{s,1}/I_{s,0}$, b_1/b_0 VS. α FOR A LINEAR CIRCUIT PHASE VELOCITY TAPER. ($C = 0.05$, $QC = 0$, $d = 0$)

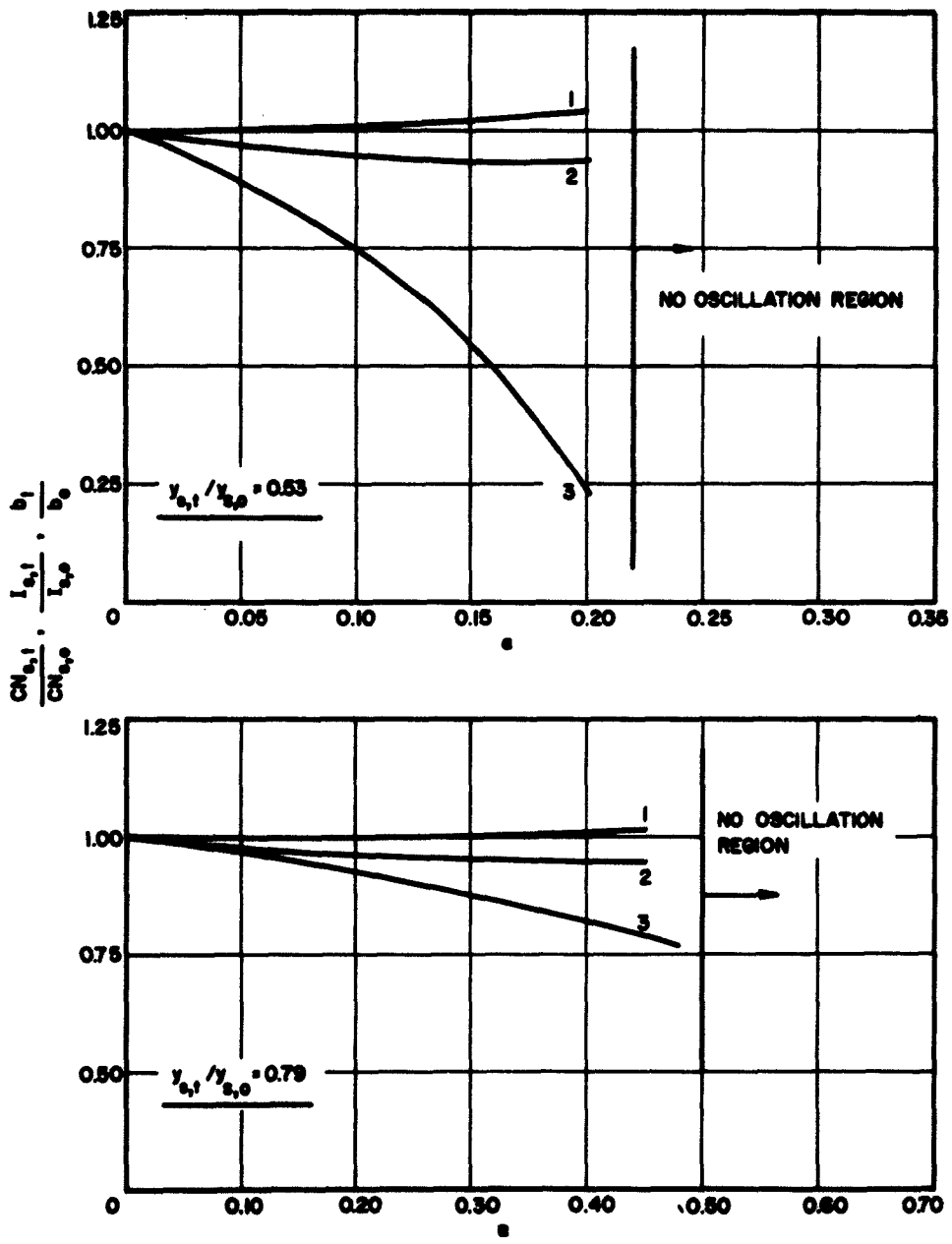

1. $\frac{CN_{s,1}}{CN_{s,o}}$ 2. $\frac{I_{s,1}}{I_{s,o}}$ 3. $\frac{b_1}{b_o}$

FIG. 3.3 $CN_{s,1}/CN_{s,o}$, $I_{s,1}/I_{s,o}$, b_1/b_o VS. α FOR A LINEAR CIRCUIT PHASE VELOCITY TAPER. ($C = 0.05$, $QC = 0$, $d = 0$)

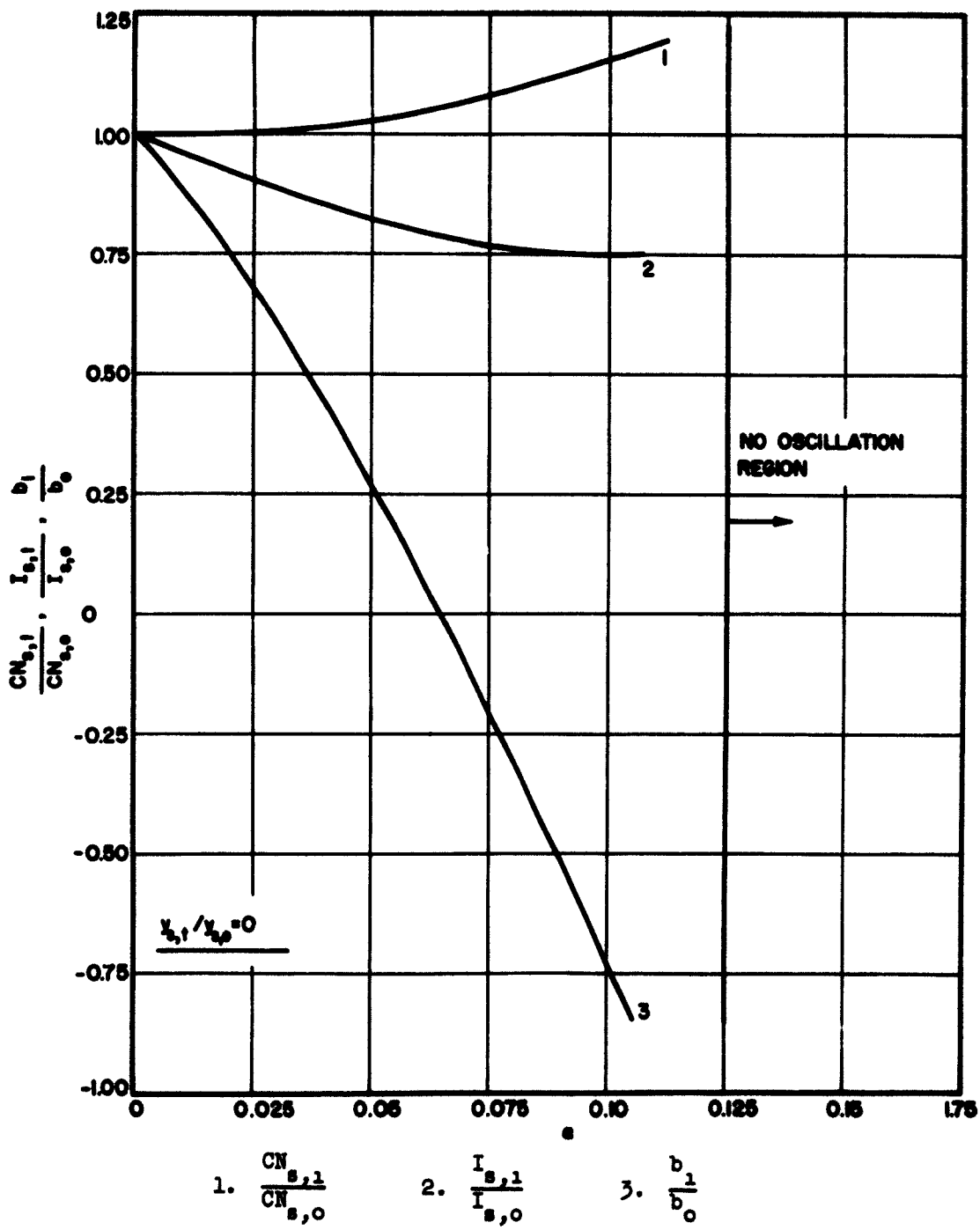

FIG. 3.4 $CN_{s,1}/CN_{s,0}$, $I_{s,1}/I_{s,0}$, b_1/b_0 VS. α FOR A LINEAR CIRCUIT PHASE VELOCITY TAPER. ($C = 0.05$, $QC = 0.2$, $d = 0$)

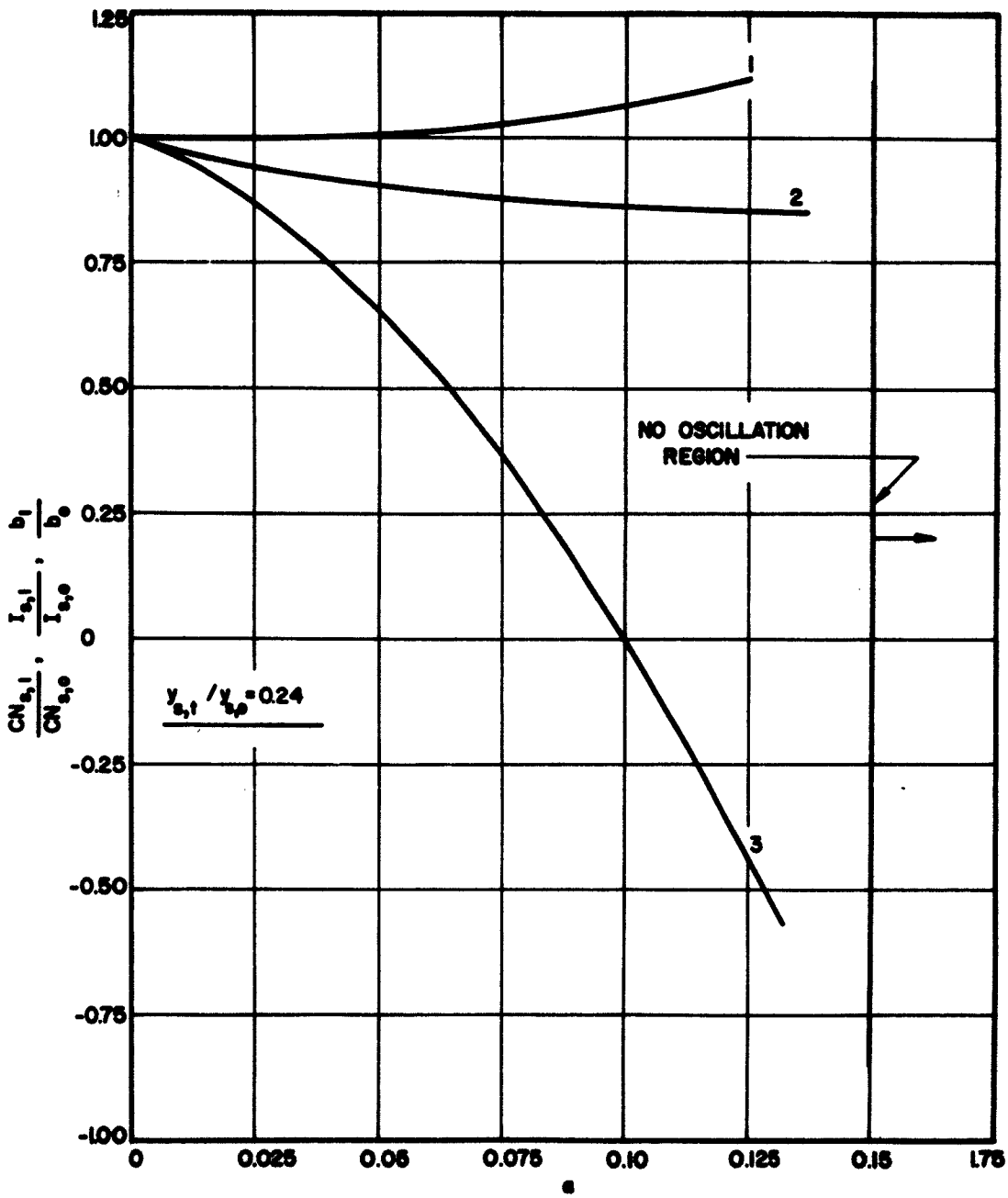

FIG. 3.5 $CN_{s,1}/CN_{s,0}$, $I_{s,1}/I_{s,0}$, b_1/b_0 VS. α FOR A LINEAR CIRCUIT PHASE VELOCITY TAPER. ($C = 0.05$, $QC = 0.2$, $d = 0$)

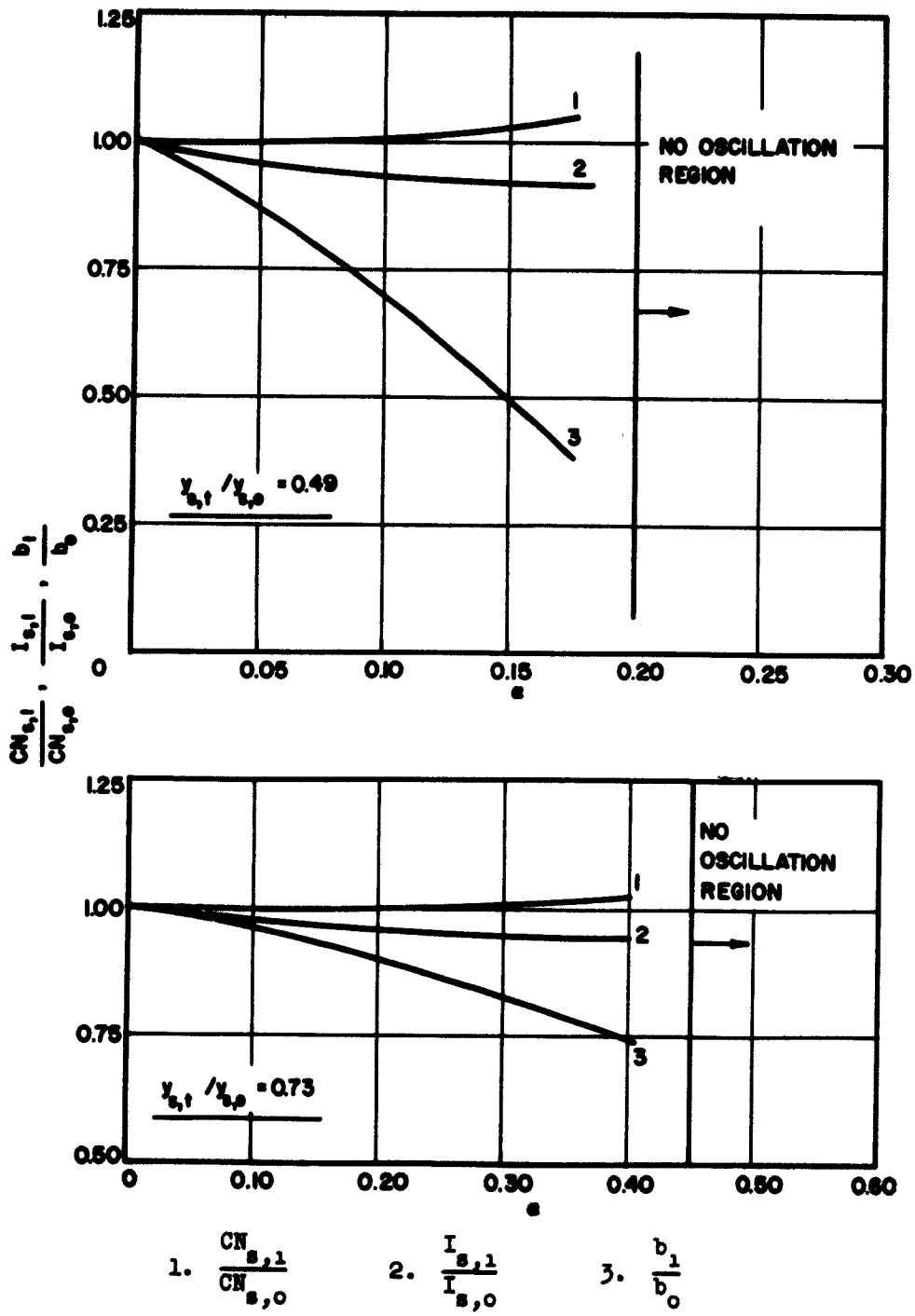

FIG. 3.6 $CN_{s,1}/CN_{s,0}$, $I_{s,1}/I_{s,0}$, b_1/b_0 VS. α FOR A LINEAR CIRCUIT PHASE VELOCITY TAPER. ($C = 0.05$, $QC = 0.2$, $d = 0$)

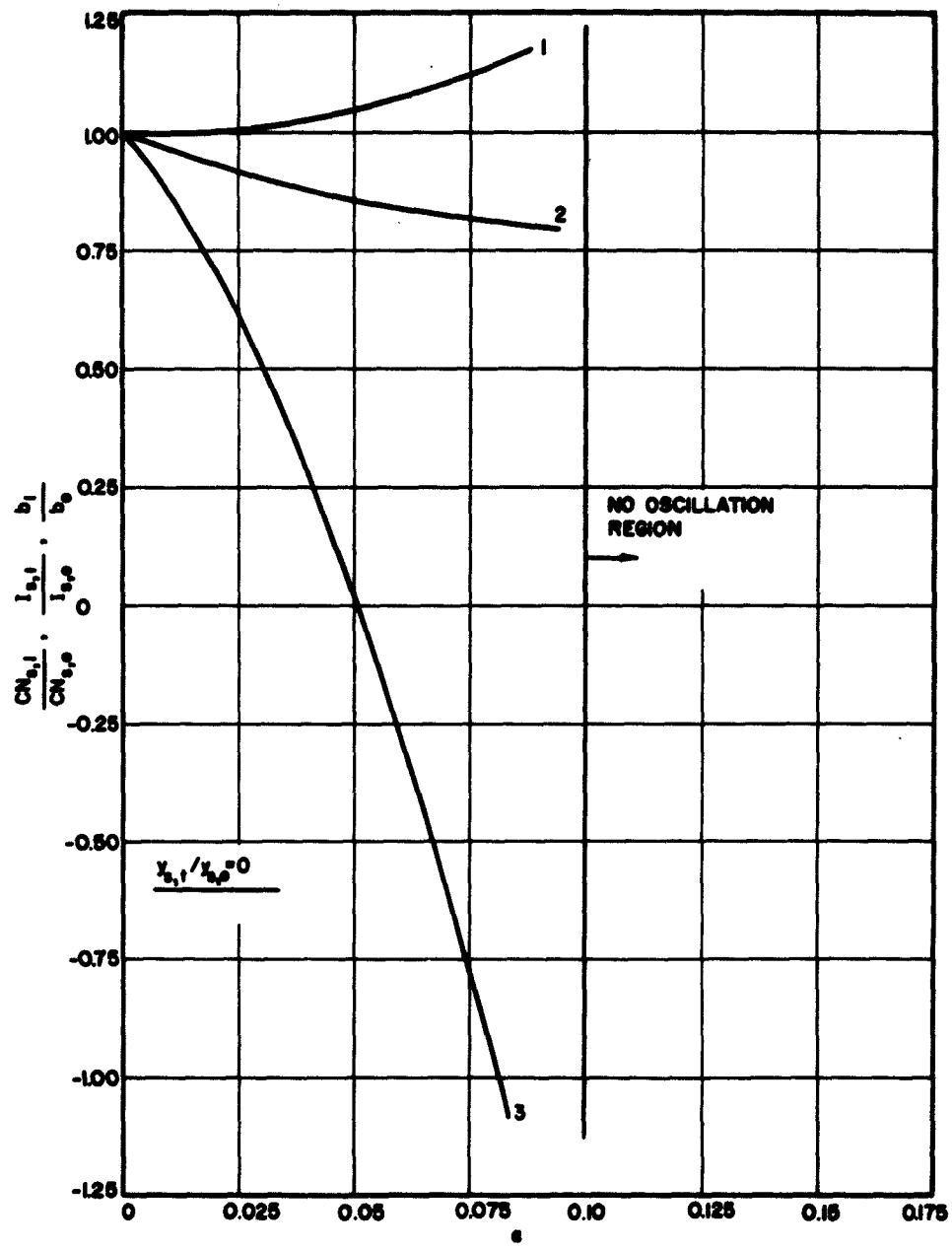

1. $\frac{CN_{s,1}}{CN_{s,0}}$ 2. $\frac{I_{s,1}}{I_{s,0}}$ 3. $\frac{b_1}{b_0}$

FIG. 3.7 $CN_{s,1}/CN_{s,0}$, $I_{s,1}/I_{s,0}$, b_1/b_0 VS. α FOR A LINEAR CIRCUIT PHASE VELOCITY TAPER. (C = 0.05, QC = 0.5, d = 0)

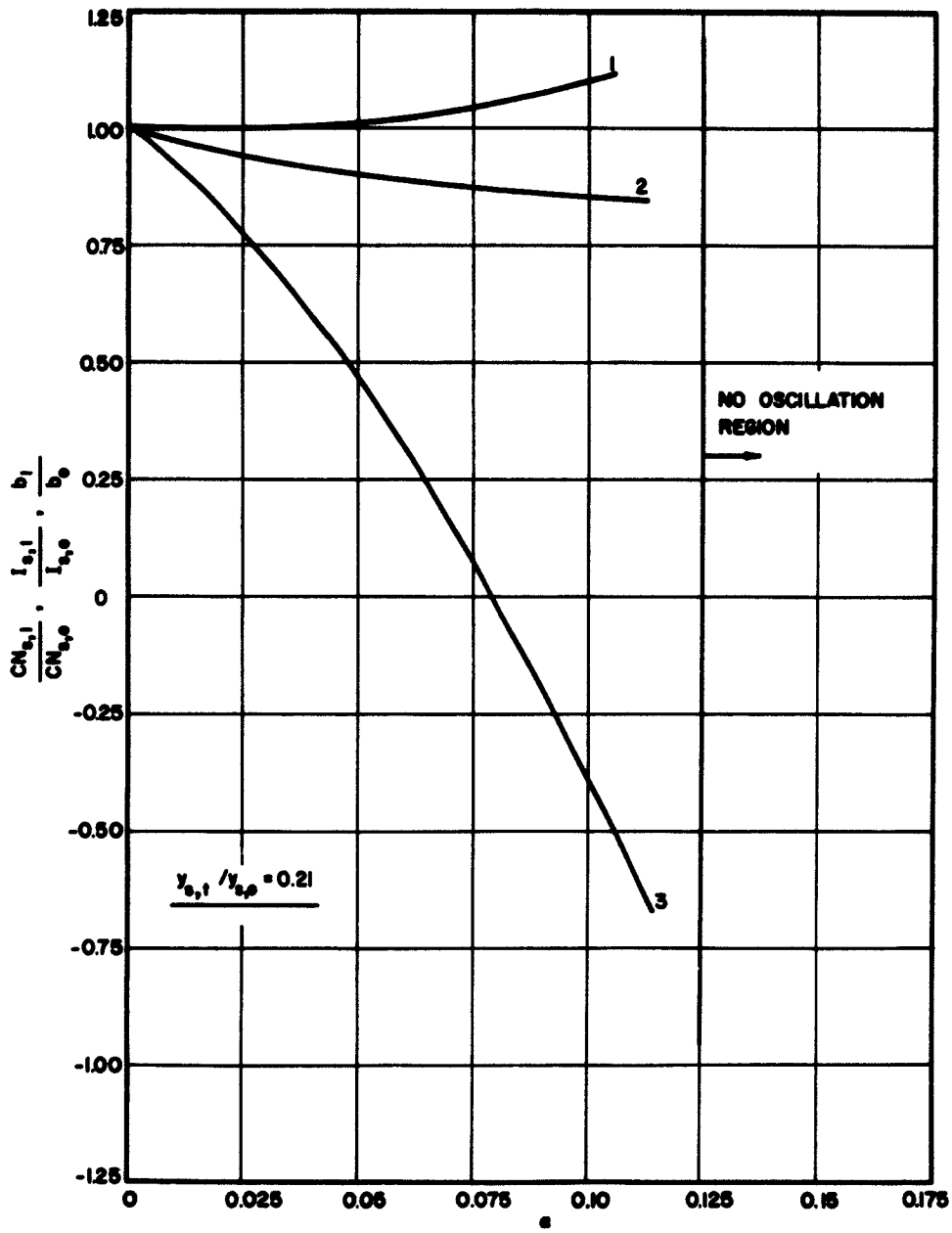

1. $\frac{CN_{s,1}}{CN_{s,o}}$ 2. $\frac{I_{s,1}}{I_{s,o}}$ 3. $\frac{b_1}{b_o}$

FIG. 3.8 $CN_{s,1}/CN_{s,o}$, $I_{s,1}/I_{s,o}$, b_1/b_o VS. α FOR A LINEAR CIRCUIT PHASE VELOCITY TAPER. ($C = 0.05$, $QC = 0.5$, $d = 0$)

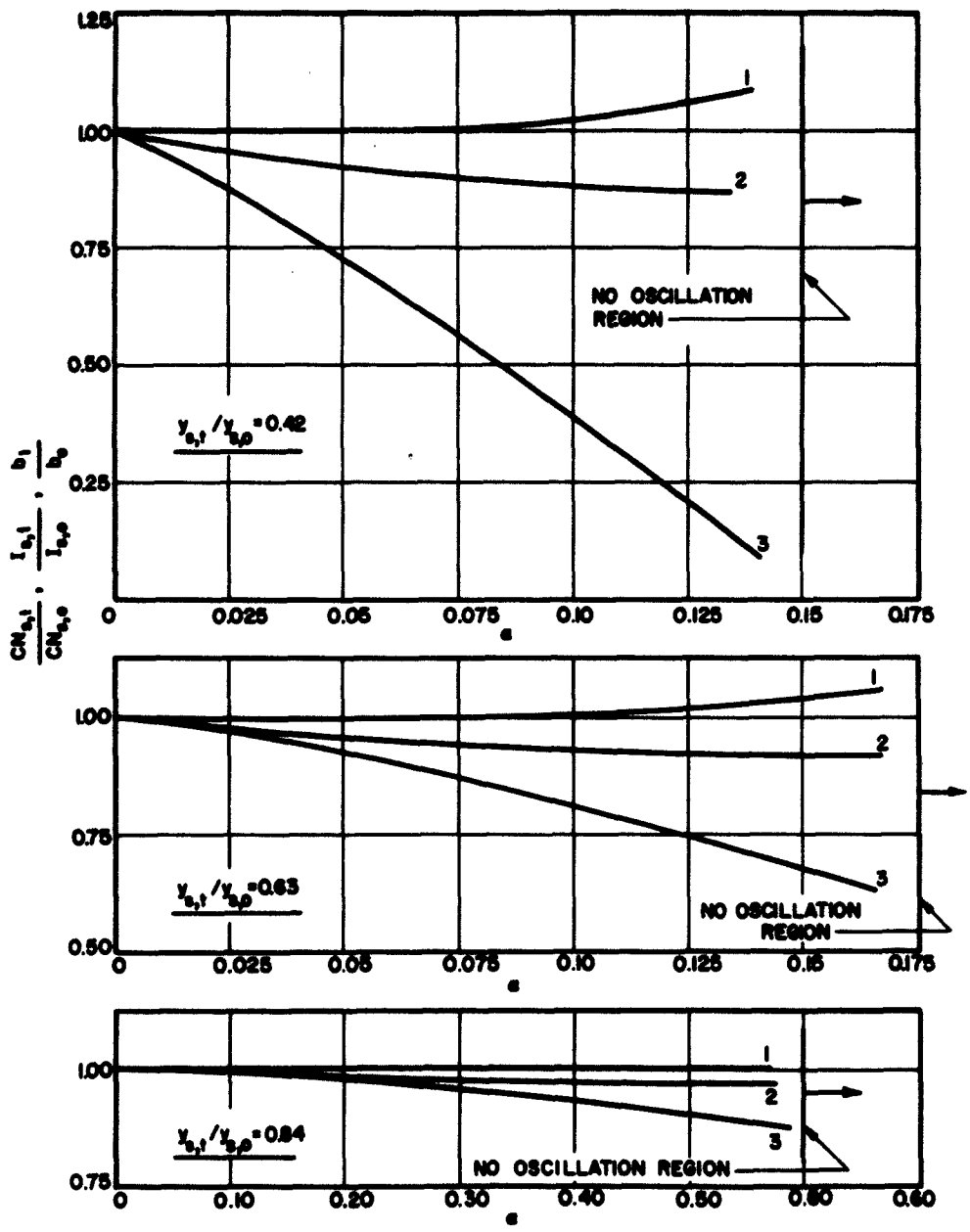

1. $\frac{CN_{s,1}}{CN_{s,0}}$ 2. $\frac{I_{s,1}}{I_{s,0}}$ 3. $\frac{b_1}{b_0}$

FIG. 3.9 $CN_{s,1}/CN_{s,0}$, $I_{s,1}/I_{s,0}$, b_1/b_0 VS. α FOR A LINEAR CIRCUIT PHASE VELOCITY TAPER. ($C = 0.05$, $QC = 0.5$, $d = 0$)

value, no value of b could be found to force the circuit voltage to vanish and thus no oscillation condition could be found. The region beyond this particular value of α has been designated as the "no oscillation region" in the figures.

3.5.2 Quadratic Circuit Phase Velocity Tapers. Here it is also assumed that the beam velocity is constant and the circuit phase velocity varies in the following manner,

$$v_o(y) = v_{oo}(1 - \alpha y^2) \quad . \tag{3.61}$$

This makes

$$\xi(y) = (1 - \alpha y^2) \tag{3.62}$$

and

$$\zeta(y) = 1 \quad . \tag{3.63}$$

Substituting the above values of $\xi(y)$ and $\zeta(y)$ into Eqs. 3.42 through 3.44 yields the following set of equations which characterize the behavior of the oscillator when a quadratic phase velocity taper is introduced on the slow-wave structure,

$$\frac{d^2V_{cn}(y)}{dy^2} + \left(\frac{1 + C_o b}{C_o}\right)^2 \frac{1}{(1 - \alpha y^2)^2} - \frac{2\alpha y}{(1 - \alpha y^2)} \frac{dV_{cn}(y)}{dy}$$

$$- j2 \frac{d}{C_o} (1 + C_o b)^2 \frac{1}{(1 - \alpha y^2)} V_{cn}(y)$$

$$= \frac{4C_o(1 + C_o b)}{(1 - \alpha y^2)} \rho_{1n}(y) - j \frac{8C_o^2 \, d(1 + C_o b)}{(1 - \alpha y^2)} \rho_{1n}(y) \quad , \tag{3.64}$$

$$\frac{du_{1n}(y)}{dy} + \frac{d\rho_{1n}(y)}{dy} + \frac{1}{C_o} \rho_{1n}(y) = 0 \quad , \tag{3.65}$$

$$\frac{1}{2}\frac{dV_{cn}(y)}{dy} + j\frac{4C_o QC}{[1 - 2C_o\sqrt{QC}]^2}\frac{1}{(1 + C_o b)}(1 - \alpha y^2)\rho_{in}(y)$$

$$= \frac{j}{C_o}u_{in}(y) + \frac{du_{in}(y)}{dy} \quad . \quad (3.66)$$

The solution of these equations is discussed in detail in Appendix B.1. The results are presented in Figs. 3.10 through 3.15.

Here also, the start-oscillation conditions of the tapered tube are compared to the uniform one as a function of the taper parameter α. The oscillation frequencies and the physical lengths of the two tubes are assumed equal. The taper was also introduced at different points along the length of the tube. As in the linear velocity taper case, the start-oscillation current decreases for weak tapers and when the taper gets stronger than a certain value no oscillation condition could be found. This region is also designated the "no oscillation region" on the figures.

3.5.3 Exponential Circuit Phase Velocity Tapers. In this section it is assumed that the circuit phase velocity varies in the following manner,

$$v_o(y) = v_{oo}\, e^{-\alpha y} \quad (3.67)$$

and the beam velocity is constant along the length of the tube. This makes $\xi(y)$ and $\zeta(y)$ assume the following values,

$$\xi(y) = e^{-\alpha y} \quad , \quad (3.68)$$

$$\zeta(y) = 1 \quad . \quad (3.69)$$

Substituting these values of $\xi(y)$ and $\zeta(y)$ in Eqs. 3.42 through 3.44 results in the following set of equations which characterize a

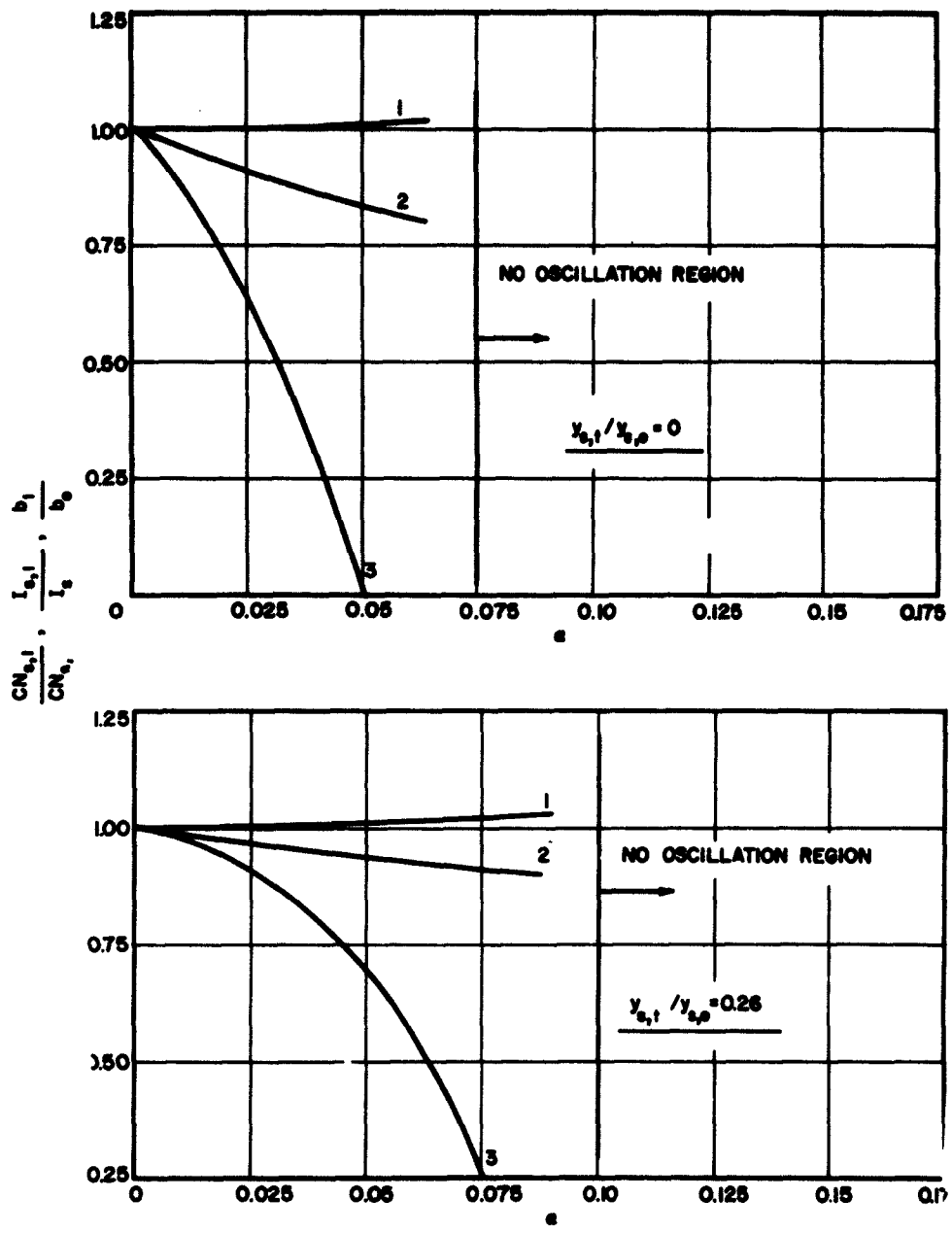

1. $\frac{CN_{s,1}}{CN_{s,o}}$ 2. $\frac{I_{s,1}}{I_{s,o}}$ 3. $\frac{b_1}{b_o}$

FIG. 3.10 $CN_{s,1}/CN_{s,o}$, $I_{s,1}/I_{s,o}$, b_1/b_o VS. α FOR A QUADRATIC CIRCUIT PHASE VELOCITY TAPER. (C = 0.05, QC = 0, d = 0)

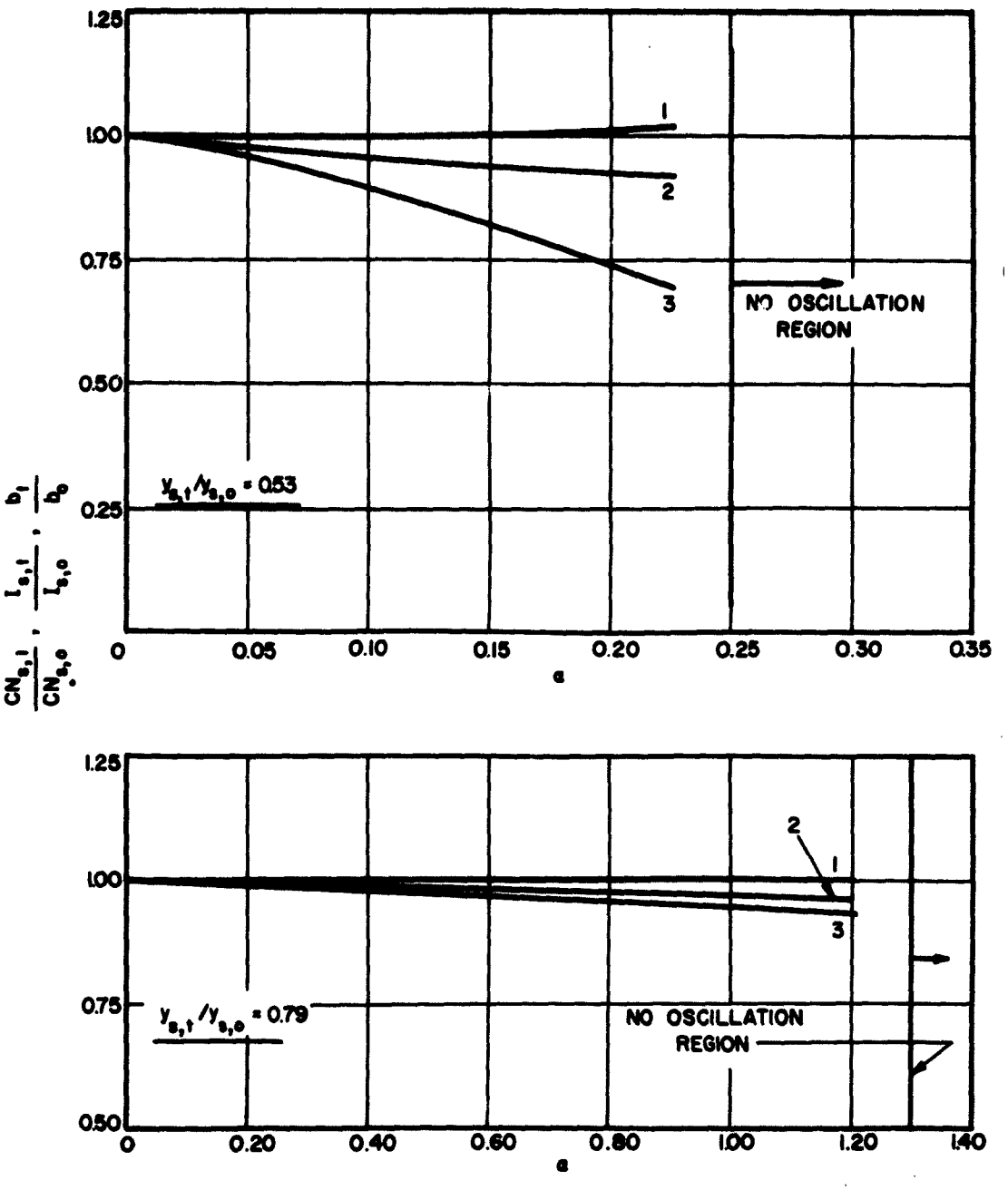

1. $\frac{CN_{s,1}}{CN_{s,0}}$ 2. $\frac{I_{s,1}}{I_{s,0}}$ 3. $\frac{b_1}{b_0}$

FIG. 3.11 $CN_{s,1}/CN_{s,0}$, $I_{s,1}/I_{s,0}$, b_1/b_0 VS. α FOR A QUADRATIC CIRCUIT PHASE VELOCITY TAPER. ($C = 0.05$, $QC = 0$, $d = 0$)

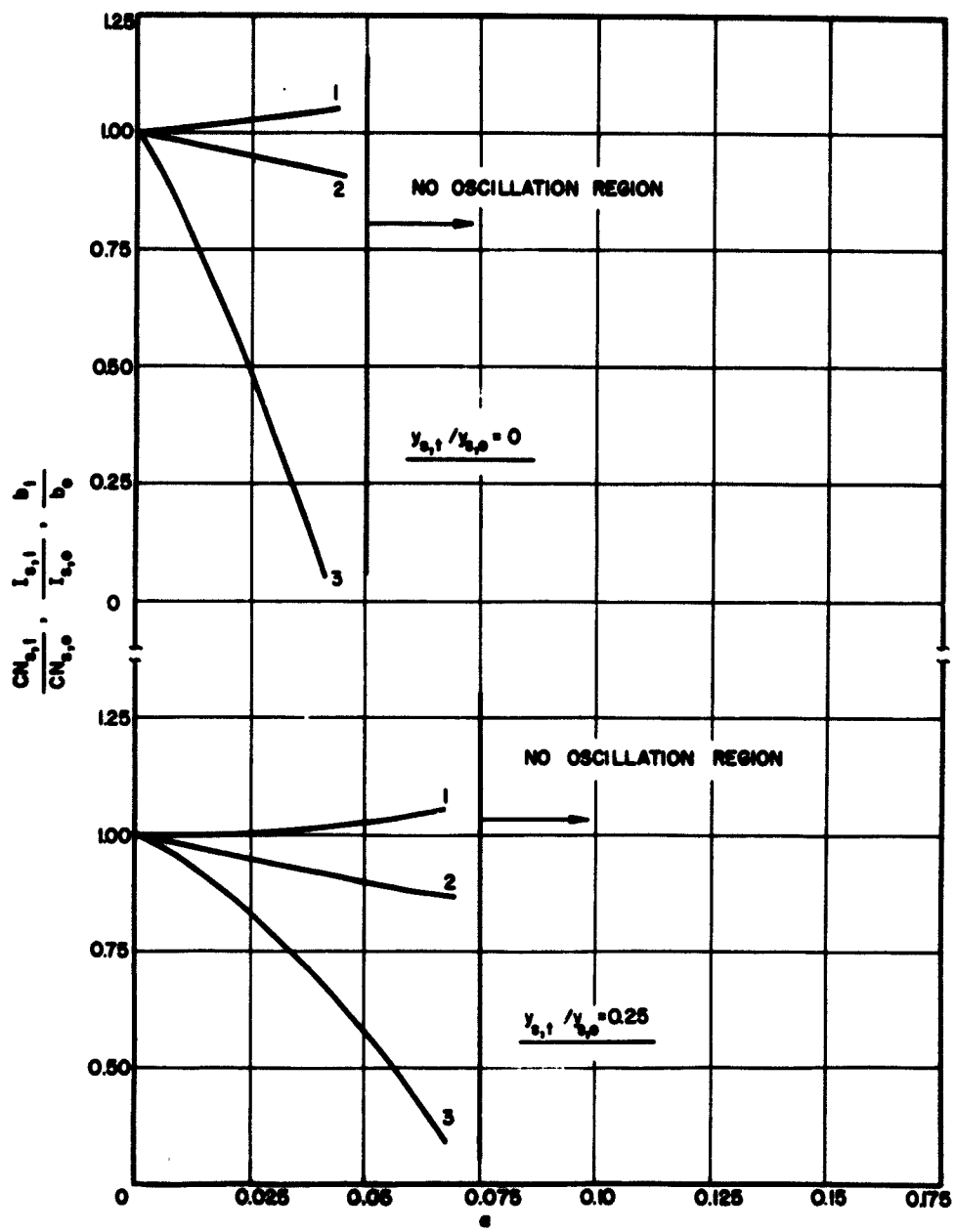

1. $\frac{CN_{s,1}}{CN_{s,o}}$ 2. $\frac{I_{s,1}}{I_{s,o}}$ 3. $\frac{b_1}{b_o}$

FIG. 3.12 $CN_{s,1}/CN_{s,o}$, $I_{s,1}/I_{s,o}$, b_1/b_o VS. α FOR A QUADRATIC CIRCUIT PHASE VELOCITY TAPER. (C = 0.05, QC = 0.2, d = 0)

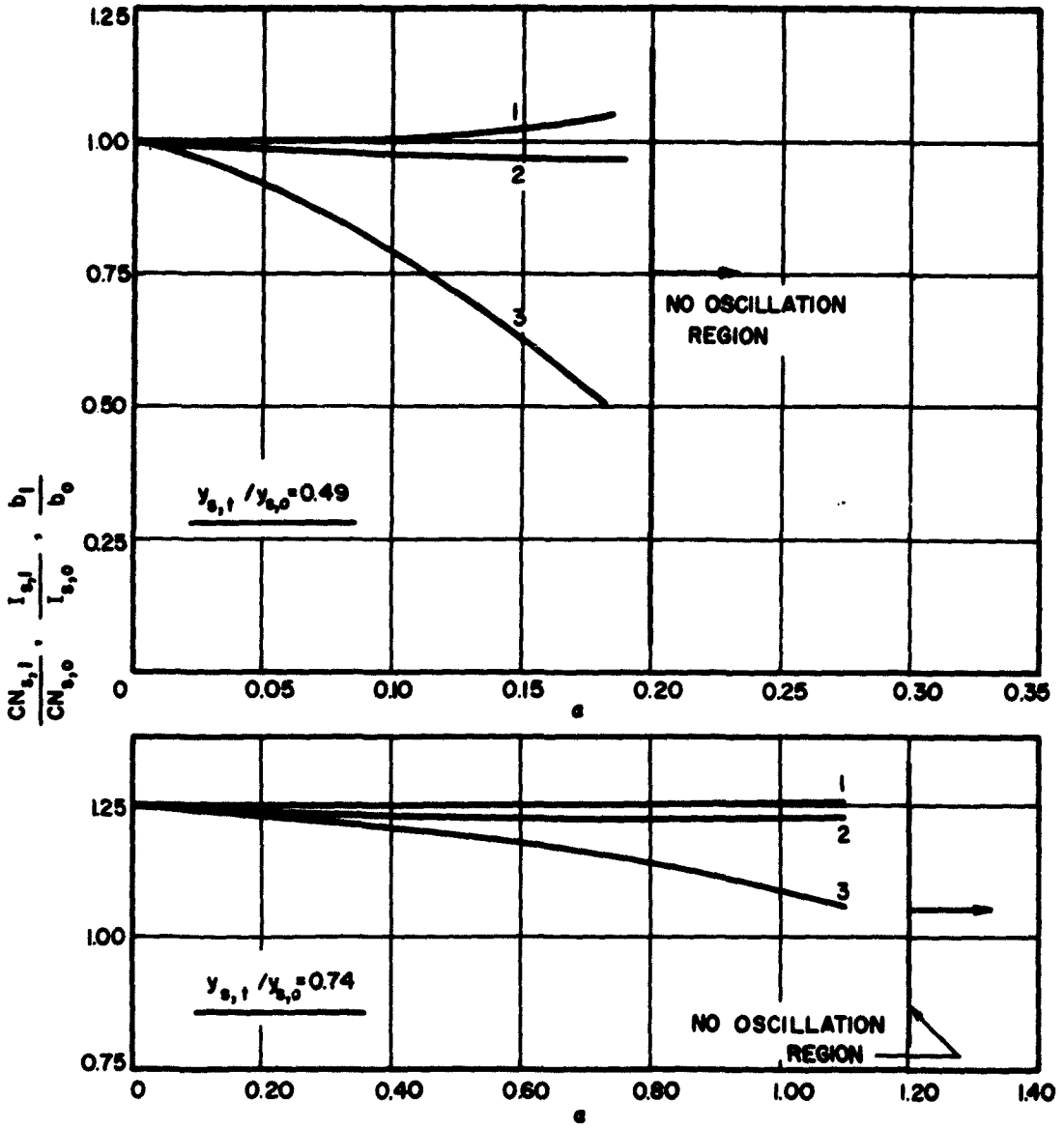

1. $\frac{CN_{s,1}}{CN_{s,0}}$ 2. $\frac{I_{s,1}}{I_{s,0}}$ 3. $\frac{b_1}{b_0}$

FIG. 3.13 $CN_{s,1}/CN_{s,0}$, $I_{s,1}/I_{s,0}$, b_1/b_0 VS. α FOR A QUADRATIC CIRCUIT PHASE VELOCITY TAPER. ($C = 0.05$, $QC = 0.2$, $d = 0$)

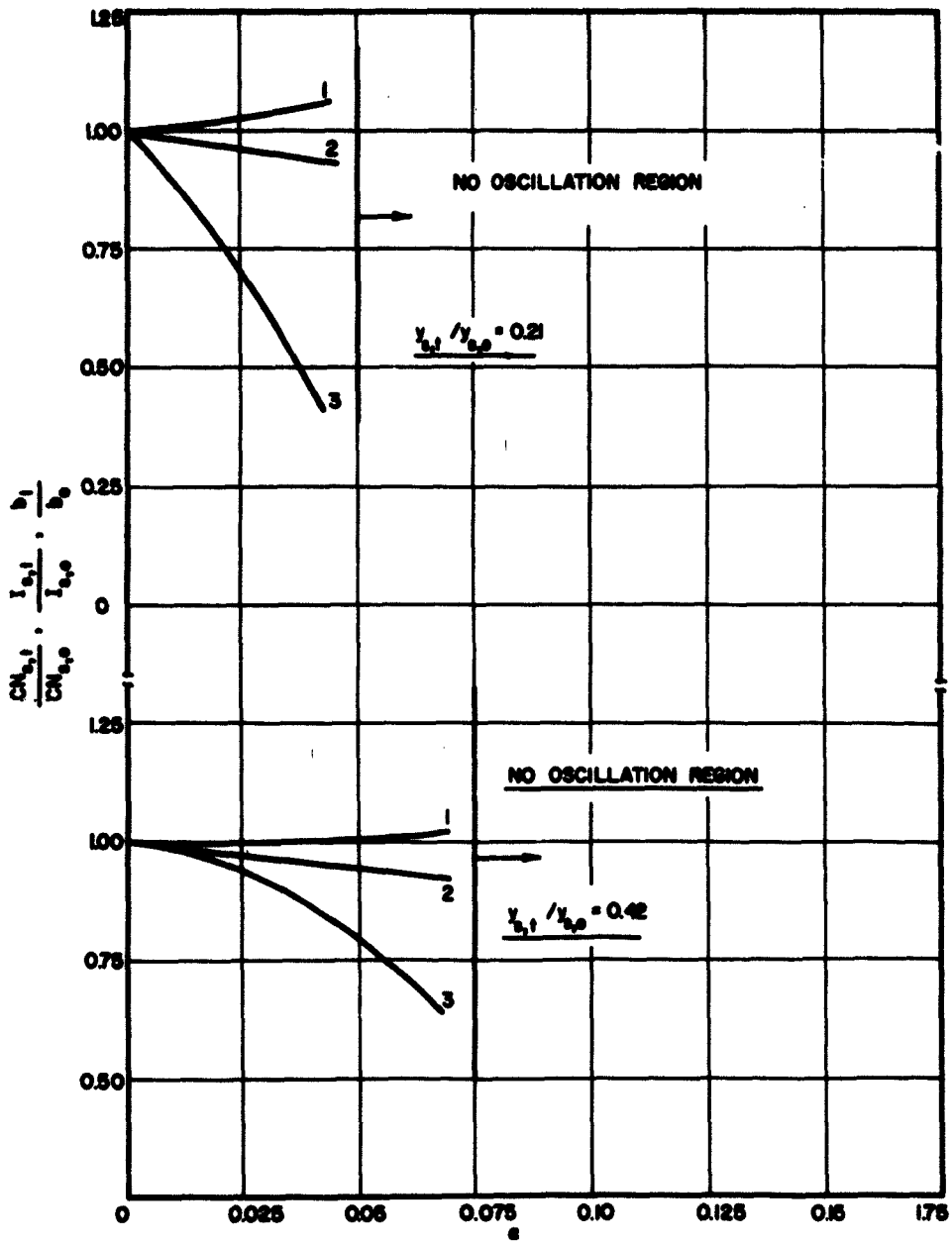

1. $\frac{CN_{s,1}}{CN_{s,0}}$ 2. $\frac{I_{s,1}}{I_{s,0}}$ 3. $\frac{b_1}{b_0}$

FIG. 3.14 $CN_{s,1}/CN_{s,0}$, $I_{s,1}/I_{s,0}$, b_1/b_0 VS. α FOR A QUADRATIC CIRCUIT PHASE VELOCITY TAPER. ($C = 0.05$, $QC = 0.5$, $d = 0$)

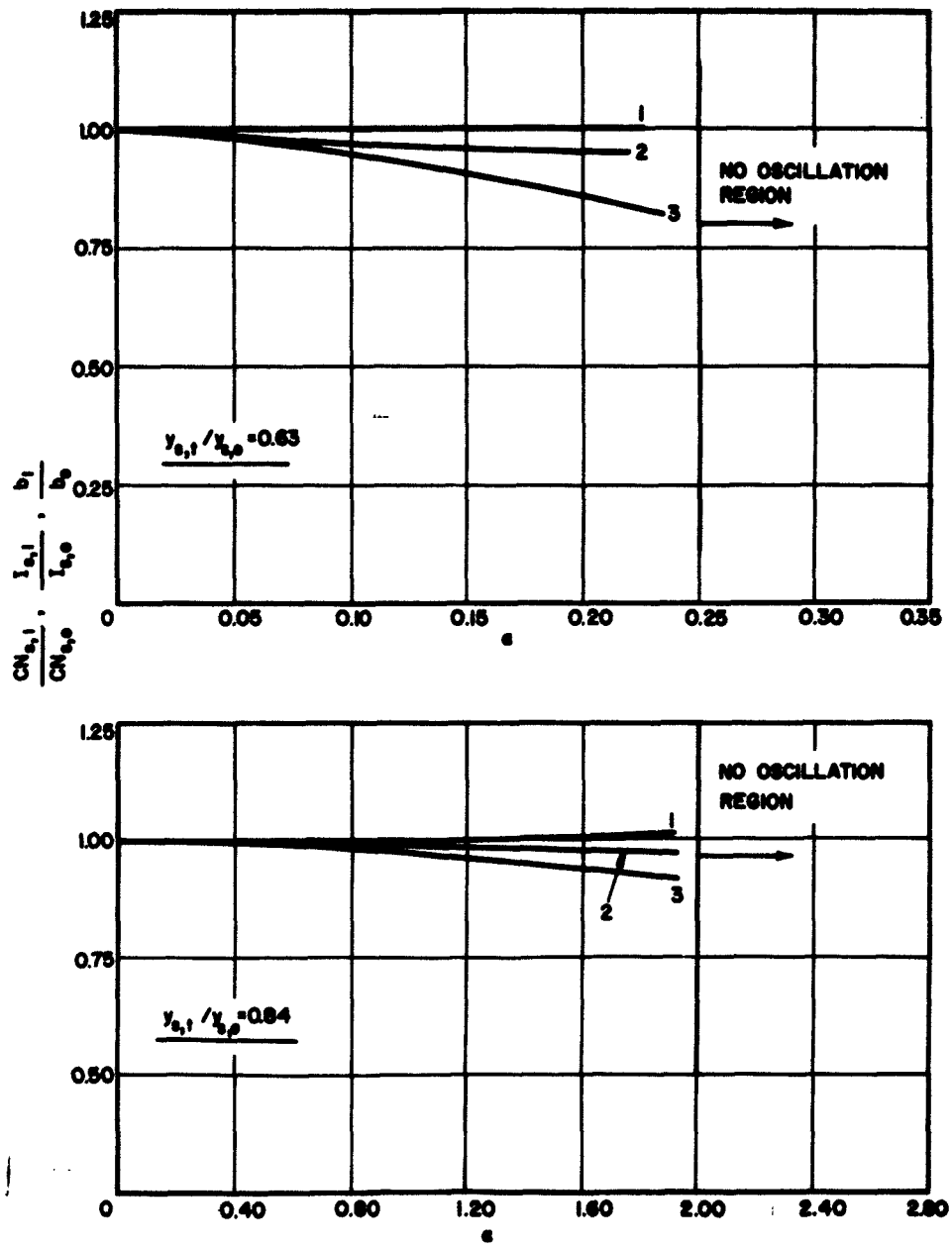

1. $\frac{CN_{s,1}}{CN_{s,o}}$ 2. $\frac{I_{s,1}}{I_{s,o}}$ 3. $\frac{b_1}{b_o}$

FIG. 3.15 $CN_{s,1}/CN_{s,o}$, $I_{s,1}/I_{s,o}$, b_1/b_o VS. α FOR A QUADRATIC CIRCUIT PHASE VELOCITY TAPER. (C = 0.05, QC = 0.5, d = 0)

backward-wave amplifier or oscillator whose phase velocity decreases exponentially with distance along the tube,

$$\frac{d^2V_{cn}(y)}{dy^2} + \left(\frac{1 + C_o b}{C_o}\right)^2 e^{2\alpha y} V_{cn}(y) - \alpha \frac{dV_{cn}(y)}{dy}$$

$$- j2 \frac{d}{C_o} (1 + C_o b)^2 e^{2\alpha y} V_{cn}(y)$$

$$= 4C_o(1 + C_o b) e^{\alpha y} \rho_{1n}(y) - j8C_o^2 d(1 + C_o b) e^{\alpha y} \rho_{1n}(y) \quad , \quad (3.70)$$

$$\frac{du_{1n}(y)}{dy} + \frac{d\rho_{1n}(y)}{dy} + \frac{j}{C_o} \rho_{1n}(y) = 0 \quad , \quad (3.71)$$

$$\frac{1}{2} \frac{dV_{cn}(y)}{dy} + j \frac{4C_o QC}{[1 - 2C_o\sqrt{QC}]^2} \frac{1}{(1 + C_o b)} e^{-\alpha y} \rho_{1n}(y)$$

$$= \frac{j}{C_o} u_{1n}(y) + \frac{du_{1n}(y)}{dy} \quad . \quad (3.72)$$

The solution of these equations on the analog computer is discussed in detail in Appendix B.1. The results are presented in Figs. 3.16 through 3.23.

Here again the start-oscillation conditions of the tapered tube are compared to those of the uniform one as a function of the taper parameter α. The oscillation frequencies and the physical length of the two tubes are assumed to be the same. The taper was also introduced here at different points along the length of the tube. It can be seen from the graphs that for weak tapers the start-oscillation current decreases and when the taper gets stronger than a certain value no oscillation

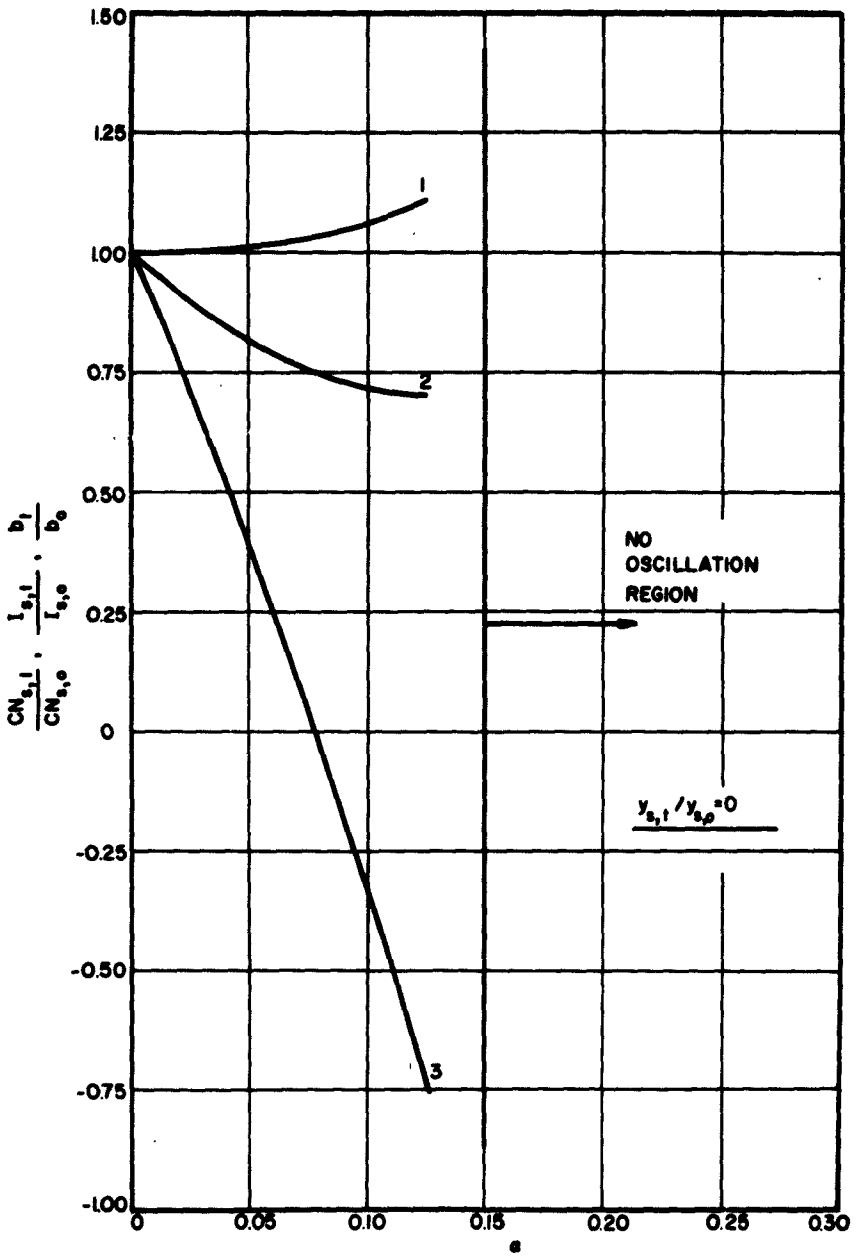

1. $\frac{CN_{s,1}}{CN_{s,o}}$ 2. $\frac{I_{s,1}}{I_{s,o}}$ 3. $\frac{b_1}{b_o}$

FIG. 3.16 $CN_{s,1}/CN_{s,o}$, $I_{s,1}/I_{s,o}$, b_1/b_o VS. α FOR AN EXPONENTIAL CIRCUIT PHASE VELOCITY TAPER. (C = 0.05, QC = 0, d = 0)

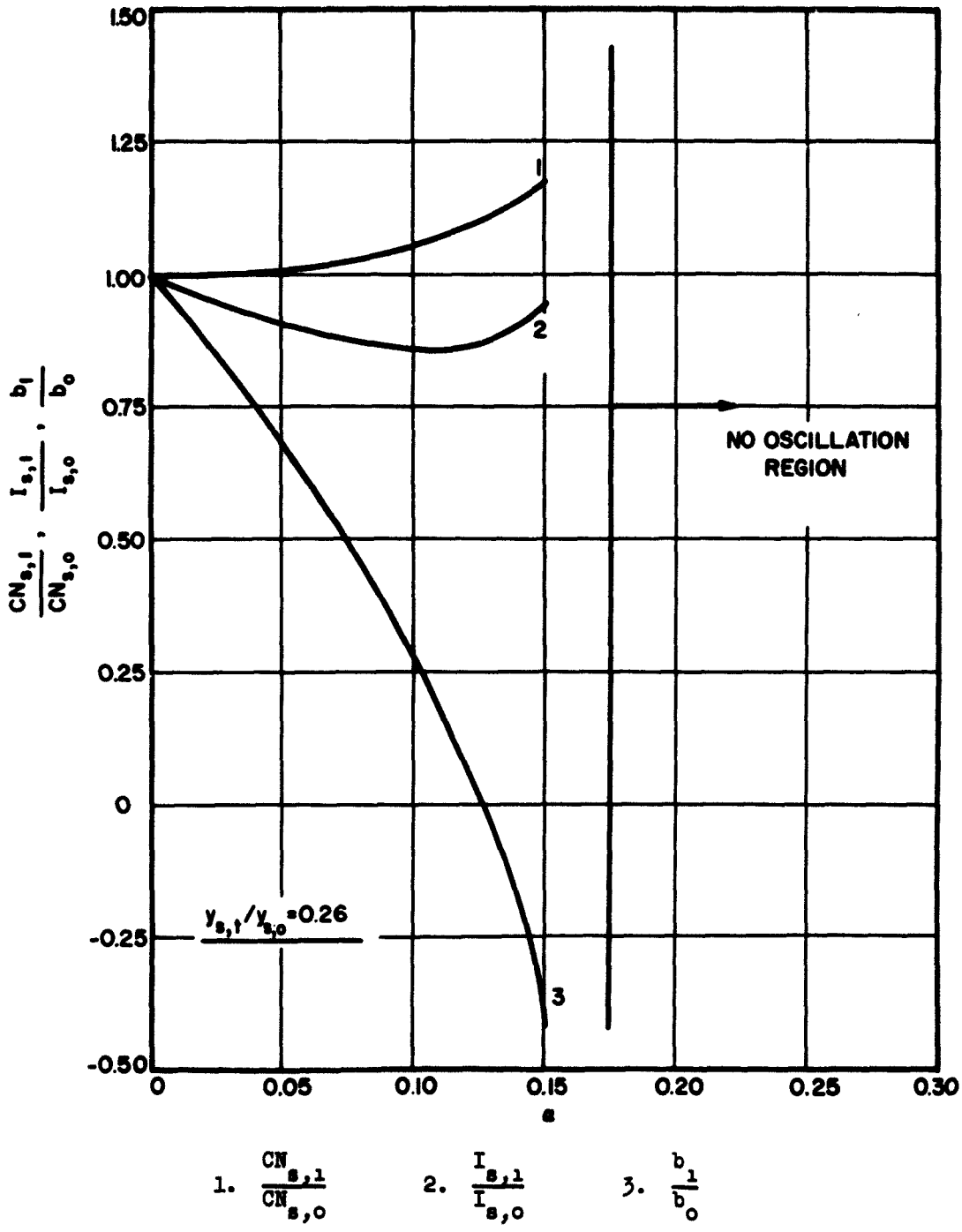

FIG. 3.17 $CN_{s,1}/CN_{s,o}$, $I_{s,1}/I_{s,o}$, b_1/b_o VS. α FOR AN EXPONENTIAL CIRCUIT PHASE VELOCITY TAPER. (C = 0.05, QC = 0, d = 0)

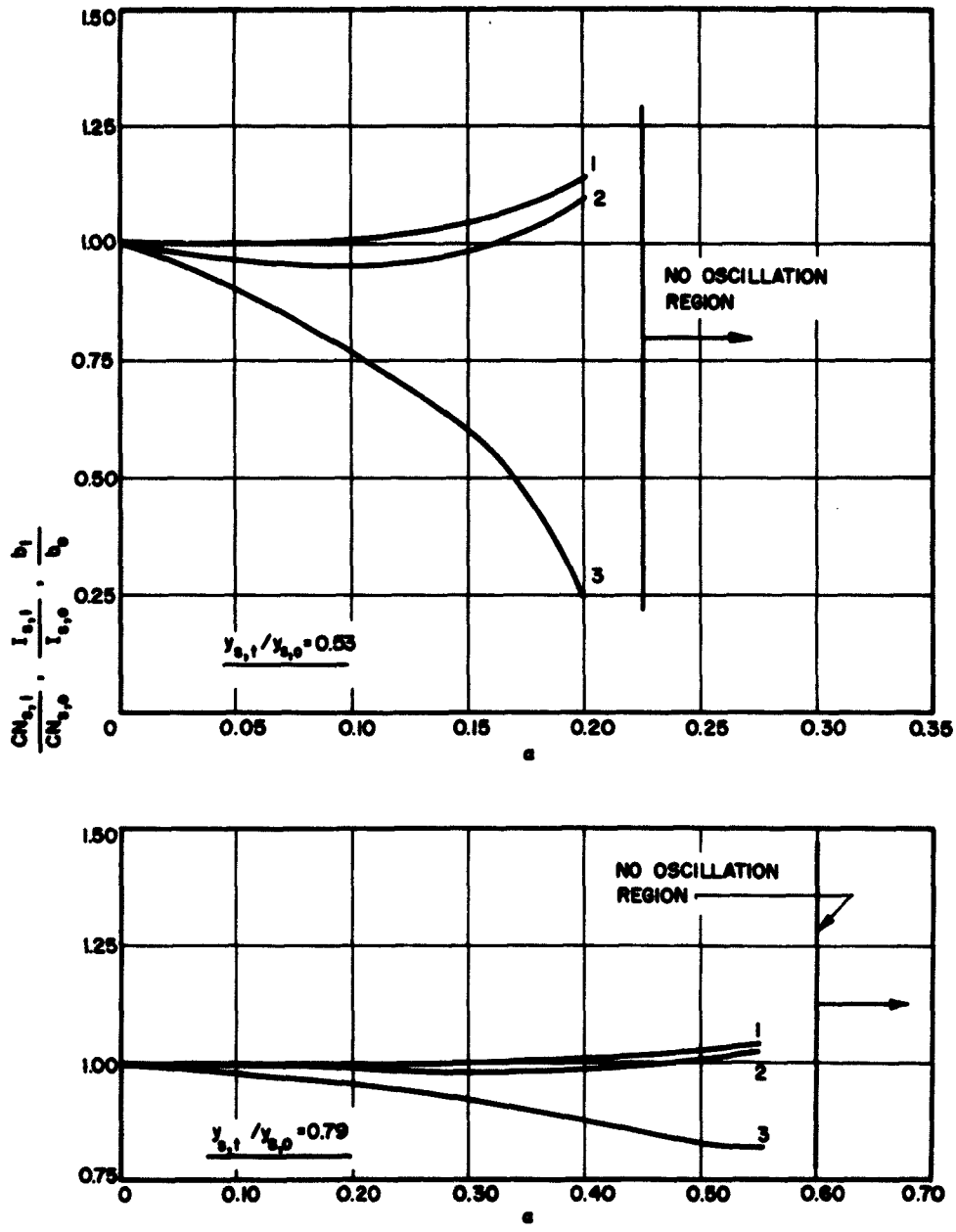

1. $\frac{CN_{s,1}}{CN_{s,0}}$ 2. $\frac{I_{s,1}}{I_{s,0}}$ 3. $\frac{b_1}{b_0}$

FIG. 3.18 $CN_{s,1}/CN_{s,0}$, $I_{s,1}/I_{s,0}$, b_1/b_0 VS. α FOR AN EXPONENTIAL CIRCUIT PHASE VELOCITY TAPER. ($C = 0.05$, $QC = 0$, $d = 0$)

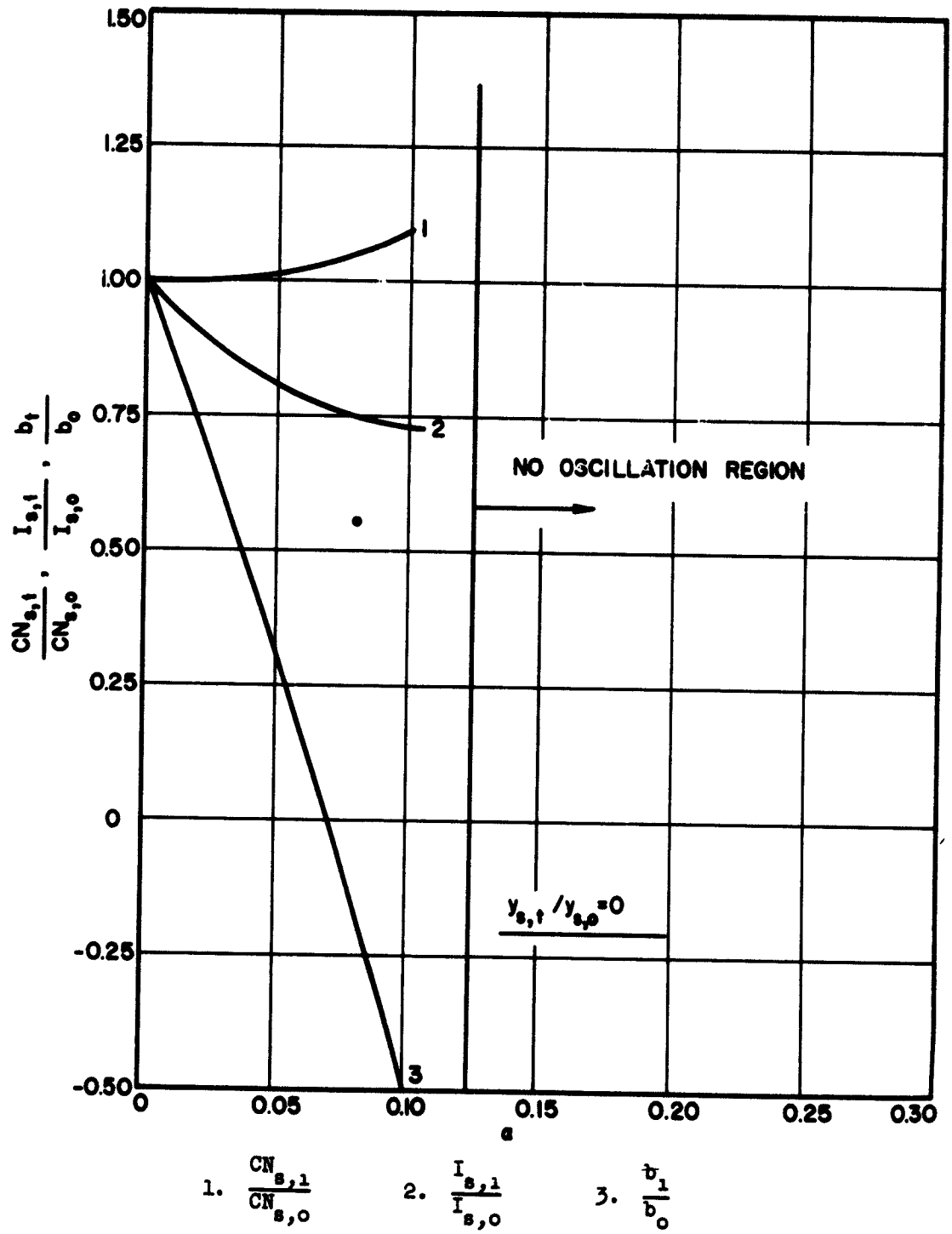

1. $\frac{CN_{s,1}}{CN_{s,o}}$ 2. $\frac{I_{s,1}}{I_{s,o}}$ 3. $\frac{b_1}{b_o}$

FIG. 3.19 $CN_{s,1}/CN_{s,o}$, $I_{s,1}/I_{s,o}$, b_1/b_o VS. α FOR AN EXPONENTIAL CIRCUIT PHASE VELOCITY TAPER. ($C = 0.05$, $QC = 0.2$, $d = 0$)

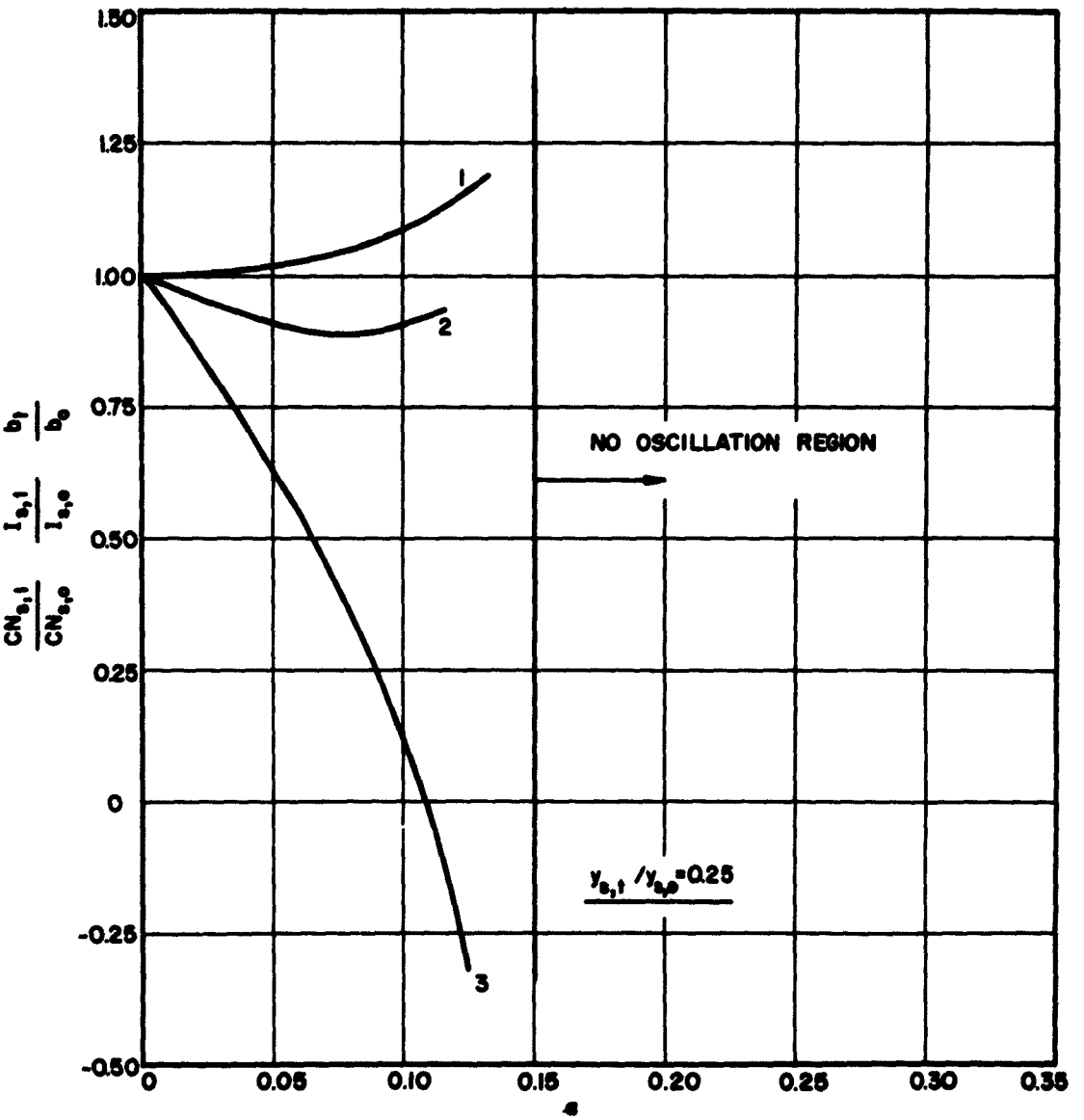

1. $\frac{CN_{s,1}}{CN_{s,o}}$ 2. $\frac{I_{s,1}}{I_{s,o}}$ 3. $\frac{b_1}{b_o}$

FIG. 3.20 $CN_{s,1}/CN_{s,o}$, $I_{s,1}/I_{s,o}$, b_1/b_o VS. α FOR AN EXPONENTIAL CIRCUIT PHASE VELOCITY TAPER. (C = 0.05, QC = 0.2, d = 0)

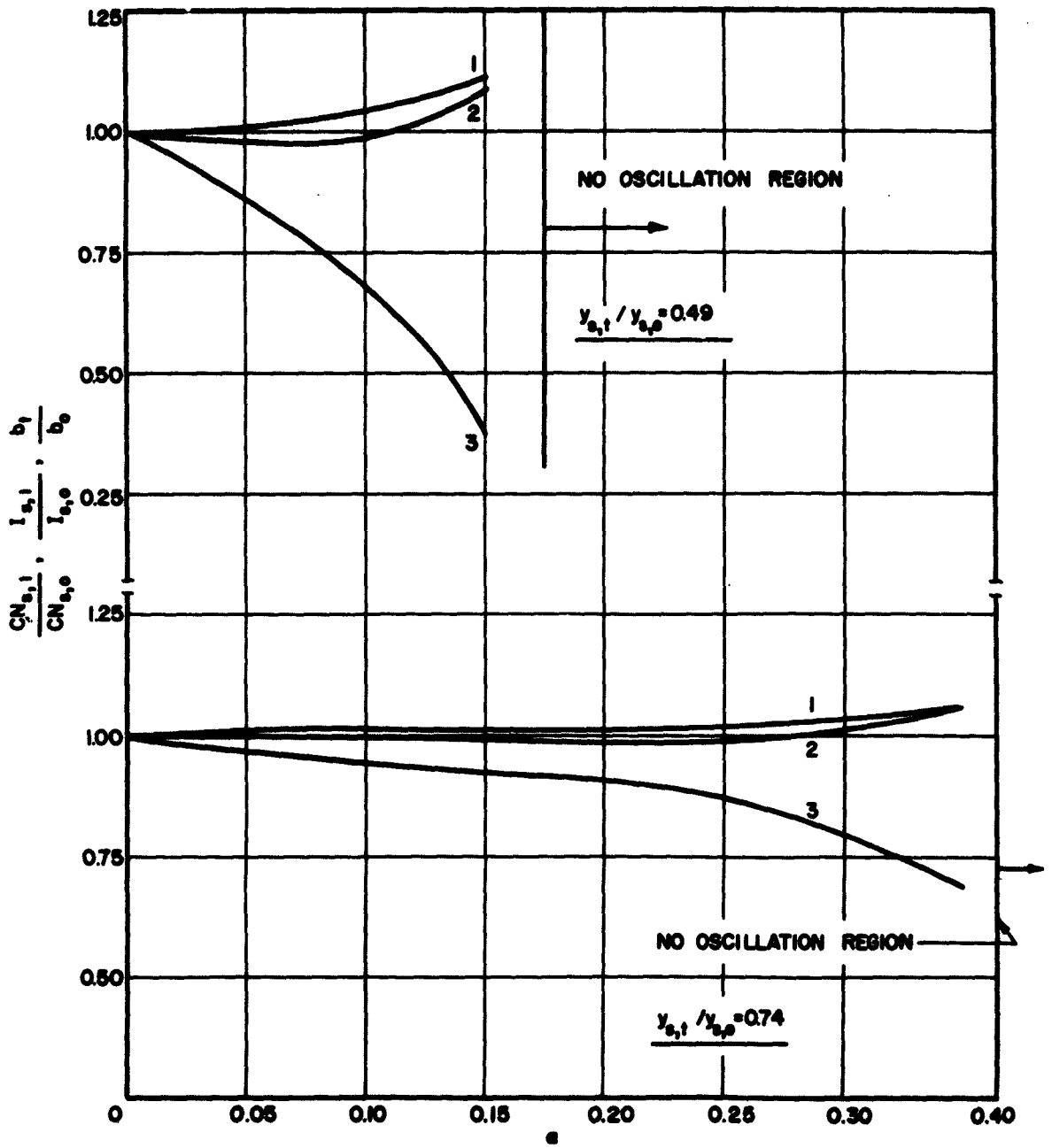

1. $\frac{CN_{s,1}}{CN_{s,0}}$ 2. $\frac{I_{s,1}}{I_{s,0}}$ 3. $\frac{b_1}{b_0}$

FIG. 3.21 $CN_{s,1}/CN_{s,0}$, $I_{s,1}/I_{s,0}$, b_1/b_0 VS. α FOR AN EXPONENTIAL CIRCUIT PHASE VELOCITY TAPER. (C = 0.05, QC = 0.2, d = 0)

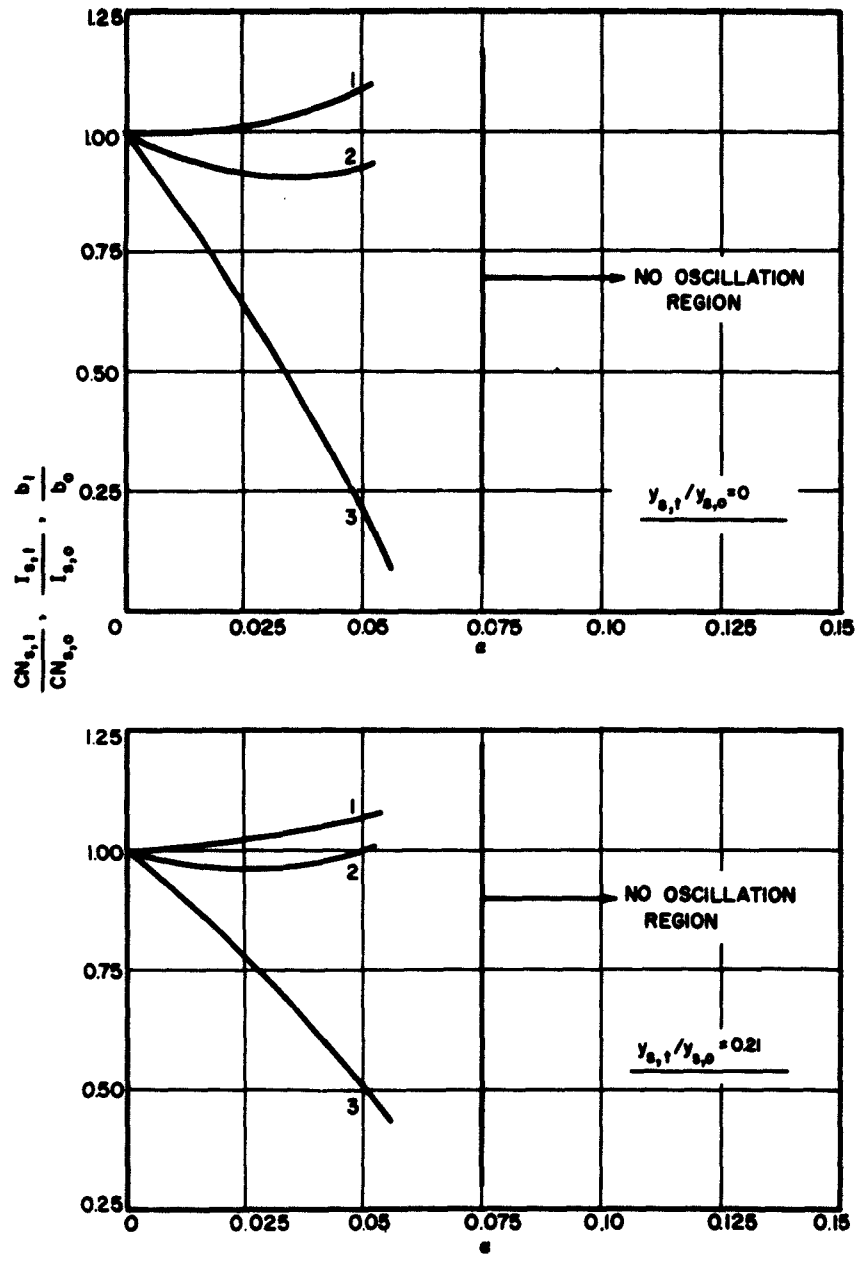

1. $\frac{CN_{s,1}}{CN_{s,o}}$ 2. $\frac{I_{s,1}}{I_{s,o}}$ 3. $\frac{b_1}{b_o}$

FIG. 3.22 $CN_{s,1}/CN_{s,o}$, $I_{s,1}/I_{s,o}$, b_1/b_o VS. α FOR AN EXPONENTIAL CIRCUIT PHASE VELOCITY TAPER. ($C = 0.05$, $QC = 0.5$, $d = 0$)

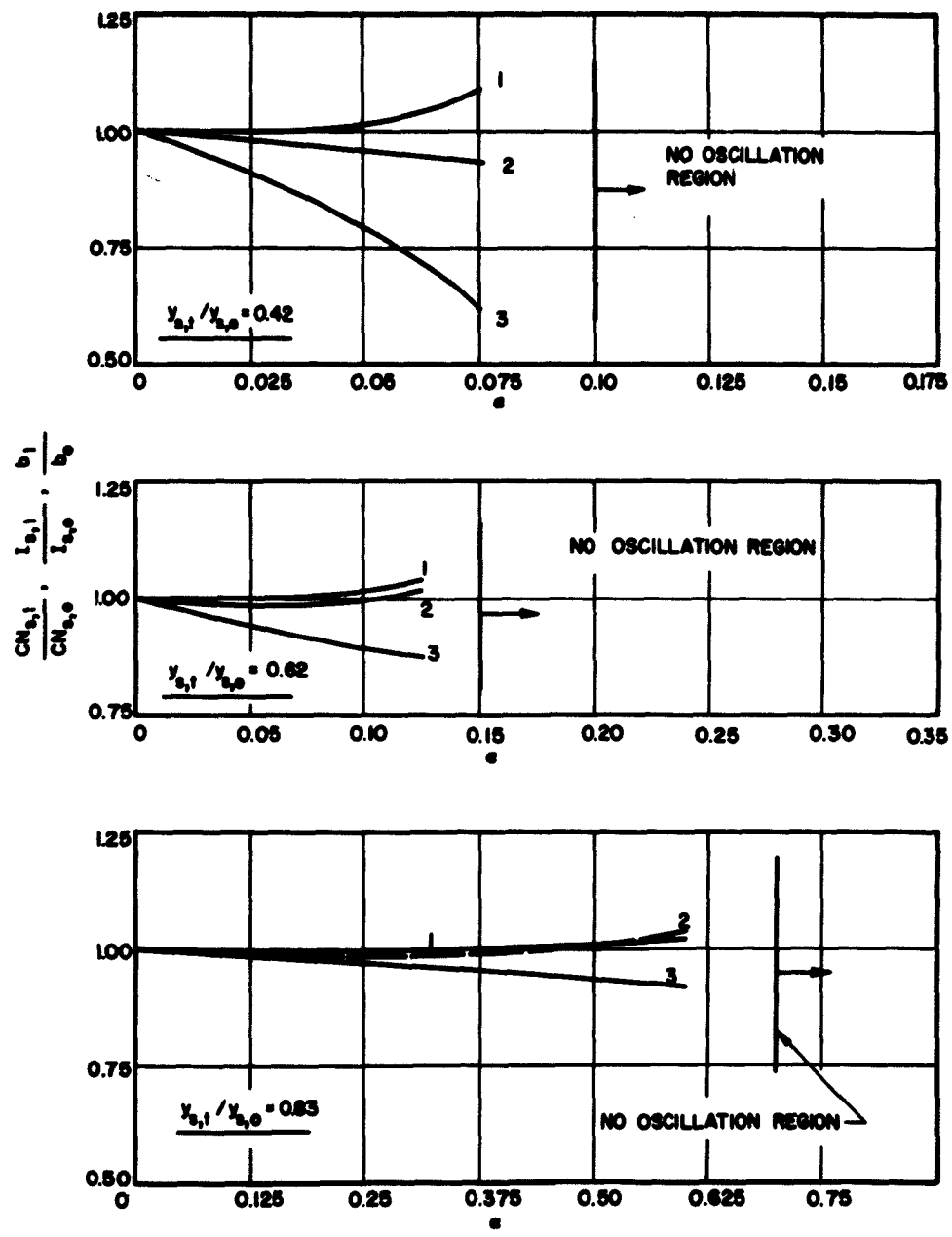

1. $\frac{CN_{s,1}}{CN_{s,o}}$ 2. $\frac{I_{s,1}}{I_{s,o}}$ 3. $\frac{b_1}{b_o}$

FIG. 3.23 $CN_{s,1}/CN_{s,o}$, $I_{s,1}/I_{s,o}$, b_1/b_o VS. α FOR AN EXPONENTIAL CIRCUIT PHASE VELOCITY TAPER. ($C = 0.05$, $QC = 0.5$, $d = 0$)

condition could be found. This region is also designated on the figures as the "no oscillation region".

3.5.4 Summary of the Effect of Circuit Phase Velocity Tapers on the Start-Oscillation Conditions of a Backward-Wave Oscillator. It has been demonstrated that the analog computer results for linear circuit phase velocity tapers are in agreement with the results obtained in Chapter II using a two-wave coupled-mode theory for very weak tapers. In both cases the circuit interaction impedance was assumed to be constant. This is not an unreasonable approximation for tubes in which the beam flows very close to the circuit. The farther the beam is from the circuit the worse the approximation becomes. As the phase velocity decreases the fields fall off more rapidly away from the circuit thus reducing the interaction impedance which tends to increase the start-oscillation current. For the kinds of tapers encountered here and for a hollow-beam helix backward-wave oscillator in which the beam is made to flow very close to the helix the above approximation is valid.

With the above in mind the following statements can be made about the effect of velocity tapers on the start-oscillation conditions.

1. For a tapered tube whose length and oscillation frequency are the same as that of a uniform one, the beam voltage in the tapered tube will be slightly lower.

2. The kind of velocity taper is not critical, but the strength of taper is very critical. For a particular value of C_o, there exists a certain strength of taper beyond which no oscillation conditions could be found. It is believed that the higher C_o is, the stronger the taper can be made before the "no oscillation" region sets in.

3. The higher C_o is at start oscillation the more the start-oscillation current is decreased by tapering. For low values of C_o it was shown in Chapter II that the start-oscillation current will increase in a tapered tube.

4. Since for strong tapers "no oscillation" conditions are possible, strong tapers can be utilized in forward-wave amplifiers to enhance efficiency[14] and at the same time suppress backward-wave oscillations.

3.5.5 Linear Voltage Gradient. Here the circuit phase velocity is assumed to be constant along the length of the tube and that the beam potential varies as,

$$V_o = V_{oo}(1 + \alpha y) \quad . \tag{3.73}$$

$\xi(y)$ and $\zeta(y)$ in Eqs. 3.42 through 3.44 then assume the following form,

$$\xi(y) = 1 \quad , \tag{3.74}$$

$$\zeta(y) = (1 + \alpha y) \quad . \tag{3.75}$$

Substituting the above values of $\xi(y)$ and $\zeta(y)$ in Eqs. 3.42 through 3.44 results in the following set of equations which characterize a backward-wave oscillator whose phase velocity is constant and whose beam potential increases linearly with distance along the tube.

$$\frac{d^2V_{cn}(y)}{dy^2} + \left(\frac{1 + C_o b}{C_o}\right)^2 V_{cn}(y) - j2\frac{d}{C_o}(1 + C_o b)^2 V_{cn}(y)$$

$$= \left[4C_o(1 + C_o b) - j8C_o^2 d(1 + C_o b)\right] \rho_{1n}(y) \quad , \tag{3.76}$$

$$\frac{1}{[1-\alpha y]^{1/2}} \frac{du_{1n}(y)}{dy} - \frac{\alpha}{2(1+\alpha y)} u_{1n}(y) + (1+\alpha y)^{1/2} \frac{d\rho_{1n}(y)}{dy}$$

$$+ \left[\frac{\alpha}{2(1+\alpha y)^{1/2}} + \frac{j}{C_o} \right] \rho_{1n}(y) = 0 \quad , \quad (3.77)$$

$$\frac{1}{2} \frac{dV_{cn}(y)}{dy} + j \frac{4C_o QC}{[1-2C_o\sqrt{QC}]^2} \frac{1}{(1+C_o b)} \rho_{1n}(y)$$

$$= \left[\frac{j}{C_o} + \frac{\alpha}{2(1+\alpha y)^{1/2}} \right] u_{1n}(y) + (1+\alpha y)^{1/2} \frac{du_{1n}(y)}{dy} \quad . \quad (3.78)$$

The solution of the above equations is discussed in detail in Appendix B.2. The results are presented here in Figs. 3.24 through 3.34.

It is seen that these curves are quite similar to those of the circuit phase velocity tapered ones. In certain cases when the voltage gradient is weak the start-oscillation current decreases and there exists a certain strength of gradient beyond which no oscillation condition could be found. This is also designated on the figures as the "no oscillation" region.

3.5.6 Quadratic Voltage Gradient. Here the circuit phase velocity is assumed constant and the beam potential varies as,

$$V_o = V_{oo}(1+\alpha y^2) \quad . \quad (3.79)$$

$\xi(y)$ and $\zeta(y)$ in Eqs. 3.42 through 3.44 then assume the following form,

$$\xi(y) = 1 \quad , \quad (3.80)$$

$$\zeta(y) = (1+\alpha y^2) \quad . \quad (3.81)$$

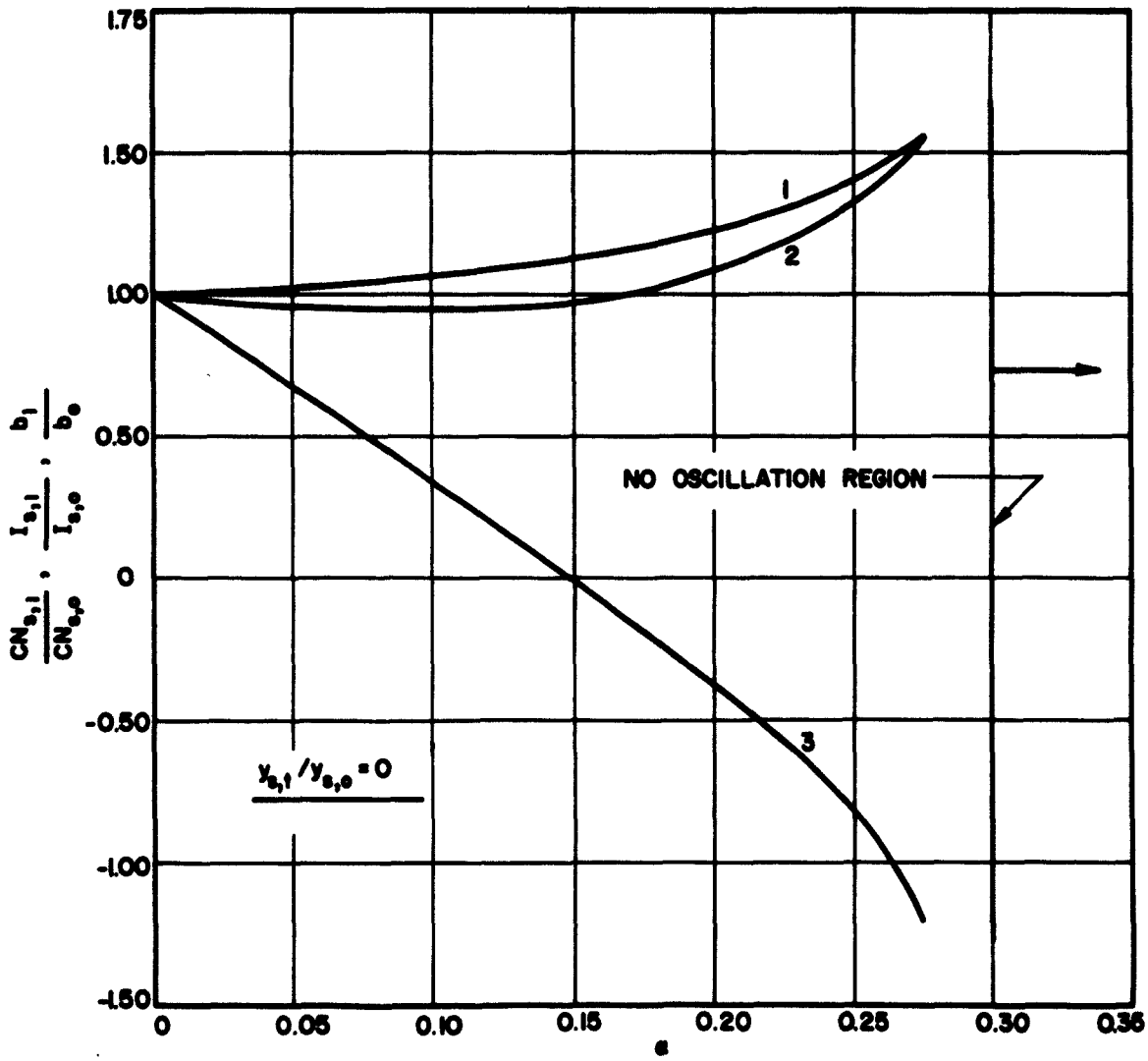

1. $\frac{CN_{s,1}}{CN_{s,o}}$ 2. $\frac{I_{s,1}}{I_{s,o}}$ 3. $\frac{b_1}{b_o}$

FIG. 3.24 $CN_{s,1}/CN_{s,o}$, $I_{s,1}/I_{s,o}$, b_1/b_o VS. α FOR A LINEAR BEAM VOLTAGE VARIATION. ($C = 0.05$, $QC = 0$, $d = 0$)

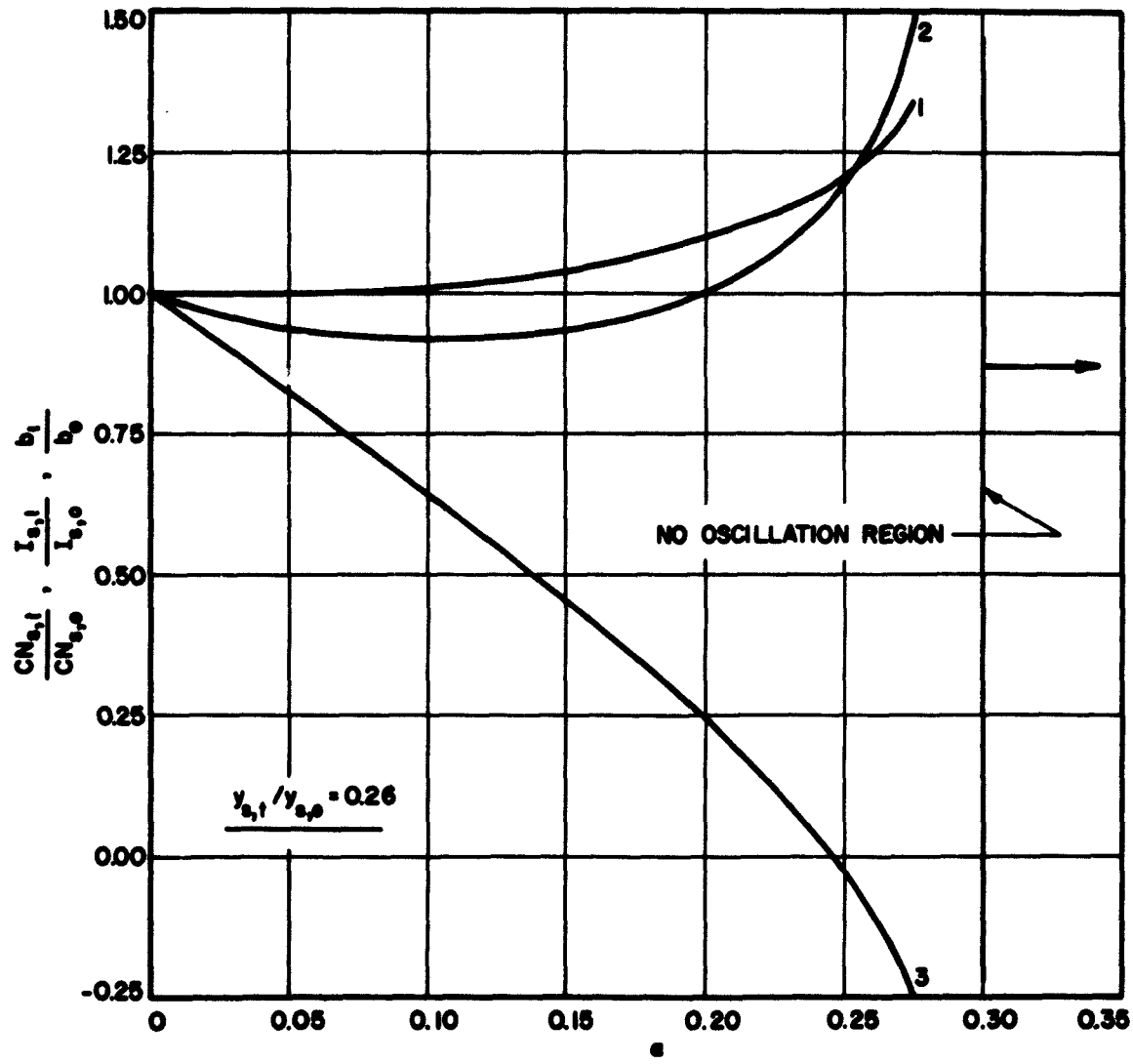

1. $\frac{CN_{s,1}}{CN_{s,o}}$ 2. $\frac{I_{s,1}}{I_{s,o}}$ 3. $\frac{b_1}{b_o}$

FIG. 3.25 $CN_{s,1}/CN_{s,o}$, $I_{s,1}/I_{s,o}$, b_1/b_o VS. α FOR A LINEAR BEAM VOLTAGE VARIATION. ($C = 0.05$, $QC = 0$, $d = 0$)

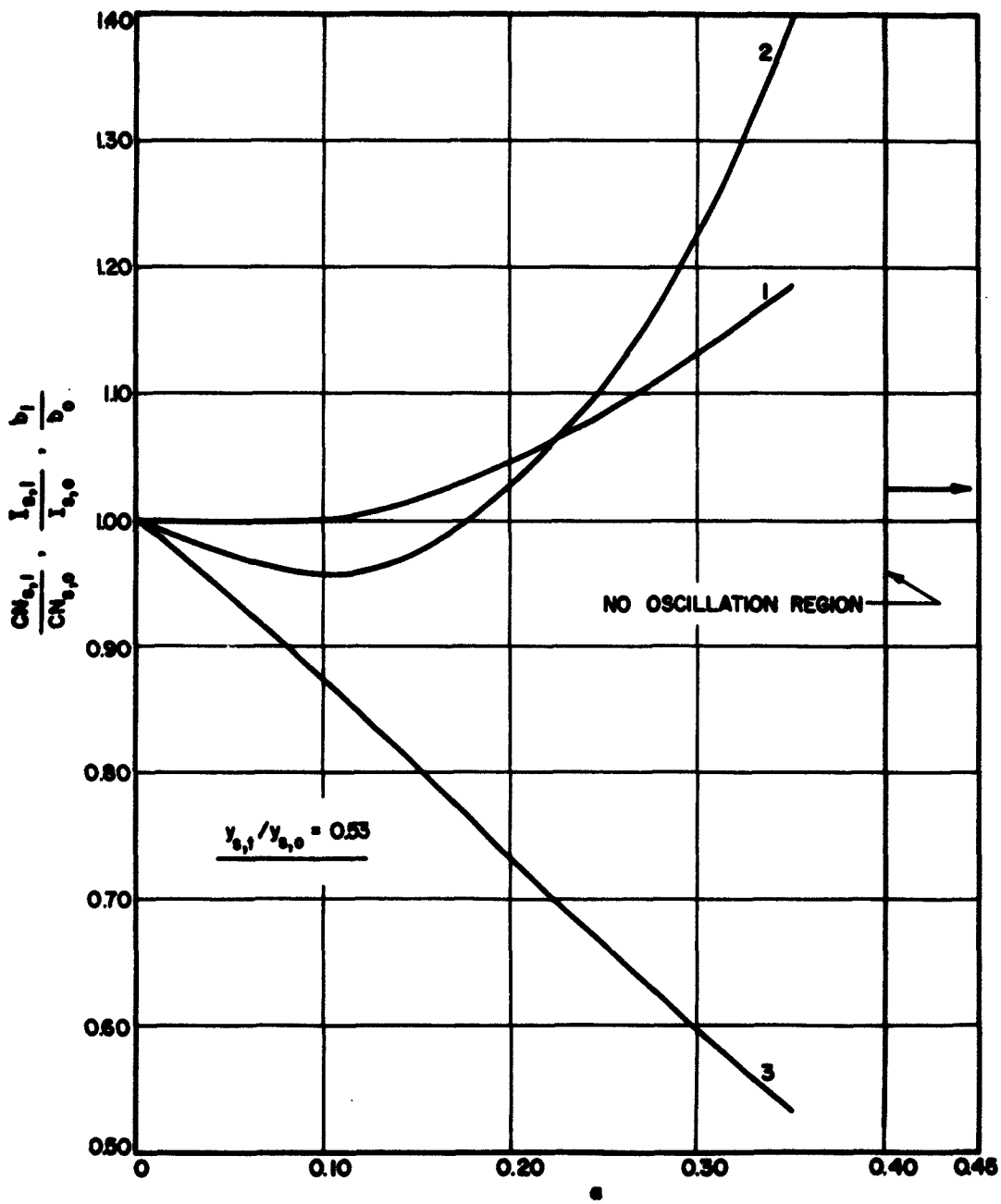

FIG. 3.26 $CN_{s,1}/CN_{s,0}$, $I_{s,1}/I_{s,0}$, b_1/b_0 VS. α FOR A LINEAR BEAM VOLTAGE VARIATION. ($C = 0.05$, $QC = 0$, $d = 0$)

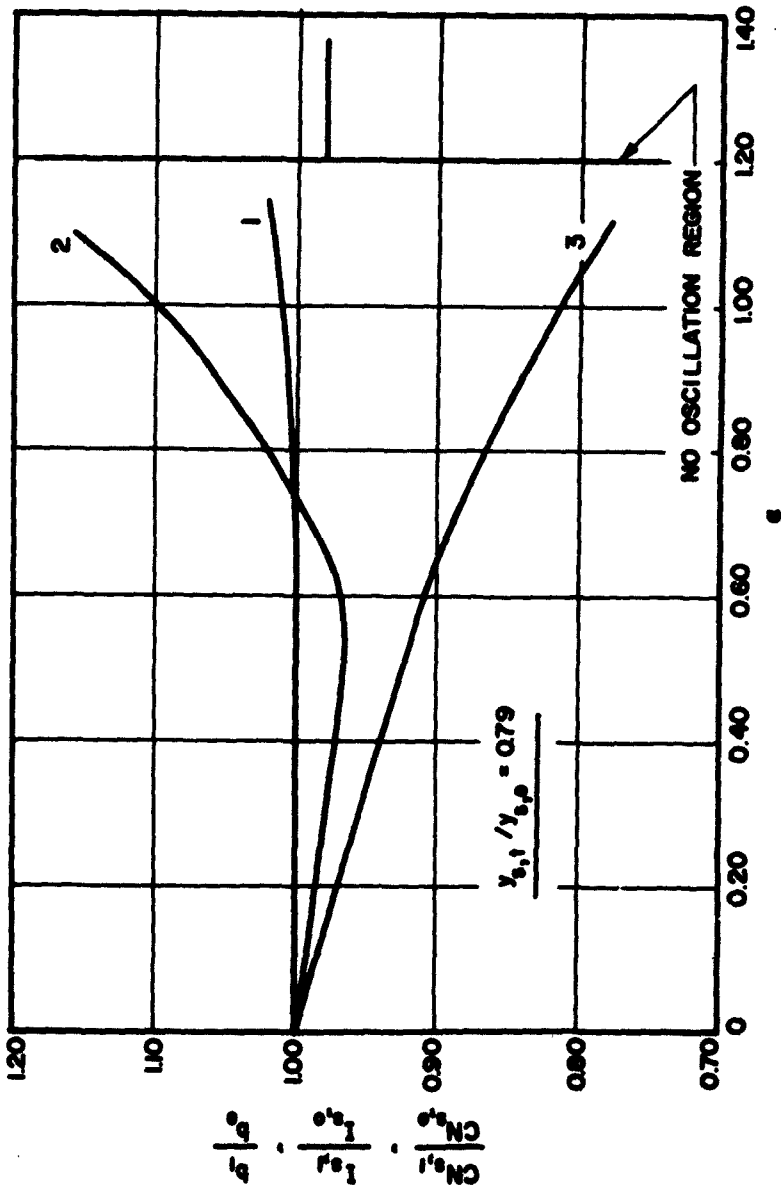

1. $\frac{CN_{s,1}}{CN_{s,o}}$ 2. $\frac{I_{s,1}}{I_{s,o}}$ 3. $\frac{b_1}{b_o}$

FIG. 3.27 $CN_{s,1}/CN_{s,o}$, $I_{s,1}/I_{s,o}$, b_1/b_o VS. α FOR A LINEAR BEAM VOLTAGE VARIATION. ($C = 0.05$, $QC = 0$, $d = 0$)

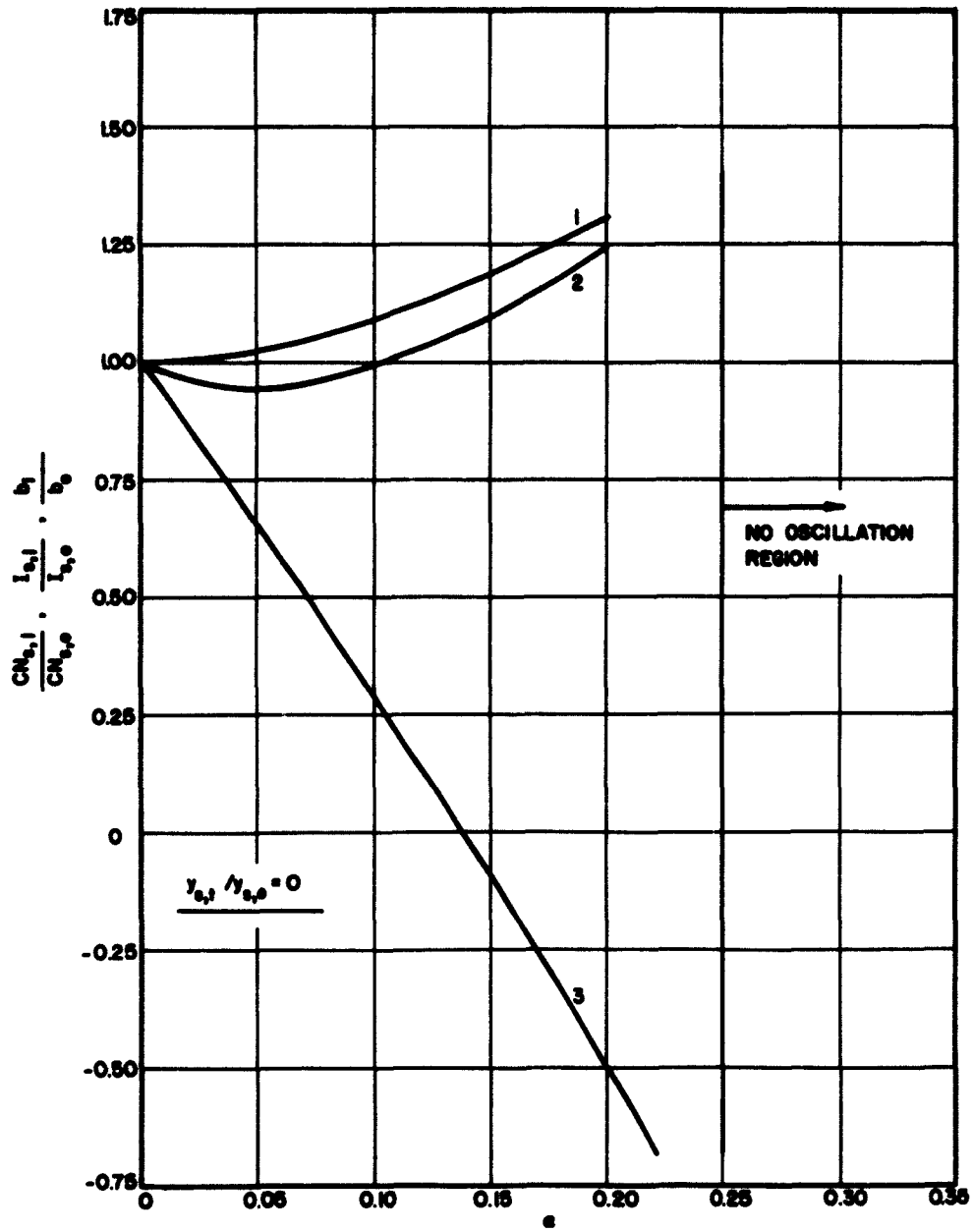

1. $\frac{CN_{s,1}}{CN_{s,0}}$ 2. $\frac{I_{s,1}}{I_{s,0}}$ 3. $\frac{b_1}{b_0}$

FIG. 3.28 $CN_{s,1}/CN_{s,0}$, $I_{s,1}/I_{s,0}$, b_1/b_0 VS. α FOR A LINEAR BEAM VOLTAGE VARIATION. ($C = 0.05$, $QC = 0.2$, $d = 0$)

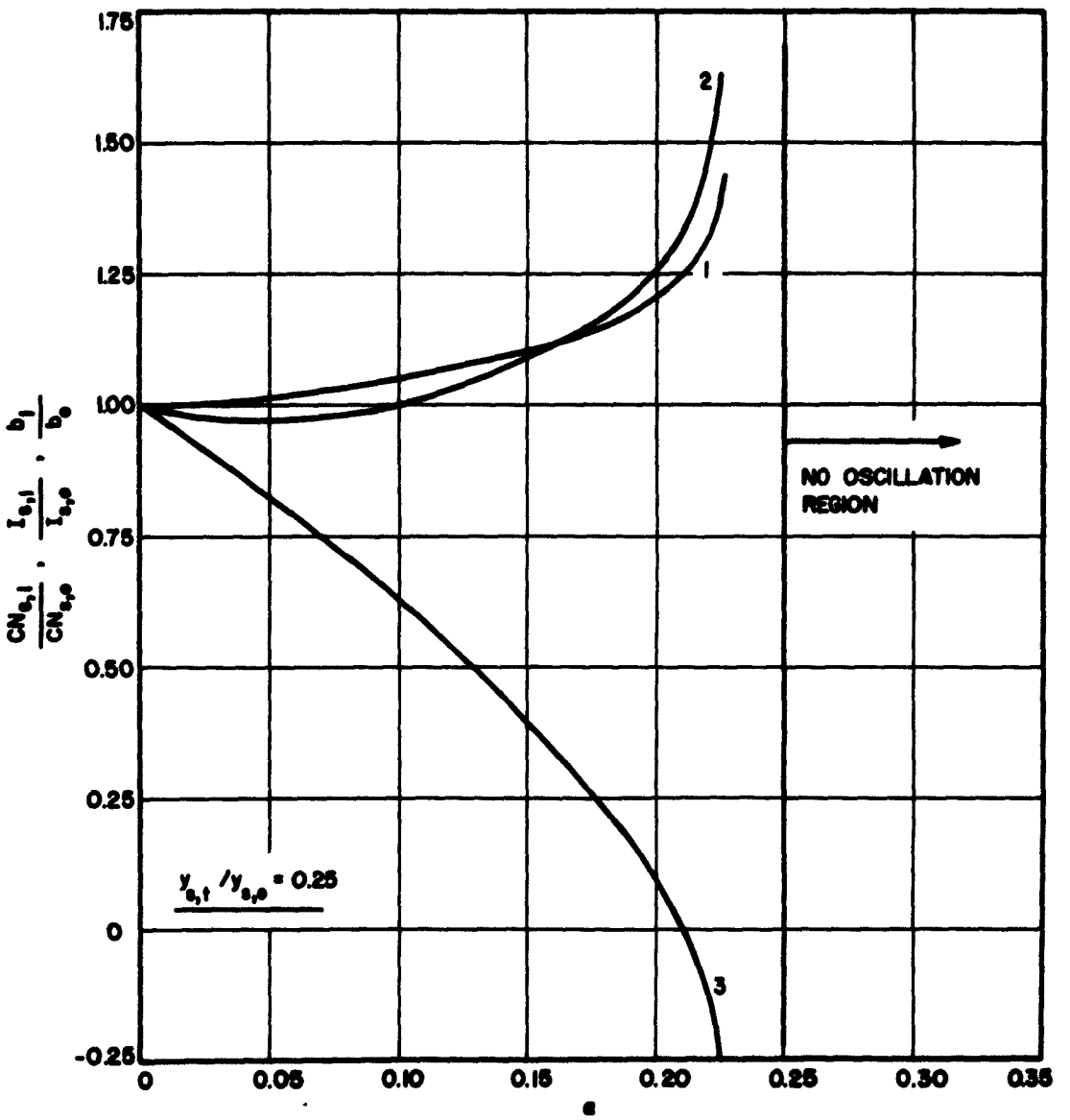

1. $\frac{CN_{s,1}}{CN_{s,o}}$ 2. $\frac{I_{s,1}}{I_{s,o}}$ 3. $\frac{b_1}{b_o}$

FIG. 3.29 $CN_{s,1}/CN_{s,o}$, $I_{s,1}/I_{s,o}$, b_1/b_o VS. α FOR A LINEAR BEAM VOLTAGE VARIATION. (C = 0.05, QC = 0.2, d = 0)

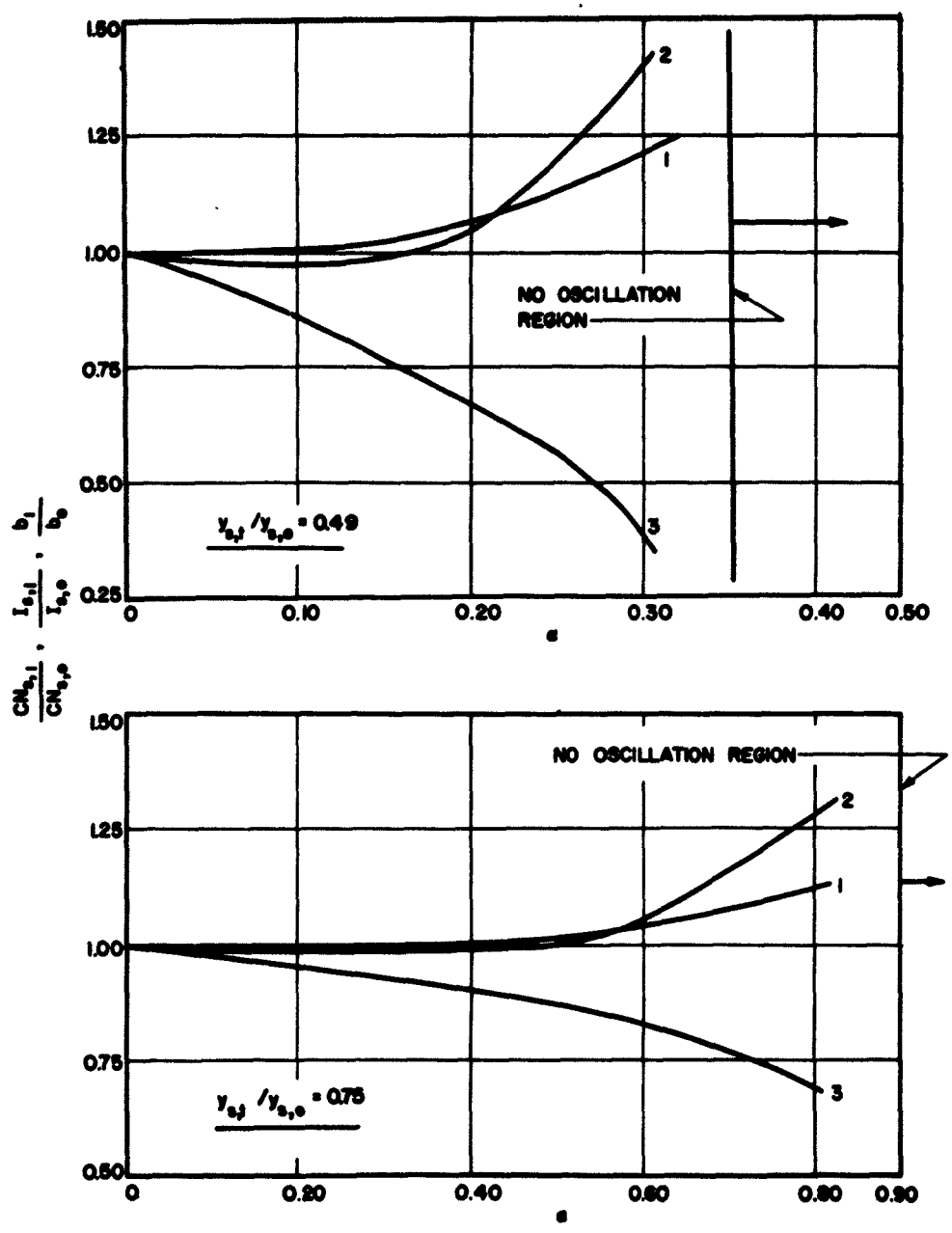

1. $\frac{CN_{s,1}}{CN_{s,0}}$ 2. $\frac{I_{s,1}}{I_{s,0}}$ 3. $\frac{b_1}{b_0}$

FIG. 3.30 $CN_{s,1}/CN_{s,0}$, $I_{s,1}/I_{s,0}$, b_1/b_0 VS. α FOR A LINEAR BEAM VOLTAGE VARIATION. ($C = 0.05$, $QC = 0.2$, $d = 0$)

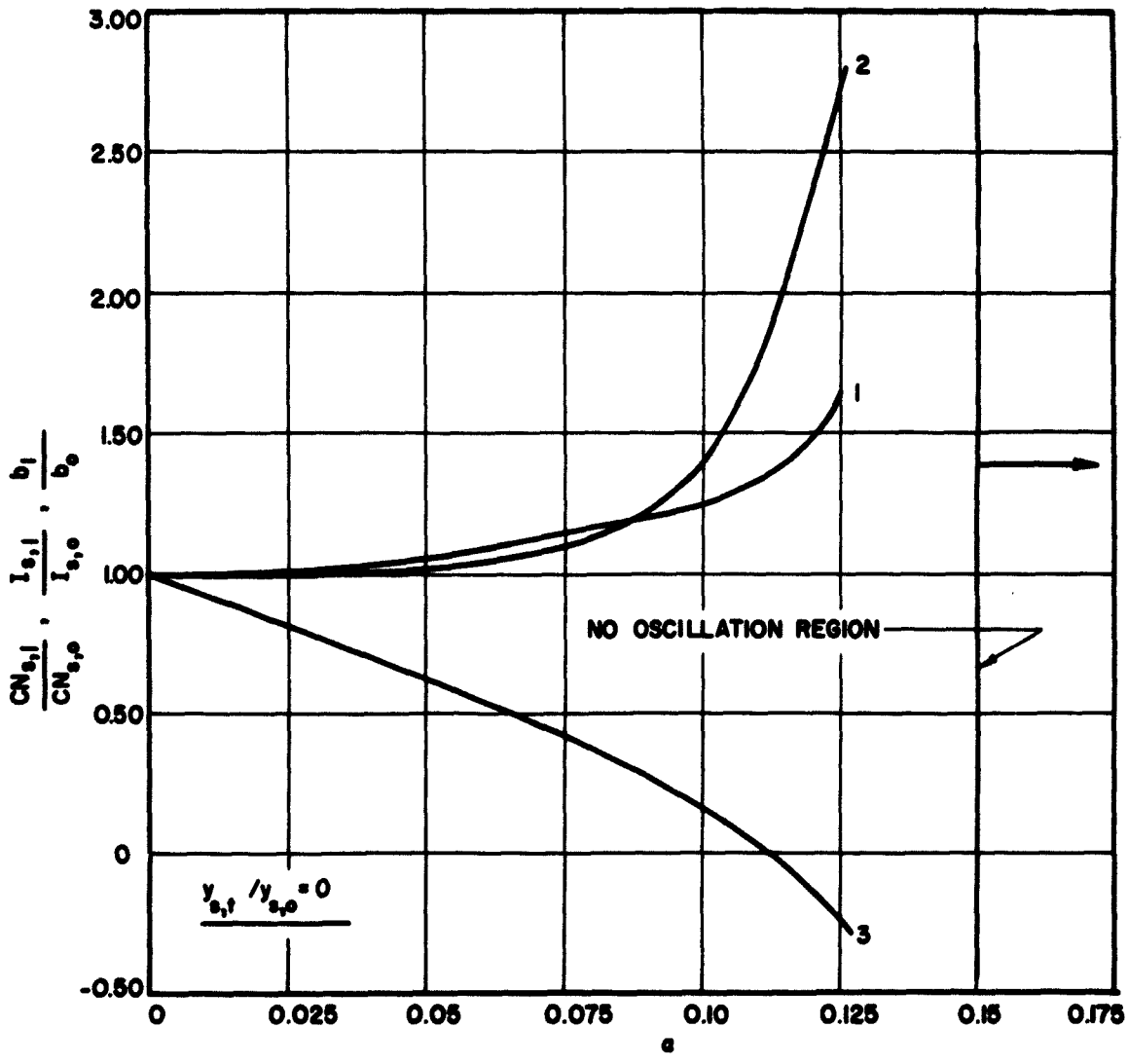

1. $\frac{CN_{s,1}}{CN_{s,o}}$ 2. $\frac{I_{s,1}}{I_{s,o}}$ 3. $\frac{b_1}{b_o}$

FIG. 3.31 $CN_{s,1}/CN_{s,o}$, $I_{s,1}/I_{s,o}$, b_1/b_o VS. α FOR A LINEAR BEAM VOLTAGE VARIATION. ($C = 0.05$, $QC = 0.5$, $d = 0$)

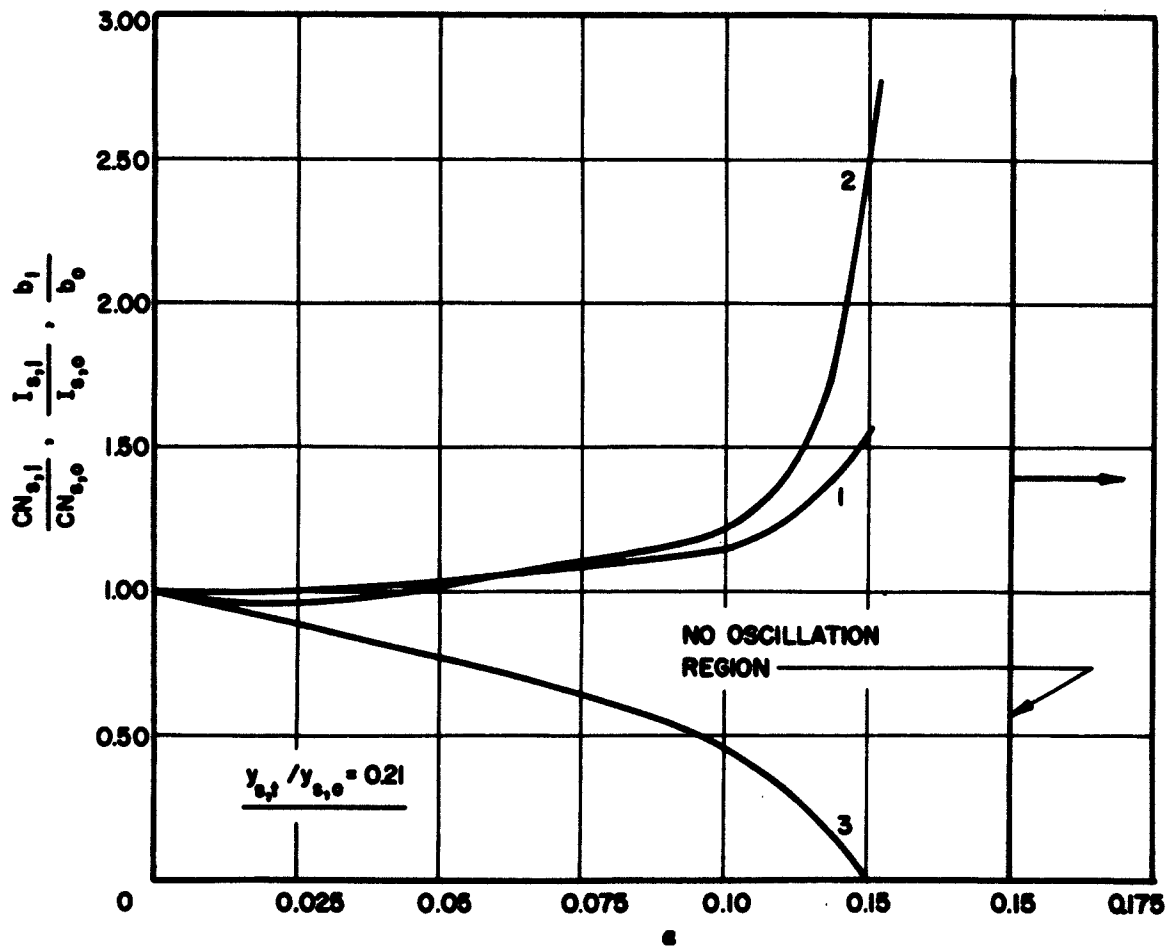

1. $\frac{CN_{s,1}}{CN_{s,o}}$ 2. $\frac{I_{s,1}}{I_{s,o}}$ 3. $\frac{b_1}{b_o}$

FIG. 3.32 $CN_{s,1}/CN_{s,o}$, $I_{s,1}/I_{s,o}$, b_1/b_o VS. α FOR A LINEAR BEAM VOLTAGE VARIATION. ($C = 0.05$, $QC = 0.5$, $d = 0$)

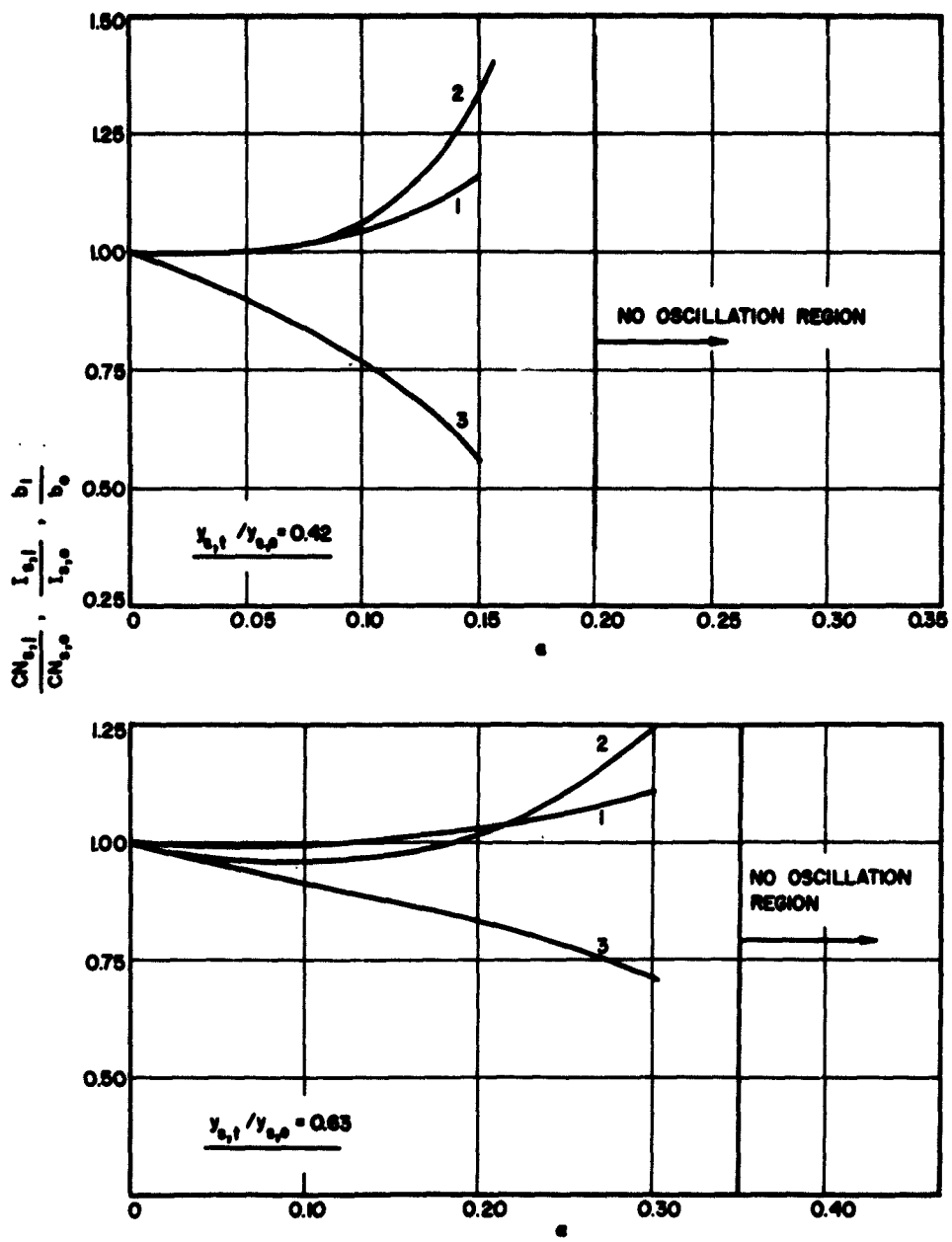

1. $\frac{CN_{s,1}}{CN_{s,o}}$ 2. $\frac{I_{s,1}}{I_{s,o}}$ 3. $\frac{b_1}{b_o}$

FIG. 3.33 $CN_{s,1}/CN_{s,o}$, $I_{s,1}/I_{s,o}$, b_1/b_o VS. α FOR A LINEAR BEAM VOLTAGE VARIATION. (C = 0.05, QC = 0.5, d = 0)

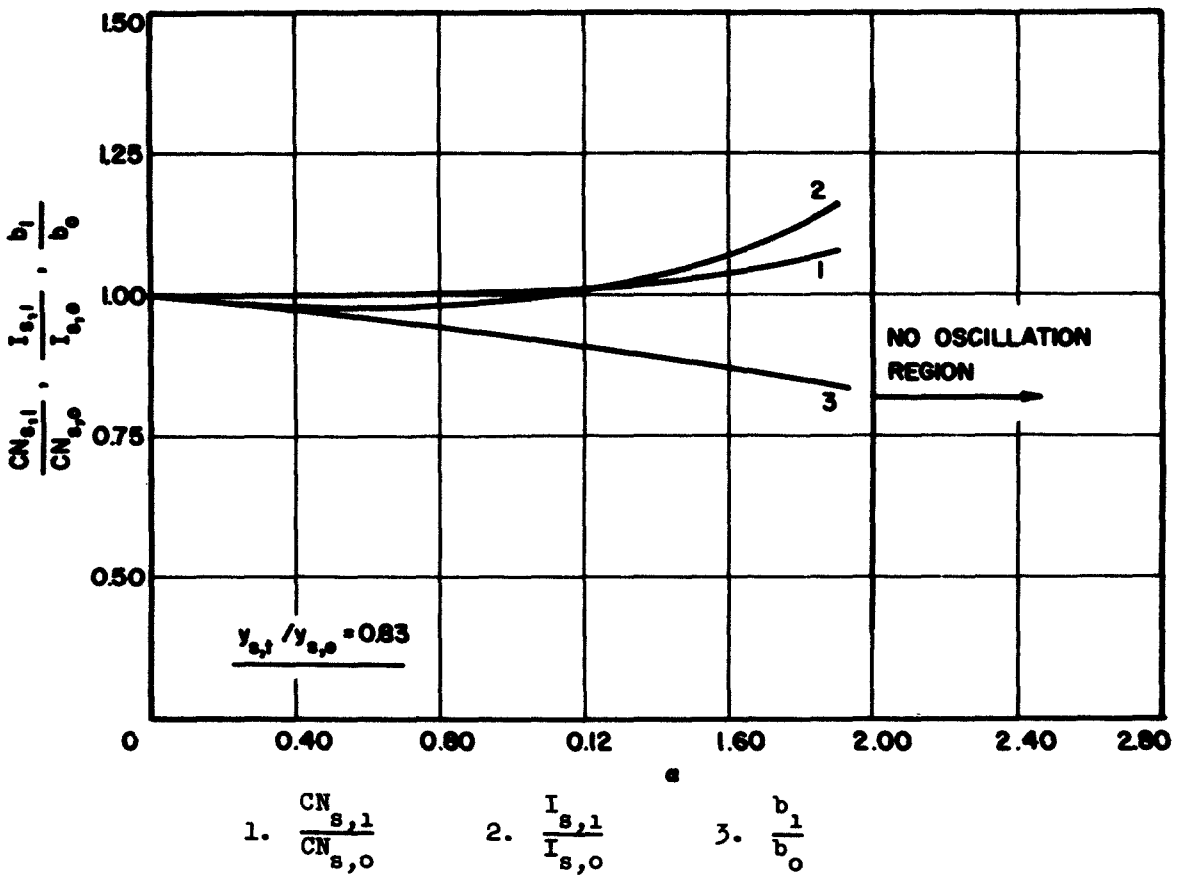

FIG. 3.34 $CN_{s,1}/CN_{s,o}$, $I_{s,1}/I_{s,o}$, b_1/b_o VS. α FOR A LINEAR BEAM VOLTAGE VARIATION. (C = 0.05, QC = 0.5, d = 0)

Substituting the above values of $\xi(y)$ and $\zeta(y)$ in Eqs. 3.42 through 3.44 results in the following set of equations

$$\frac{d^2V_{cn}(y)}{dy^2} + \left(\frac{1 + C_o b}{C_o}\right)^2 V_{cn}(y) - j2 \frac{d}{C_o}(1 + C_o b)^2 V_{cn}(y)$$

$$= \left[4C_o(1 + C_o b) - j8C_o^2 d(1 + C_o b)\right] \rho_{1n}(y) \quad , (3.82)$$

$$\frac{1}{[1 + \alpha y^2]^{1/2}} \frac{du_{1n}(y)}{dy} - \frac{\alpha y}{(1 + \alpha y^2)} u_{1n}(y) + (1 + \alpha y^2) \frac{d\rho_{1n}(y)}{dy}$$

$$+ \left[\frac{\alpha y}{(1 + \alpha y^2)^{1/2}} + \frac{j}{C_o}\right] \rho_{1n}(y) = 0 \quad , (3.83)$$

$$\frac{1}{2} \frac{dV_{cn}(y)}{dy} + j \frac{4C_o QC}{[1 - 2C_o\sqrt{QC}]^2} \frac{1}{(1 + C_o b)} \rho_{1n}(y)$$

$$= \left[\frac{j}{C_o} + \frac{\alpha y}{(1 + \alpha y^2)^{1/2}}\right] u_{1n}(y) + (1 + \alpha y^2)^{1/2} \frac{du_{1n}(y)}{dy} \quad . (3.84)$$

The solution of these equations is discussed in detail in Appendix B.2. The results are presented here in Figs. 3.35 through 3.38.

It is again seen here that for weak tapers the start-oscillation current has a tendency to decrease, however, beyond a certain strength of taper the current increases very rapidly and a "no oscillation" region sets in.

3.5.7 Exponential Voltage Gradient. Here the circuit phase velocity is assumed constant and the beam potential varies as

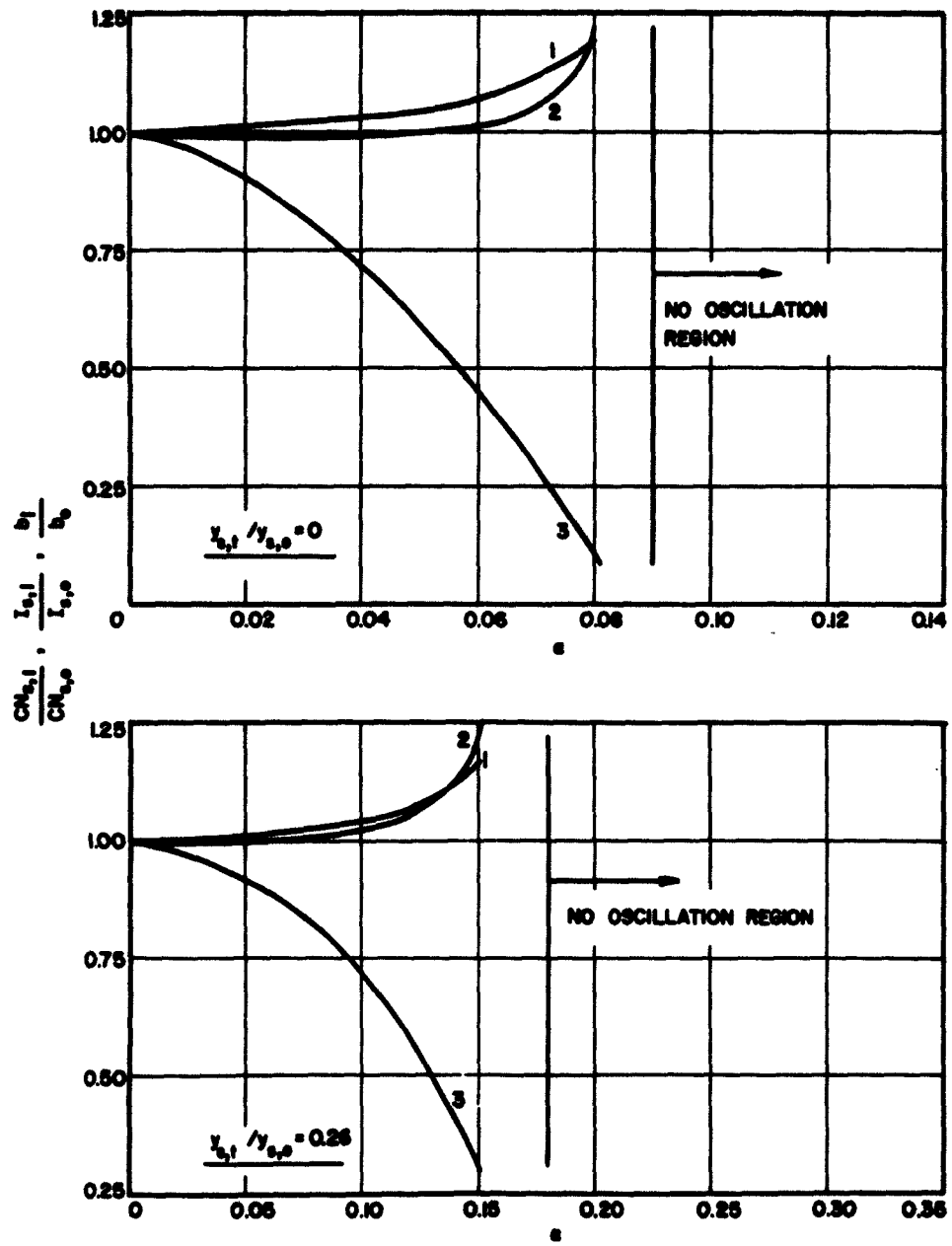

1. $\frac{CN_{s,1}}{CN_{s,o}}$ 2. $\frac{I_{s,1}}{I_{s,o}}$ 3. $\frac{b_1}{b_o}$

FIG. 3.35 $CN_{s,1}/CN_{s,o}$, $I_{s,1}/I_{s,o}$, b_1/b_o VS. α FOR A QUADRATIC VOLTAGE GRADIENT. ($C = 0.05$, $QC = 0$, $d = 0$)

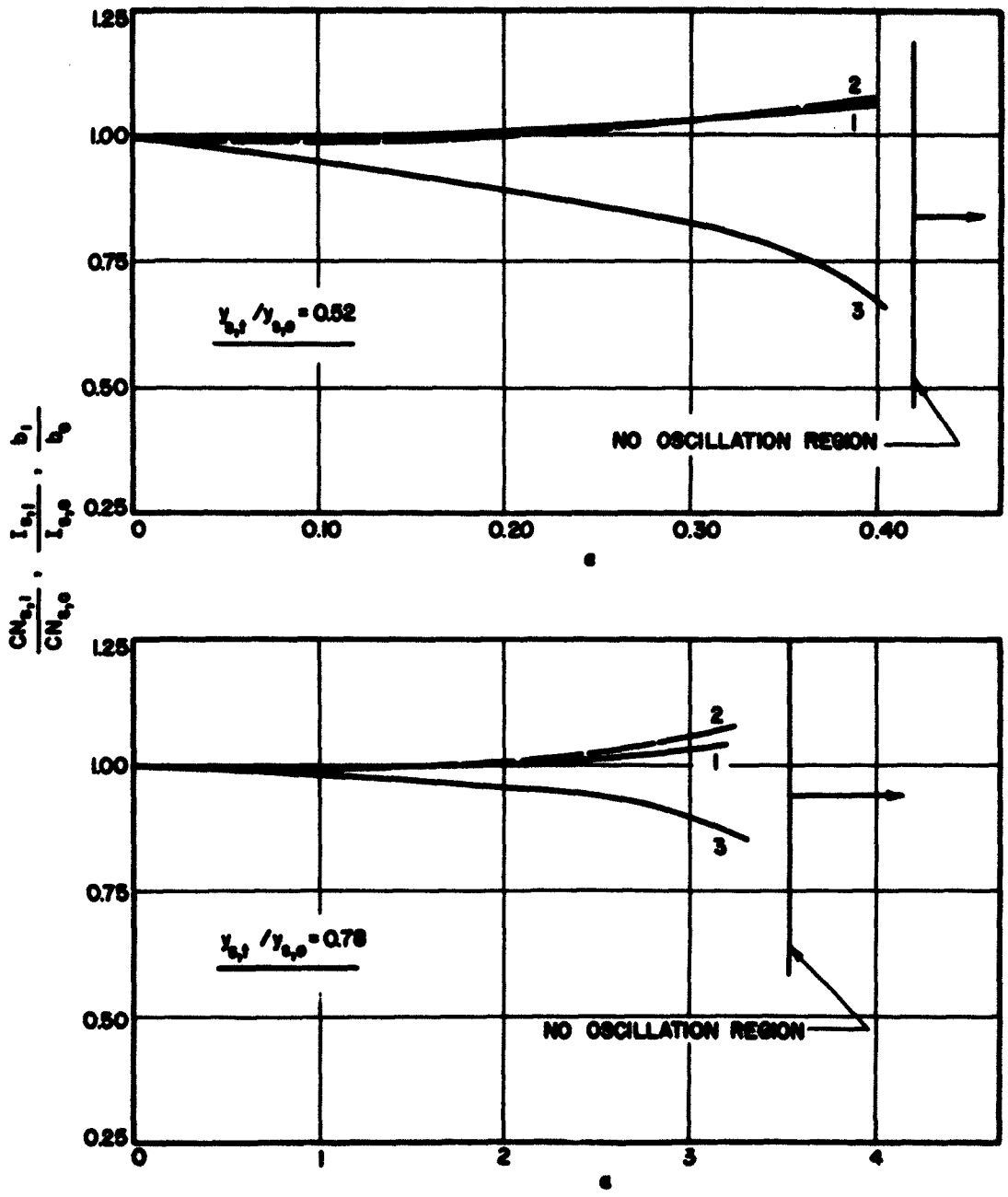

1. $\frac{CN_{s,1}}{CN_{s,0}}$ 2. $\frac{I_{s,1}}{I_{s,0}}$ 3. $\frac{b_1}{b_0}$

FIG. 3.36 $CN_{s,1}/CN_{s,0}$, $I_{s,1}/I_{s,0}$, b_1/b_0 VS. α FOR A QUADRATIC VOLTAGE GRADIENT. ($C = 0.05$, $QC = 0$, $d = 0$)

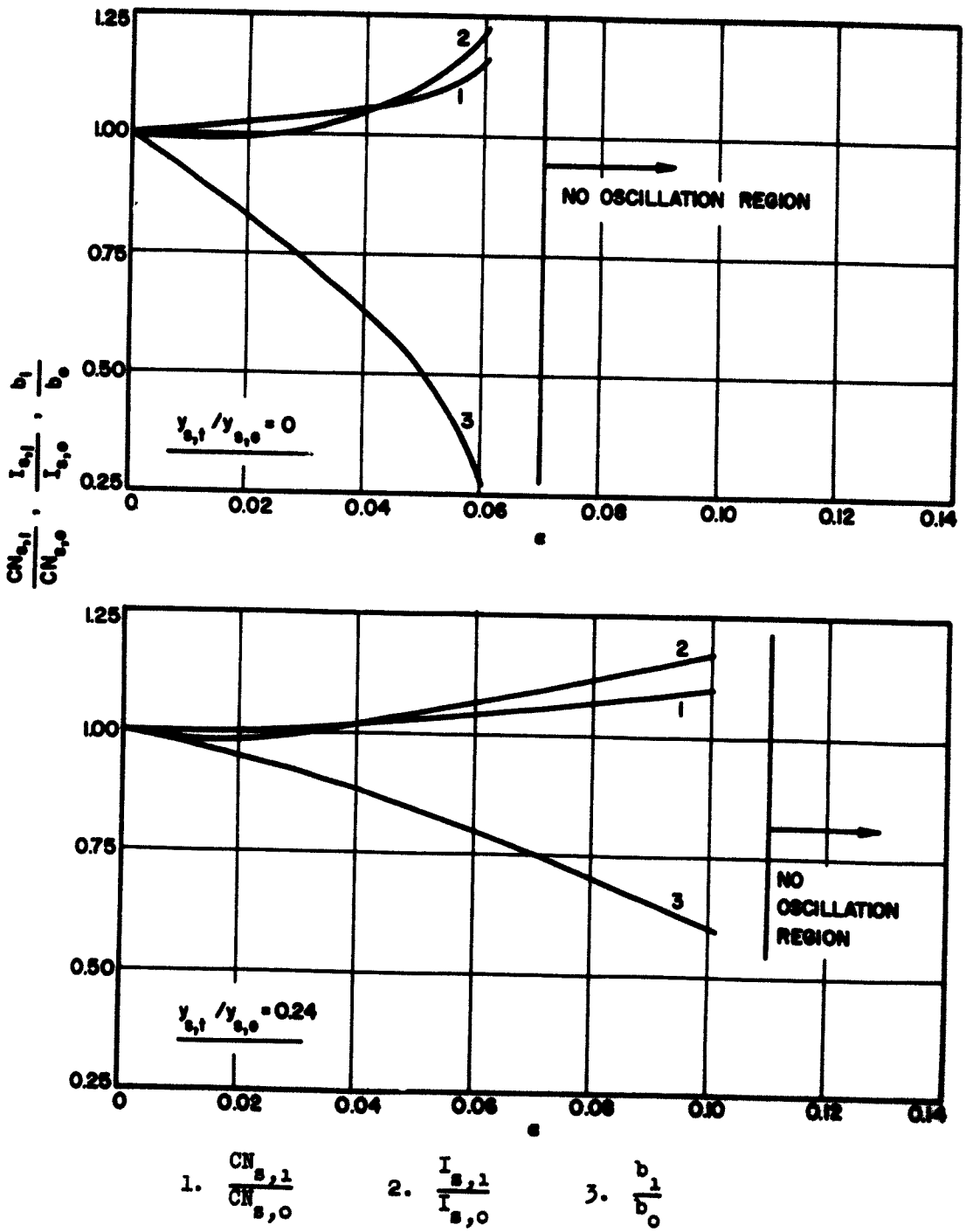

1. $\frac{CN_{s,1}}{CN_{s,o}}$ 2. $\frac{I_{s,1}}{I_{s,o}}$ 3. $\frac{b_1}{b_o}$

FIG. 3.37 $CN_{s,1}/CN_{s,o}$, $I_{s,1}/I_{s,o}$, b_1/b_o VS. α FOR A QUADRATIC VOLTAGE GRADIENT. ($C = 0.05$, $QC = 0.2$, $d = 0$)

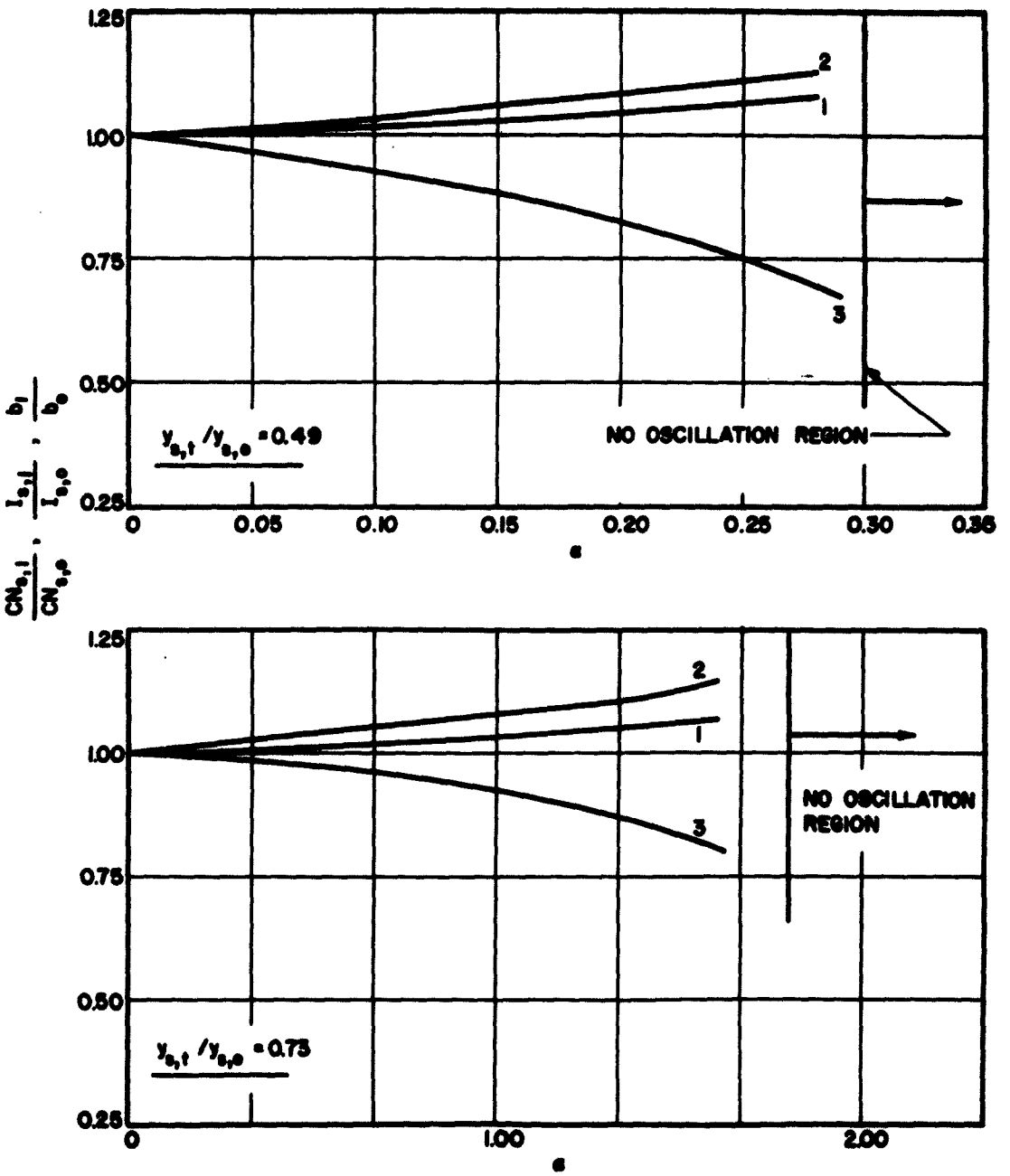

1. $\frac{CN_{s,1}}{CN_{s,o}}$ 2. $\frac{I_{s,1}}{I_{s,o}}$ 3. $\frac{b_1}{b_o}$

FIG. 3.38 $CN_{s,1}/CN_{s,o}$, $I_{s,1}/I_{s,o}$, b_1/b_o VS. α FOR A QUADRATIC VOLTAGE GRADIENT. (C = 0.05, QC = 0.2, d = 0)

$$V_o = V_{oo} e^{2\alpha y} \quad . \tag{3.85}$$

This makes $\xi(y)$ and $\zeta(y)$ in Eqs. 3.42 through 3.44 assume the following values,

$$\xi(y) = 1 \quad , \tag{3.86}$$

$$\zeta(y) = e^{2\alpha y} \quad . \tag{3.87}$$

Substituting the above values of $\xi(y)$ and $\zeta(y)$ into Eqs. 3.42 through 3.44 results in the following set of equations,

$$\frac{d^2V_{cn}(y)}{dy^2} + \left(\frac{1 + C_o b}{C_o} \right)^2 V_{cn}(y) - j2 \frac{j}{C_o} (1 + C_o b)^2 V_{cn}(y)$$

$$= \left[4C_o(1 + C_o b) - j8C_o^2 \, d(1 + C_o b) \right] \rho_{1n}(y) \quad , \tag{3.88}$$

$$e^{-\alpha y} \frac{du_{1n}(y)}{dy} - \alpha e^{-\alpha y} u_{1n}(y) + e^{\alpha y} \frac{d\rho_{1n}(y)}{dy} + \left[\alpha e^{\alpha y} + \frac{j}{C_o} \right] \rho_{1n}(y) = 0 \quad , \tag{3.89}$$

$$\frac{1}{2} \frac{dV_{cn}(y)}{dy} + j \frac{4C_o QC}{[1 - 2C_o \sqrt{QC}]^2} \frac{1}{(1 + C_o b)} \rho_{1n}(y)$$

$$= \left[\frac{j}{C_o} + \alpha e^{\alpha y} \right] u_{1n}(y) + e^{\alpha y} \frac{du_{1n}(y)}{dy} \quad . \tag{3.90}$$

The solution of these equations is discussed in detail in Appendix B.2. The results are presented here in Figs. 3.39 through 3.43.

Here again it is seen that for weak tapers the start-oscillation current tends to decrease, however, after a certain strength of taper the

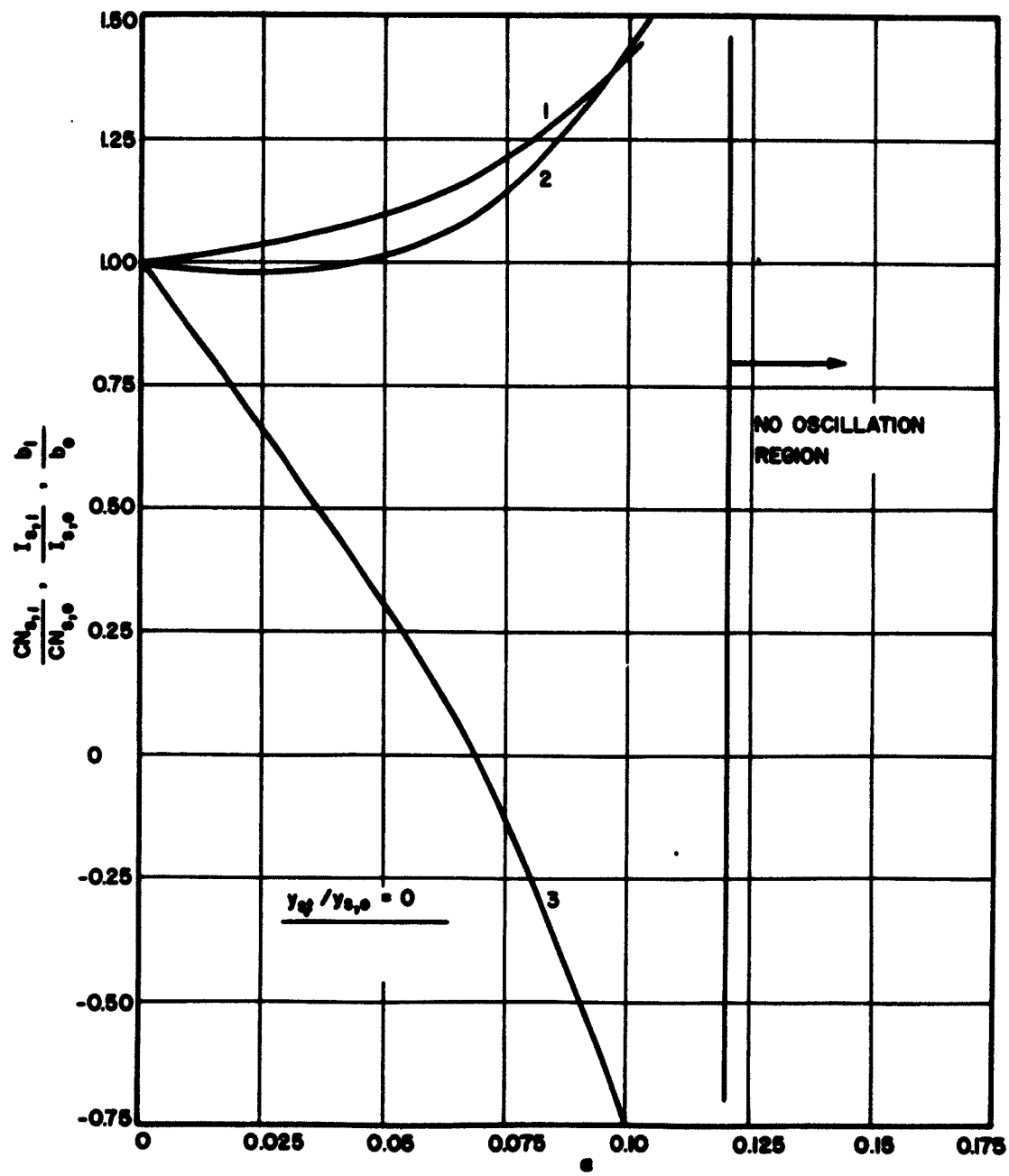

1. $\frac{CN_{s,1}}{CN_{s,o}}$ 2. $\frac{I_{s,1}}{I_{s,o}}$ 3. $\frac{b_1}{b_o}$

FIG. 3.39 $CN_{s,1}/CN_{s,o}$, $I_{s,1}/I_{s,o}$, b_1/b_o VS. α FOR AN EXPONENTIAL VOLTAGE GRADIENT. ($C = 0.05$, $QC = 0$, $d = 0$)

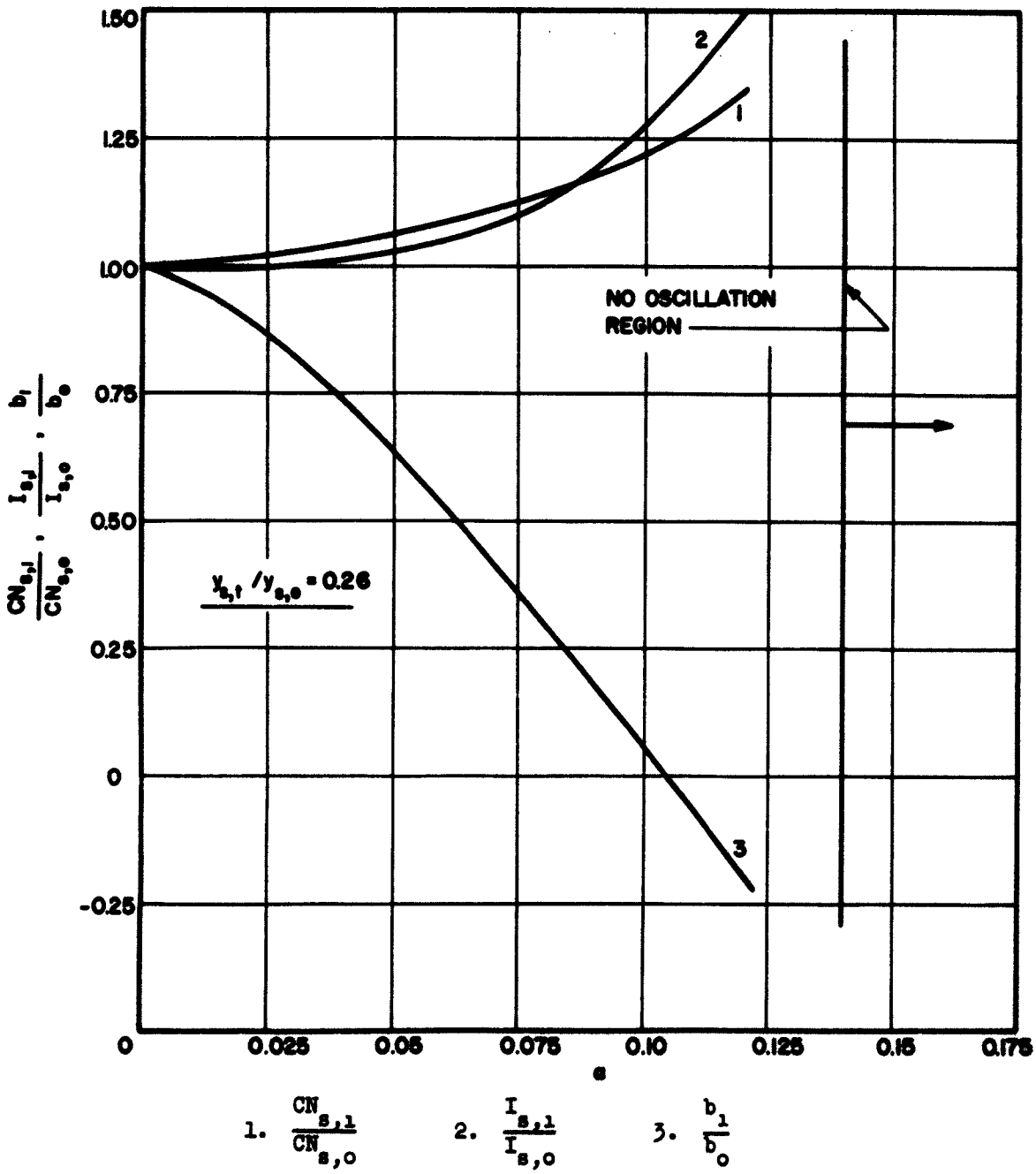

1. $\frac{CN_{s,1}}{CN_{s,0}}$ 2. $\frac{I_{s,1}}{I_{s,0}}$ 3. $\frac{b_1}{b_0}$

FIG. 3.40 $CN_{s,1}/CN_{s,0}$, $I_{s,1}/I_{s,0}$, b_1/b_0 VS. α FOR AN EXPONENTIAL VOLTAGE GRADIENT. ($C = 0.05$, $QC = 0$, $d = 0$)

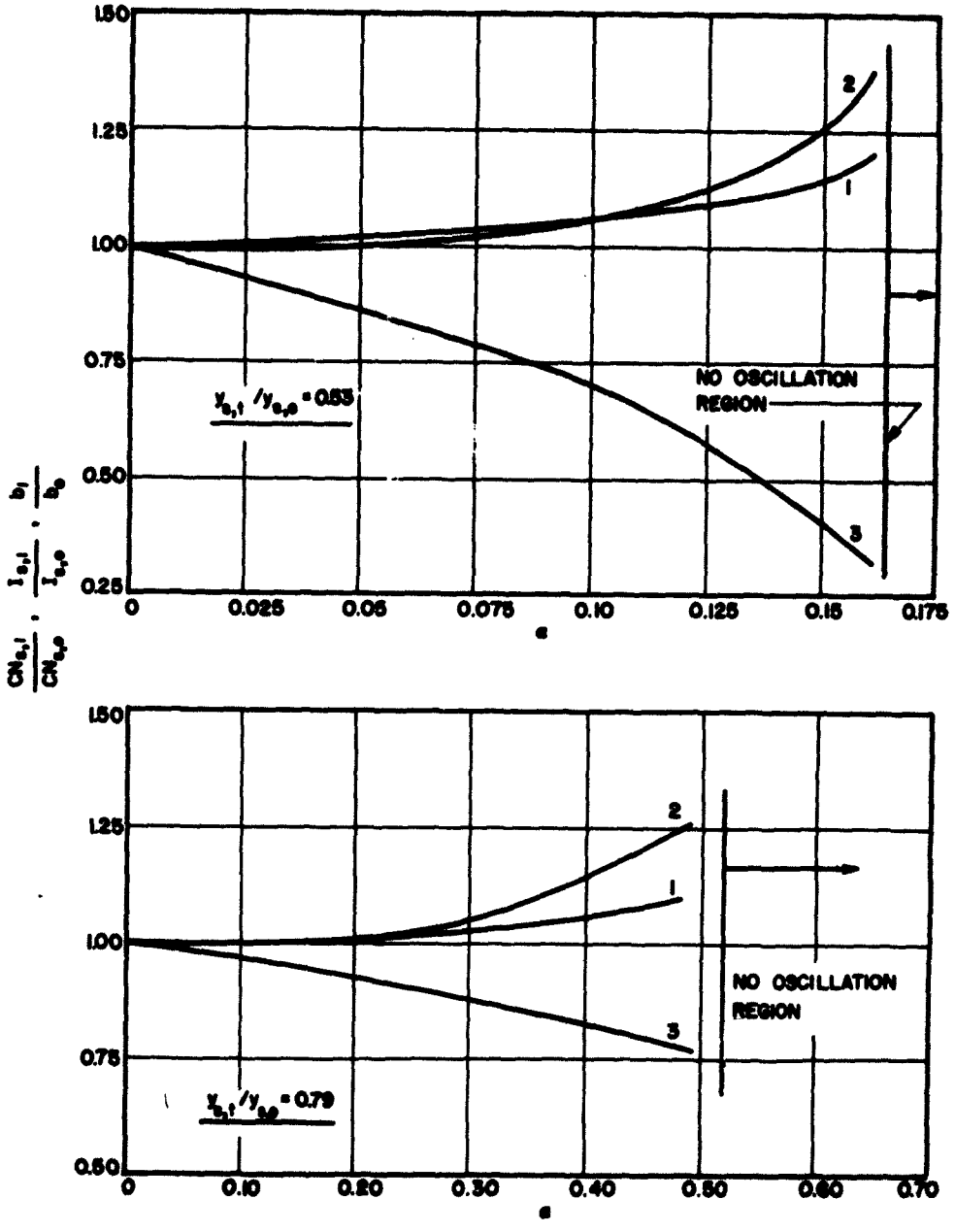

1. $\frac{CN_{s,1}}{CN_{s,o}}$ 2. $\frac{I_{s,1}}{I_{s,o}}$ 3. $\frac{b_1}{b_o}$

FIG. 3.41 $CN_{s,1}/CN_{s,o}$, $I_{s,1}/I_{s,o}$, b_1/b_o VS. α FOR AN EXPONENTIAL VOLTAGE GRADIENT. (C = 0.05, QC = 0, d = 0)

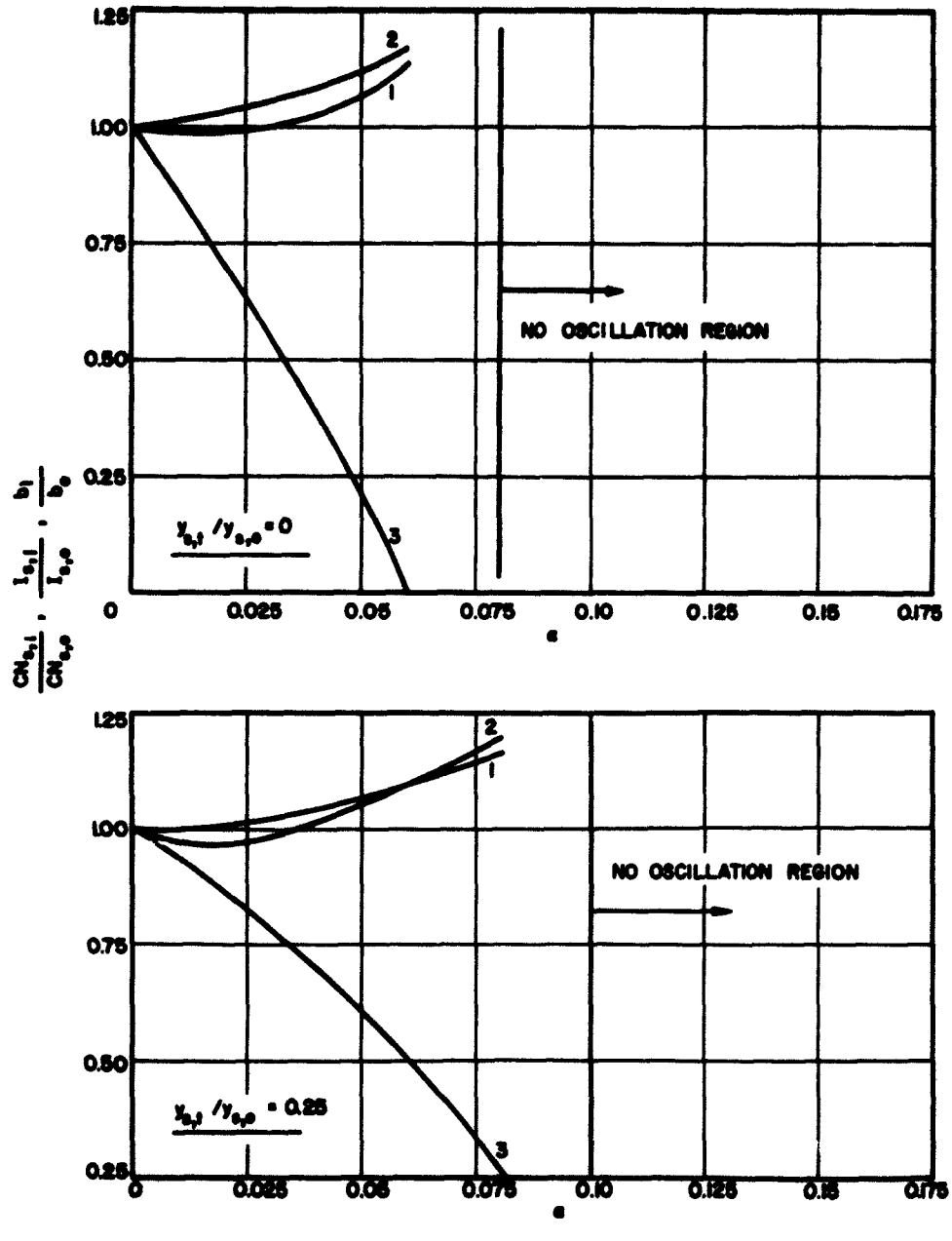

1. $\frac{CN_{s,1}}{CN_{s,0}}$ 2. $\frac{I_{s,1}}{I_{s,0}}$ 3. $\frac{b_1}{b_0}$

FIG. 3.42 $CN_{s,1}/CN_{s,0}$, $I_{s,1}/I_{s,0}$, b_1/b_0 VS. α FOR AN EXPONENTIAL VOLTAGE GRADIENT. ($C = 0.05$, $QC = 0.2$, $d = 0$)

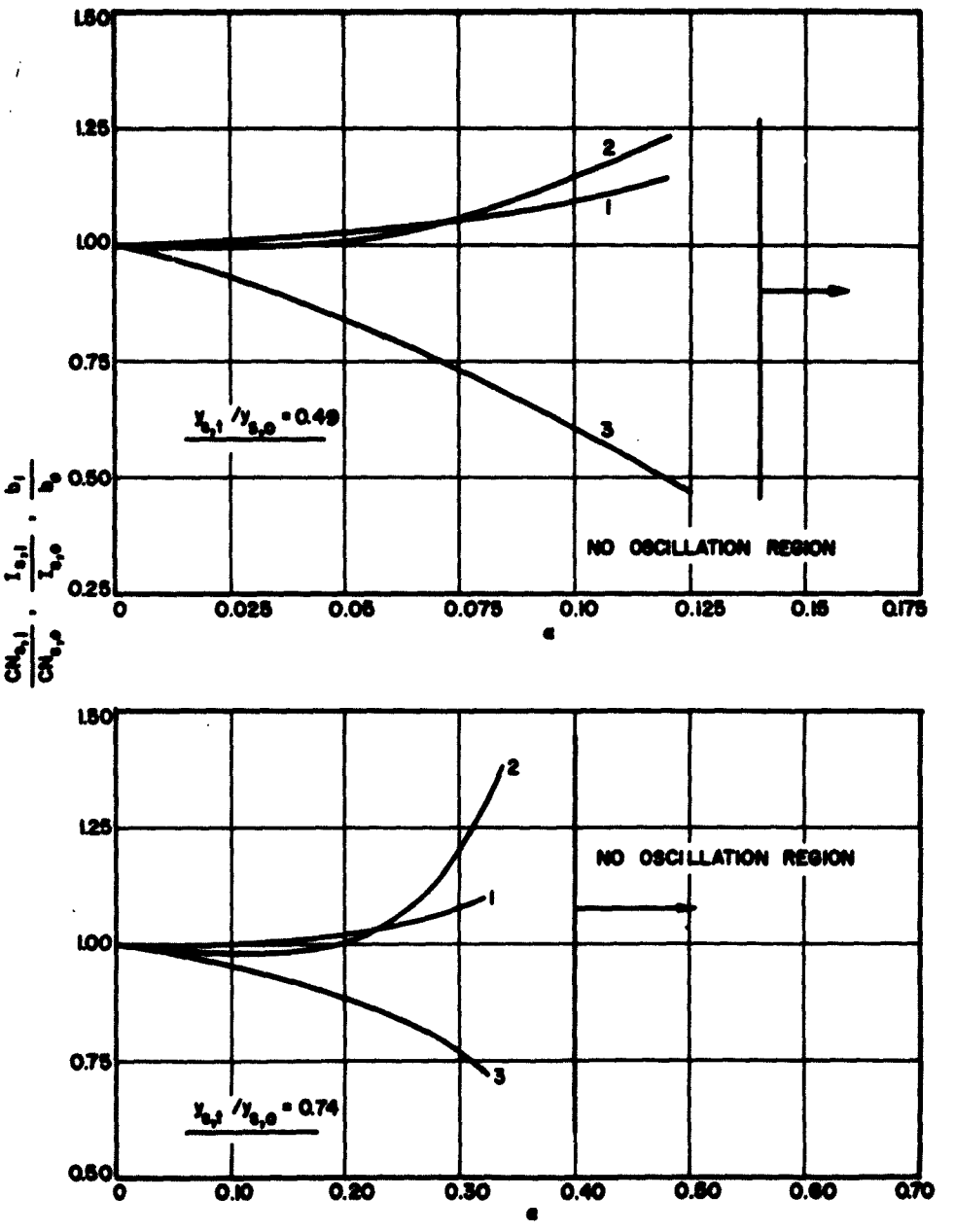

1. $\frac{CN_{s,1}}{CN_{s,o}}$ 2. $\frac{I_{s,1}}{I_{s,o}}$ 3. $\frac{b_1}{b_o}$

FIG. 3.43 $CN_{s,1}/CN_{s,o}$, $I_{s,1}/I_{s,o}$, b_1/b_o VS. α FOR AN EXPONENTIAL VOLTAGE GRADIENT. (C = 0.05, QC = 0.2, d = 0)

oscillation currents start to increase very rapidly and a "no oscillation" region sets in.

3.5.8 Summary of the Effect of Voltage-Gradients on the Start-Oscillation Conditions. It has been shown that the start-oscillation current in a backward-wave oscillator whose beam potential is non-uniform can be lower than one with a uniform potential if both are to oscillate at the same frequency and are of the same length. This was found to be the case for weak gradients. The kind of gradient is not critical, but the strength of the gradient is certainly significant. It has been found that for the kinds of gradients investigated above, the start-oscillation current starts to increase very rapidly when a certain strength of gradient is reached. For those cases a "no oscillation" region sets in when the gradient becomes stronger than a certain value. This suggests that the voltage gradient can be chosen to either decrease the start-oscillation current or to suppress backward-wave oscillations in forward-wave amplifiers.

It is worthy to note here that some experimental results obtained at Stanford[6] on a linear voltage gradient agree qualitatively with those obtained here. Figure 2, page 42 of that report shows a slight decrease in the start-oscillation current for a weak gradient and rapid increase in the oscillation current when the gradient is made stronger.

3.5.9 Sinusoidal Beam Potential Variation. In this section the effect of a sinusoidally varying beam potential on the start-oscillation conditions is investigated. It was mentioned earlier that this type of beam potential variation is inherent in the operation of electrostatically focused backward-wave oscillators[4,5]. Here then, the circuit phase

velocity is assumed constant and the beam potential varies as a function of distance along the tube as follows:

$$V_o = V_{oo}\left[1 - A\cos\frac{2\pi z}{L}\right] , \tag{3.91}$$

where L = the length of the focusing period.

We can express Eq. 3.91 in terms of the normalized coordinate y as follows:

$$V_o = V_{oo}\left[1 - A\cos\frac{2\pi z_o}{L}\left(\frac{y}{y_o}\right)\right] \tag{3.92}$$

or

$$V_o = V_{oo}\left[1 - A\cos\alpha y\right] , \tag{3.93}$$

where

$$\alpha = \frac{2\pi N_{d\text{-}c}}{y_o}$$

and $N_{d\text{-}c}$ = the number of d-c focusing periods in the tube.

$\xi(y)$ and $\zeta(y)$ in Eqs. 3.42 through 3.44 then become,

$$\xi(y) = 1 , \tag{3.94}$$

$$\zeta(y) = \left[1 - A\cos\alpha y\right] . \tag{3.95}$$

Substituting the above values of $\xi(y)$ and $\zeta(y)$ in Eqs. 3.42 through 3.44 results in the following set of equations:

$$\frac{d^2V_{cn}(y)}{dy^2} + \left(\frac{1 + C_o b}{C_o}\right)^2 V_{cn}(y) - j2\frac{1}{C_o}(1 + C_o b)^2 V_{cn}(y)$$

$$= \left[4C_o(1 + C_o b) - j8C_o^2\, d(1 + C_o b)\right]\rho_{1n}(y) , \tag{3.96}$$

$$\frac{1}{[1 - A \cos \alpha y]^{1/2}} \frac{du_{1n}(y)}{dy} - \frac{\alpha A}{2} \frac{\sin \alpha y}{[1 - A \cos \alpha y]^{3/2}} u_{1n}(y)$$

$$+ [1 - A \cos \alpha y]^{1/2} \frac{d\rho_{1n}(y)}{dy}$$

$$+ \left[\frac{\alpha A \sin \alpha y}{2[1 - A \cos \alpha y]^{1/2}} + \frac{j}{C_o} \right] \rho_{1n}(y) = 0 \quad , \quad (3.97)$$

$$\frac{1}{2} \frac{dV_{cn}(y)}{dy} + j \frac{4C_o QC}{[1 - 2C_o \sqrt{QC}]^2} \frac{1}{(1 + C_o b)} \rho_{1n}(y)$$

$$= \left[\frac{j}{C_o} + \frac{\alpha A \sin \alpha y}{2[1 - A \cos \alpha y]^{1/2}} \right] u_{1n}(y)$$

$$+ [1 - A \cos \alpha y]^{1/2} \frac{du_{1n}(y)}{dy} \quad . \quad (3.98)$$

The solution of the above equations is discussed in detail in Appendix B.2. The results are presented here in Figs. 3.44 through 3.53. In these figures the start-oscillation conditions in the nonuniform oscillator are compared to those of a uniform one for different values of α, which is a measure of the number of d-c focusing periods. These conditions are plotted as a function of A which is a measure of the deviation from the uniform potential.

It can be seen from the figures that the average potential in the two cases is the same. The start-oscillation current increases when either α or A is increased. However, in most of the cases that were investigated the increase is slight. Another way of interpreting these results which are mentioned earlier, is outlined below.

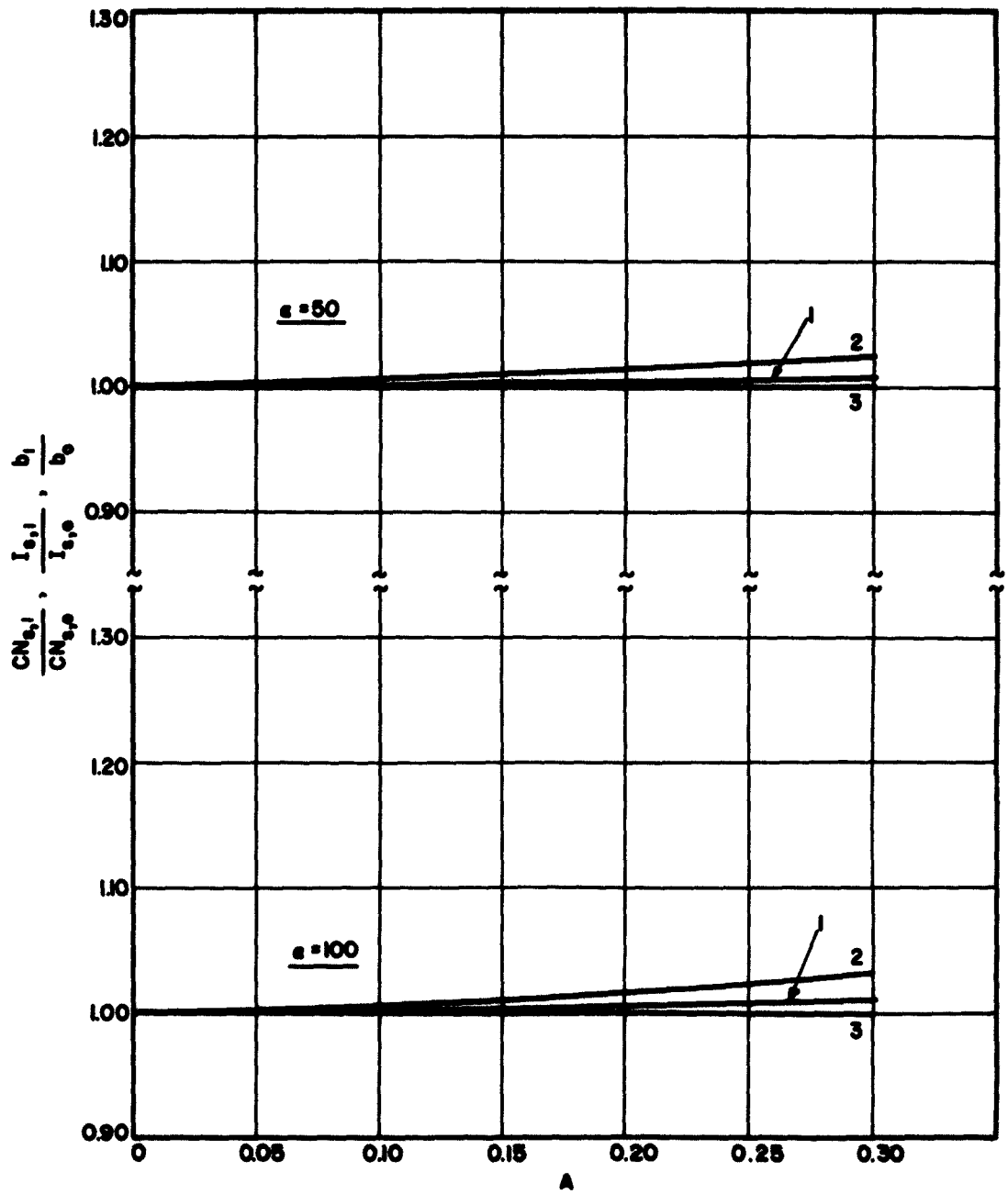

1. $\frac{CN_{s,1}}{CN_{s,o}}$ 2. $\frac{I_{s,1}}{I_{s,o}}$ 3. $\frac{b_1}{b_o}$

FIG. 3.44 $CN_{s,1}/CN_{s,o}$, $I_{s,1}/I_{s,o}$, b_1/b_o VS. A FOR A SINUSOIDAL BEAM POTENTIAL VARIATION. (C = 0.05, QC = 0, d = 0)

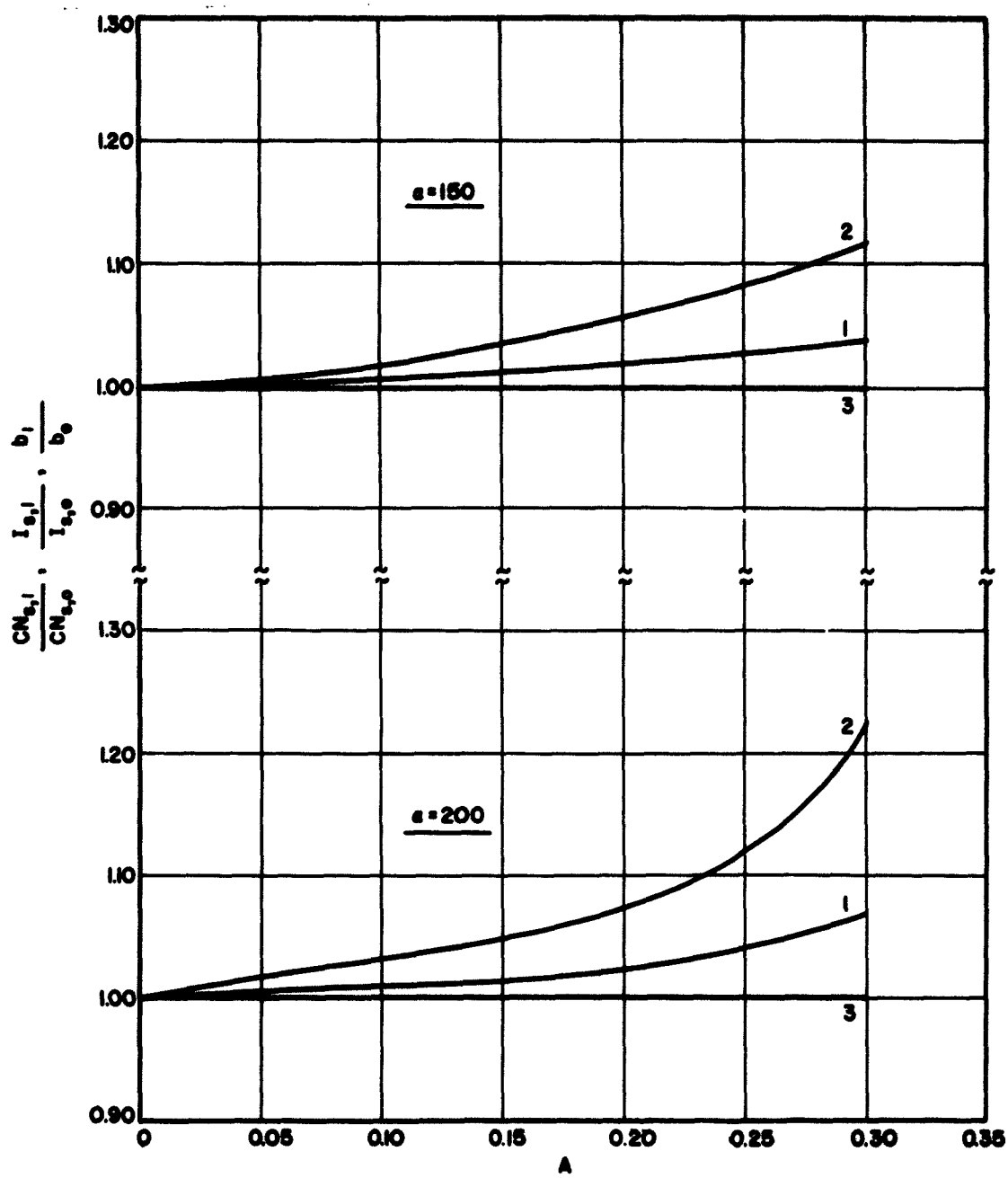

1. $\frac{CN_{s,1}}{CN_{s,o}}$ 2. $\frac{I_{s,1}}{I_{s,o}}$ 3. $\frac{b_1}{b_o}$

FIG. 3.45 $CN_{s,1}/CN_{s,o}$, $I_{s,1}/I_{s,o}$, b_1/b_o VS. A FOR A SINUSOIDAL BEAM POTENTIAL VARIATION. (C = 0.05, QC = 0, d = 0)

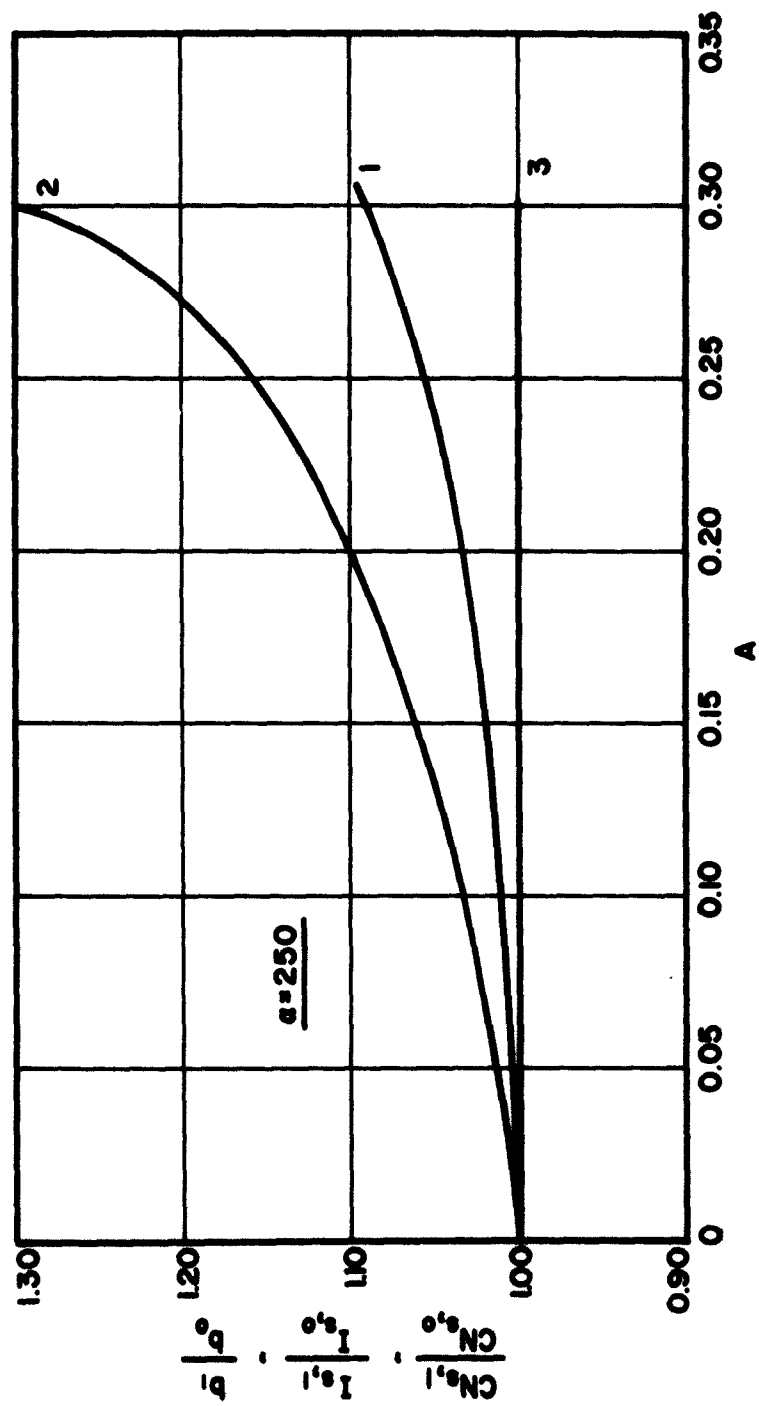

1. $\frac{CN_{s,1}}{CN_{s,o}}$ 2. $\frac{I_{s,1}}{I_{s,o}}$ 3. $\frac{b_1}{b_o}$

FIG. 3.46 $CN_{s,1}/CN_{s,o}$, $I_{s,1}/I_{s,o}$, b_1/b_o VS. A FOR A SINUSOIDAL BEAM POTENTIAL VARIATION. (C = 0.05, QC = 0, d = 0)

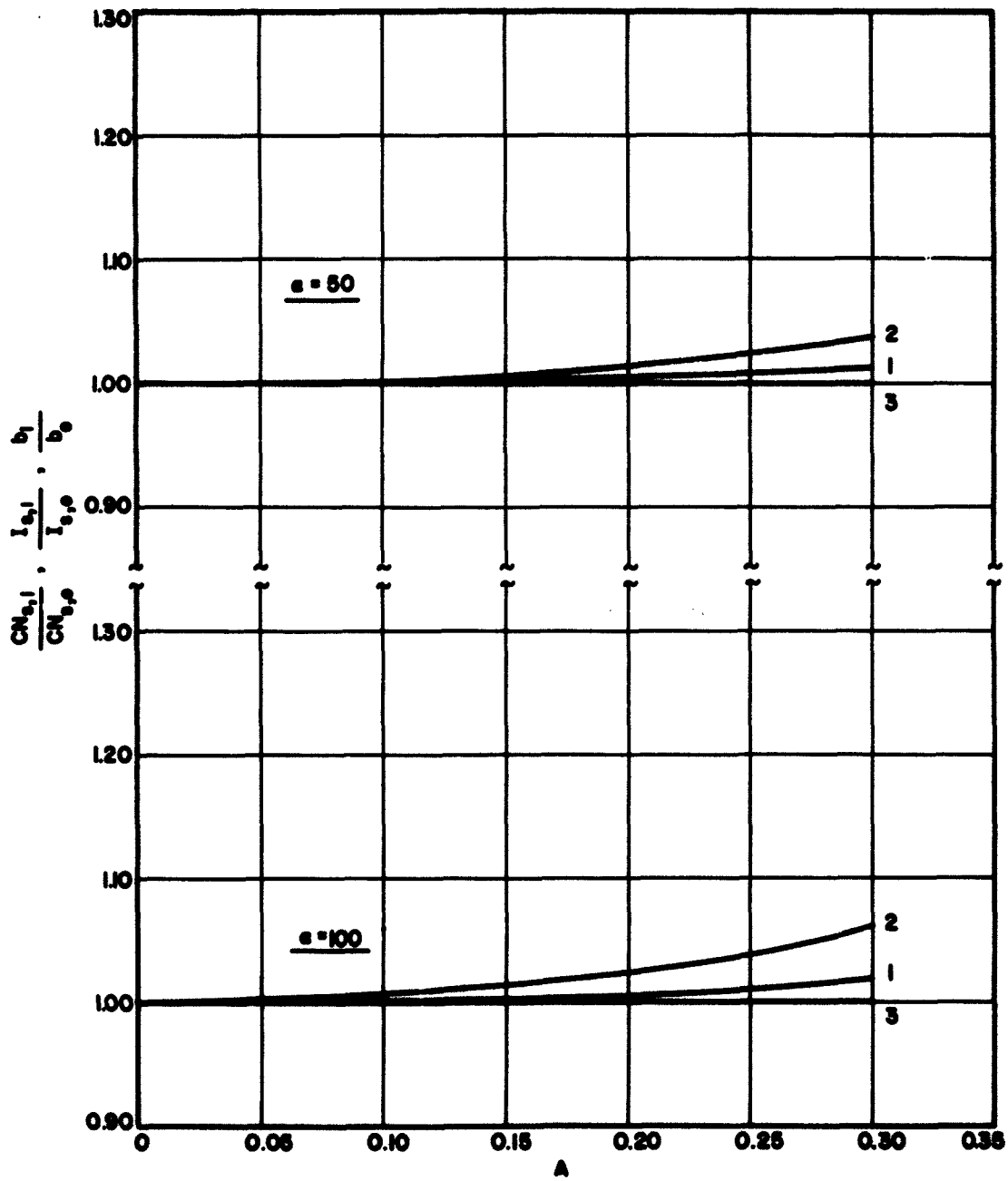

$\frac{CN_{s,1}}{CN_{s,o}} \cdot \frac{I_{s,1}}{I_{s,o}} \cdot \frac{b_1}{b_o}$

1. $\frac{CN_{s,1}}{CN_{s,o}}$ 2. $\frac{I_{s,1}}{I_{s,o}}$ 3. $\frac{b_1}{b_o}$

FIG. 3.47 $CN_{s,1}/CN_{s,o}$, $I_{s,1}/I_{s,o}$, b_1/b_o VS. A FOR A SINUSOIDAL BEAM POTENTIAL VARIATION. (C = 0.05, QC = 0.2, d = 0)

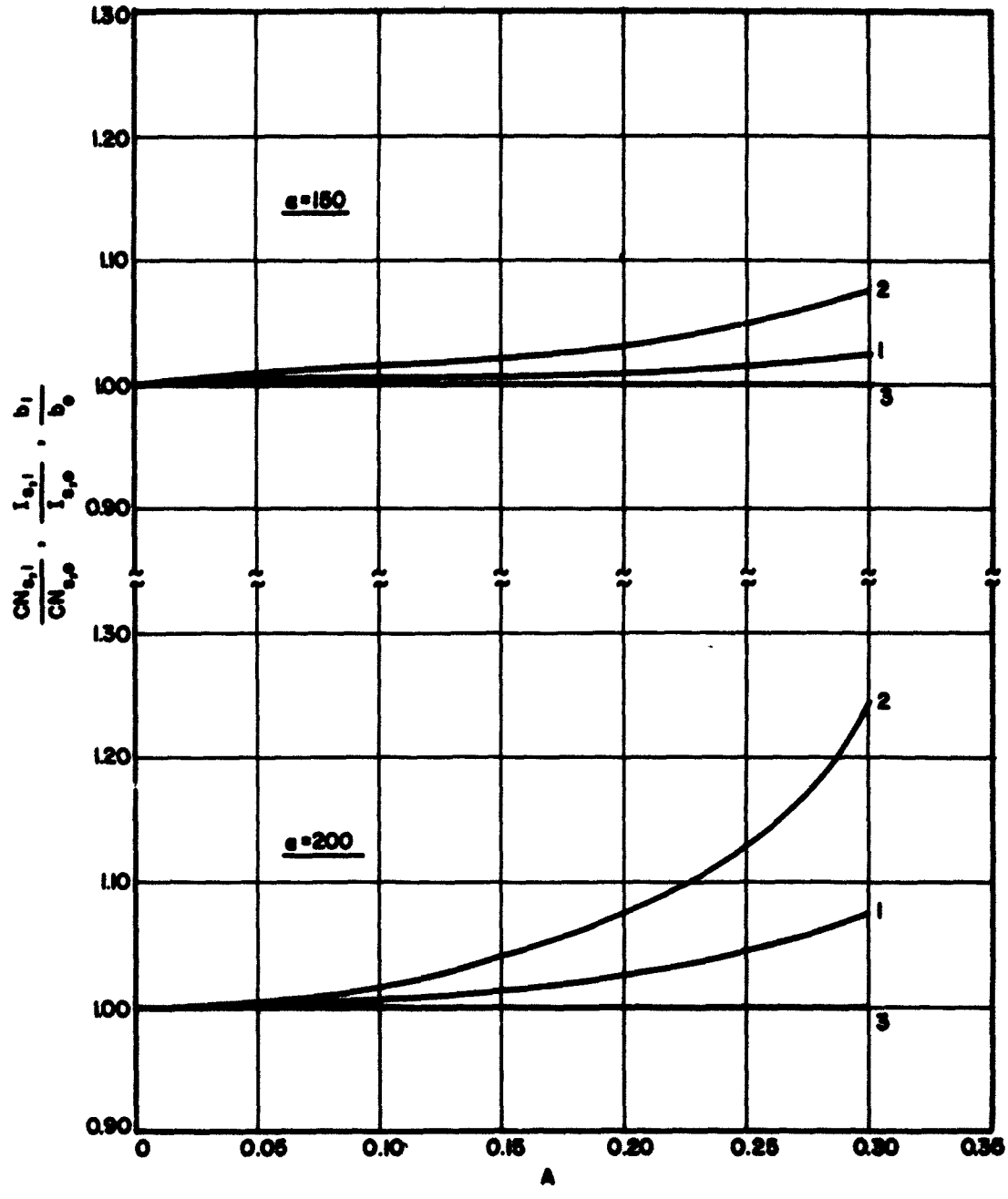

1. $\frac{CN_{s,1}}{CN_{s,o}}$ 2. $\frac{I_{s,1}}{I_{s,o}}$ 3. $\frac{b_1}{b_o}$

FIG. 3.48 $CN_{s,1}/CN_{s,o}$, $I_{s,1}/I_{s,o}$, b_1/b_o VS. A FOR A SINUSOIDAL BEAM POTENTIAL VARIATION. (C = 0.05, QC = 0.2, d = 0)

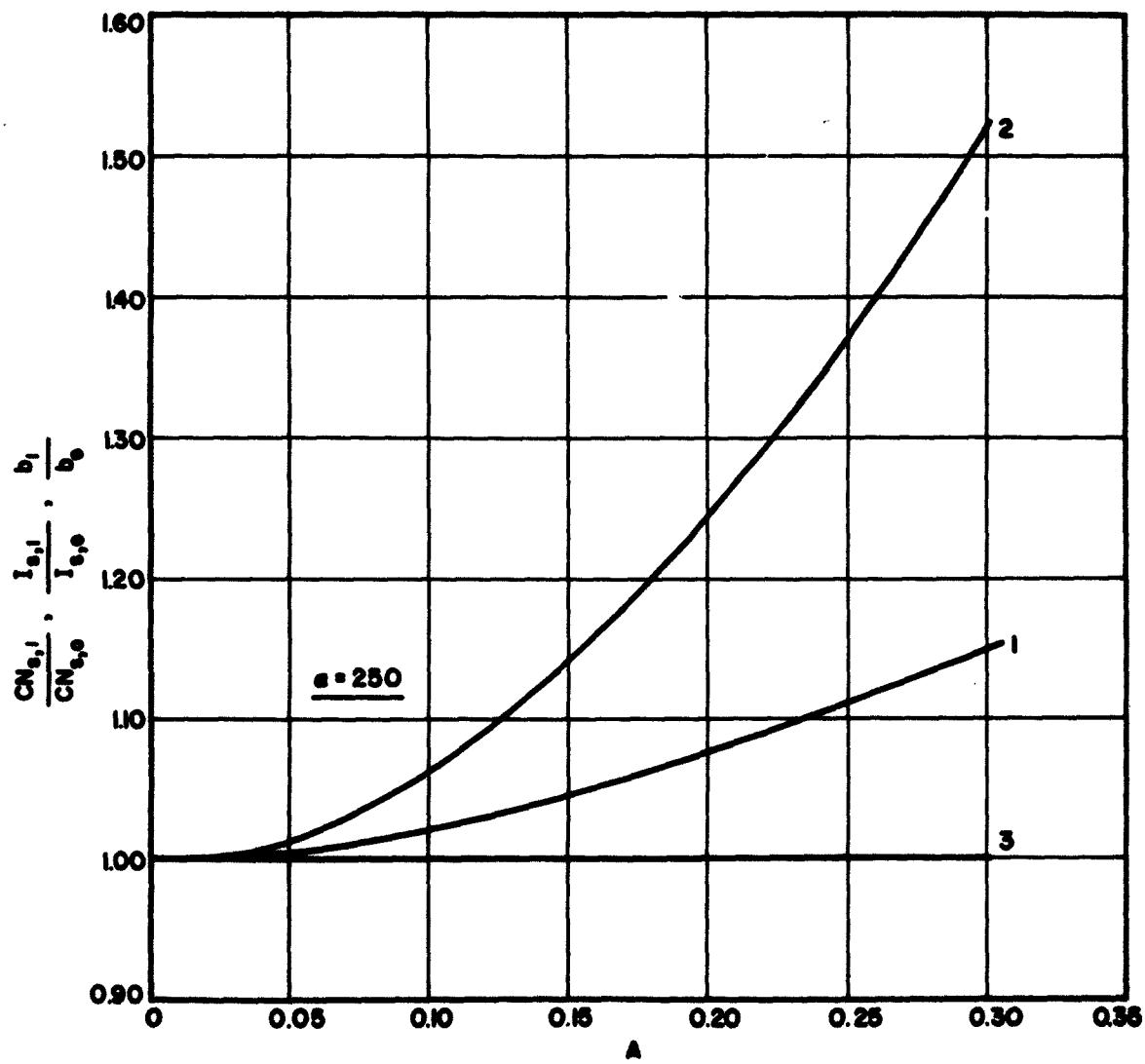

1. $\frac{CN_{s,1}}{CN_{s,o}}$ 2. $\frac{I_{s,1}}{I_{s,o}}$ 3. $\frac{b_1}{b_o}$

FIG. 3.49 $CN_{s,1}/CN_{s,o}$, $I_{s,1}/I_{s,o}$, b_1/b_o VS. A FOR A SINUSOIDAL BEAM POTENTIAL VARIATION. (C = 0.05, QC = 0.2, d = 0)

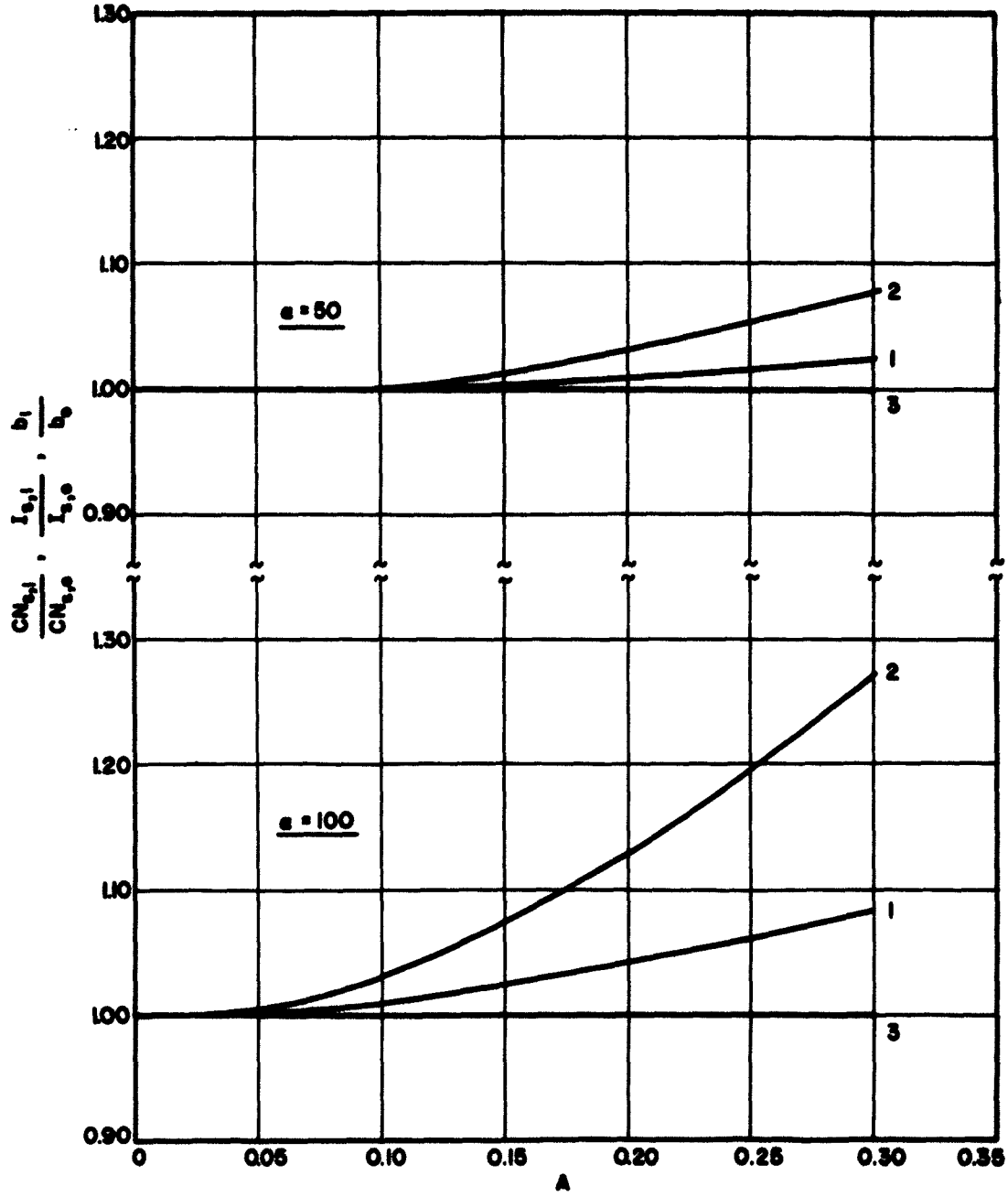

1. $\frac{CN_{s,1}}{CN_{s,o}}$ 2. $\frac{I_{s,1}}{I_{s,o}}$ 3. $\frac{b_1}{b_o}$

FIG. 3.50 $CN_{s,1}/CN_{s,o}$, $I_{s,1}/I_{s,o}$, b_1/b_o VS. A FOR A SINUSOIDAL BEAM POTENTIAL VARIATION. (C = 0.05, QC = 0.5, d = 0)

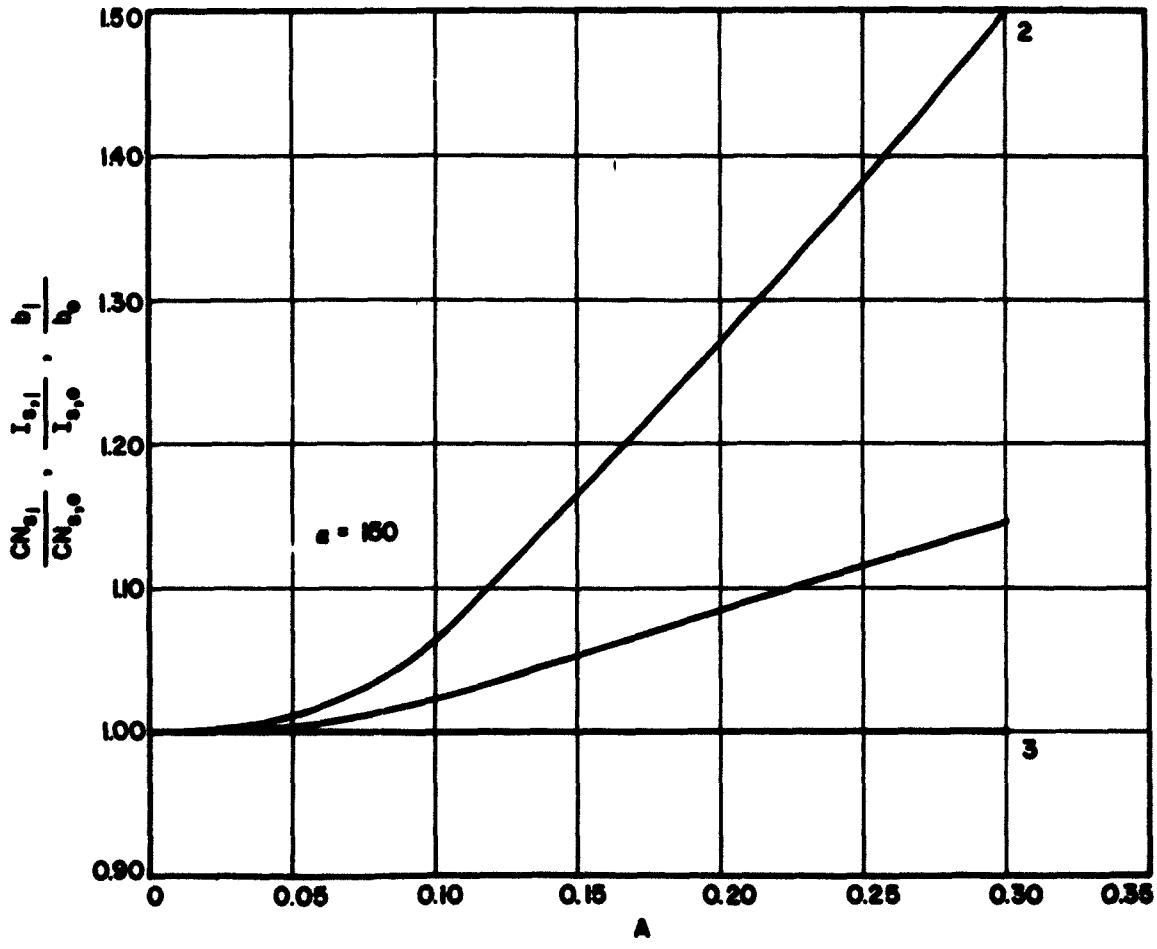

1. $\frac{CN_{s,1}}{CN_{s,0}}$ 2. $\frac{I_{s,1}}{I_{s,0}}$ 3. $\frac{b_1}{b_0}$

FIG. 3.51 $CN_{s,1}/CN_{s,0}$, $I_{s,1}/I_{s,0}$, b_1/b_0 VS. A FOR A SINUSOIDAL BEAM POTENTIAL VARIATION. (C = 0.05, QC = 0.5, d = 0)

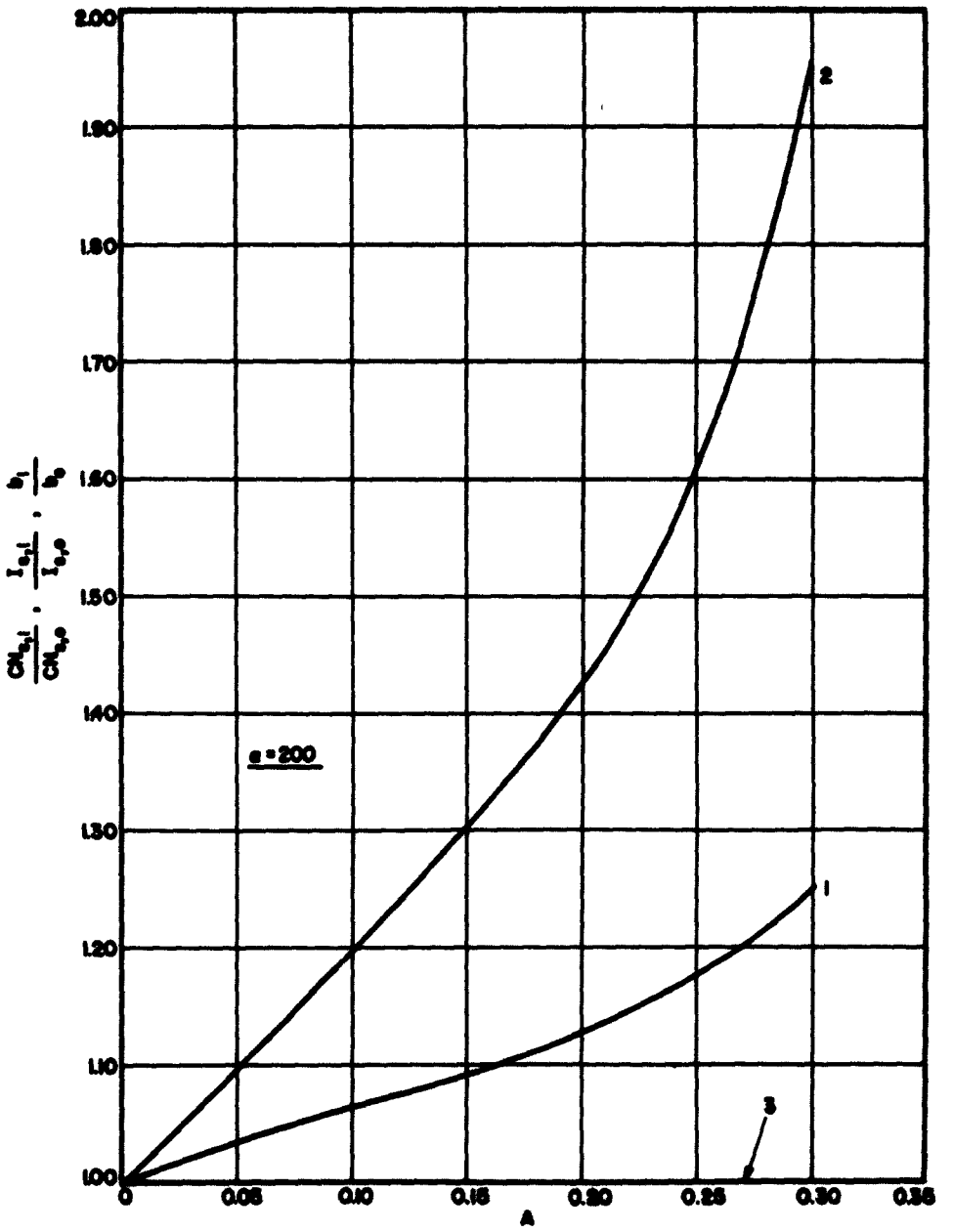

1. $\frac{CN_{s,1}}{CN_{s,o}}$ 2. $\frac{I_{s,1}}{I_{s,o}}$ 3. $\frac{b_1}{b_o}$

FIG. 3.52 $CN_{s,1}/CN_{s,o}$, $I_{s,1}/I_{s,o}$, b_1/b_o VS. A FOR A SINUSOIDAL BEAM POTENTIAL VARIATION. (C = 0.05, QC = 0.5, d = 0)

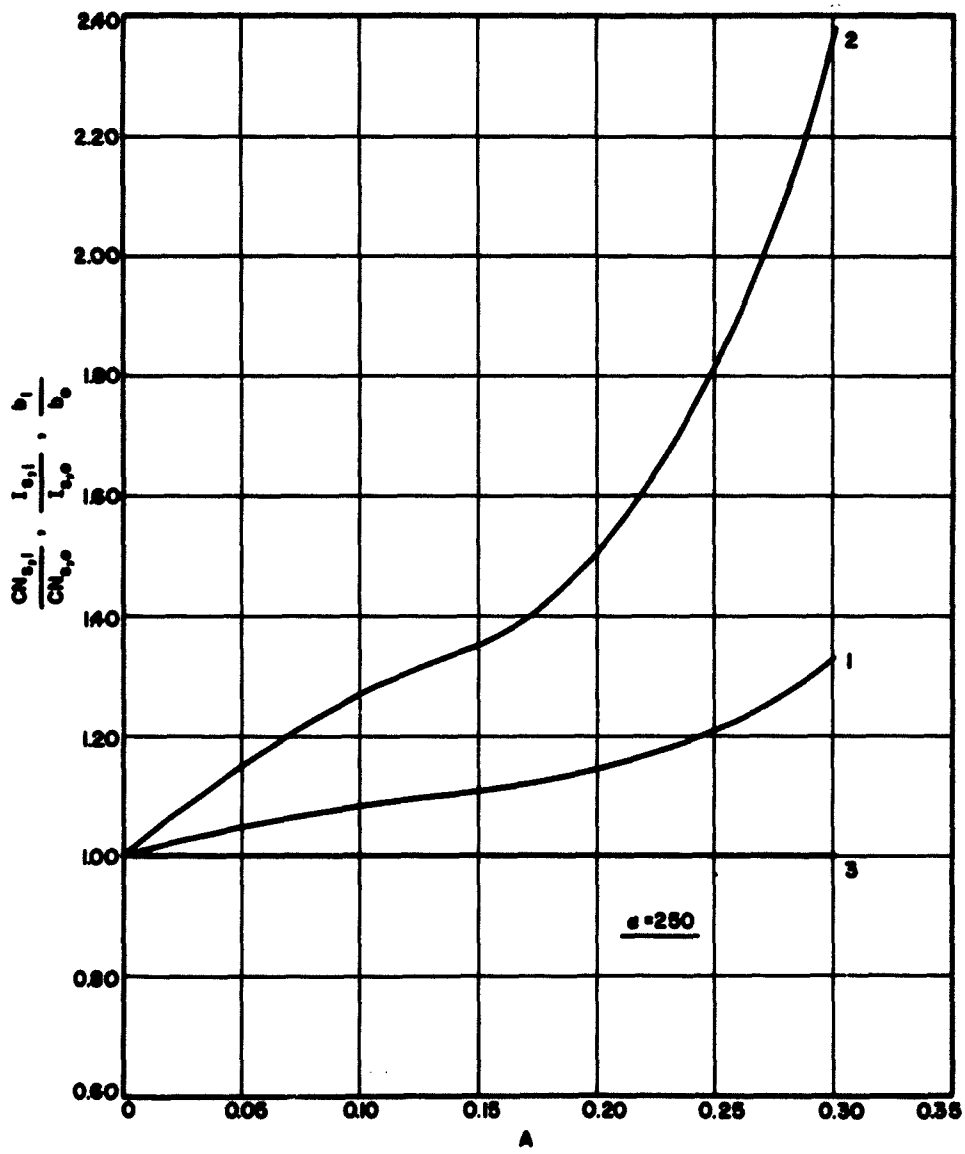

1. $\frac{CN_{s,1}}{CN_{s,o}}$ 2. $\frac{I_{s,1}}{I_{s,o}}$ 3. $\frac{b_1}{b_o}$

FIG. 3.53 $CN_{s,1}/CN_{s,o}$, $I_{s,1}/I_{s,o}$, b_1/b_o VS. A FOR A SINUSOIDAL BEAM POTENTIAL VARIATION. (C = 0.05, QC = 0.5, d = 0)

Since the average beam potential is the same in both tubes, then holding C_o constant means the start-oscillation current is the same in both of them. The start-oscillation length can then be compared as,

$$\frac{z_1}{z_o} = \frac{y_1}{y_o} = \frac{CN_{s,1}}{CN_{s,o}} \quad . \tag{3.99}$$

$CN_{s,1}/CN_{s,o}$ is plotted in the figures. It is seen that for the wide range of cases considered here the increase in the start-oscillation length is slight.

CHAPTER IV. EFFICIENCY OF NONUNIFORM BACKWARD-WAVE OSCILLATORS

4.1 Introduction

In the last two chapters the start-oscillation conditions were determined by employing a linear theory which is valid up to start oscillation. This was valid, since up to start oscillation the r-f signal levels are very small and thus products of a-c quantities could be neglected. Also the hydrodynamical equation of flow was employed which is valid up to start oscillation because the spread in electron velocities up to this point is small compared to the d-c velocity so that all electrons passing a given point can be assumed to have the same velocity.

In an operating* backward-wave oscillator, however, where the r-f fields are appreciable, a nonlinear analysis of the device becomes essential since it is the nonlinearities that ultimately determine the output levels and operating frequency. Due to the severe bunching effects shown theoretically by Sedin[12] and experimentally by Gewartowski[13] the hydrodynamical equation of flow becomes invalid since the spread in electron velocities now becomes appreciable and the possibility of electron trajectory crossing becomes more likely. Thus a nonlinear analysis employing a Lagrangian formulation must be utilized in order to study the characteristics of an operating tube. Rowe[20] and Sedin[12] have utilized such an analysis to study the characteristics of a uniform backward-wave oscillator. In this chapter Rowe's[20] equations are

---

* An operating backward-wave oscillator is one which is operating at currents well above the start-oscillation current.

modified to accommodate a nonuniformity in the circuit phase velocity or the beam potential. The resulting set of nonlinear integro-differential equations are then solved on a digital computer.

4.2 Nonlinear Large-Signal Equations

In the following paragraphs the equations describing the behavior of an operating backward-wave oscillator are derived. The following simplifying assumptions, which aid the treatment of the interaction problem but do not essentially limit the applicability of these equations to a practical situation, are introduced.

1. The problem is restricted to one dimension. Thus the r-f fields are assumed to be uniform in the transverse plane, and no density variations exist within the stream. There is no lateral motion of electrons under these conditions and hence no scalloping of the beam boundary. Such a case is essentially true in a backward-wave oscillator where a thin hollow stream is employed and a strong d-c focusing magnetic field colinear with the stream is employed.

2. The electrons are assumed to enter the slow-wave structure at the same velocity. That is, thermal velocity distribution of the electrons is neglected.

3. The electron velocities are assumed to be very small compared to the velocity of light. Thus nonrelativistic equations are employed. Therefore the magnetic field generated by the electron's own motion is negligible. The effect of the magnetic vector potential can also be neglected and the equations of electrostatics are applicable.

4. The field interaction problem which is actually present here is represented by an equivalent lumped-constant transmission-line model. The inductance and capacitance per unit length of the line are chosen to

match the wave phase velocity and the longitudinal electric field acting on the electrons for the pertinent slow-wave structure to be employed. This is essentially true for a single mode of a structure where the phase velocity is very small compared to the velocity of light. This also adds flexibility to the equations in that it makes the theory more general and applicable to any structure.

With the above assumptions we now proceed to the development of the basic equations.

4.3 The Circuit Equation of a Nonuniform Transmission Line in the Presence of the Stream

This equation has been derived in Section 3.2.1 and is written below for convenience,

$$\frac{\partial^2 V_c(z,t)}{\partial z^2} - \frac{1}{v_o^2(z)} \frac{\partial^2 V_c(z,t)}{\partial t^2} - \left[\frac{1}{Z_o(z)} \frac{dZ_o(z)}{dz} - \frac{1}{v_o(z)} \frac{dv_o(z)}{dz} \right] \frac{\partial V_c(z,t)}{\partial t} - \frac{2\omega C_o(z) d(z)}{v_o^2(z)} \frac{\partial V_c(z,t)}{\partial t}$$

$$= \mp \frac{Z_o(z)}{v_o(z)} \left[\frac{\partial^2 \rho(z,t)}{\partial t^2} + 2\omega C_o(z) d(z) \frac{\partial \rho(z,t)}{\partial t} \right] \quad (4.1)$$

whenever a double sign appears, the top one refers to the forward-wave amplifier and the lower one to the backward-wave oscillator. The quantities appearing in the above equations have already been defined in Section 3.2.1 and will not be repeated here. A similar equation has also been employed by Meeker and Rowe[14] in the forward-wave amplifier study.

4.4 The Force Equation

With the assumptions introduced in Section 4.2 the newton force equation can be written as,

$$\frac{d^2z}{dt^2} = -|\eta| \left[\vec{E}_c(z,t) + \vec{E}_{sc_1}(z,t) + \vec{E}_{d\text{-}c}(z) \right] \tag{4.2a}$$

$$= |\eta| \left[\frac{\partial V_c(z,t)}{\partial z} + \frac{\partial V_{sc_1}(z,t)}{\partial z} + \frac{dV_{d\text{-}c}(z)}{dz} \right] , \tag{4.2b}$$

where

η = the charge-to-mass ratio of an electron, coul./kg.,

$\vec{E}_c(z,t) = -\partial V_c(z,t)/\partial z$ = the r-f circuit field intensity, volts/m,

$\vec{E}_{sc_1}(z,t) = -\partial V_{sc_1}(z,t)/\partial z$ = the space-charge field intensity, volts/m,

$\vec{E}_{d\text{-}c}(z) = -dV_{d\text{-}c}(z)/dz$ = the d-c field, volts/m, and is a measure of the nonuniformity of the d-c beam potential.

4.5 Lagrangian Formulation

4.5.1 Large-Signal Independent Variables and Normalized Coordinates.

In the large-signal operation of the backward-wave oscillator, the electron spread will be appreciable and thus electron groups will have different velocities at different points along the tube. This may lead to electron trajectory crossings, i.e., electrons which enter the tube later overtake those that entered earlier. It is then necessary to introduce a set of independent variables suited to following the individual electron groups along the tube. This is achieved by introducing a new coordinate which is essentially a tag designating, for each electron group, the time at which such a group enters the tube, i.e., t_{o1},

$t_{o2}\ldots,t_{oj}$ are the different times at which electron groups 1,2,...,j enter the tube. This coordinate system was outlined by Rowe[35] where it was employed to describe the behavior of traveling-wave amplifiers. The large-signal variables are illustrated in Fig. 4.1a where four flight-line diagrams are shown. The dashed line represents a fictitious reference trajectory of an electron starting at zero time and position and moving through the tube with constant velocity u_o. Since, as was mentioned above, due to large-signal interactions all electron groups are either speeded up or slowed down and thus acquire different velocities, the velocities of the different electron groups are defined at any position as,

$$\left.\frac{dz}{dt}\right|_{z,t_{oj}} \triangleq u_o[1+2\ C_o u(z,t_{oj})] \quad , \tag{4.3}$$

where u_o = the d-c electron velocity at the entrance to the tube, m/sec. and $2\ C_o u(z,t_{oj})\ u_o$ = the change in velocity of the jth electron due to any of the three forces acting on it; namely, the r-f circuit field, the d-c gradient, and the coulomb forces of the other electrons.

The cold circuit phase velocity which is now a function of distance is defined as follows:

$$v_o(z) \triangleq \frac{u_o}{1+C_o b(z)} \tag{4.4}$$

and it is obvious that any nonuniformity in the cold circuit phase velocity can be introduced through b(z).

The actual wave phase velocity is defined as,

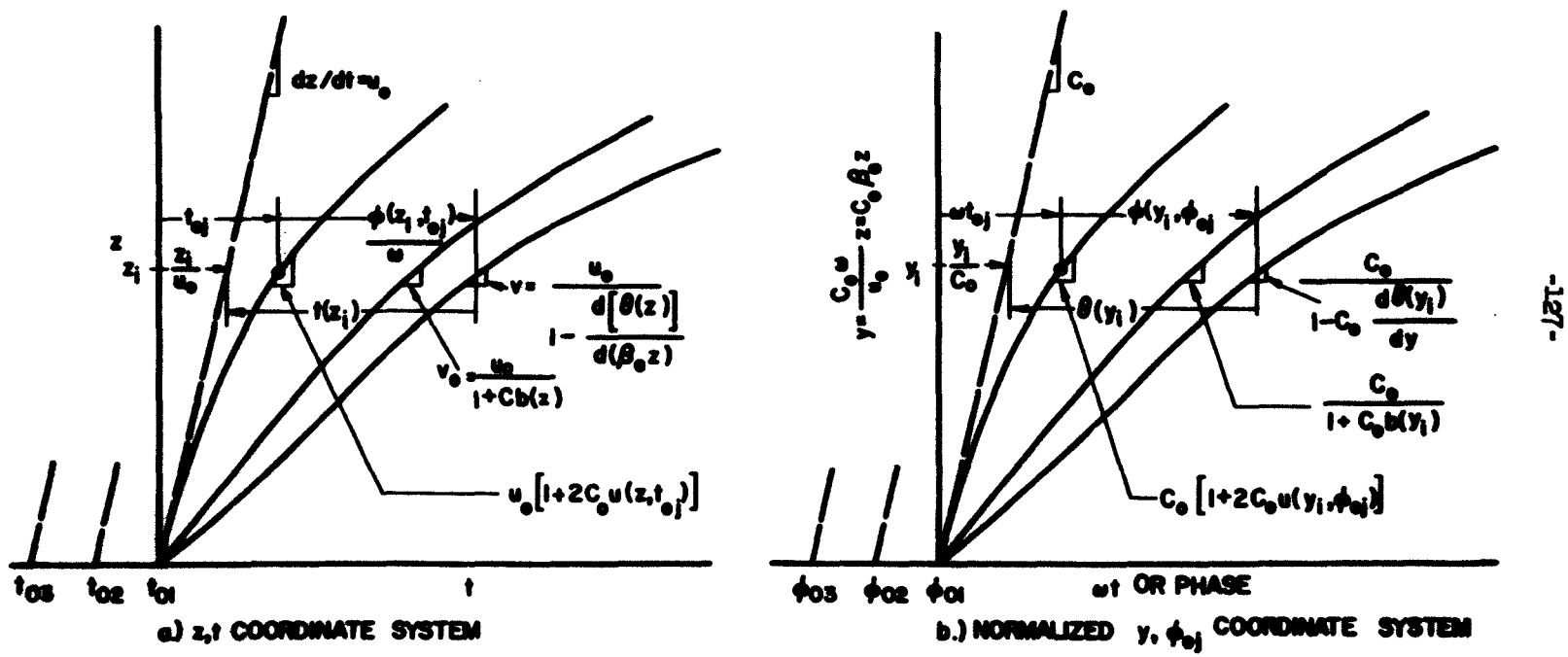

FIG. 4.1 LARGE-SIGNAL FLIGHT-LINE DIAGRAMS.

$$v(z) \triangleq \frac{u_o}{\left[1 - \frac{d\theta(z)}{d(\beta_e z)}\right]} , \tag{4.5}$$

where $\theta(z)$ is the phase lag of the actual r-f wave behind the fictitious reference wave propagating at velocity u_o.

Let us now introduce the following normalized variables,

$$y \triangleq \beta_e C_o z = \frac{\omega}{u_o} C_o z = 2\pi C_o N \tag{4.6}$$

which is a normalized distance, where N = the number of stream wavelengths, and

$$\varphi_{oj} \triangleq \omega t_{oj} \tag{4.7}$$

which is a time-phase of entry.

The newly evolved phase plane is shown in Fig. 4.1b, where the flight lines behave the same as in Fig. 4.1a except for the scale changes.

4.5.2 Large-Signal Dependent Variables. The large-signal dependent variables now then become, $\theta(y)$ which is the phase lag of the actual r-f wave behind the fictitious reference wave propagating at velocity u_o, and the set of $\varphi(y,\varphi_{oj})$'s which specify the phases of the j electrons per r-f cycle relative to the actual wave at position y. Later in the development of the equations a wave solution is assumed and φ will then mean simply the phase of the traveling wave at any point, referred to a reference phase of the wave which is the phase at z = 0 and t = 0. Meanwhile, a basic relationship among the variables can be written down by referring to Fig. 4.1b and summing the phase angles at any fixed distance, y_1. This is,

$$\frac{y_i}{C_o} - \theta(y_i) = \omega t + \varphi(y_i, \varphi_{oj}) \quad . \tag{4.8}$$

4.6 Development of the Working Equations

In this section the working equations are developed in a form which is convenient for solution on a digital computer. Since these equations are very similar to the large-signal forward-wave amplifier equations which have been developed in detail in the literature[35], except for a change in the impedance sign, the development here will be very brief.

4.6.1 Phase Equation. The phase equation is actually a set of equations relating the change of phase of each electron to the electron's velocity and the actual traveling-wave phase velocity. There are as many equations as the number of chosen electron groups per wavelength. It can be written as follows[14,34]:

$$\frac{\partial \varphi(y, \varphi_{oj})}{\partial y} + \frac{d\theta(y)}{dy} = \frac{2u(y, \varphi_{oj})}{1 + 2C_o u(y, \varphi_{oj})} \quad . \tag{4.9}$$

4.6.2 Circuit Equation. Since in this case the periodicity of the transmission system is a function of distance along it, a wave-type solution of the following form is assumed,

$$\begin{aligned} V_c(z,t) &= R_e \left\{ \tilde{V}(z) \exp j \left[\omega t - \int_0^z \beta(z)\, dz \right] \right. \\ &= \tilde{V}(z) \cos \left[\omega t - \int_0^z \beta(z)\, dz \right] \\ &= \tilde{V}(z) \cos [-\varphi(z,t)] \quad , \end{aligned} \tag{4.10}$$

where

$$-\varphi(z,t) = \omega t - \int_0^z \beta(z)\, dz \quad . \tag{4.11}$$

Here $(-\varphi)$ represents the phase angle of the wave relative to a reference phase of the wave which is the phase angle at $z = 0$ and $t = 0$.

Substituting the value of $V_c(z,t)$ from Eq. 4.10 into Eq. 4.1 and arranging results in,

$$\cos(-\varphi)\left[\frac{d^2\tilde{V}(z)}{dz^2} - \beta^2(z)\tilde{V}(z) + \frac{\omega^2}{v_o^2(z)}\tilde{V}(z) \right.$$

$$\left. - \frac{d}{dz} \ln \frac{Z_o(z)}{v_o(z)} \frac{d\tilde{V}(z)}{dz} \right] + \sin(-\varphi)\left[2\beta(z) \frac{d\tilde{V}(z)}{dz} \right.$$

$$+ \tilde{V}(z) \frac{d\beta(z)}{dz} - \frac{d}{dz} \ln \frac{Z_o(z)}{v_o(z)} \tilde{V}(z)\beta(z)$$

$$\left. + \frac{2\omega^2 C_o d(z)}{v_o^2(z)} \tilde{V}(z) \right] = \mp \frac{Z_o(z)}{v_o(z)} \left[\frac{\partial^2 \rho(z,t)}{\partial t^2} \right.$$

$$\left. + 2\omega C_o(z) d(z) \frac{\partial \rho(z,t)}{\partial t} \right] \quad . \tag{4.12}$$

The space-charge density $\rho(z,t)$ is next expanded in a Fourier series in the phase dimension as follows:

$$\rho(z,t) = \sum_{n=1}^{\infty} A_n \cos n(-\varphi) + B_n \sin n(-\varphi) \quad , \tag{4.13}$$

where

$$n(-\varphi) = n\omega t - \int_0^z n\beta(z)\, dz \quad , \tag{4.14}$$

$$A_n = \frac{1}{\pi} \int_0^{2\pi} \rho(z,t) \cos n(-\varphi) d\varphi(z,t) \quad , \tag{4.15}$$

$$B_n = \frac{1}{\pi} \int_0^{2\pi} \rho(z,t) \sin n(-\varphi) d\varphi(z,t) \quad . \tag{4.16}$$

The above expansion is equivalent to a frequency expansion which expresses the harmonic content of a bunched beam. It is assumed here that the induced voltage on the circuit is limited to the fundamental frequency, so that $\rho(z,t)$ on the right-hand side of Eq. 4.12 becomes just,

$$\rho(z,t) = A_1 \cos(-\varphi) + B_1 \sin(-\varphi) \quad , \tag{4.17}$$

where A_1 and B_1 are given by Eqs. 4.15 and 4.16.

Substituting Eq. 4.17 into 4.12 and equating the coefficients of $\sin(-\varphi)$ and $\cos(-\varphi)$ on both sides of the equation results in the following two equations:

$$\frac{d^2\tilde{V}(z)}{dz^2} - \tilde{V}(z)\left[\beta^2(z) - \frac{\omega^2}{v_o^2(z)}\right] - \frac{d}{dz} \ln \frac{Z_o(z)}{v_o(z)} \frac{d\tilde{V}(z)}{dz}$$

$$= \mp \frac{Z_o(z)}{v_o(z)} \omega^2 \frac{1}{\pi} \int_0^{2\pi} \rho[z,\varphi(z,t)] \cos(-\varphi) d\varphi$$

$$\mp 2\omega^2 C_o(z)\, d(z) \frac{Z_o(z)}{v_o(z)} \frac{1}{\pi} \int_0^{2\pi} \rho[z,\varphi(z,t)] \sin(-\varphi) d\varphi \quad , \tag{4.18}$$

$$2\,\beta(z)\,\frac{d\tilde{V}(z)}{dz} + \tilde{V}(z)\,\frac{d\beta(z)}{dz} - \frac{d}{dz}\,\ell n\,\frac{Z_o(z)}{v_o(z)}\,\beta(z)\,\tilde{V}(z)$$

$$+\frac{2\,\omega^2\,C_o(z)\,d(z)}{v_o^2(z)}\,\tilde{V}(z) \;=\; \pm\,\frac{Z_o(z)}{v_o(z)}\,\omega^2\,\frac{1}{\pi}\int_0^{2\pi}\rho[z,\varphi(z,t)]\,\sin(-\varphi)d\varphi$$

$$\pm\,2\,\omega^2\,C_o(z)d(z)\,\frac{Z_o(z)}{v_o(z)}\,\frac{1}{\pi}\int_0^{2\pi}\rho[z,\varphi(z,t)]\,\cos(-\varphi)d\varphi\;. \qquad (4.19)$$

The space-charge density must now be expressed in terms of the Lagrangian variables. This can be achieved by considering the conservation of charge so that the following expression can be written down,

$$\rho(z,t)\;dz \;=\; \rho(0,0)dz_o \;=\; \frac{I_o}{u_o}\,dz_o \quad , \qquad (4.20)$$

where I_o is a negative quantity defined as $I_o = \rho(0,0)u_o$. Introducing the normalized and Lagrangian variables into the above equations results in[14,34]

$$\rho(z,t) \;=\; \rho(y,\varphi) \;=\; \frac{I_o}{u_o}\,\frac{d\varphi_o}{[1+2C_o u(y,\varphi_{oj})]d\varphi} \quad . \qquad (4.21)$$

The following quantity is now defined,

$$A(y) \;\triangleq\; \frac{C_o\tilde{V}(y)}{I_o Z_o} \quad . \qquad (4.22)$$

With this definition the ratio of the r-f power at any point y to the stream d-c power can now be expressed approximately as[34],

$$\frac{\text{Ratio of r-f power}}{\text{d-c power}} \;=\; 2\,C_o\,A^2(y) \quad . \qquad (4.23)$$

Substituting Eqs. 4.21 and 4.22 in Eqs. 4.18 and 4.19 and introducing the normalized variables we finally obtain the following two circuit working equations,

$$\frac{d^2A(y)}{dy^2} - A(y)\left[\left(\frac{1}{C_o} - \frac{d\theta(y)}{dy}\right)^2 - \left(\frac{1+C_o b(y)}{C_o}\right)^2\right] - \frac{dA(y)}{dy}$$

$$\left[\frac{d}{dy}\ln\frac{Z(z)}{Z_o} + \frac{C_o}{1+C_o b(y)}\frac{db(y)}{dy}\right] = \mp\left(\frac{Z(y)}{Z_o}\right)\frac{1+C_o b(y)}{\pi C_o}$$

$$\left[\int_0^{2\pi}\frac{\cos\varphi(y,\varphi'_{oj})d\varphi'_{oj}}{1+2C_o u(y,\varphi'_{oj})} + 2C_o d(y)\int_0^{2\pi}\frac{\sin\varphi(y,\varphi'_{oj})d\varphi'_{oj}}{1+2C_o u(y,\varphi'_{oj})}\right], \qquad (4.24)$$

$$A(y)\left[\frac{d^2\theta(y)}{dy^2} - \left(\frac{d\theta(y)}{dy} - \frac{1}{C_o}\right)\left(\frac{d}{dy}\ln\frac{Z(y)}{Z_o} + \frac{C_o}{1+C_o b(y)}\frac{db(y)}{dy}\right)\right.$$

$$\left. - \frac{2d(y)}{C_o}[1+C_o b(y)]^2\right] + 2\left[\frac{d\theta(y)}{dy} - \frac{1}{C_o}\right]\frac{dA(y)}{dy}$$

$$= \mp\frac{Z(y)}{Z_o}\left(\frac{1+C_o b(y)}{\pi C_o}\right)\left[\int_0^{2\pi}\frac{\sin\varphi(y,\varphi'_{oj})d\varphi'_{oj}}{1+2C_o u(y,\varphi'_{oj})}\right.$$

$$\left. - 2C_o d(y)\int_0^{2\pi}\frac{\cos\varphi(y,\varphi'_{oj})d\varphi'_{oj}}{1+2C_o u(y,\varphi'_{oj})}\right]. \qquad (4.25)$$

Wherever a double sign appears in the above equations the top one refers to the forward-wave amplifier and the lower one to the backward-wave oscillator.

4.6.3 The Force Equation. The development of the force equation is straightforward. The form of the space-charge field employed here is that derived by Rowe[34]. In this method the force on a particular electron due to all other electrons was calculated under the assumption that all electrons were at a position y but each had a different phase. This method is consistent with the manner in which the problem was integrated, and the equivalence of this method to that employed by Tien[36] has been illustrated by Rowe[37] in another paper. In that paper good agreement was obtained between the nonlinear TWA performance using the above method and Tien's method. Both authors essentially utilize the electron distribution in time in place of the actual space distribution.

Substituting the normalized variables and Lagrangian coordinates in the force equation (Eq. 4.2) results in,

$$\frac{\partial u(y,\varphi_{oj})}{\partial y} = \left[- A(y)\left(1 - C_o \frac{d\theta(y)}{dy}\right) \sin \varphi(y,\varphi_{oj}) \right.$$

$$\left. + C_o \frac{dA(y)}{dy} \cos \varphi(y,\varphi_{oj}) \right] = C_o \frac{dA_{d-c}(y)}{dy}$$

$$+ \frac{1}{[1+C_o b_o(y)]} \left(\frac{\omega_p}{\omega C_o}\right)^2 \int_0^{2\pi} \frac{F[\varphi(y,\varphi_{oj}) - \varphi'_{ok}]d\varphi'_{ok}}{1+2C_o u(y,\varphi'_{ok})} \quad . \quad (4.26)$$

The following definitions have been employed in the above equations,

$v_o(y)$ = cold circuit phase velocity,

$v(y)$ = actual phase velocity,

$$\frac{u_o}{v_o(y)} \triangleq 1 + C_o b(y) \quad ,$$

$$\frac{u_o}{v(y)} \triangleq 1 - C_o \frac{d\theta(y)}{dy} \quad .$$

and $A_{d\text{-}c}(y) = C_o V_{d\text{-}c}(y)/I_o Z_o$.

4.7 Discussion of the Working Equations and Boundary Conditions

In the development of the above equations a single-wave solution was assumed. For this to hold exactly the transmission-line characteristic impedance must be uniform. However, if the nonuniformity varies very slowly with distance, which is the case here, the above wave solution is approximately correct. Also the characteristic impedance of the transmission line was replaced by the interaction impedance. This is a good approximation for slow waves. For slow waves the two impedances are related as follows[3]:

$$Z_{int.} = \left[1 - \left(\frac{v}{c}\right)^2\right] Z_o \quad . \tag{4.27}$$

The independent variables in the above equations are y and φ_{oj}. The dependent variables are A(y), $\varphi(y,\varphi_{oj})$ and $u(y,\varphi_{oj})$. The boundary conditions can now be represented as follows:

1. The electrons are assumed to enter the interaction region with no modulation (unless the beam is prebunched). This results in

$$u(0,\varphi_{oj}) = 0 \quad . \tag{4.28}$$

2. The initial phases of the entering particles are uniformly spaced. This yields

$$\varphi_{oj} = \frac{2\pi j}{n} , \tag{4.29}$$

where n is the total number of electron groups chosen per r-f cycle. The value of n chosen in later computations is 32.

3. $\theta(0) = 0$.

4. A(0) is arbitrarily chosen and a trial and error procedure is employed to find the correct A(0) for different operating conditions.

5. The boundary conditions $dA(y)/dy\big|_{y=0}$ and $d\theta(y)/dy\big|_{y=0}$ can be easily obtained by considering Eq. 3.2, namely,

$$\frac{\partial V_c(z,t)}{\partial z} = - L(z) \frac{\partial I_c(z,t)}{\partial t} - I_c R(z) . \tag{4.30}$$

The characteristic impedance of the line Z at z = 0 can be expressed as,

$$Z_o = \frac{\bar{V}_c(0)}{\bar{I}_c(0)} . \tag{4.31}$$

Equation 4.30 can then be expressed as follows,

$$\frac{\partial V_c(z,t)}{\partial z}\bigg|_{z=0} = - V_c(0)\left[j \frac{\omega}{v_o(0)} - \frac{2\pi C_o d(0)}{v_o(0)}\right] . \tag{4.32}$$

However, from Eq. 4.10 we have,

$$V_c(z,t) = \bar{V}(z) \cos[-\varphi(z,t)] . \tag{4.33}$$

By differentiating Eq. 4.33 with respect to z and evaluating it at z = 0, we get,

$$\frac{\partial V_c(z,t)}{\partial t}\bigg|_{z=0} = - j \bar{V}_c(0)\beta(0) \cos(-\varphi) + \frac{d\bar{V}(z)}{dz}\bigg|_{z=0} \cos(-\varphi) . \tag{4.34}$$

Equating the real and imaginary parts of Eqs. 4.32 and 4.34 gives

$$\beta(0) = \frac{\omega}{v_o(0)} = \beta_o(0) \tag{4.35}$$

and

$$\left.\frac{d\bar{V}(z)}{dz}\right|_{z=0} = 2\beta_o(0)C_o d(0)V_c(0) \quad , \tag{4.36}$$

dividing Eq. 4.35 by β_e yields

$$\frac{\beta(0)}{\beta_e} = 1 - C_o \left.\frac{d\theta}{dy}\right|_{y=0} = \frac{\beta_o(0)}{\beta_e} = 1 + C_o b(0) \tag{4.37}$$

and thus

$$\left.\frac{d\theta}{dy}\right|_{y=0} = - b(0) \quad . \tag{4.38}$$

Introducing the normalized variable y into Eq. 4.36 results in,

$$\left.\frac{dA(y)}{dy}\right|_{y=0} = 2[1 + C_o b(0)]d(0)A(0) \quad , \tag{4.39}$$

where as mentioned above A(0) is arbitrary.

The working equations have been programmed on a digital computer and solved for different operating parameters. A detailed discussion of the solution of these equations on the digital computer can be found in the literature[36] and will not be included here.

4.8 Phase Focusing in O-Type Backward-Wave Devices

The idea of phase focusing has been successfully applied to the forward-wave amplifier[14]. There a considerable enhancement in the

efficiency of the device was obtained. Since the operation of "O-type" forward and backward devices is similar in several respects, the application of phase focusing to backward-wave devices is investigated here.

An understanding of phase focusing in backward-wave devices is facilitated by examining the phase and velocity of the electron groups at different positions along the tube. It should be recalled that the output in a backward-wave device is at y = 0. Figures 4.2 and 4.3 illustrate the velocity versus phase for the different electron groups (32 in total) in a uniform tube, and a tapered tube respectively. A plot of the r-f amplitudes as a function of normalized distance y is shown in Fig. 4.4. It can be seen from Fig. 4.2 that the electrons all start out with the same velocity u_o and the phases at y = 0 are uniformly distributed over the period of the r-f cycle so that at y = 0, $\varphi_{oj} = 2\pi j/n$, where n is the total number of electron groups chosen. It is thus seen that at y = 0, half of the electron groups are in a decelerating phase and the other half in an accelerating phase. The velocity versus phase diagram also shows that at points farther down the tube more electrons are in the decelerating than the accelerating phase and on the average more electrons are decelerated and thus kinetic energy is converted into r-f energy. However at a certain y position the electron groups start to slip back into the accelerating phase and thus on the average the electrons start to gain energy from the r-f wave. Up to this point the r-f field is decreasing with distance (see Fig. 4.4) but it starts to increase with distance when more electron groups are present in the accelerating phase than the decelerating phase. This situation can be alleviated somewhat by trying to keep the electrons in a favorable decelerating phase and thus extract more energy from them.

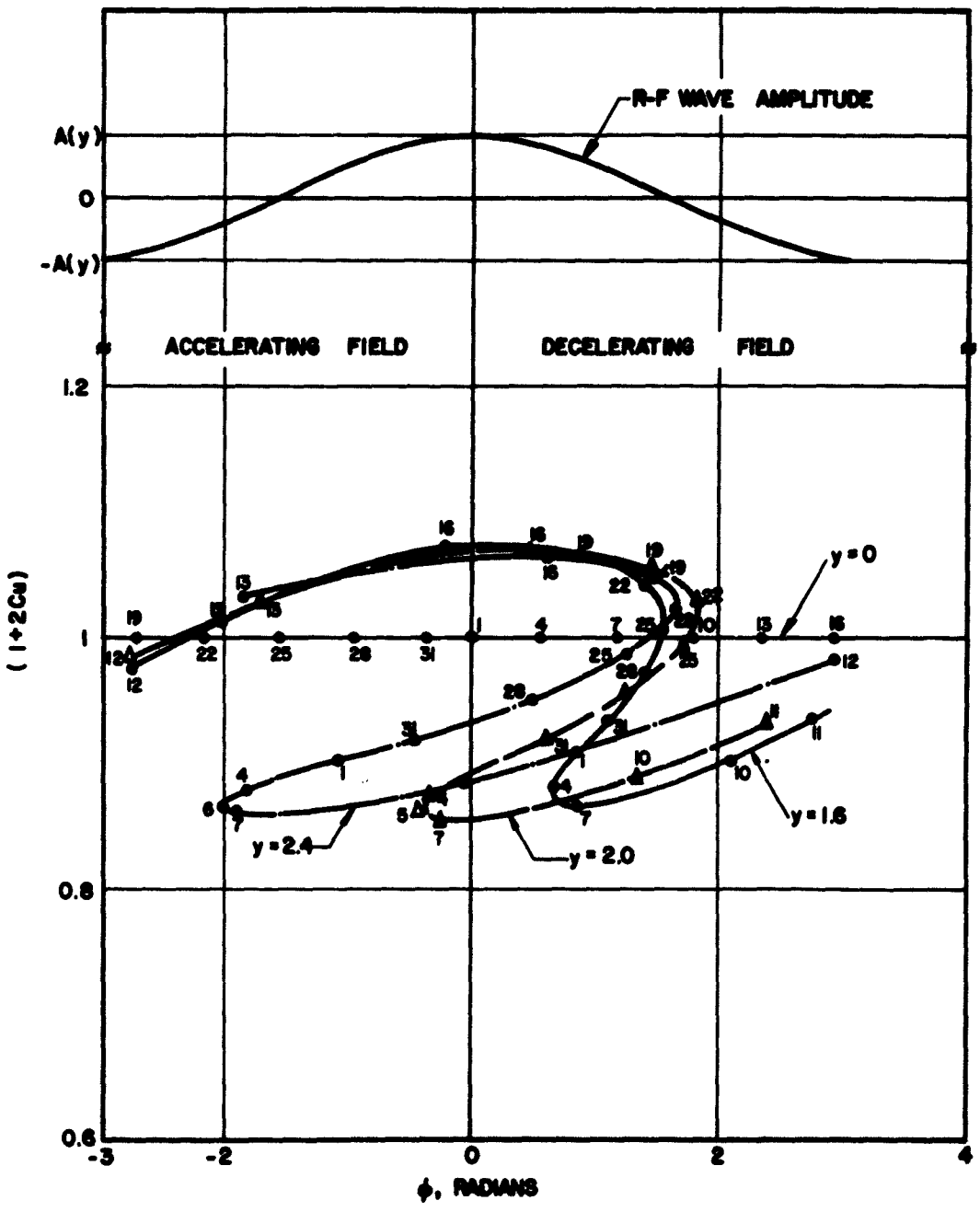

FIG. 4.2 (1 + 2Cu) VS. φ AT DIFFERENT y POSITIONS FOR A UNIFORM TUBE. (C = 0.05, b = 1.625, QC = 0)

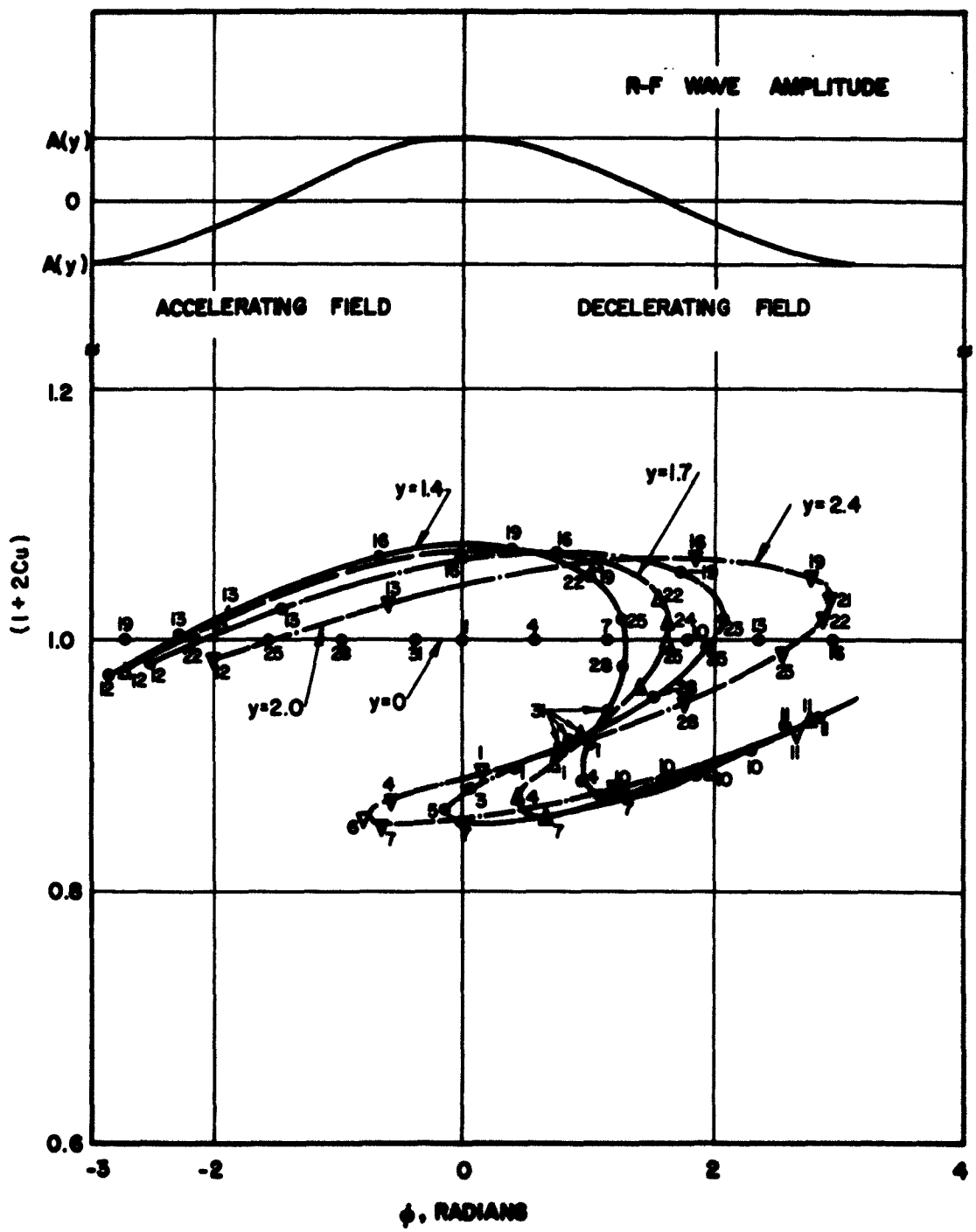

FIG. 4.3 (1 + 2Cu) VS. φ AT DIFFERENT y POSITIONS FOR A TAPERED TUBE; TAPER STARTS AT y = 1.7.

(C = 0.05, b = 1.625, QC = 0)

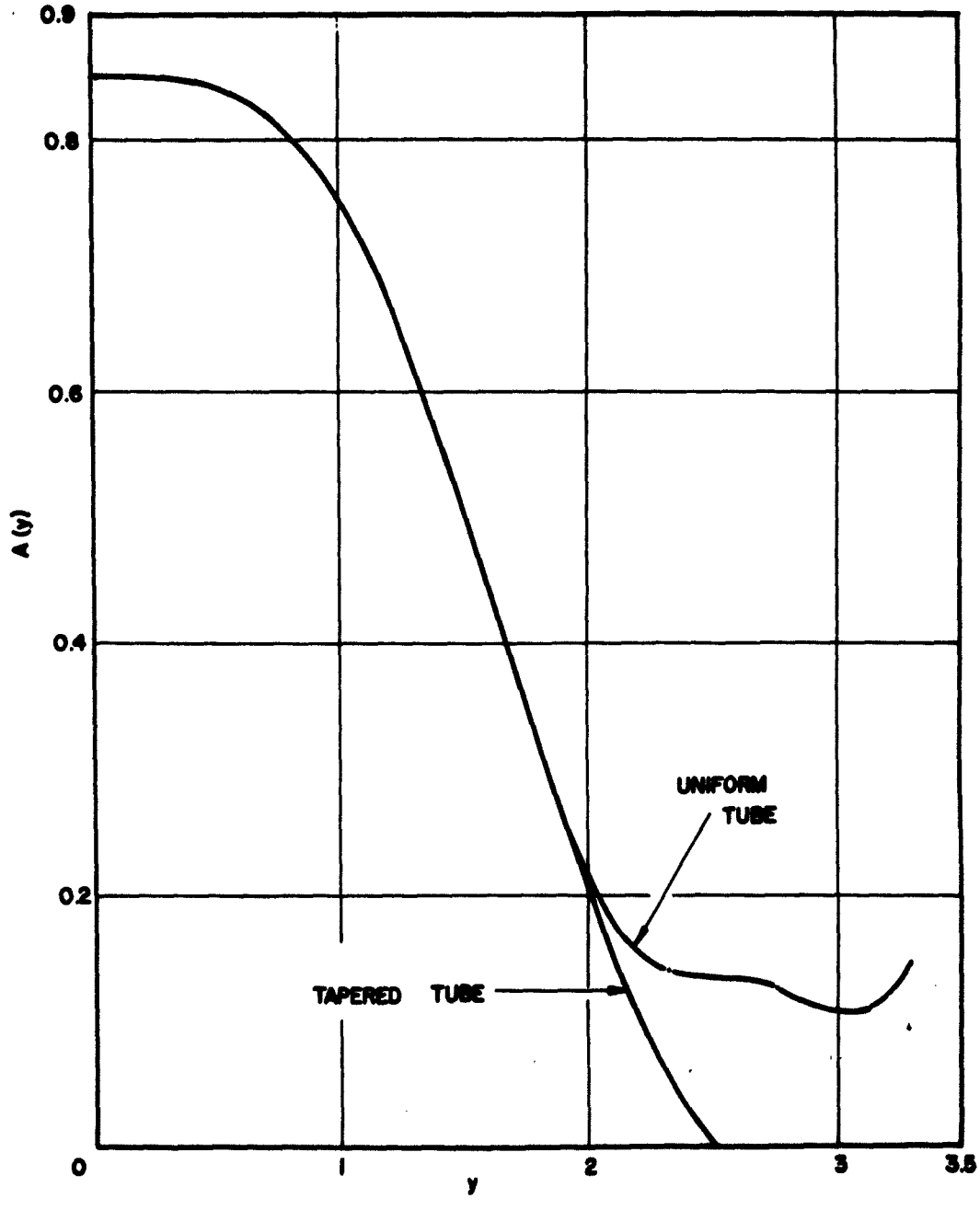

FIG. 4.4 A(y) VS. y FOR UNIFORM AND TAPERED TUBES. TAPER STARTS AT y = 1.7. (C = 0.05, b_o = 1.625, QC = 0)

This can be achieved by either of two methods[14], the first employs a circuit phase velocity taper and the other a d-c voltage gradient. Figure 4.3 illustrates the phase-focusing criteria using a circuit phase velocity taper. This figure is similar to Fig. 4.2 for a uniform tube, but it is seen here that the electrons are kept in a favorable decelerating phase and thus more kinetic energy is extracted from the beam. The normalized r-f voltage amplitude is plotted as a function of y for the two cases in Fig. 4.4. The input r-f power in each case would correspond to the minimum value of A(y) and the output r-f power correspond to the value of A(y) at y = 0. The efficiency η can be expressed as

$$\eta = 2C_o[A^2(0) - A^2_{min}(y)] \quad . \tag{4.40}$$

Since a circuit phase velocity taper is more practical and much easier to achieve than a d-c gradient it is considered in detail in the following section.

4.9 Circuit Phase Velocity Tapers for Phase Focusing

By examining the velocity versus phase diagrams of Figs. 4.2 and 4.3 it can be appreciated that due to the difference of phase of the electron groups, a certain circuit phase velocity taper which is applied to keep a certain group of electrons in a favorable phase might tend to defocus other electron groups. Had it not been for the difference in phase among the electron groups, i.e., if all the electron groups were at one phase angle relative to the r-f wave, then a circuit velocity taper can be developed to keep the electron group at this phase angle and thus extract all the kinetic energy from it. Since at some point down the tube the electron beam becomes "bunched" and the spread in phase is not as great as it is at the beginning of the tube, the velocity taper should

be applied at some point down the tube at which the phase difference among electrons is smallest.

In order to obtain some guideline as to what form the circuit taper must take, a hypothetical situation where all the electron groups are assumed to have the same phase with respect to the r-f wave and the same velocity is assumed. This of course results in one "big" electron at a certain phase angle φ_f. This kind of approximation is referred to as the "hard-kernel-bunch" approximation which was employed by Meeker and Rowe[14] for phase focusing in forward-wave amplifiers. Under this approximation circuit phase velocity tapers can be developed which keep this "big" electron in a favorable phase and thus extract all the kinetic energy from it. These approximate velocity tapers can then be applied to realistic situations where the electron phases and velocities are different, but with their weighted average phase and velocity corresponding to that of the "big" electron.

4.9.1 Circuit Phase Velocity Tapers Under Hard-Kernel-Bunch Approximation. Under this approximation the phase Eq. 4.9, and the force Eq. 4.26, equations which are actually a set of equations containing as many equations each as the number of electron groups chosen, now reduce to one equation each.

Since the electron phase angle φ_f is now forced to stay constant along the tube, the phase equation reduces to,

$$\frac{d\theta(y)}{dy} = \frac{2\,u(y,\varphi_f)}{1+2C_o u(y,\varphi_f)} \quad . \tag{4.41}$$

Equation 4.41 can be easily transformed into the following form,

$$\frac{u_o}{1 - C_o \frac{d\theta(y)}{dy}} = u_o[1 + 2 C_o u(y,\varphi_f)] \quad , \tag{4.42}$$

which actually says that in order to keep the electron at a constant phase, the electron velocity and the actual wave phase velocity must be equal; a result which is intuitively obvious.

The following quantities are now defined:

$$x(y) \triangleq [1 + 2 C_o u(y,\varphi_f)] \tag{4.43}$$

and

$$q(y) \triangleq \frac{v_o(y)}{u_o} = \frac{1}{1 + C_o b(y)} \quad . \tag{4.44}$$

Neglecting space-charge effects and the d-c gradient and utilizing Eqs. 4.42 through 4.44, the force equation reduces to

$$\frac{dx(y)}{dy} = - \frac{2 C_o A(y)}{x^2(y)} \sin \varphi_f + \frac{2 C_o^2}{x(y)} \frac{dA(y)}{dy} \cos \varphi_f \quad , \tag{4.45}$$

Neglecting circuit loss, the first of the circuit equations, (Eq. A.24) now becomes,

$$\frac{d^2A(y)}{dy^2} - A(y)\left[\left(\frac{1}{C_o} - \frac{d\theta(y)}{dy}\right)^2 - \left(\frac{1+C_o b(y)}{C_o}\right)^2\right]$$

$$- \frac{dA(y)}{dy}\left[\frac{d}{dy}\ln\frac{Z_o(y)}{Z_o} + \frac{C_o}{1+C_o b(y)}\frac{db(y)}{dy}\right]$$

$$= \mp\left(\frac{Z_o(y)}{Z_o}\right)\frac{[1+C_o b(y)]\cos\varphi_f}{\pi C_o[1+2C_o u(y,\varphi_f)}\int_0^{2\pi} d\varphi_o' \qquad (4.46)$$

and the second circuit equation (Eq. 4.25) becomes,

$$A(y)\left[\frac{d^2\theta(y)}{dy^2} - \left(\frac{d\theta(y)}{dy} - \frac{1}{C_o}\right)\left(\frac{d}{dy}\ln\frac{Z_o(y)}{Z_o}\right.\right.$$

$$\left.\left. + \frac{C_o}{1+C_o b(y)}\frac{db(y)}{dy}\right)\right] + 2\left[\frac{d\theta(y)}{dy} - \frac{1}{C_o}\right]\frac{dA(y)}{dy}$$

$$= \mp\frac{Z_o(y)}{Z_o}\left(\frac{1+C_o b(y)}{\pi C_o}\right)\frac{\sin\varphi_f}{1+2C_o u(y,\varphi_f)}\int_0^{2\pi} d\varphi_o' \quad . \qquad (4.47)$$

Whenever a double sign appears the top one refers to a forward-wave amplifier and the bottom one to a backward-wave device.

By employing Eqs. 4.42 through 4.44 and arranging, Eq. 4.46 can be written in the following form,

$$\frac{d^2A(y)}{dy^2} - \frac{A(y)}{C_o^2}\left[\frac{1}{x^2} - \frac{1}{q^2}\right] - \frac{dA(y)}{dy}\left[\frac{d}{dy} \ln \frac{Z_o(y)}{Z_o} - \frac{1}{q(y)} \frac{dq(y)}{dy}\right]$$

$$= \mp \left(\frac{Z_o(y)}{Z_o}\right) \frac{2 \cos - \varphi_f}{C_o x(y) q(y)} \quad (4.48)$$

and Eq. 4.47 becomes

$$\frac{dA(y)}{dy} = \pm \frac{Z(y)}{Z_o} \frac{\sin \varphi_f}{q(y)} + A(y)\left[\frac{1}{2x(y)} \frac{dx(y)}{dy}\right.$$

$$\left. + \frac{1}{2}\left(\frac{d}{dy} \ln \frac{Z_o(y)}{Z_o} - \frac{1}{q(y)} \frac{dq(y)}{dy}\right)\right] . \quad (4.49)$$

Equations 4.45, 4.48 and 4.49 were solved on a digital computer for one representative case where $Z_o(y)$ was assumed equal to Z_o and a value of $C_o = 0.05$ and $\varphi_f = \pi/2$ were chosen. The result is shown in Fig. 4.5 where it is compared to the result from an approximate solution for the same parameters. It is seen there that the agreement is excellent. The approximate solution of the above equations follows.

4.9.2 Approximate Velocity Profiles for Tapered Backward-Wave Oscillators. In this section the cold circuit phase velocity is assumed to be equal to the actual wave phase velocity which as was shown above is equal to the phase-focused electron velocity. This is a very good approximation for small values of C_o which is the usual case in a backward-wave oscillator. This of course makes $x(y) = q(y)$ in the equations of the preceding section. Under this assumption, and neglecting terms containing C_o^2 since they will be very small, Eq. 4.45 reduces to,

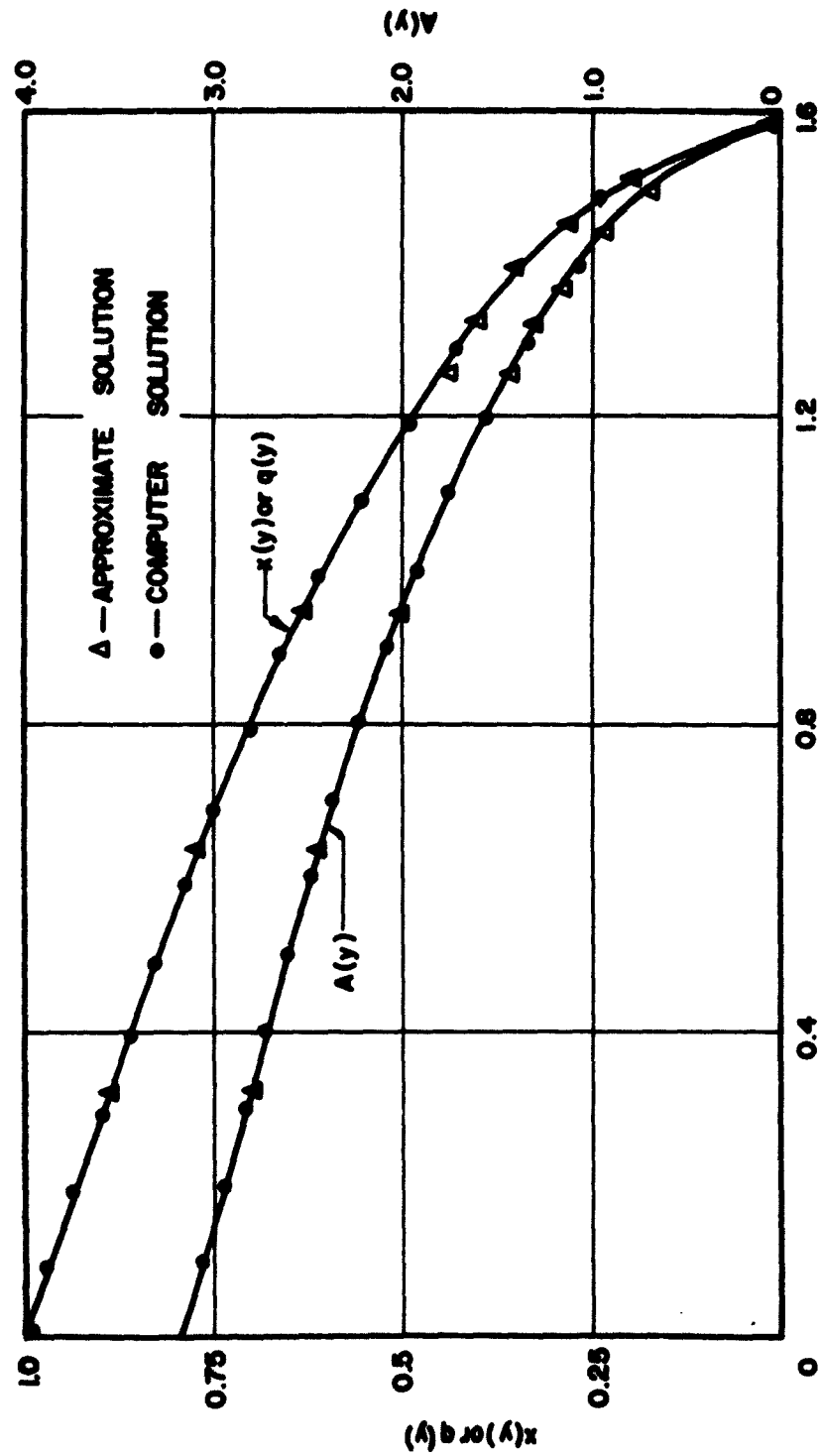

FIG. 4.5 COMPARISON OF EXACT AND APPROXIMATE SOLUTIONS FOR DETERMINING THE CIRCUIT PHASE VELOCITY VARIATION FOR A HARD-KERMEL-BUNCH APPROXIMATION.

($C_o = 0.05$, $QC = 0$, $d = 0$, $z_o(y) = z_o$, $\varphi_f = \pi/2$)

$$\frac{dx(y)}{dy} = -\frac{2\,C_o A(y)}{x^2(y)} \sin \varphi_f \qquad (4.50)$$

and Eq. 4.49 becomes

$$\frac{dA(y)}{dy} = \pm \frac{Z_o(y)}{Z_o} \frac{\sin \varphi_f}{x(y)} + \frac{A(y)}{2} \frac{1}{Z_o(y)} \frac{dZ_o(y)}{dy} \quad . \qquad (4.51)$$

From Eq. 4.50 we can write

$$\frac{\sin \varphi_f}{x(y)} = -\frac{1}{2\,C_o A(y)} x(y) \frac{dx(y)}{dy} \quad . \qquad (4.52)$$

Substituting Eq. 4.52 into 4.51 and arranging results in,

$$2\,C_o \frac{d}{dy}\left[\frac{Z_o}{Z_o(y)} A^2(y)\right] = \mp \frac{dx^2(y)}{dy} \quad . \qquad (4.53)$$

Integrating Eq. 4.53 gives

$$2\,C_o \frac{Z_o}{Z_o(y)} A^2(y) = \mp x^2(y) + k \quad , \qquad (4.54)$$

where k is the integration constant. The boundary conditions at y = 0 are $A(0) = A_o, Z_o(0) = Z_o$ and x(0) = 1. Substituting these in Eq. 4.54 we find,

$$k = 2\,C_o A_o^2 \pm 1 \quad . \qquad (4.55)$$

Substituting in Eq. 4.54 we get

$$2\,C_o \frac{Z_o}{Z_o(y)} A^2(y) = \mp x^2(y) + 2\,C_o A_o^2 \pm 1 \quad . \qquad (4.56)$$

This is essentially a statement of energy conservation. It represents the fact that the r-f power gained is equal to the kinetic power lost by the electron.

Solving for A(y) from Eq. 4.56 we obtain,

$$A(y) = \sqrt{\frac{Z_o(y)}{2C_oZ_o}\left[\mp x^2(y) + 2C_o A_o^2 \pm 1\right]} \quad . \tag{4.57}$$

Substituting this value of A(y) in Eq. 4.50 and arranging yields

$$\sqrt{2C_o}\,\sin\varphi_f\,dy = -\frac{x^2(y)\,dx(y)}{\sqrt{\frac{Z_o(y)}{Z_o}\left[2C_oA_o^2 \pm 1 \mp x^2(y)\right]}} \quad . \tag{4.58}$$

When $Z_o(y)$ is specified the above equation can be solved for x(y) which gives the required taper to achieve phase focusing. Since the main concern here is the backward-wave oscillator the solution of the above equation will be obtained for different variations in $Z_o(y)$. Before this is done, however, a few words about velocity tapers in forward-wave amplifiers are in order here.

Meeker and Rowe[14,36] have derived tapers for forward-wave amplifiers which are specialized to a focusing angle $\varphi_f = 90°$. Equation 4.58 applies to a forward-wave amplifier, with the same assumptions as those of theirs, when the top sign in this equation is considered. It can thus be seen that the above restriction, namely $\varphi_f = 90°$ is not necessary because the tapers can be obtained for any φ_f by a slight modification. This modification is the inclusion of sin φ_f in the equation. The only effect this has on the tapers derived by Meeker and Rowe is to change the abscissa scale in their figures from $\sqrt{2C_o}\,y$ to $\sqrt{2C_o}\,y \sin\varphi_f$.

This makes the tapers applicable to any phase focusing angle and thus makes the tapers general.

We now turn to the main concern here which is the backward-wave oscillator. The velocity tapers in this case are obtained for two variations of $Z_o(y)$ as follows:

Case A. Constant Impedance in the Nonuniform Region. This case is a good approximation for a tube where a thin hollow beam moving very close to the slow-wave structure is employed. We then have here, $Z_o(y) = Z_o$ and Eq. 4.58 applied to a backward-wave oscillator now becomes,

$$\sqrt{2\,C_o}\,\sin\varphi_f\,dy = -\frac{x^2(y)\,dx(y)}{\sqrt{[2\,C_o\,A_o^2 - 1 + x^2(y)]}} \quad . \tag{4.59}$$

Integrating Eq. 4.59 we obtain,

$$\sqrt{2\,C_o}\,y\,\sin\varphi_f = \frac{1}{2}\left[\sqrt{2\,C_o\,A_o^2}\,-\,x(y)\,\sqrt{(2\,C_o\,A_o^2 - 1) + x^2(y)}\,\right]$$

$$+\,\frac{2\,C_o\,A_o^2 - 1}{2}\left[\ln\frac{x(y) + \sqrt{2\,C_o\,A_o^2 - 1) + x^2(y)}}{1 + \sqrt{2\,C_o\,A_o^2}}\right] \quad . \tag{4.60}$$

$x(y) = q(y)$ is plotted as a function of $\sqrt{2\,C_o}\,y\,\sin\varphi_f$ for different values of $2\,C_o\,A_o^2$ in Fig. 4.6.

Case B. Realistic Impedance Variation. A realistic impedance variation can be prescribed when the fields for the slow-wave structure are known. For a tape helix which is widely used in backward-wave oscillators, such an impedance variation can be estimated by reference to the paper by Ash

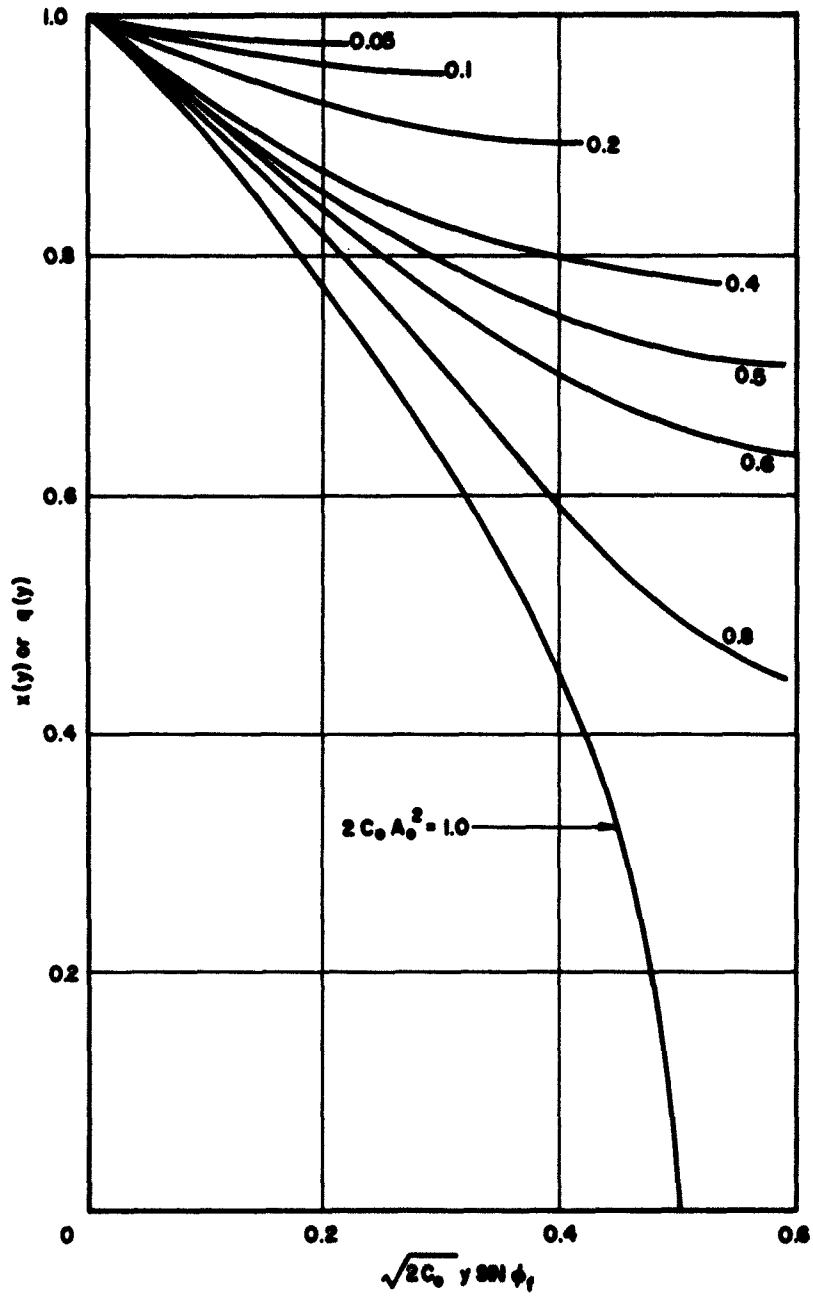

FIG. 4.6 VELOCITY PROFILES BASED UPON A HARD-KERNEL-BUNCH APPROXIMATION; CONSTANT INTERACTION IMPEDANCE IS ASSUMED.

and Watkins[39]. There, the reduction factor, for a hollow beam with mean radius r_o and small thickness, is given approximately by

$$R_m = \left[\frac{I_m(\gamma r_o)}{I_m(\gamma a)} \right]^2 , \tag{4.61}$$

where m refers to the space harmonic under consideration, namely (-1) in this case, and a is the mean radius of the helix. The ratio of the impedance at a radius r_o in the tapered section to that at the same radius in the uniform section can be represented as follows*:

$$\frac{Z(r_o)_t}{Z(r_o)_u} = \left[\frac{I_{-1}(\gamma_{-1t} r_o)/I_{-1}(\gamma_{-1t} a)}{I_{-1}(\gamma_{-1u} r)/I_{-1}(\gamma_{-1u} a)} \right]^2 . \tag{4.62}$$

This ratio is plotted in Fig. 4.7 as a function of the ratio of the tapered to the uniform phase velocity. An impedance variation which is equal to $(v_{p-1t}/v_{p-1u})^2$ is plotted in the figure and it is seen that such a variation is quite realistic for a tape helix. v_p is the cold circuit phase velocity.

With such an impedance variation, $Z_o(y)/Z_o$ in Eq. 4.58 becomes

$$\frac{Z_o(y)}{Z_o} = x^2(y) . \tag{4.63}$$

Substituting Eq. 4.63 in Eq. 4.58 we obtain,

$$\sqrt{2\,C_o}\,\sin\Phi_f\,dy = -\frac{x(y)\,dx(y)}{\sqrt{[2\,C_o\,A_o^2 - 1 + x^2(y)}} . \tag{4.64}$$

---

* "t" refers to a tapered section and "u" to a uniform one.

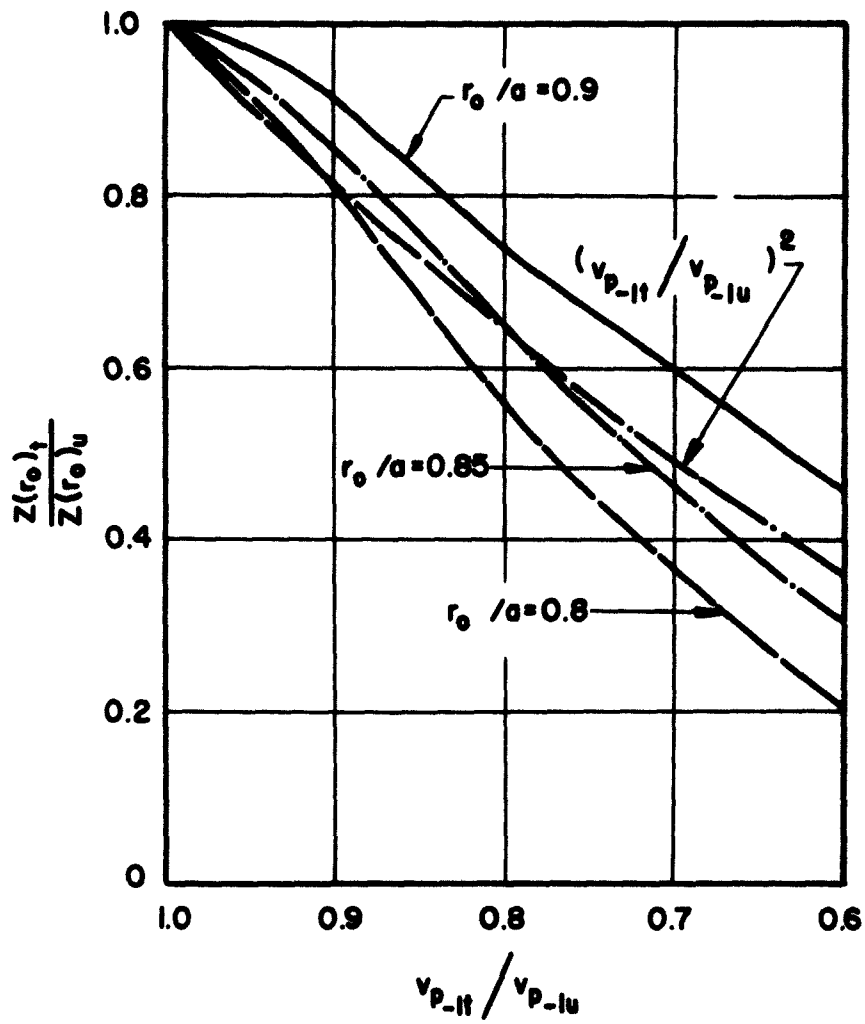

FIG. 4.7 IMPEDANCE VARIATION FOR THE -1 SPACE HARMONIC OF A TAPE HELIX AS A FUNCTION OF PHASE VELOCITY. ($\gamma_{-1u}a = 6.0$)

Integrating Eq. 4.64 and arranging gives

$$\sqrt{2\,C_o}\,\sin\varphi_f\,y = \sqrt{2\,C_o\,A_o^2} - \sqrt{(2\,C_o\,A_o^2 - 1) + x^2(y)} \quad . \quad (4.65)$$

x(y), which it should be recalled here is equal to q(y) in this analysis, is plotted as a function of $\sqrt{2\,C_o}\;y\sin\varphi_f$ in Fig. 4.8. It can be easily deduced by comparing Figs. 4.6 and 4.8 that when a circuit impedance variation which decreases with distance along the tube is present, the tube will be longer than one where the impedance is constant. This is to be expected of course, since a decrease in the interaction impedance means the energy conversion process is weaker and thus a longer distance is required to achieve the same amount of energy conversion.

4.9.3 Application of Velocity Tapers to Practical Backward-Wave Oscillators. In the last section a "hard-kernel-bunch" was assumed and circuit velocity tapers to focus this bunch in the decelerating field of the r-f wave and thus extract all or part of its kinetic energy were developed. The case of a "hard-kernel-bunch", however, is highly idealized and in an actual operating backward-wave oscillator the different electron groups are diffused in phase and possess varying electron velocities as shown in Fig. 4.2. This situation can be approximated, however, if a premodulated or strongly prebunched beam[39] is employed. The difficulty, of course, is to be able to achieve this prebunching over a wide frequency band without resorting to mechanical tuning and thus negating the advantage of a backward-wave oscillator.

The velocity tapers derived under the above assumptions do serve, however, as a guideline to the kind of tapers to be used in actual situations. By reference to Fig. 4.2 it can be seen that at some y value removed from the input the majority of electron groups are in a favorable

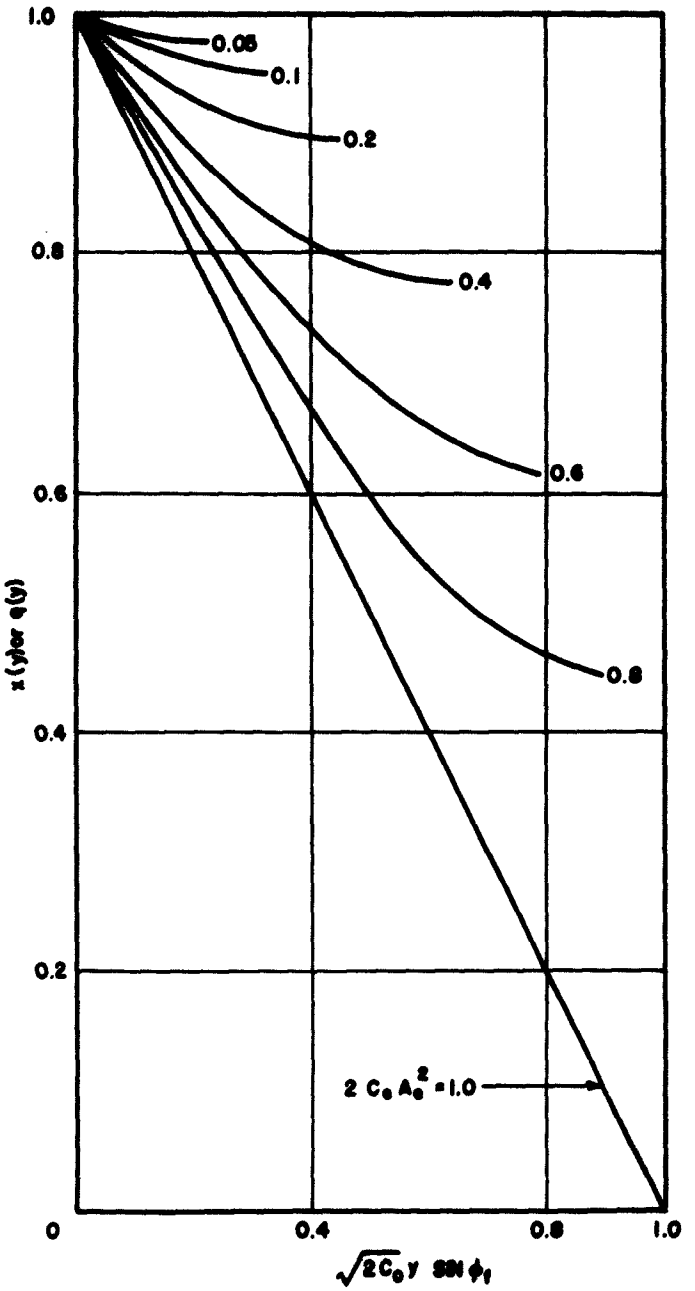

FIG. 4.8 VELOCITY PROFILES BASED UPON HARD-KERNEL-BUNCH APPROXIMATION; INTERACTION IMPEDANCE VARIATION AS $x^2(y)$ IS ASSUMED.

decelerating phase. A velocity taper can then be employed which tends to keep these electrons in that favorable phase and thus extract more kinetic energy from them. Since the electron phases and velocities are diffused, one would try to focus the center of gravity of the different electron groups, so that on the average more energy can be extracted. This was performed here, and the results are reported in this section where they are compared to the results obtained in a similar uniform tube.

Before these results are presented a few words as to how they were obtained are in order. The equations characterizing the behavior of the interaction mechanism, namely Eqs. 4.9, 4.24, 4.25 and 4.26 were programmed on an I.B.M. 7090 digital computer. For a uniform backward-wave oscillator, choosing a set of operating parameters, namely C_o, QC and d, one would then have to make a guess about the output r-f power level, i.e., A_o and the corresponding beam-circuit synchronism parameter b which would force the circuit voltage A(y) to zero and thus obtain an oscillation condition. Thus a trial and error procedure which could be very lengthy must be employed to obtain oscillation conditions. When a circuit velocity taper is introduced the problem becomes even more complicated. It can be appreciated by reference to the preceding section that the kind of taper and the point at which the taper should be applied depend on the level of r-f output or A_o and the taper itself will affect A_o. Unlike the forward-wave amplifier[14], where a certain input r-f level can be chosen, a circuit velocity taper is then applied at some point along the tube where a good bunch is formed, the solution of the equations is then completed and the output r-f level determined, one is at a loss in this case as to what should be chosen first. The procedure

employed here in determining the effect of velocity tapers on the efficiency is discussed below.

First a phase velocity variation was assumed. The choice of the phase velocity variation was based on the tapers derived in the previous section under a "hard-kernel-bunch" assumption and also from a knowledge of the behavior of a uniform tube[20]. Since an analytic expression for the velocity taper is desirable, the following variation was assumed,

$$\frac{v_o(y)}{v_o(0)} = e^{-\sqrt{2\,C_o}\, y \sin \varphi_f} \quad . \tag{4.66}$$

This exponential variation fits the derived tapers best and is consistent with the actual r-f voltage variation in the tube. For a particular C_o, the strength of the taper can be easily varied by varying $\sin \varphi_f$. The taper can then be introduced at different points along the tube and its effect on the output r-f level determined. Since the velocity variation appears in the equations in the form of b(y), an expression for b(y) can be easily written as follows:

$$b(y) = \left\{ \left(\frac{1 + C_o b_o}{C_o} \right) \exp \left[\sqrt{2\,C_o}\ (y - y_{s,t}) \sin \varphi_f \right] - \frac{1}{C_o} \right\} \quad , \tag{4.67}$$

where $b_o = b(0)$,

$y_{s,t}$ = the point at which the taper starts

and

$$(y - y_{s,t}) = 0 \quad \text{for} \quad y \leq y_{s,t} \quad .$$

Since a trial and error procedure must be employed to determine the r-f output level, i.e., A_o and the beam-circuit synchronism parameter

b for an operating oscillator, a downhill method was incorporated into the computer program. The procedure employed in finding an operating point was then as follows:

1. A certain set of parameters for the operating tube is chosen, namely C_o, QC, and d.

2. A taper in the form of b(y) (Eq. 4.67) is applied at some point $y = y_{s,t}$ down the tube.

3. Initial values of A_o and b_o are then chosen.

4. Using these initial values of A_o and b_o as the central point, the computer determines the minimum value of A(y) for a 3 x 3 mesh of points in the A_o, b_o plane. The value of A_o and b_o at which the minimum value of A(y) is lowest is used as the central point for the next computations. The process is repeated until a set of values of A_o and b_o are found which force A(y) to go to zero. This then represents an operating point. The process can then be repeated of course for different tapers and parameters. This process eliminates any operating points which were observed by Rowe[20] in his study of the uniform oscillator, where the r-f voltage on the helix reaches a minimum nonzero value at some point but does reach a zero value at some later point.

The results of the cases investigated here are presented in Figs. 4.9 through 4.20 and are discussed in the following section.

4.10 Discussion of Results on Tapered Backward-Wave Oscillators

In the following figures the oscillation conditions in an operating tapered backward-wave oscillator are compared to those in a uniform one. Essentially, the efficiency, oscillator length and the point at which the taper starts are presented in the figures for different operating parameters. Only a few points which represent computer

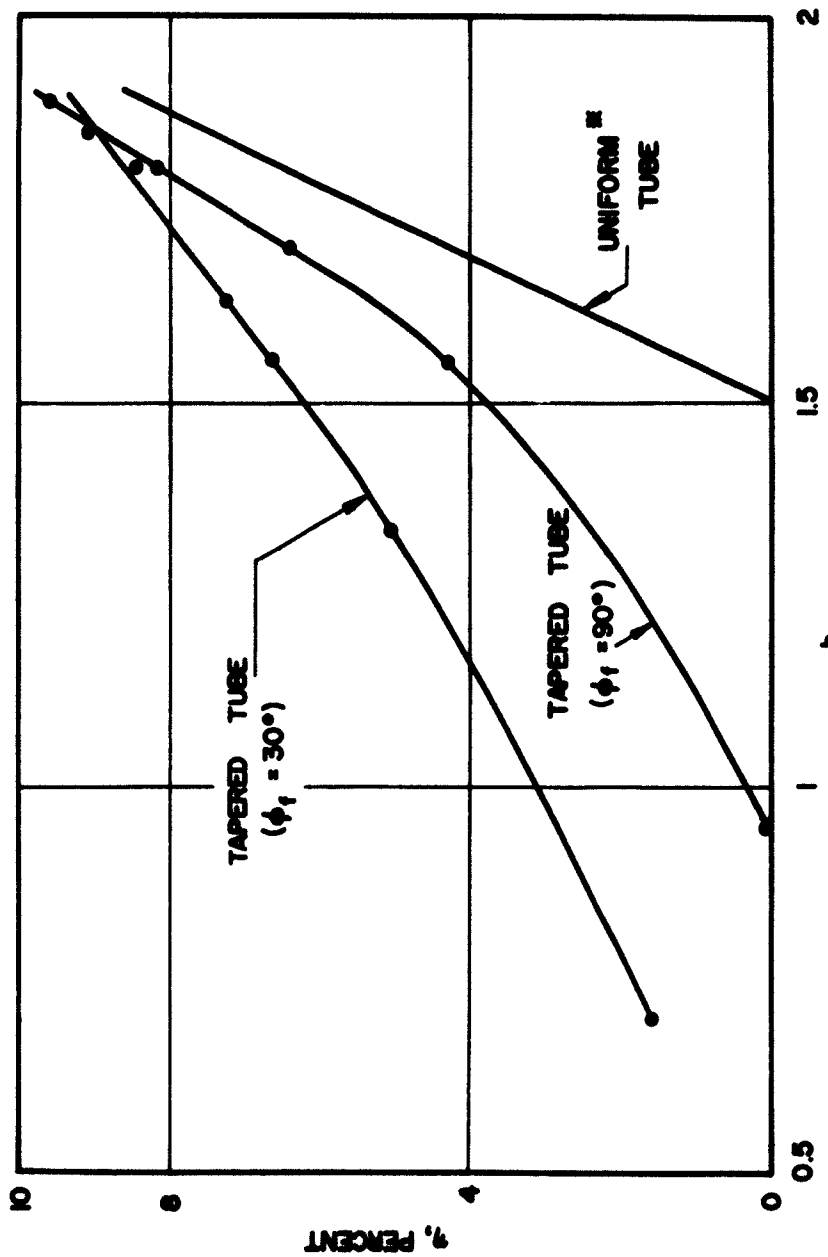

* Uniform tube data was obtained from Rowe's paper[20].

FIG. 4.9 COMPARISON OF EFFICIENCY IN TAPERED AND UNIFORM BACKWARD-WAVE OSCILLATORS. INTERACTION IMPEDANCE IS ASSUMED TO BE CONSTANT. (C_o = 0.05, d = 0, QC = 0)

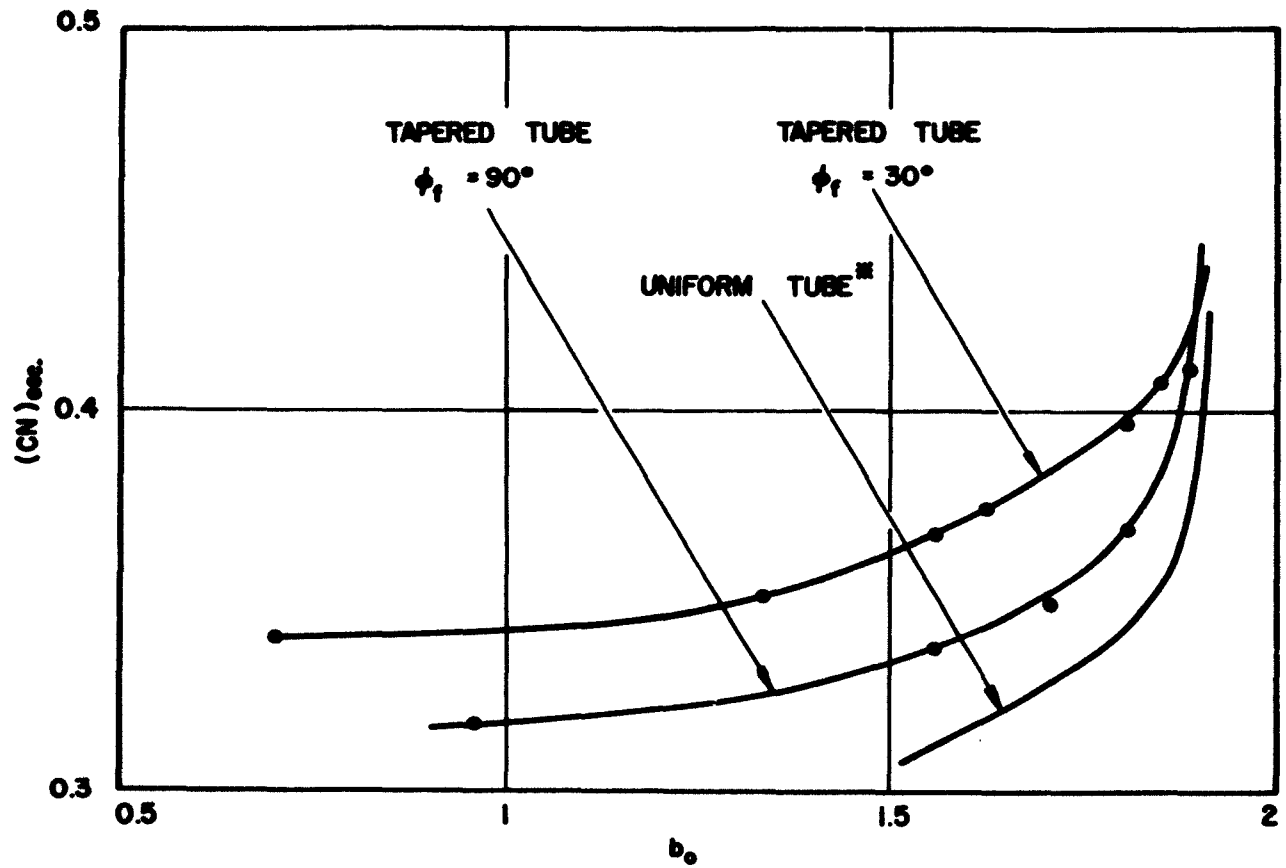

* Uniform tube data was obtained from Rowe's paper[20].

FIG. 4.10 UNIFORM AND TAPERED NORMALIZED TUBE LENGTHS VS. b_o. THESE OSCILLATION LENGTHS CORRESPOND TO THE EFFICIENCIES SHOWN IN FIG. 4.9. (C = 0.05, d = 0, QC = 0)

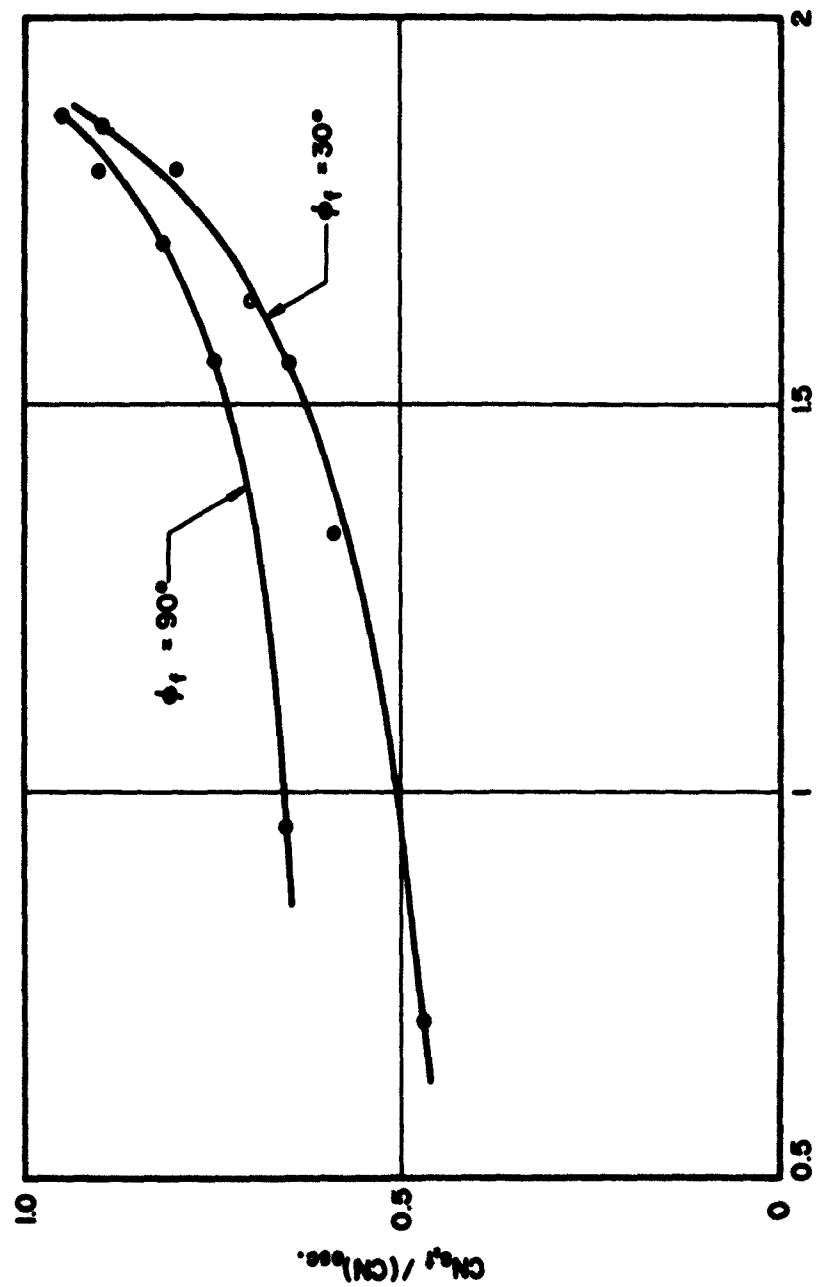

FIG. 4.11 RATIO OF THE LENGTH AT WHICH THE TAPER STARTS TO THE TOTAL LENGTH OF THE TUBE.
THESE CURVES CORRESPOND TO THE TAPERED TUBES OF FIGS. 4.9 AND 4.10.

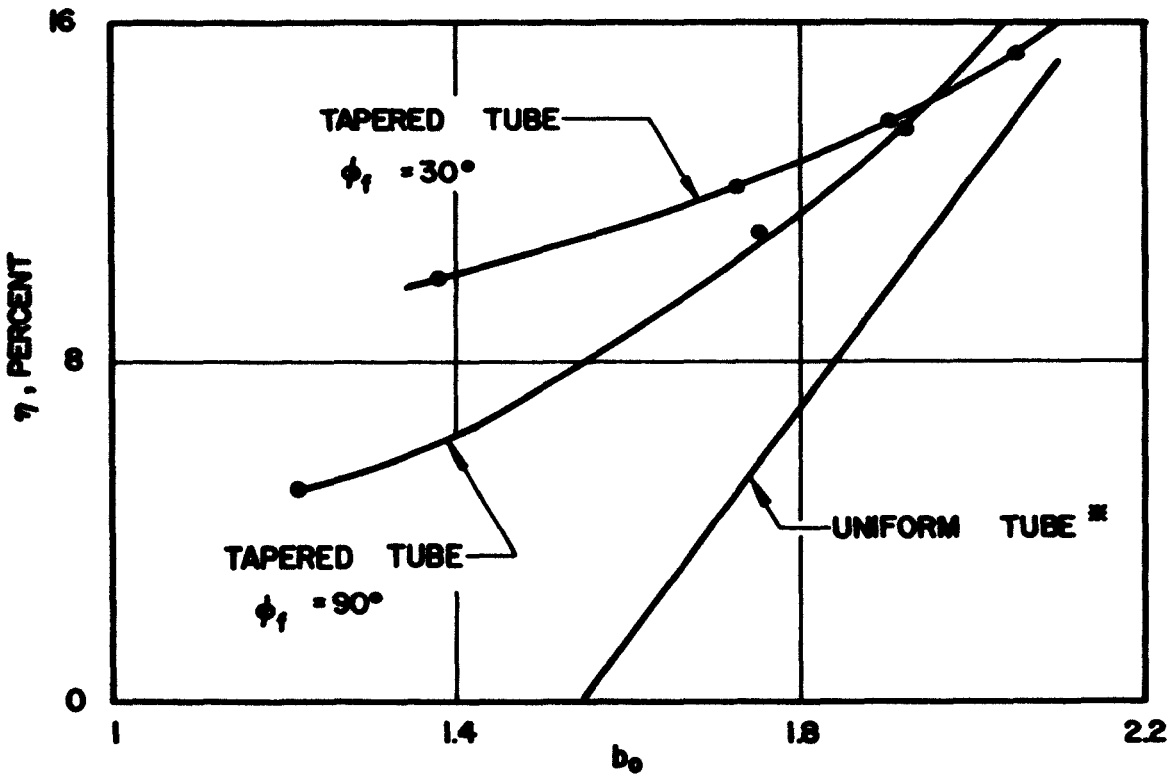

* Uniform tube data was obtained from Rowe's paper[20].

FIG. 4.12 COMPARISON OF EFFICIENCY IN TAPERED AND UNIFORM BACKWARD-WAVE OSCILLATORS. INTERACTION IMPEDANCE IS ASSUMED TO BE CONSTANT. (C_0 = 0.1, QC = 0, d = 0)

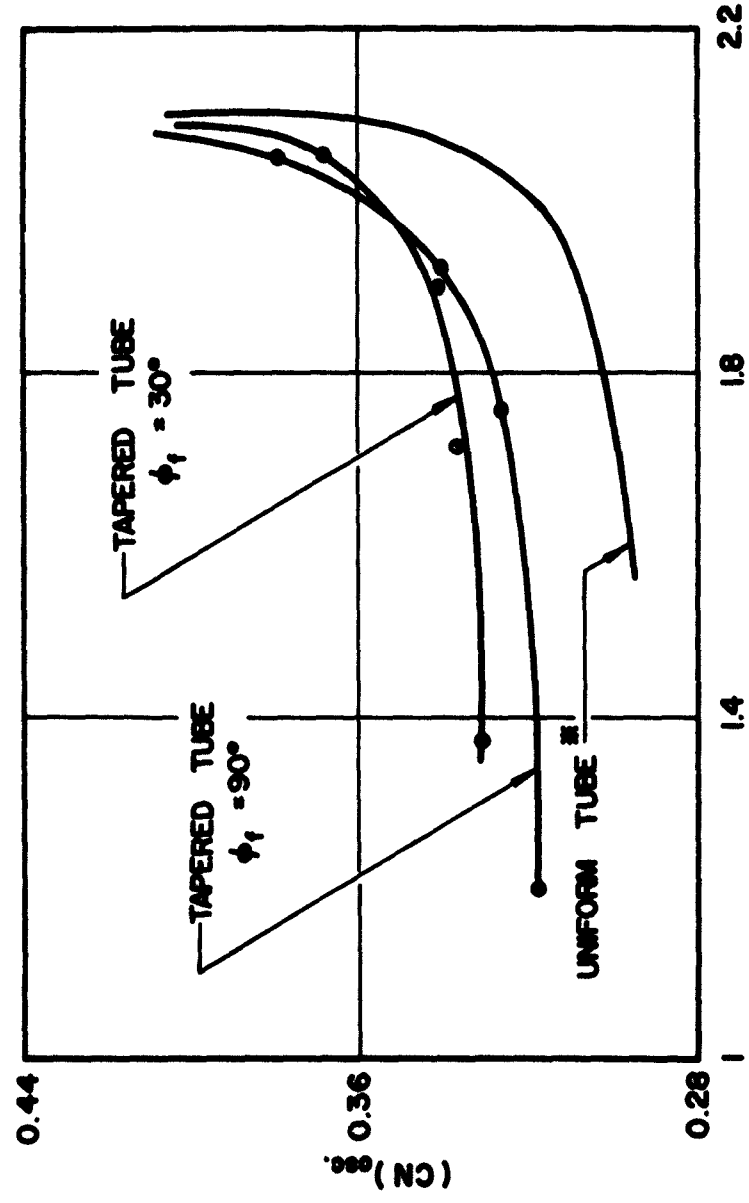

* Uniform tube data was obtained from Rowe's paper[20].

FIG. 4.13 UNIFORM AND TAPERED NORMALIZED TUBE LENGTHS VS. b_o. THESE NORMALIZED OSCILLATION LENGTHS CORRESPOND TO THE EFFICIENCIES SHOWN IN FIG. 4.12. (C = 0.1, QC = 0, d = 0)

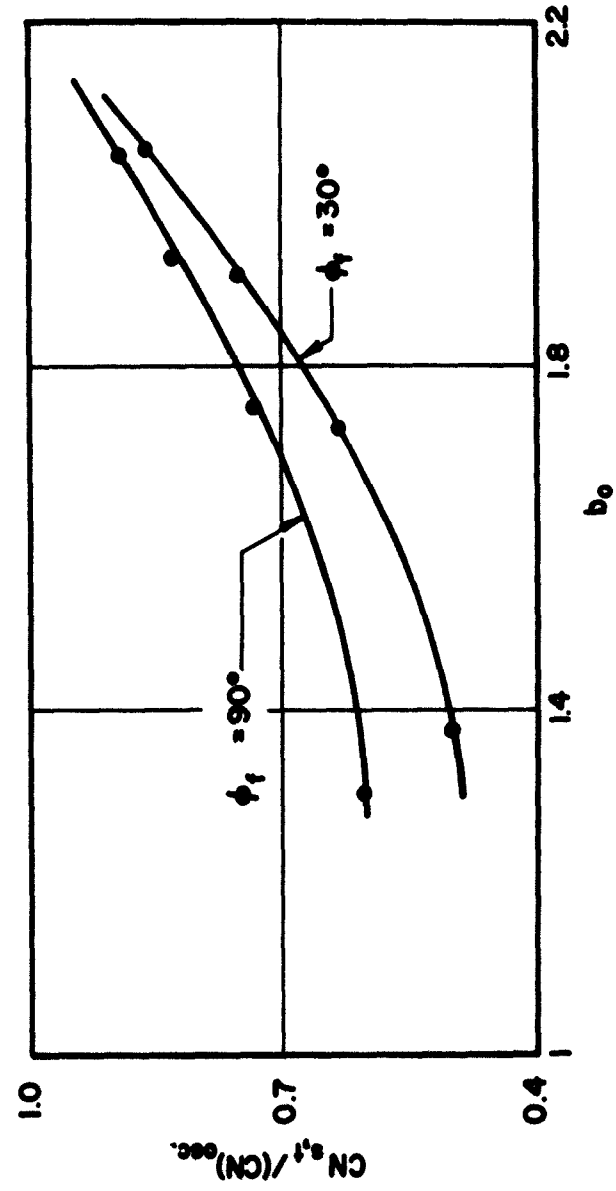

FIG. 4.14 RATIO OF THE LENGTH AT WHICH THE TAPER STARTS TO THE TOTAL LENGTH OF THE TUBE. THESE CURVES CORRESPOND TO THE TAPERED TUBES OF FIGS. 4.12 AND 4.13.

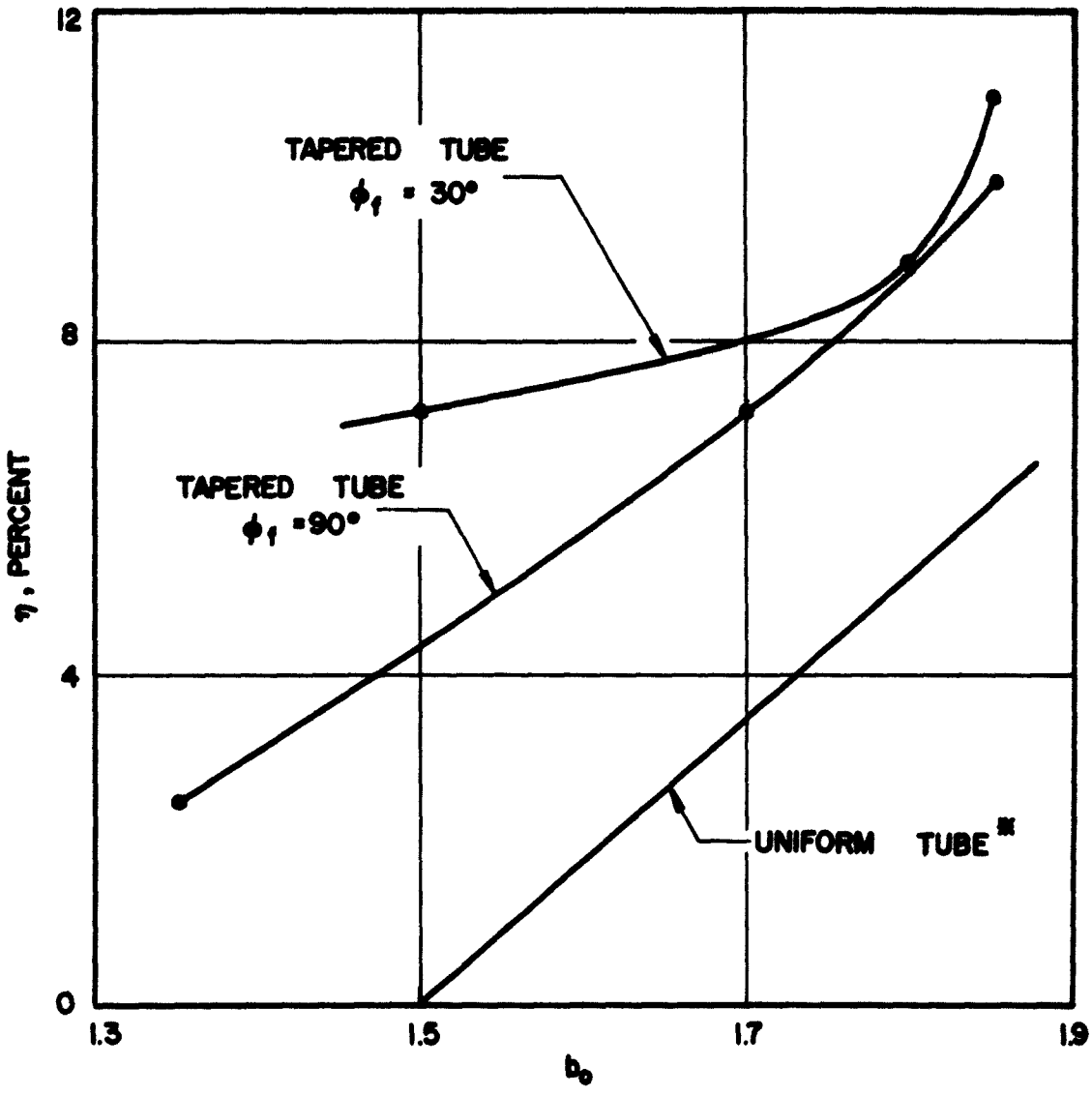

* Uniform tube data was obtained from Rowe's paper[20].

FIG. 4.15 COMPARISON OF EFFICIENCY IN UNIFORM AND TAPERED BACKWARD-WAVE OSCILLATORS. INTERACTION IMPEDANCE IS ASSUMED CONSTANT. (C = 0.05, QC = 0.25, d = 0, B = 1.0, a'/b' = 2.0)

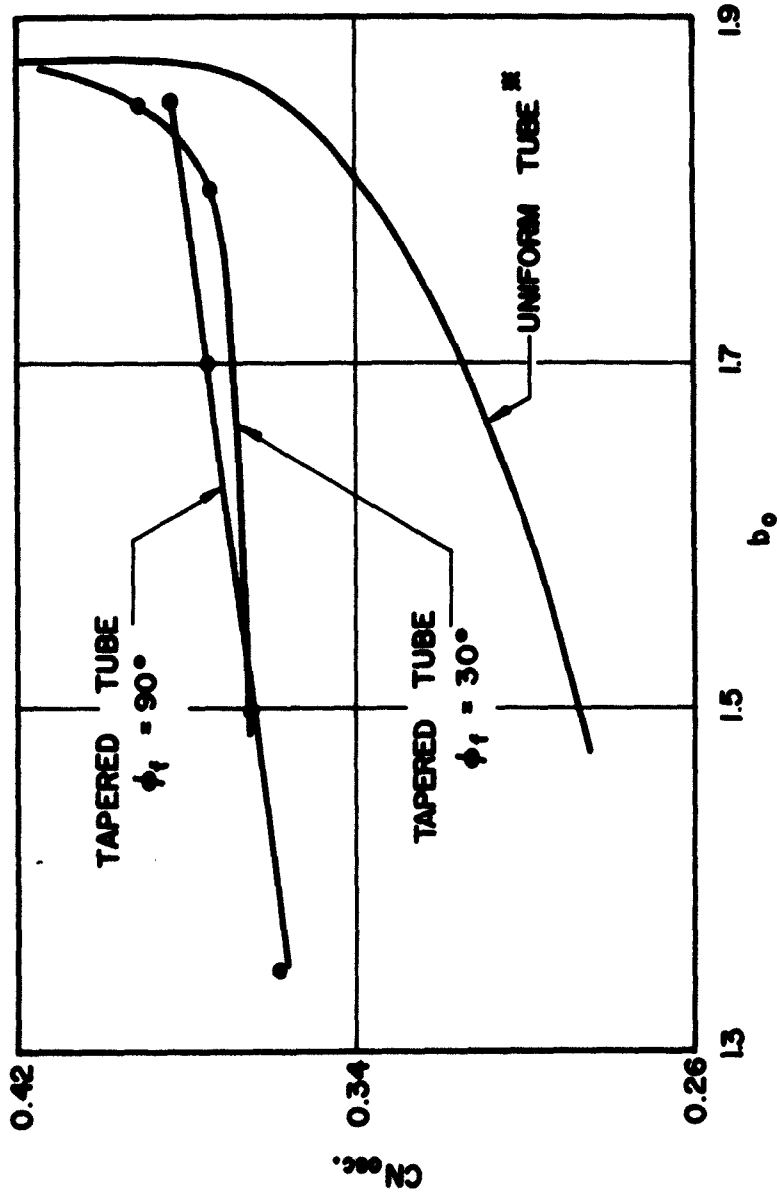

* Uniform tube data was obtained from Rowe's paper[20].

FIG. 4.16 UNIFORM AND TAPERED NORMALIZED TUBE LENGTHS VS. b_o. THESE NORMALIZED OSCILLATION LENGTHS CORRESPOND TO THE EFFICIENCIES SHOWN IN FIG. 4.15.

(C = 0.05, d = 0, QC = 0.25, B = 1.0, a'/b' = 2.0)

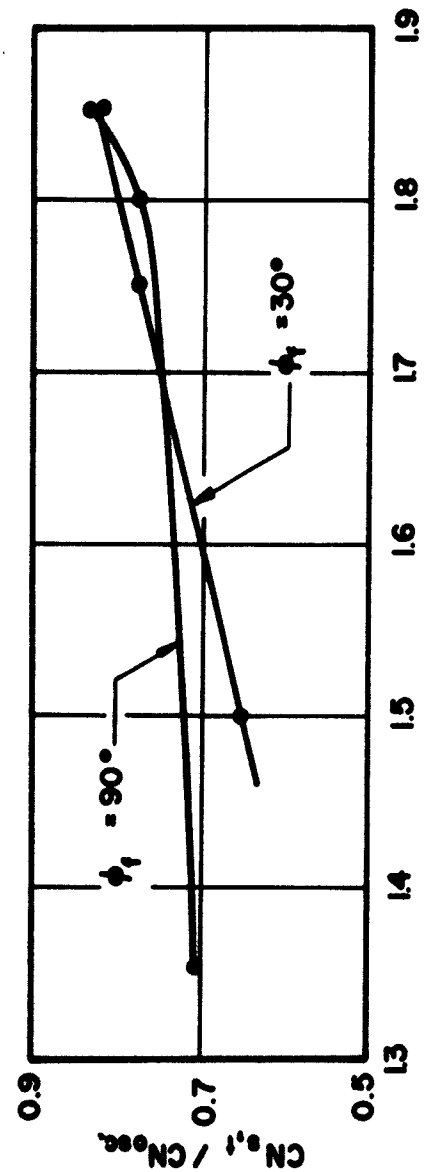

FIG. 4.17 RATIO OF THE LENGTH AT WHICH THE TAPER STARTS TO THE TOTAL LENGTH OF THE TUBE. THESE CURVES CORRESPOND TO THE TAPERED TUBES OF FIGS. 4.15 AND 4.16.

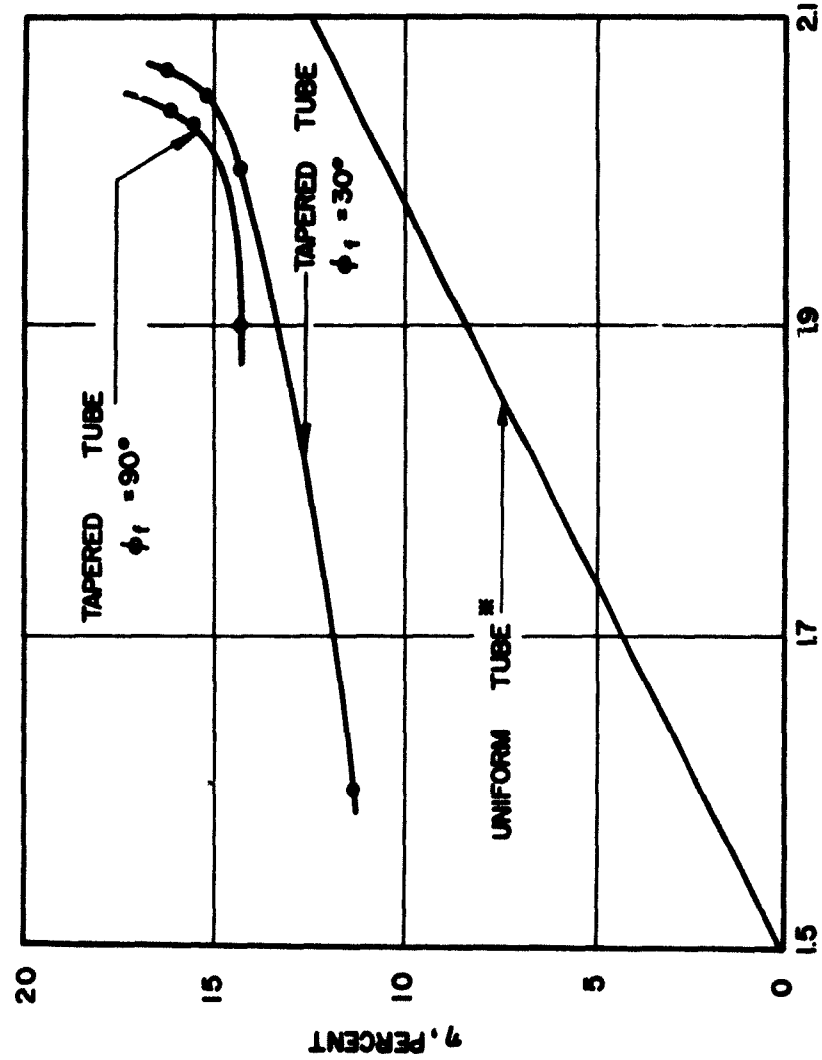

* Uniform tube data was obtained from Rowe's paper[20].

FIG. 4.18 COMPARISON OF EFFICIENCY IN UNIFORM AND TAPERED BACKWARD-WAVE OSCILLATORS. INTERACTION IMPEDANCE IS ASSUMED CONSTANT. ($C = 0.1$, $QC = 0.25$, $d = 0$, $B = 1.0$, $s'/b' = 2.0$)

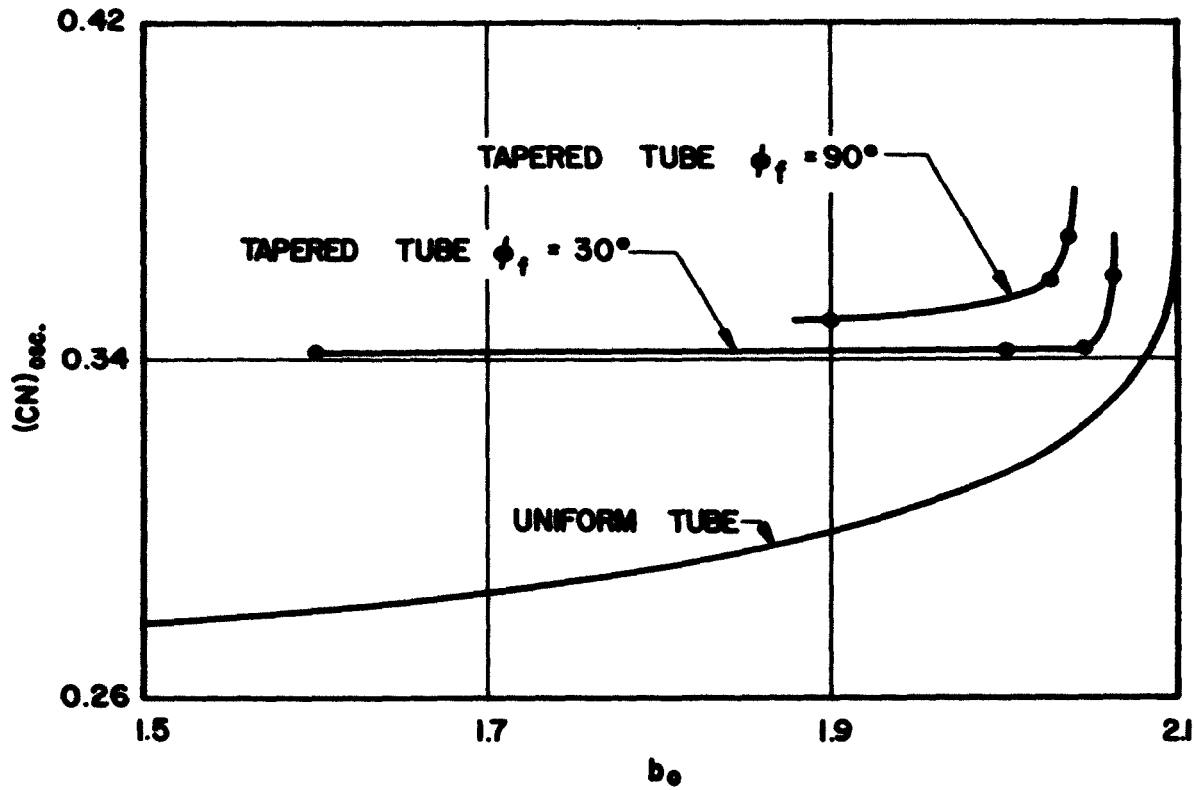

* Uniform tube data was obtained from Rowe's paper[20].

FIG. 4.19 UNIFORM AND TAPERED NORMALIZED TUBE LENGTHS VS. b_o. THESE NORMALIZED OSCILLATION LENGTHS CORRESPOND TO THE EFFICIENCIES SHOWN IN FIG. 4.18. (C = 0.1, QC = 0.25, d = 0, B = 1.0, a'/b' = 2.0)

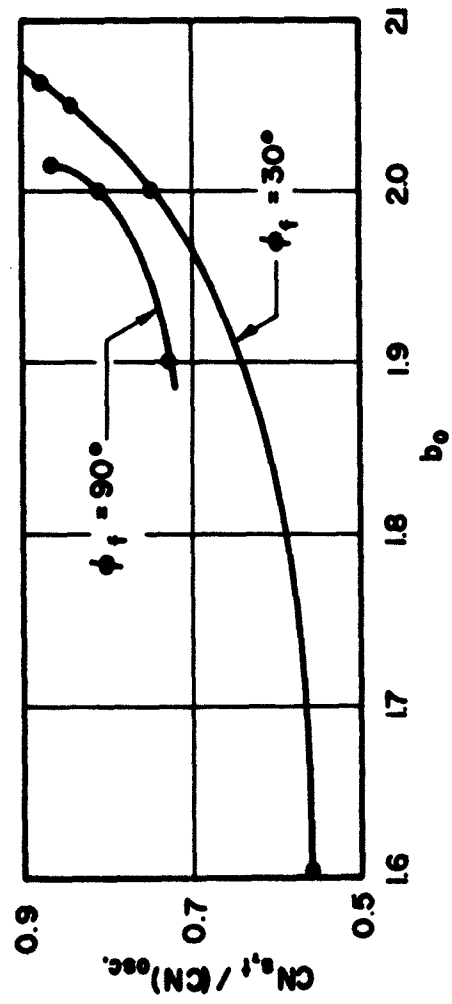

FIG. 4.20 RATIO OF THE LENGTH AT WHICH THE TAPER STARTS TO THE TOTAL LENGTH OF THE TUBE. THESE CURVES CORRESPOND TO THE TAPERED TUBES OF FIGS. 4.18 AND 4.19.

solutions have been obtained. This is because the computer time required for finding an oscillation point is quite long and thus very expensive.

The tapers investigated here should not be considered optimum. Other more elaborate schemes can be devised where the computer can be programmed to automatically determine the kind of velocity tapers required to achieve higher efficiencies. However, such schemes would even be more expensive since they would require more computer time. The results presented in the following figures do show the usefulness of the tapers derived under the "hard-kernel-bunch" approximation. In all the cases considered, higher efficiencies were obtained in a tapered tube than that in a uniform one.

When comparing the oscillation conditions of a uniform and a tapered tube, it is assumed that the two tubes are operating at the same voltage, same current and same frequency. This makes C_o in the two tubes the same since no impedance variation is assumed, and the oscillation conditions are plotted as a function of the synchronism parameter b_o. It can then be seen from the figures that the efficiency of a tapered tube is greater than that in a uniform one, but the physical length in the tapered tube would be slightly higher. The percentage increase in efficiency is seen to be higher at an operating point where the efficiency of the uniform tube is low than that at which the efficiency of the uniform tube is high. It can also be seen that a tapered tube will start oscillating at a lower value of b_o (lower voltage) than that of a uniform one which confirms the results of the small-signal analysis of the previous chapters. It was also found that when these tapers that were investigated here were applied at the beginning of the

tube, no oscillation condition could be found. This was also predicted by the small-signal analysis of the previous chapter.

From these results we can then conclude that velocity tapers can be chosen to improve the efficiency of a backward-wave oscillator. The strength of the taper depends on how efficient a uniform tube is to start with, i.e., the value of C_o. The higher C_o is the stronger the taper. One has to be careful in choosing a taper, for if the taper is made stronger than a certain value at a certain operating parameter C_o, the tube will not start oscillating. Since forward-wave amplifiers are much more efficient than backward-wave oscillators a much stronger taper would be needed there to achieve phase focusing[14]. Such a strong taper while improving the efficiency of the forward-wave amplifier may also serve to suppress backward-wave oscillations in those cases.

4.11 Efficiency in Electrostatically Focused Backward-Wave Oscillators

It is inherent in the operation of an electrostatically focused tube[31,32] that the beam potential varies approximately in a sinusoidal manner as follows:

$$V_o(z) = V_{oo}\left[1 - A\cos\frac{2\pi z}{L}\right] , \qquad (4.68)$$

where L = the d-c focusing period.

The d-c gradient force term appears in the force Eq. 4.26 in the form $C_o[dA_{d-c}(y)/dy]$, where $A_{d-c}(y) = [C_o V_{d-c}(y)/I_o Z_o]$. Representing the voltage as a function of the normalized coordinate y as was done in Section 3.5.9 and substituting we obtain,

$$C_o\frac{dA_{d-c}(y)}{dy} = \frac{Aq}{4C_o}\sin qy , \qquad (4.69)$$

where

$$\alpha = \frac{2\pi N_{d-c}}{y_o}$$

and N_{d-c} = the total number of d-c focusing periods in the tube.

Including the above term of Eq. 4.69 in the force Eq. 4.26, the oscillation conditions can be determined for specified values of α and A. The equations were solved for a few cases and are presented in Table 4.1 where they are compared to the oscillation conditions in a uniform tube whose constant beam potential is equal to the average beam potential in the sinusoidal case. For the operating parameters considered here it should be recalled that the maximum efficiency[20] of a uniform tube is approximately 15 percent and no oscillation can take place for b_o values less than 1.5.

Table 4.1

Comparison of Efficiency of an Electrostatically-Focused BWO and a Uniform One

$C_o = 0.1$, QC = 0		d = 0	Uniform Tube A = 0		Tube with Sinusoidal Beam Potential	
A	α	b_o	η %	$CN_{osc.}$	η %	$CN_{osc.}$
0.05	100	2.0	11.2	0.32	15.1	0.37
0.1	100	1.05	no oscillation		19.0	0.48
0.2	100				no oscillation	
0.1	50	2.10	15	>0.36	14	0.334
0.2	50	1.3	no oscillation		22	0.58
0.4	50				no oscillation	

It is seen from Table 4.1 that the efficiency in an electrostatically focused backward-wave oscillator is generally greater than that in a uniform one. In order to obtain these higher efficiencies the physical tube length must be longer than that of a uniform tube. It should be noticed that these higher efficiencies are obtained at an average beam potential which is slightly lower than the uniform tube beam potential. For the operating parameters investigated here, it was found that for $\alpha A = 200$ and above no oscillation point could be found on the computer.

The author sees no apparent physical explanation for the higher efficiencies obtained. However, a possible explanation is offered. It is possible that a sinusoidal beam potential variation might inherently phase focus the electron groups and make it possible to extract more energy from them. This is borne out by the fact that at these higher efficiencies if one examines the velocities and phases of the different electron groups at different y positions along the tube, one finds that in the sinusoidal beam potential tube the electrons stay in the decelerating field a longer distance and give up more of their kinetic energy to the r-f field. It is apparent that the degree of energy conversion under such conditions warrants further study.

CHAPTER V. EXPERIMENTAL TAPERED BACKWARD-WAVE OSCILLATOR

5.1 Tapered BWO

In order to study the effect of circuit velocity tapers on the start-oscillation current and efficiency, the parts for a commercially available Huggins "HO-1" backward-wave oscillator were obtained and the tape helix slow-wave circuit was modified to include a pitch variation toward the collector end of the tube. This oscillator operates in the S-band frequency range and the pertinent dimensions are given in Table 5.1.

Table 5.1

Beam and Helix Dimensions of Experimental Tube

Uniform Helix Pitch	0.133 inch
Helix Tape Thickness	0.010 inch
Helix Tape Width	0.040 inch
Helix O.D.	0.375 inch
Helix I.D.	0.355 inch
Beam O.D.	0.331 inch
Beam I.D.	0.290 inch

This oscillator operates at fairly low power levels. The theoretical C and QC values for this tube are shown in Fig. 5.1 where they are given as a function of frequency. The impedance of the (-1) space harmonic for the tape helix which is needed in computing the C values was obtained

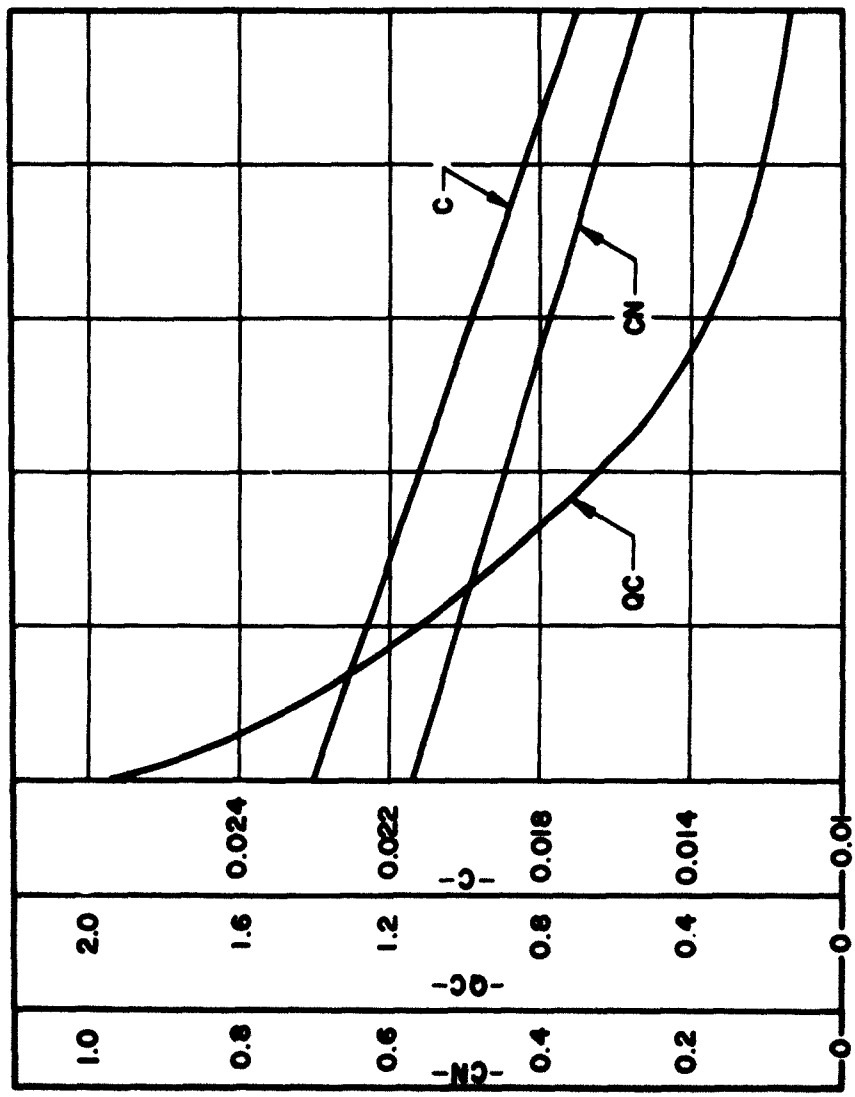

FIG. 5.1 THEORETICAL C, QC AND CN VS. FREQUENCY FOR THE EXPERIMENTAL TUBE.

($I_{COLLECTOR}$ = 15 ma, TUBE LENGTH = 5 INCHES)

from the paper by Ash and Watkins[38]. The space-charge parameter QC was computed using Johnson's paper[5].

Knowing the C and QC values one can then obtain the tapers and the points at which these tapers should be applied from a digital computer solution for these values. However, first this would be a c stly process and second it is realized that a computer might not be available to each person who might be interested in employing such tapers. The computer solutions obtained in Chapter IV for realistic backward-wave oscillators do not cover a wide range of operating parameters and were intended to get a general idea of the utility of the tapers derived under the "hard-kernel-bunch" approximation when such tapers are applied to realistic situations. It was found there that these tapers result in higher efficiencies. The design of the tapered section for this oscillator was based on the tapers derived from the above approximation and also assuming a realistic impedance variation which for this tube corresponds to the impedance variation assumed in deriving the tapers in Chapter IV. In Section 4.9, it should be recalled, the impedance was assumed to vary as the square of the phase velocity on the helix.

The procedure that was followed in designing the tapered section is as follows. Since the C parameter varies across the band, an average C value was chosen to design the taper. For this tube the C value chosen was approximately 0.02 which is the C value at mid-frequency. Next the uniform section of the tube was made approximately 5 inches long. The choice of the uniform length is affected by the available length of solenoid for focusing the electron beam, and also one has to be careful not to start the taper too soon. The uniform length should be chosen so that its CN value is about 1.5 to 2.0 times the value of CN at start

oscillation. For this tube, the CN value at the above chosen C value is approximately equal to 0.45 which is approximately 1.5 times the value of CN at start oscillation for a uniform tube. Since the tapers that must be used in a backward-wave oscillator are very weak, an exponential velocity variation is approximately the same as a linear velocity variation thus a linear velocity variation was chosen for the tapered section. The velocity variation can then be written in the following form,

$$\frac{v_o(y)}{v_o(0)} = 1 - \sqrt{2C}\, y \sin \varphi_f \quad , \tag{5.1}$$

where $y = 2\pi$ CN and

N = the number of stream wavelengths.

Since the phase velocity on the helix is directly proportional to the pitch, the pitch variation is now determined from Eq. 5.1 and can be written as follows,

$$\frac{p}{p_o} = 1 - (2\pi)(0.2)\ \text{CN} \quad . \tag{5.2}$$

The rate of taper has been established, but the question arises as to how far must the pitch be tapered? An idea about this can be obtained by referring to the computer solutions of the previous chapter. From there it can be concluded that a maximum pitch variation of 15 to 20 percent should be employed and the ratio of p/p_o thus should never be less than 75 percent. It should be emphasized here that it is the rate of pitch variation that is most important and a tube tapered to 25 percent* should never have a lower efficiency than one tapered to 15 percent. The

---

* An "x" percent taper means that the phase velocity of the tube is decreased by "x" percent of its value in the uniform section.

disadvantage is, of course, that in order to obtain the higher taper the tube would have to be made longer.

For the tube investigated here, a 20 percent linear taper was incorporated in the helix. For a 20 percent linear taper, the total CN for the taper length can be easily obtained from Eq. 5.2 and is approximately equal to 0.2. This corresponds to a physical length of approximately 2 inches in the S-band oscillator investigated here.

5.2 Experimental Procedure and Results

Based upon the above considerations an experimental backward-wave oscillator was assembled and tested under different configurations. Figure 5.2 shows the pertinent dimensions of the tube and the different configurations under which it was tested. The tube consists of a uniform length of helix 5.5 inches long, a tapered section 2.0 inches long and another 1.5 inch of uniform section. The first half inch and the last 1.5 inch were covered with a lossy material, namely dag dispersion No. 226, which was placed on the inside and outside of the vacuum envelope. The lossy material was tapered on both sides to minimize reflections. The different configurations were tested in the same order as their designated numbers. Tube number 5, where the lossy material is placed on the outside of the glass envelope over the whole length of the tapered section is refereed to as the uniform tube.

Since we are mainly concerned in comparing the characteristics of the different configurations, the tests were performed in each case at the same frequencies. This assures the same coupler VSWR and ohmic losses in the helix and associated components used in measuring the output power. The results are presented in Figs. 5.3 through 5.11 where efficiency versus collector current plots are shown for different operating

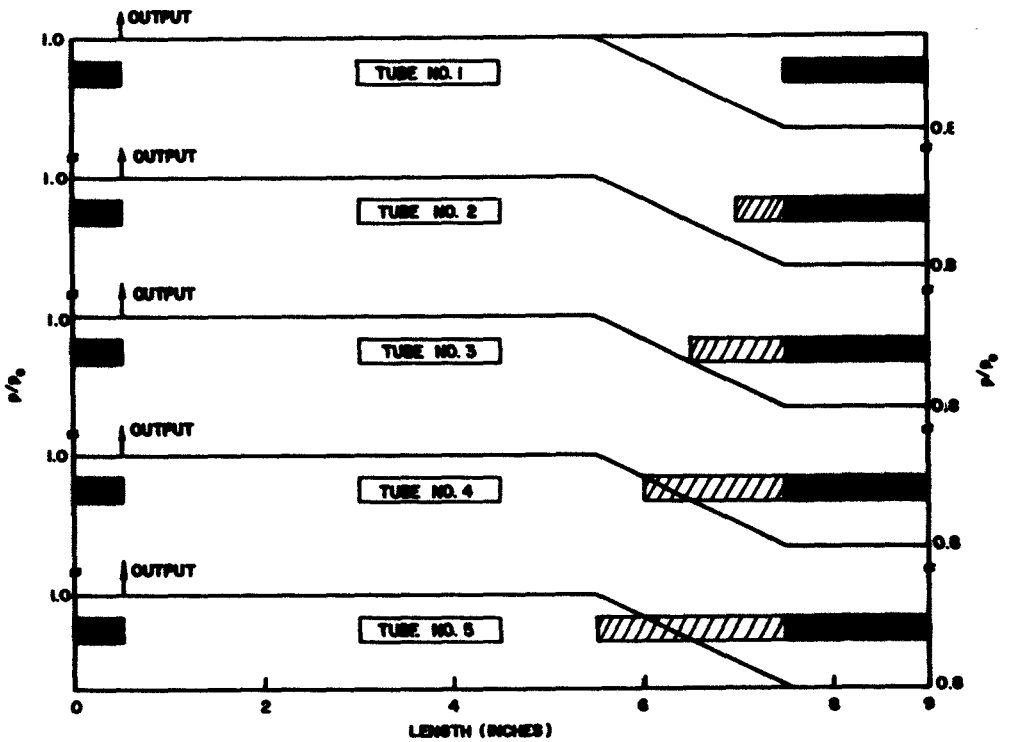

Designates the length over which "Dag Dispersion No. 226" is placed inside and outside the vacuum envelope.

Designates the length over which "Dag Dispersion No. 226" was placed outside the vacuum envelope only.

FIG. 5.2 p/p_o VS. LENGTH FOR EXPERIMENTAL BACKWARD-WAVE OSCILLATOR.

(p_o = 0.133 INCH IS THE PITCH OF THE UNIFORM SECTION)

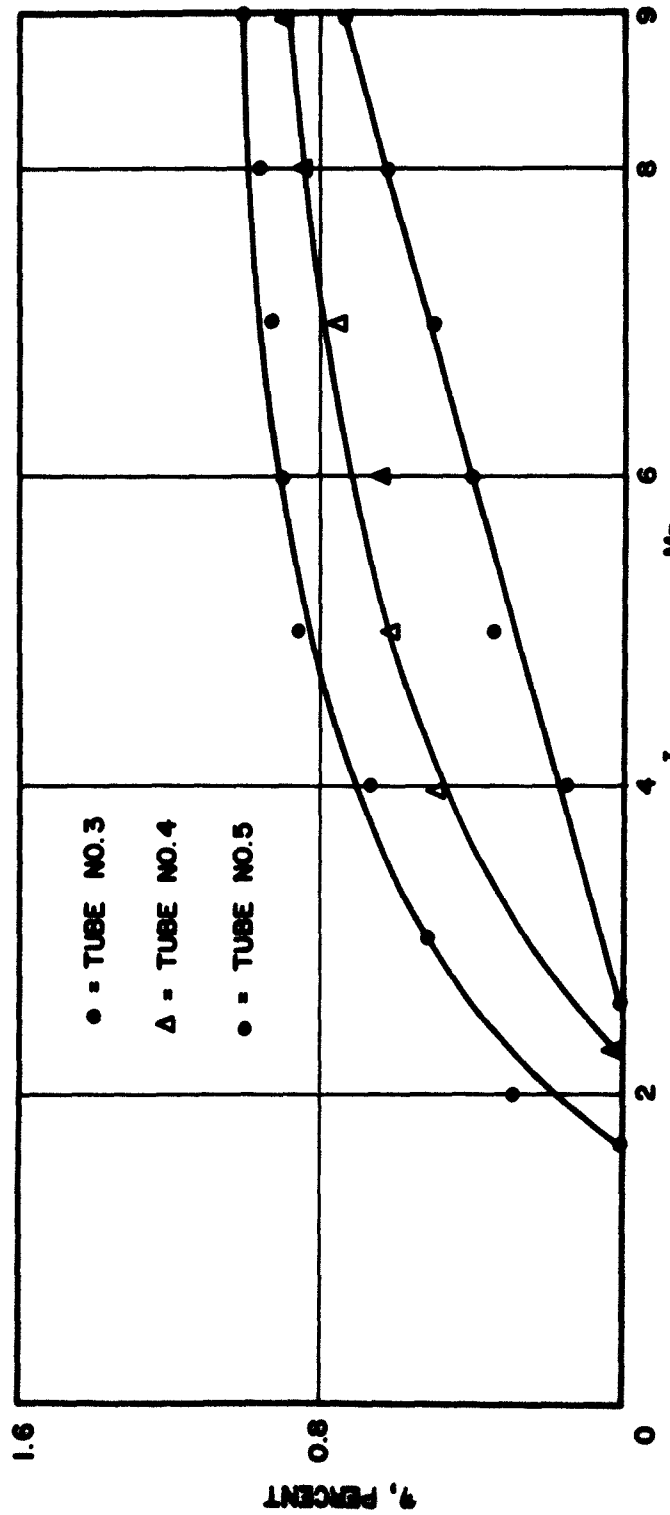

FIG. 5.3 EFFICIENCY VS. COLLECTOR CURRENT FOR EXPERIMENTAL BWO. (f = 2 Gc, V_{HELIX} = 250 VOLTS) (TUBE NUMBERS REFER TO THOSE SPECIFIED IN FIG. 5.2)

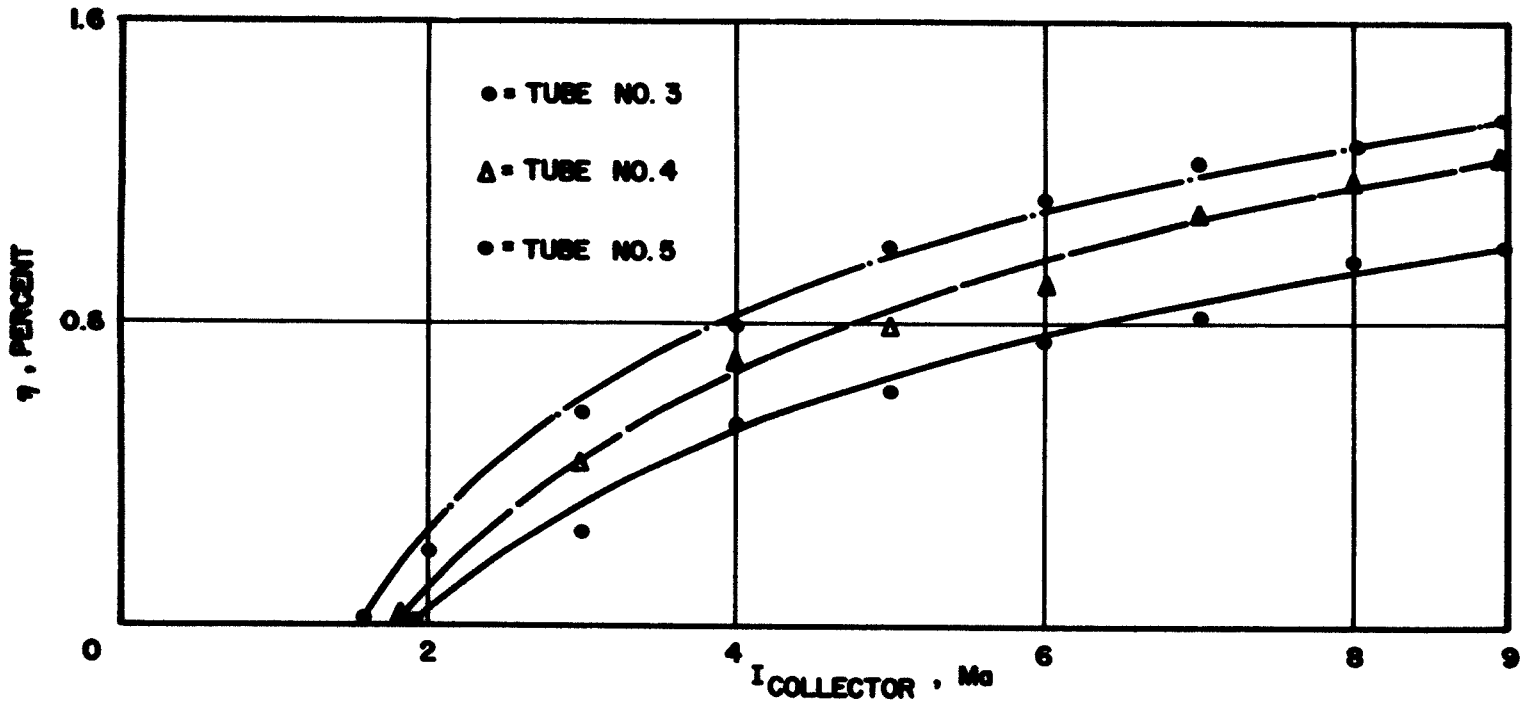

FIG. 5.4 EFFICIENCY VS. COLLECTOR CURRENT FOR EXPERIMENTAL BWO. (f = 2.2 Gc, V_{HELIX} = 350 VOLTS) (TUBE NUMBERS REFER TO THOSE SPECIFIED IN FIG. 5.2)

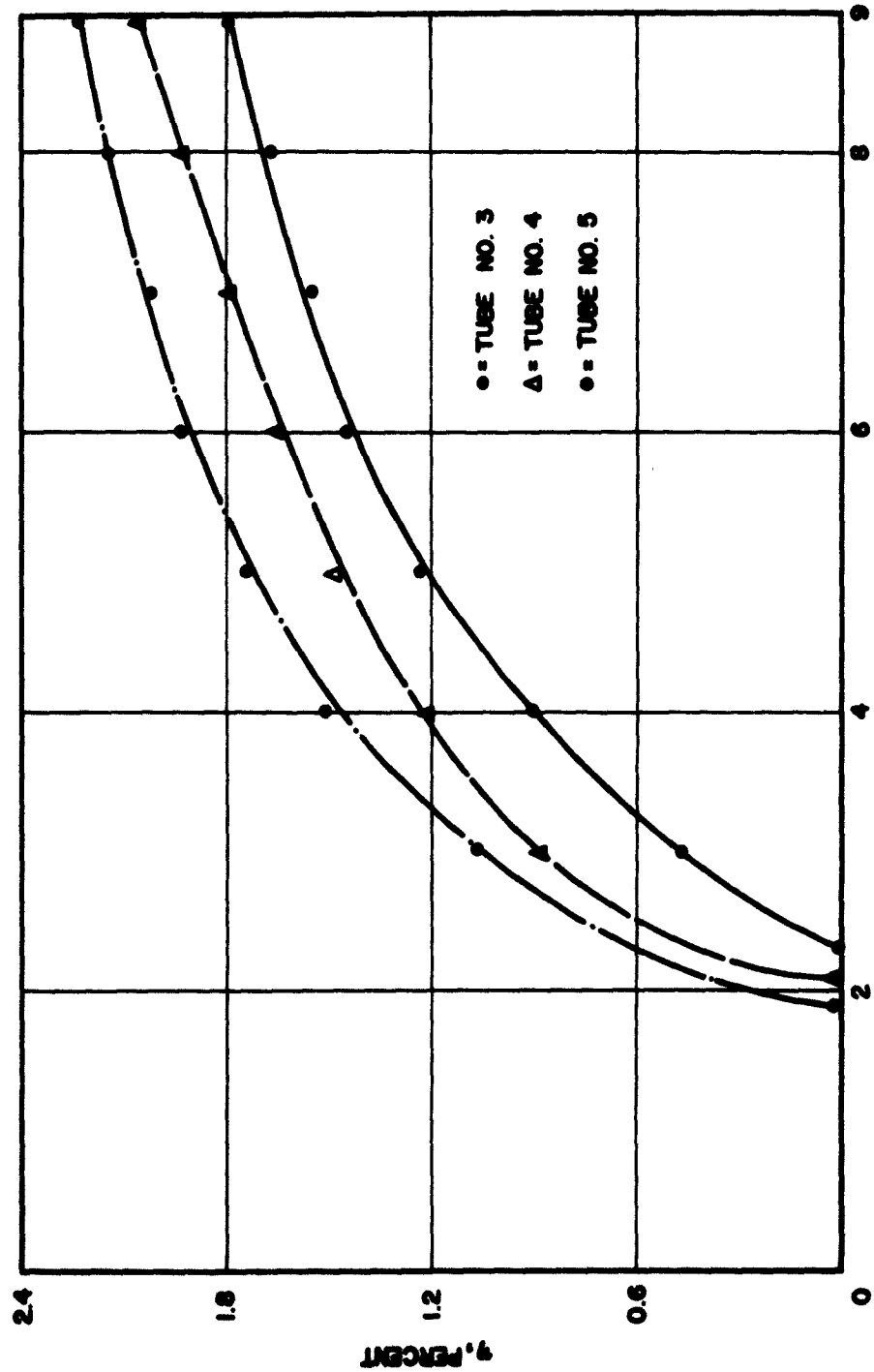

FIG. 5.5 EFFICIENCY VS. COLLECTOR CURRENT FOR EXPERIMENTAL BWO. ($f = 2.5$ Gc, $V_{HELIX} = 450$ VOLTS) (TUBE NUMBERS REFER TO THOSE SPECIFIED IN FIG. 5.2)

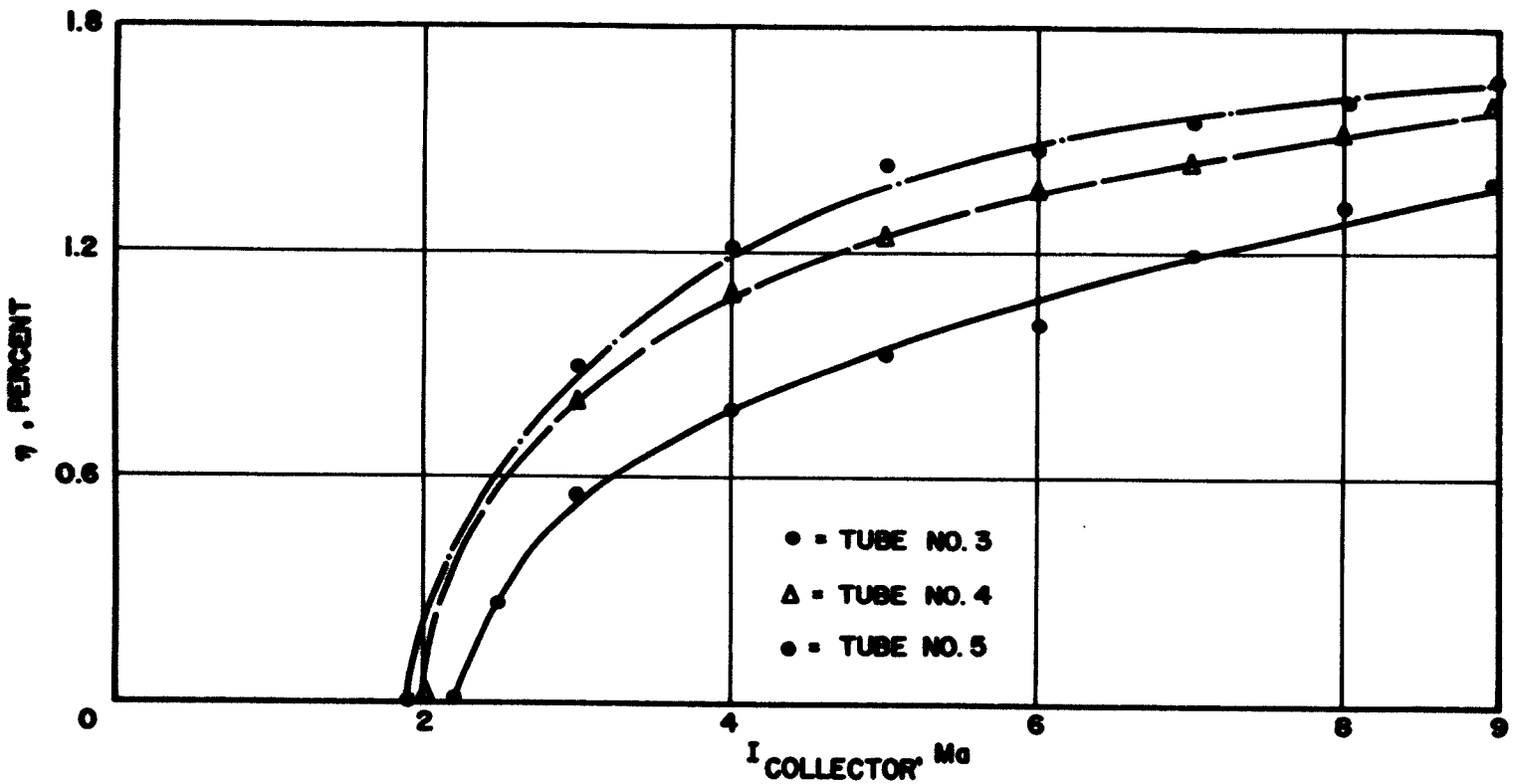

FIG. 5.6 EFFICIENCY VS. COLLECTOR CURRENT FOR EXPERIMENTAL BWO. (f = 2.6 Gc, V_{HELIX} = 560 VOLTS) (TUBE NUMBERS REFER TO THOSE SPECIFIED IN FIG. 5.2)

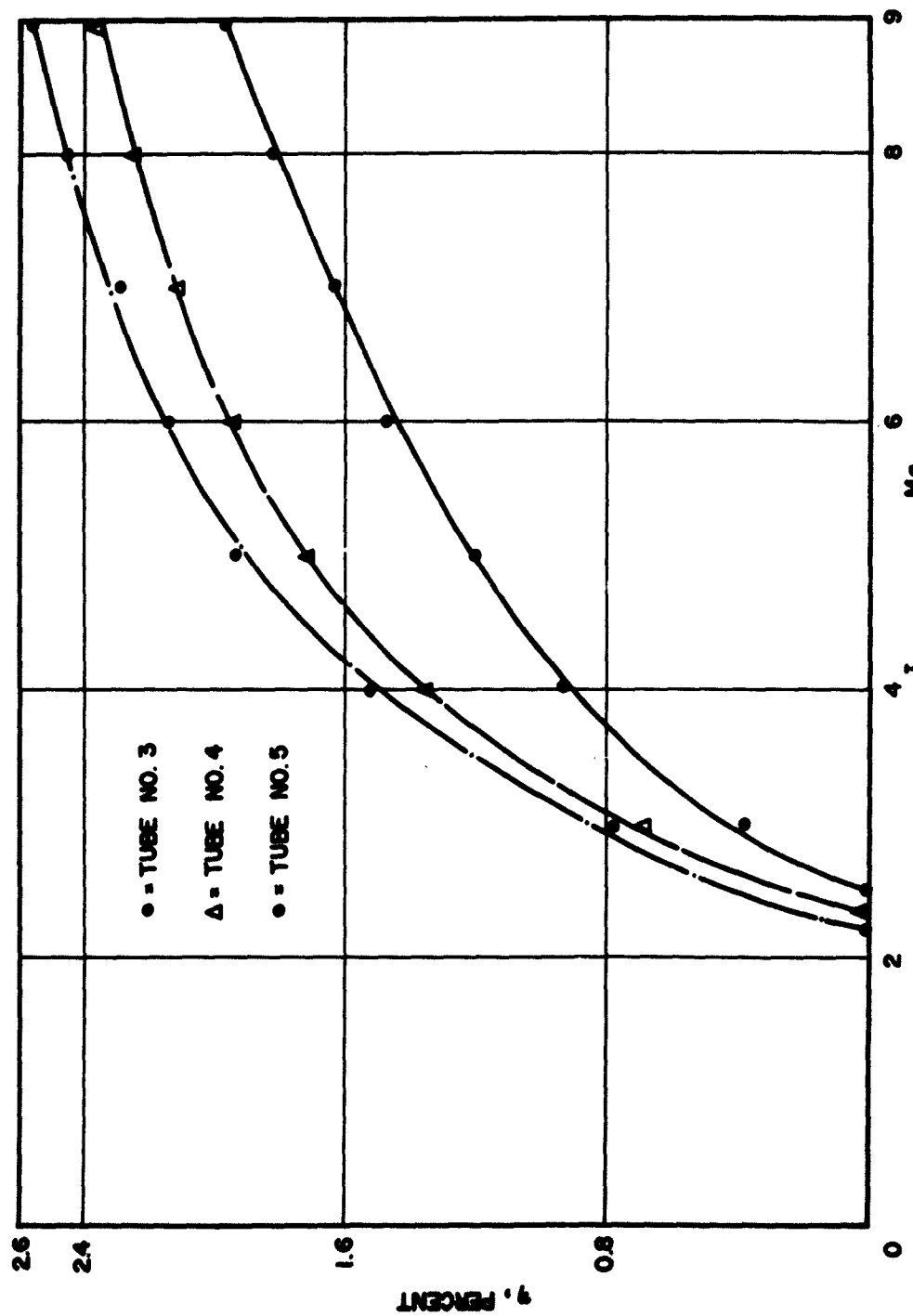

FIG. 5.7 EFFICIENCY VS. COLLECTOR CURRENT FOR EXPERIMENTAL BWO. (f = 2.8 Gc, V_{HELIX} = 700 VOLTS) (TUBE NUMBERS REFER TO THOSE SPECIFIED IN FIG. 5.2)

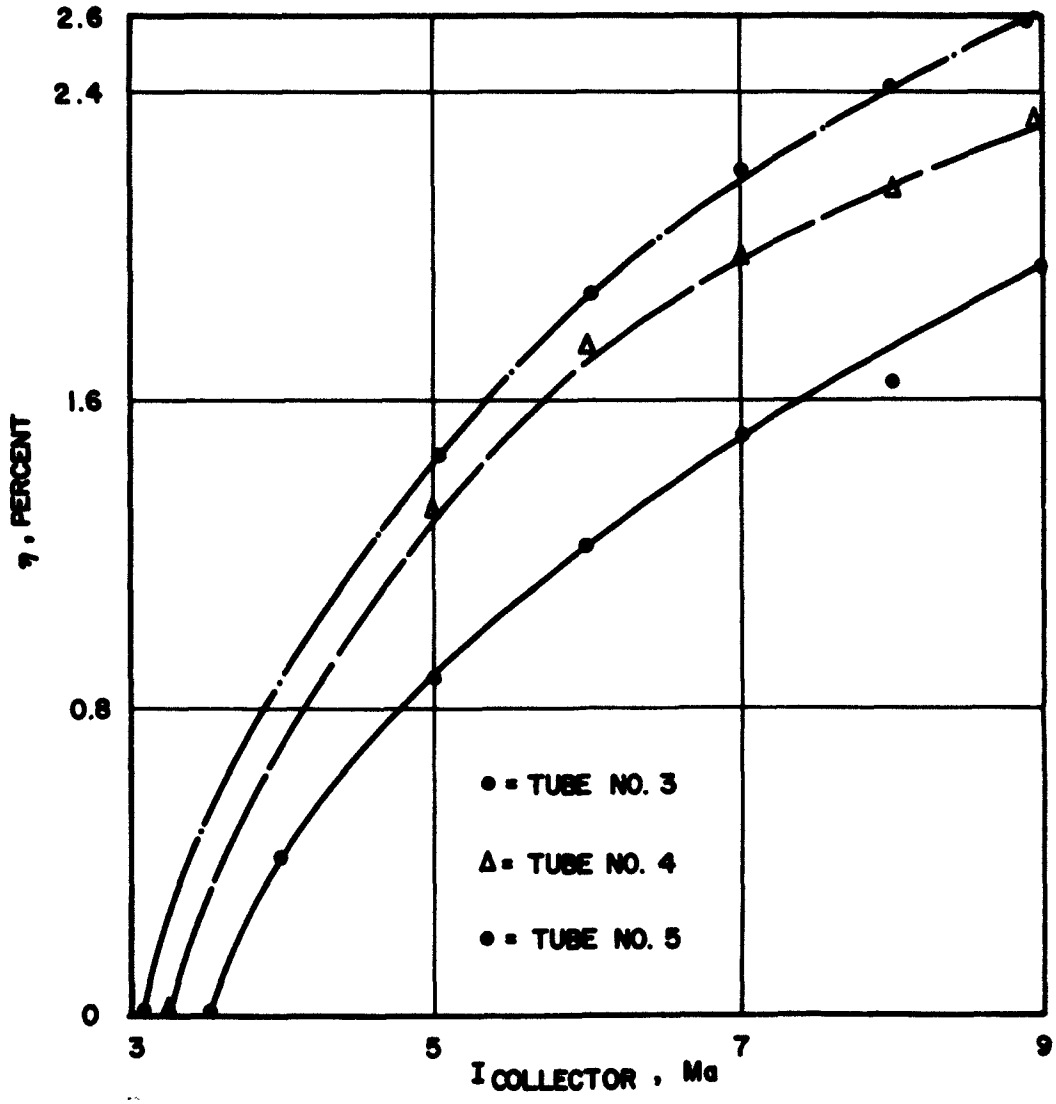

FIG. 5.8 EFFICIENCY VS. COLLECTOR CURRENT FOR EXPERIMENTAL BWO. (f = 3.0 Gc, V_{HELIX} = 900 VOLTS) (TUBE NUMBERS REFER TO THOSE SPECIFIED IN FIG. 5.2)

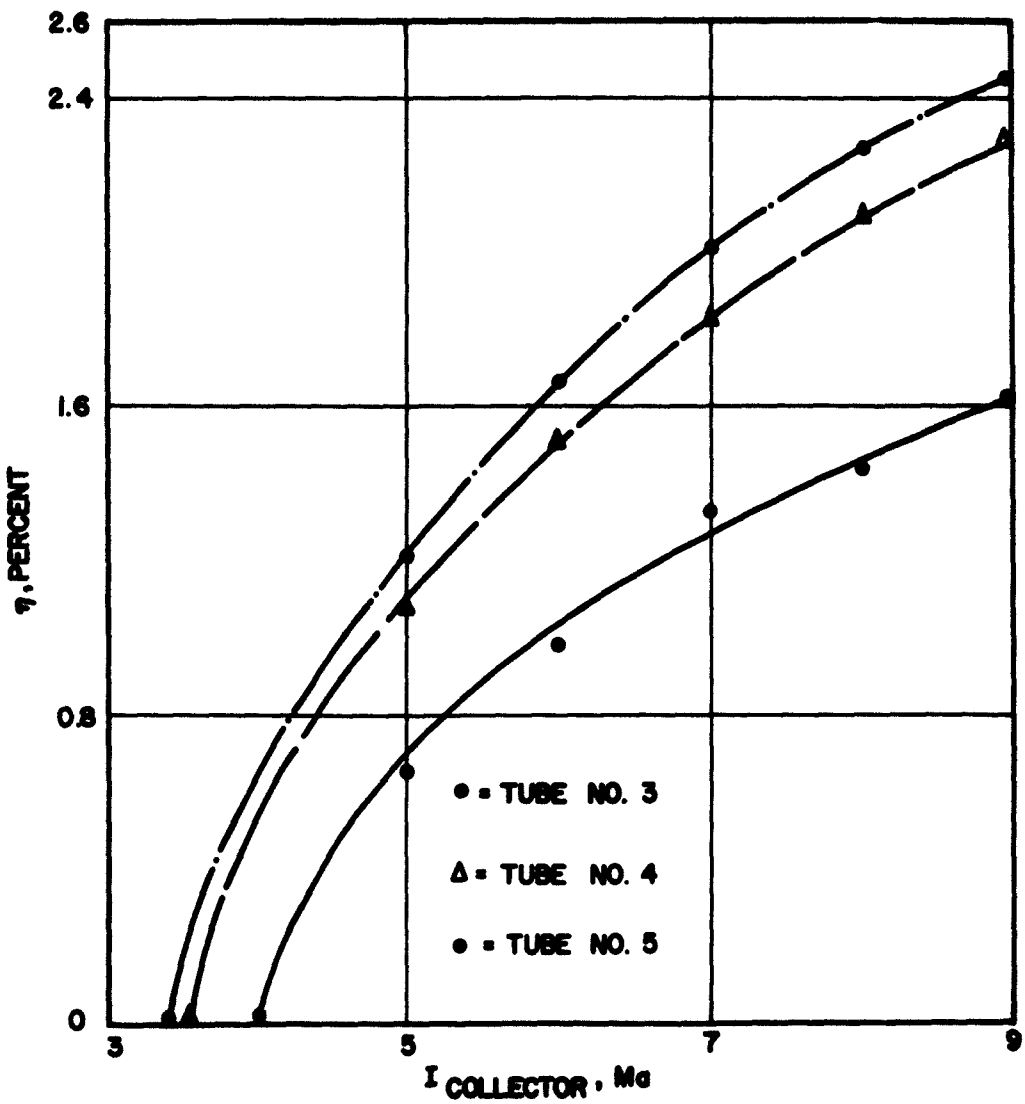

FIG. 5.9 EFFICIENCY VS. COLLECTOR CURRENT FOR EXPERIMENTAL BWO. (f = 3.2 Gc, V_{HELIX} = 1100 VOLTS) (TUBE NUMBERS REFER TO THOSE SPECIFIED IN FIG. 5.2)

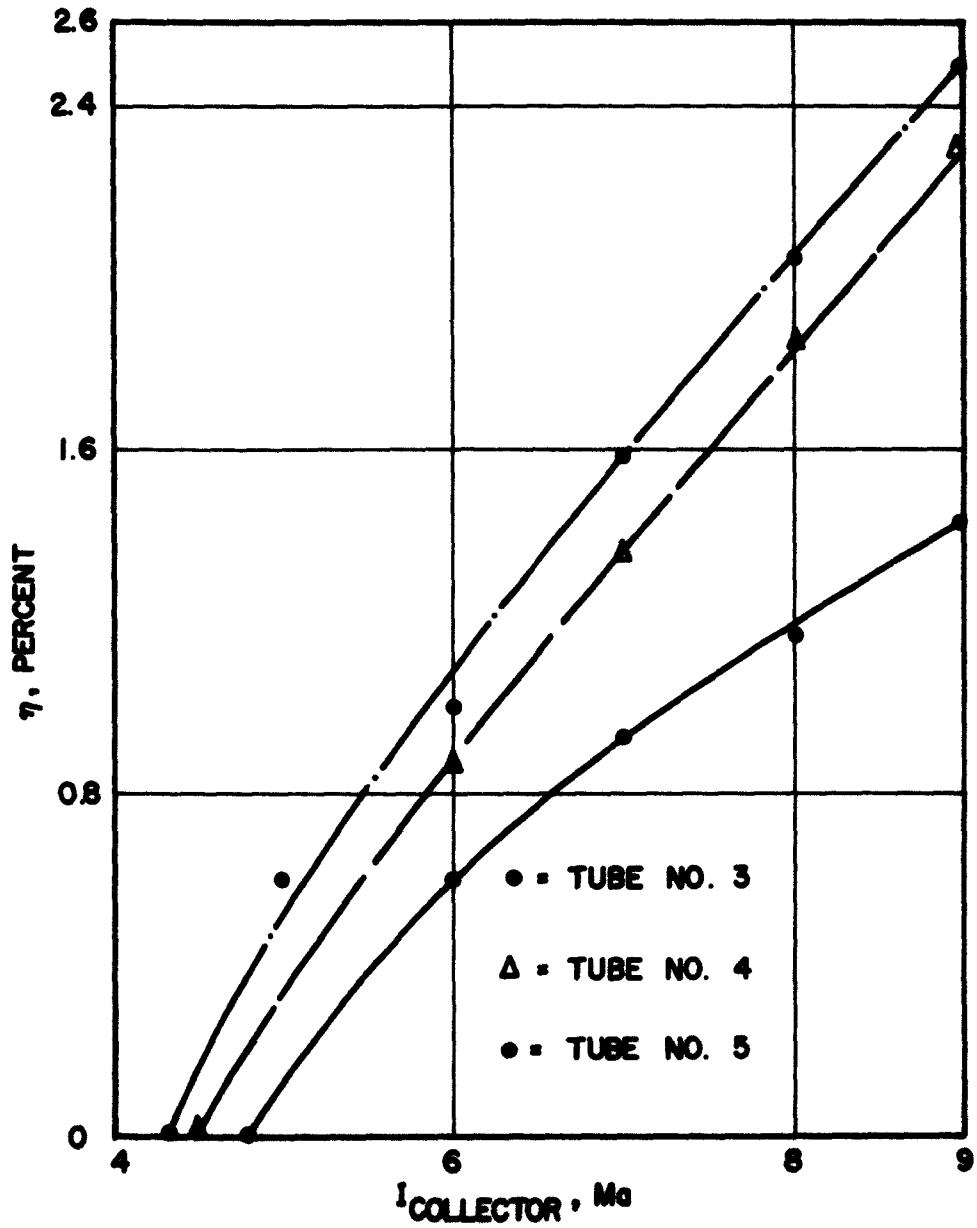

FIG. 5.10 EFFICIENCY VS. COLLECTOR CURRENT FOR EXPERIMENTAL BWO. ($f = 3.4$ Gc, $V_{HELIX} = 1350$ VOLTS) (TUBE NUMBERS REFER TO THOSE SPECIFIED IN FIG. 5.2)

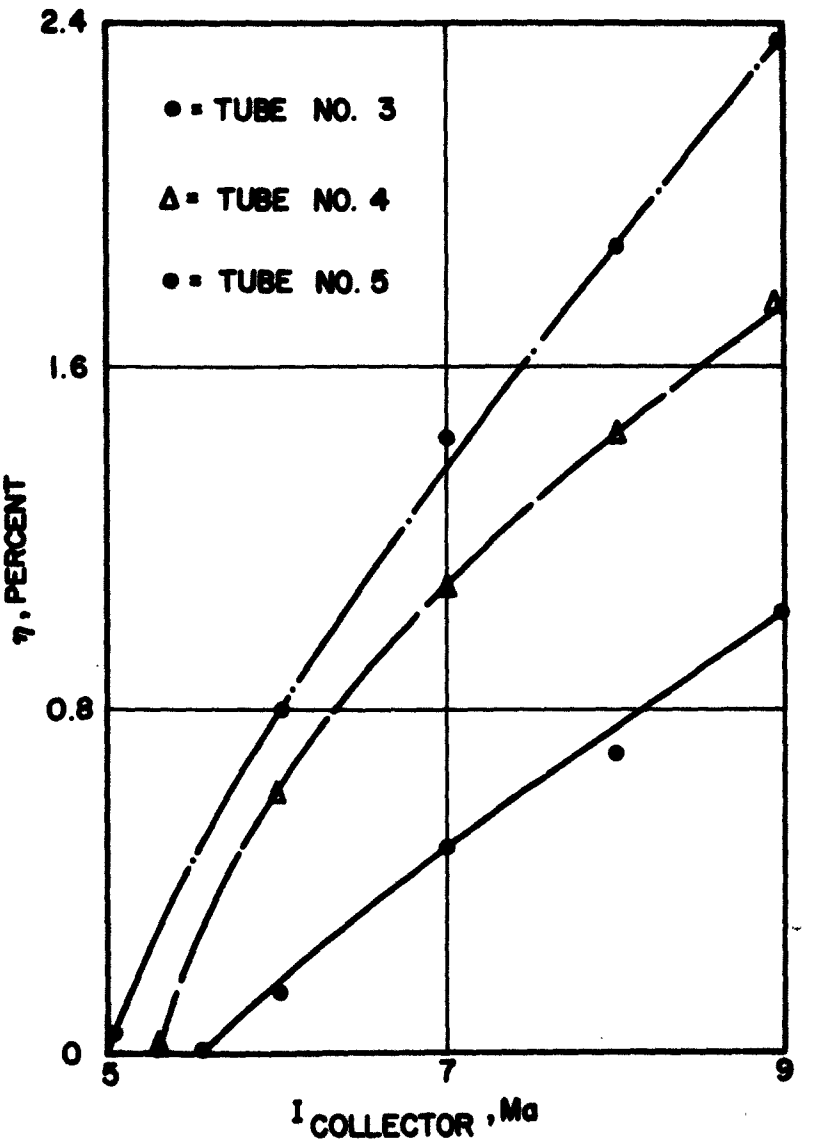

FIG. 5.11 EFFICIENCY VS. COLLECTOR CURRENT FOR EXPERIMENTAL BWO. (f = 3.75 Gc, V_{HELIX} = 1900 VOLTS) (TUBE NUMBERS REFER TO THOSE SPECIFIED IN FIG. 5.2)

frequencies. Efficiency versus frequency curves at the maximum collector current are shown in Fig. 5.12 and the start-oscillation currents versus frequency for the different configurations are shown in Fig. 5.13.

5.3 Discussion of Results and Conclusions

The start-oscillation current for different configurations is shown in Fig. 5.13. It can be seen from these plots that the start-oscillation current in the tapered tubes is lower than that of the uniform one. However, the decrease in the start-oscillation current is less than what it should have been had the tube been made uniform over the whole length. An increase in the length of a uniform tube from L_o to L_1 should result in a decrease in the start-oscillation current from I_o to I_1 where

$$\frac{I_1}{I_o} = \left(\frac{L_o}{L_1}\right)^3 \quad . \tag{5.3}$$

It can then be concluded that for this tube the start-oscillation current of the tapered tube is higher than that of a uniform one of the same length. This is in agreement with the theory of Chapter II where it was predicted that for small values of C the start-oscillation current does increase, even when the interaction impedance is assumed constant. In this tube the C value at start oscillation is very small and of course the interaction impedance of the tapered section is less than that of a uniform one thus resulting in a higher start-oscillation current.

It can be seen, however, from Figs. 5.3 through 5.12 that the efficiency is considerably enhanced by the taper. It is well known from theoretical[20] and experimental[5] results that when a BWO is operating at a current greater than approximately twice the start-oscillation current,

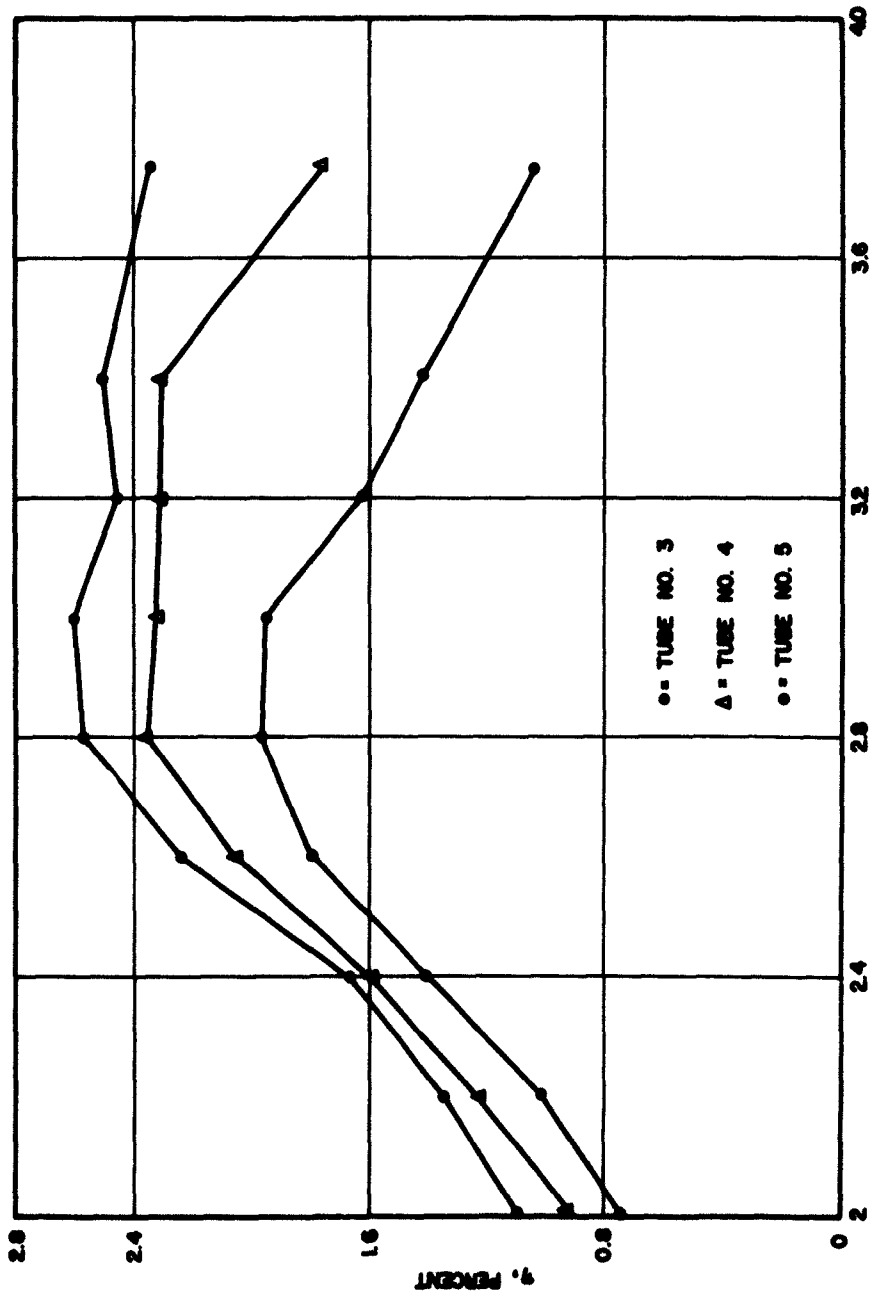

FIG. 5.12 EFFICIENCY VS. FREQUENCY FOR EXPERIMENTAL BACKWARD-WAVE OSCILLATOR.

($I_{COLLECTOR}$ = 9 ma) (TUBE NUMBERS REFER TO THOSE SPECIFIED IN FIG. 5.2)

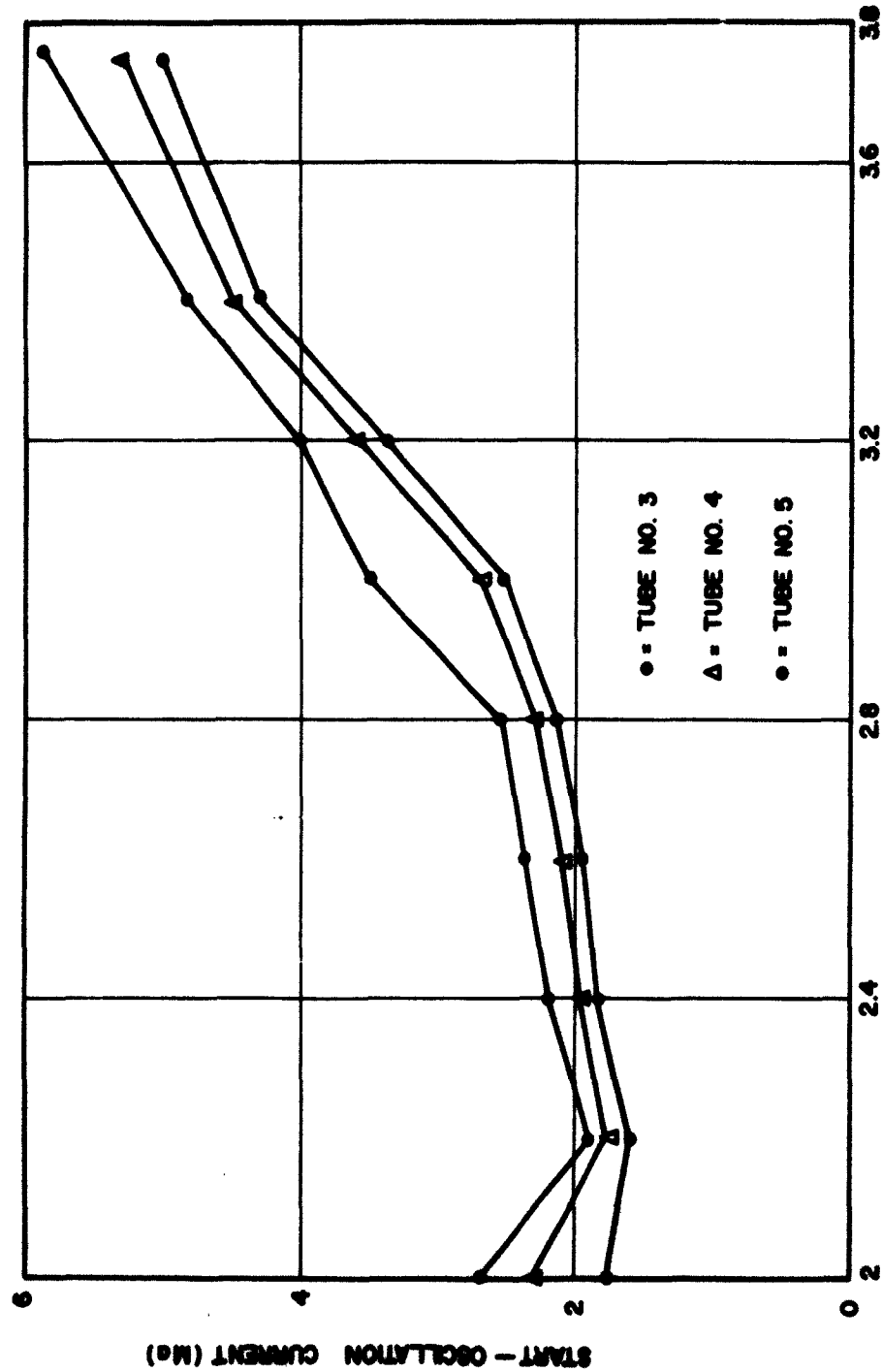

FIG. 5.13 START-OSCILLATION CURRENT VS. FREQUENCY FOR EXPERIMENTAL BWO.

(TUBE NUMBERS REFER TO THOSE SPECIFIED IN FIG. 5.2)

increasing the length of the tube will have no effect on the efficiency. For most of the cases compared here, the operating current was greater than twice the start-oscillation current and the efficiency was enhanced by the addition of a tapered section. The efficiency improvement factor varies from 1.2 to 2.0 over the frequency range 2.0 to 3.75 Gc.

It was also found that when the taper was extended beyond a certain value the efficiency was unaffected. Specifically, tubes numbers 2 and 1 with 15 and 20 percent tapers respectively gave essentially the same efficiency as tube number 3 which has a 10 percent taper.

The fact that the start-oscillation current is higher in the tapered tube than that in a uniform one of the same length but that the efficiency is enhanced by tapering can be justified by a simple physical explanation of the device operation. At start oscillation very little kinetic energy of electrons has been converted into r-f power. The electron velocity is then essentially constant along the length of the tube and negligible bunching takes place. A taper in the circuit phase velocity which is intended to phase focus a bunch of electrons in a favorable decelerating phase will not serve its purpose in this case because there actually is no bunch to focus. Since C in this tube is very small, the increase in the start-oscillation current is in agreement with the theoretical predictions. However, when the device is operating at currents well above the start-oscillation current strong r-f fields are present on the helix which modulate the electron velocity and thus give rise to a bunch at some point along the tube. Introducing a velocity taper at this point to keep this bunch in a decelerating phase will then enable the r-f fields to extract more energy from the electrons and thus enhance the efficiency.

It can then be concluded that the circuit phase velocity tapers derived under a hard-kernel-bunch approximation serve well in the design of more efficient backward-wave devices. Their usefulness has been experimentally verified here, and the taper that was employed here should not be considered as optimum.

CHAPTER VI. PREBUNCHED BEAM BACKWARD-WAVE OSCILLATOR

6.1 Introduction

All previous analyses of backward-wave oscillators have assumed that the beam enters the slow-wave structure with negligible r-f modulation. It was shown in the nonlinear analysis in Chapter IV that a tightly bunched beam introduced into a backward-wave slow-wave structure results in very high efficiencies when the structure phase velocity is tapered to keep the wave and the bunch in synchronism. It was also mentioned there that to obtain a tight bunch, a narrow-band circuit would presumably have to be employed and thus limit the tuning range of a BWO.

It is believed that a scheme similar to that of a two cavity klystron, where the output cavity is replaced by a backward-wave structure would combine the desirable high efficiency of a klystron and the voltage tunability of a BWO. The backward-wave structure can be made to operate in a fundamental backward-wave mode where a high interaction impedance can be achieved. This would require a higher voltage, however, than one operating on a backward space harmonic. The r-f structure can also be tapered to achieve better efficiencies. A diagram of this scheme is shown in Fig. 6.1.

In this chapter the start-oscillation conditions for a prebunched beam backward-wave oscillator are investigated. Both the effect of velocity and current modulation are discussed. The effect of the drift angle between the modulating electrode and the entrance plane of the slow-wave structure were examined and an optimum drift angle was found.

The method employed in this analysis and the results obtained from it are presented in the following sections.

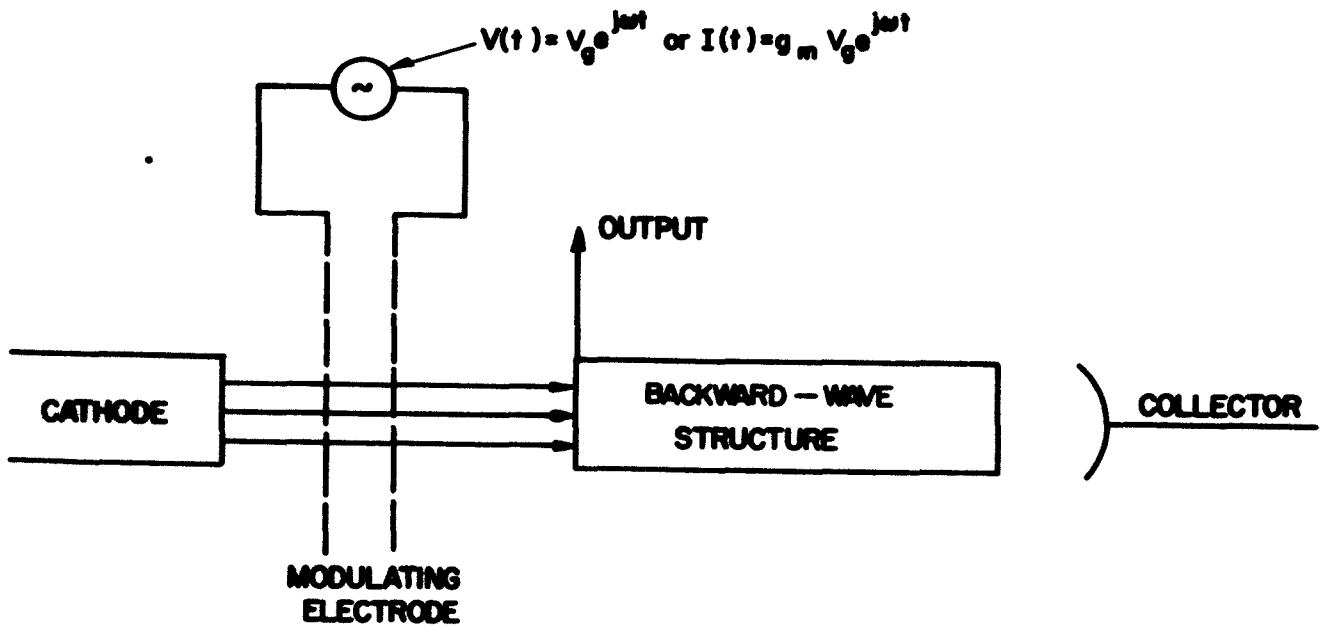

FIG. 6.1 PREMODULATED BACKWARD-WAVE OSCILLATOR.

6.2 Backward-Wave Oscillator Equations

A general set of equations describing the behavior of a backward-wave oscillator were derived in Chapter III and are given by Eqs. 3.42 through 3.44. For a uniform, lossless oscillator these equations reduce to,

$$\frac{d^2V_{cn}(y)}{dy^2} + \left(\frac{1 + C_o b}{C_o}\right)^2 V_{cn}(y) = 4C_o(1 + C_o b)\,\rho_{1n}(y) \quad , \quad (6.1)$$

$$\frac{du_{1n}(y)}{dy} + \frac{d\rho_{1n}(y)}{dy} + \frac{j}{C_o}\,\rho_{1n}(y) = 0 \quad , \quad (6.2)$$

$$\frac{1}{2}\,\frac{dV_{cn}(y)}{dy} + j\,\frac{4C_o\,QC}{[1 - 2C_o\sqrt{QC}]^2}\,\frac{1}{(1 + C_o b)}\,\rho_{1n}(y) = \frac{j}{C_o}\,u_{1n}(y) + \frac{du_{1n}(y)}{dy} \quad , \quad (6.3)$$

where all the quantities appearing in these equations have been defined already. These equations have been programmed on an analog computer and the procedure for obtaining an oscillation condition is the same as that employed in Chapter III and is discussed in detail there and in Appendix B.

The case of a premodulated beam can be easily accommodated on the analog computer. This is accomplished by merely specifying the r-f modulation on the beam at the input to the slow-wave structure. It should be recalled that for an unmodulated beam, $\rho_{1n}(0) = u_{1n}(0) = 0$. For a premodulated beam $\rho_{1n}(0)$ and $u_{1n}(0)$ will have some finite value depending on the depth of modulation.

The values of $\rho_{in}(0)$ and $u_{in}(0)$ can be determined as a function of the modulating voltage through a space-charge and gap modulation analysis. This analysis is presented in the following sections.

6.3 Space-Charge Wave and Gap Modulation Equations

Space-charge wave propagation on an electron beam has been treated in detail by several authors[41,42] and will not be repeated here. It is found that two space-charge waves that are of interest exist on the electron beam. One wave travels with a phase velocity slightly faster than the electrons and the other slightly slower. These are referred to as the fast and slow space-charge waves respectively. Their phase velocities can be expressed as*,

$$v_{ps} = \frac{u_o}{1 + \frac{\omega_p}{\omega}} \tag{6.4}$$

and

$$v_{pf} = \frac{u_o}{1 - \frac{\omega_p}{\omega}} , \tag{6.5}$$

where the quantities appearing in the above equations have been defined already. For a beam in a drift tube, ω_p is replaced by a reduced plasma radian frequency ω_q. A premodulated beam interacting with a forward-wave structure was investigated by Rowe and Meeker[40].

The total velocity, line charge density and current of the beam can be expressed as follows:

$$u = u_o + u_1 e^{j(\omega t - \beta_e z)} , \tag{6.6}$$

---

* Subscript "s" refers to slow wave and "f" to fast one.

where

$$u_1 = u_{1s} e^{-j\beta_q z} + u_{1f} e^{j\beta_q z} \quad ; \tag{6.7}$$

$$\rho = \rho_o + \rho_1 e^{j(\omega t - \beta_e z)} \quad , \tag{6.8}$$

where

$$\rho_1 = \rho_{1s} e^{-j\beta_q z} + \rho_{1f} e^{j\beta_q z} \quad , \tag{6.9}$$

$$i = \rho_t u_t = - I_o + i_1 e^{j(\omega t - \beta_e z)} \quad , \tag{6.10}$$

$$i_1 = i_{1s} e^{-j\beta_q z} + i_{1f} e^{j\beta_q z} \quad . \tag{6.11}$$

Equations 6.7, 6.9 and 6.11 can be written in a different form as follows:

$$u_1 = (u_{1s} + u_{1f}) \cos \beta_q z + j(u_{1f} - u_{1s}) \sin \beta_q z \quad , \tag{6.12}$$

$$\rho_1 = (\rho_{1s} + \rho_{1s}) \cos \beta_q z + j(\rho_{1f} - \rho_{1s}) \sin \beta_q z \tag{6.13}$$

and

$$i_1 = (i_{1s} + i_{1f}) \cos \beta_q z + j(i_{1f} - i_{1s}) \sin \beta_q z \quad . \tag{6.14}$$

6.4 Velocity Modulation of the Beam

It is assumed here that a small-amplitude voltage applied across a pair of short transit-angle grids is employed to velocity modulate the beam. If the electrodes' position is taken as z = 0, then at this position u becomes,

$$u = u_o + u_1(0) e^{j\omega t} \quad . \tag{6.15}$$

If the modulating voltage is taken as $V_g e^{j\omega t}$ and it is assumed that $V_g \ll V_o$, where V_o is the d-c beam potential, then $u_1(0)$ can be expressed as

$$u_1(0) = \frac{V_g}{2V_o} u_o \quad . \tag{6.16}$$

For this case the following conditions must be satisfied,

$$u_{1s} = u_{1f} \quad , \tag{6.17}$$

$$i_{1s} + i_{1f} = 0 \quad . \tag{6.18}$$

From these conditions, it can be readily seen from Eq. 6.12 that

$$u_{1s} = u_{1f} = \frac{u_1(0)}{2} = \frac{V_g}{4V_o} u_o \quad . \tag{6.19}$$

From Eq. 6.12 we finally obtain,

$$u_{1n} = \frac{u_1}{u_o} = \frac{V_g}{2V_o} \cos \beta_q z \quad . \tag{6.20}$$

From Eq. 6.14 we get,

$$i_{1n} = \frac{i_1}{I_o} = j2 \frac{i_{1f}}{I_o} \sin \beta_q z \quad . \tag{6.21}$$

The continuity equation is expressed as,

$$\nabla \cdot i + \frac{\partial \rho}{\partial t} = 0 \quad . \tag{6.22}$$

For this one-dimensional problem, Eq. 6.22 reduces to,

$$\frac{\partial i}{\partial z} + \frac{\partial \rho}{\partial t} = 0 \quad . \tag{6.23}$$

From Eq. 6.23 it can be easily shown that,

$$\beta_{s,f}\, i_{1s,f} = \omega\, \rho_{1s,f} \quad , \tag{6.24}$$

where

$$\beta_s = (\beta_e + \beta_q) \tag{6.25}$$

and

$$\beta_f = (\beta_e - \beta_q) \quad . \tag{6.26}$$

Now using the relation

$$i = \rho\, u \tag{6.27}$$

and assuming small-signal conditions results in,

$$I_o = -\rho_o\, u_o \tag{6.28}$$

and

$$i_{1s,f} = \rho_o\, u_{1s,f} + u_o\, \rho_{1s,f} \quad . \tag{6.29}$$

Substituting Eq. 6.29 in Eq. 6.24 we get,

$$i_{1s,f} = \left(\frac{\omega \rho_o}{\omega - \beta_{s,f}\, u_o} \right) u_{1s,f} \quad . \tag{6.30}$$

Substituting for $\beta_{s,f}$ its values from Eq. 6.25 and Eq. 6.26 and employing Eq. 6.28 and Eq. 6.19 we finally obtain,

$$\frac{i_{1s,f}}{I_o} = \pm \left(\frac{\omega}{\omega_q} \right) \frac{V_g}{4V_o} \quad . \tag{6.31}$$

Substituting Eq. 6.31 in Eq. 6.21 yields,

$$i_{1n} = \frac{i_1}{I_o} = -j \left(\frac{\omega}{\omega_q} \right) \frac{V_g}{2V_o} \sin \beta_q z \quad . \tag{6.32}$$

From Eq. 6.29 $\rho_{1s,f}$ can be expressed as,

$$\frac{\rho_{1s,f}}{\rho_o} = -\left[\frac{u_{1s,f}}{u_o} + \frac{i_{1s,f}}{I_o}\right] . \qquad (6.33)$$

Substituting Eq. 6.33 in Eq. 6.9 and employing Eq. 6.31 and Eq. 6.19 results in,

$$\rho_{1n} = \frac{\rho_1}{\rho_o} = -\frac{V_g}{2V_o}\cos\beta_q z + j\left(\frac{\omega}{\omega_q}\right)\frac{V_g}{2V_o}\sin\beta_q z . \qquad (6.34)$$

The values of u_{1n} and ρ_{1n} at the entrance to the slow-wave structure, which are needed to solve Eqs. 6.4 through 6.6, can now be computed from Eqs. 6.20 and 6.34 for specified values of V_g/V_o, (ω/ω_q) and $\beta_q z$.

The factor ω/ω_q can be calculated by assuming that it is the same in the drift region as in the interaction region. The space-charge parameter QC is related to ω_q/ω as follows:

$$4QC \approx \left(\frac{\omega_q}{C_o\omega}\right)^2 . \qquad (6.35)$$

Thus for a specified value of QC and C_o, ω/ω_q can be easily calculated.

$\beta_q z$ is determined when the drift region length is specified. This can assume any value. It is desirable, however, to have the drift region length as short as possible. $\beta_q z$ is the radian plasma drift length from the modulating structure to the input plane of the r-f structure.

The start-oscillation conditions were investigated for several values of $\beta_q z$. It was found that a minimum start-oscillation length is obtained when $\beta_q z = \pi/4$.

The start-oscillation conditions are presented in Figs. 6.2 and 6.3. In Fig. 6.2, b_1/b_o is plotted as a function of $V_g/2V_o$, where b_1

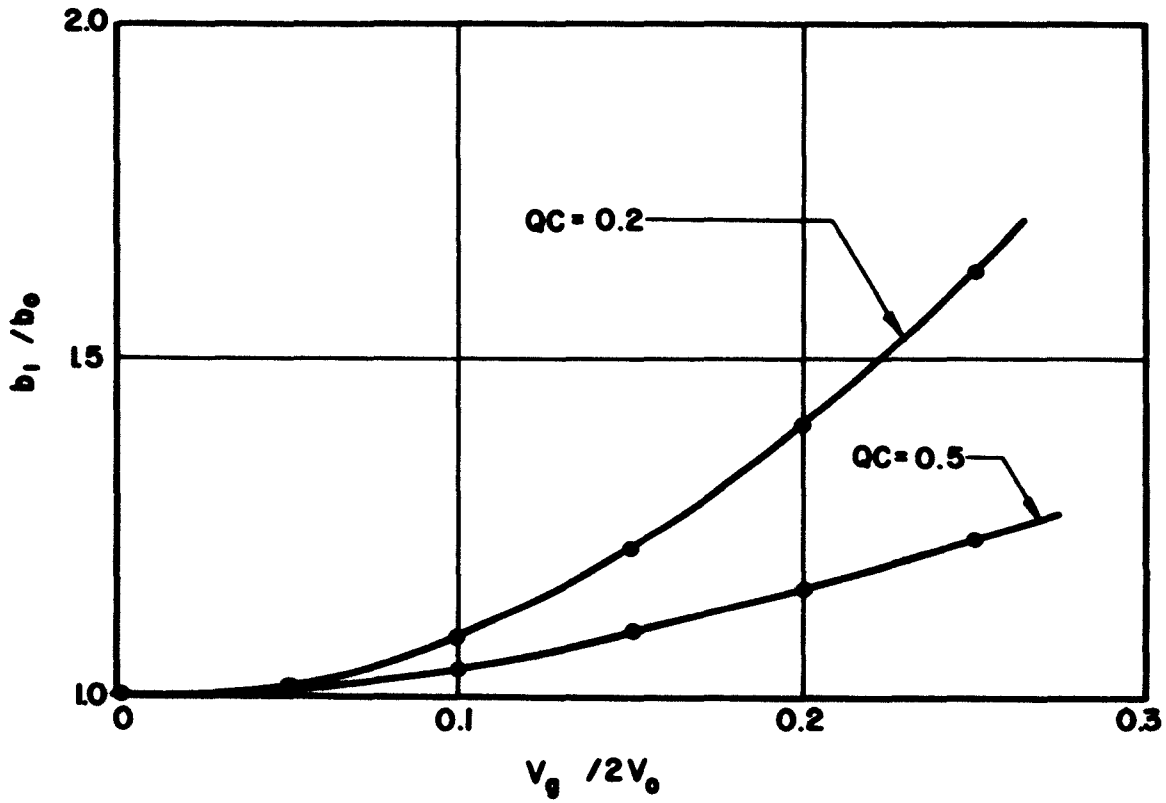

b_1 = the synchronism parameter for the premodulated BWO.

b_o = the synchronism parameter for a regular BWO.

FIG. 6.2 b_1/b_o VS. $V_g/2V_o$ FOR A VELOCITY PREMODULATED BWO. ($\beta_q z = \pi/4$, C = 0.05)

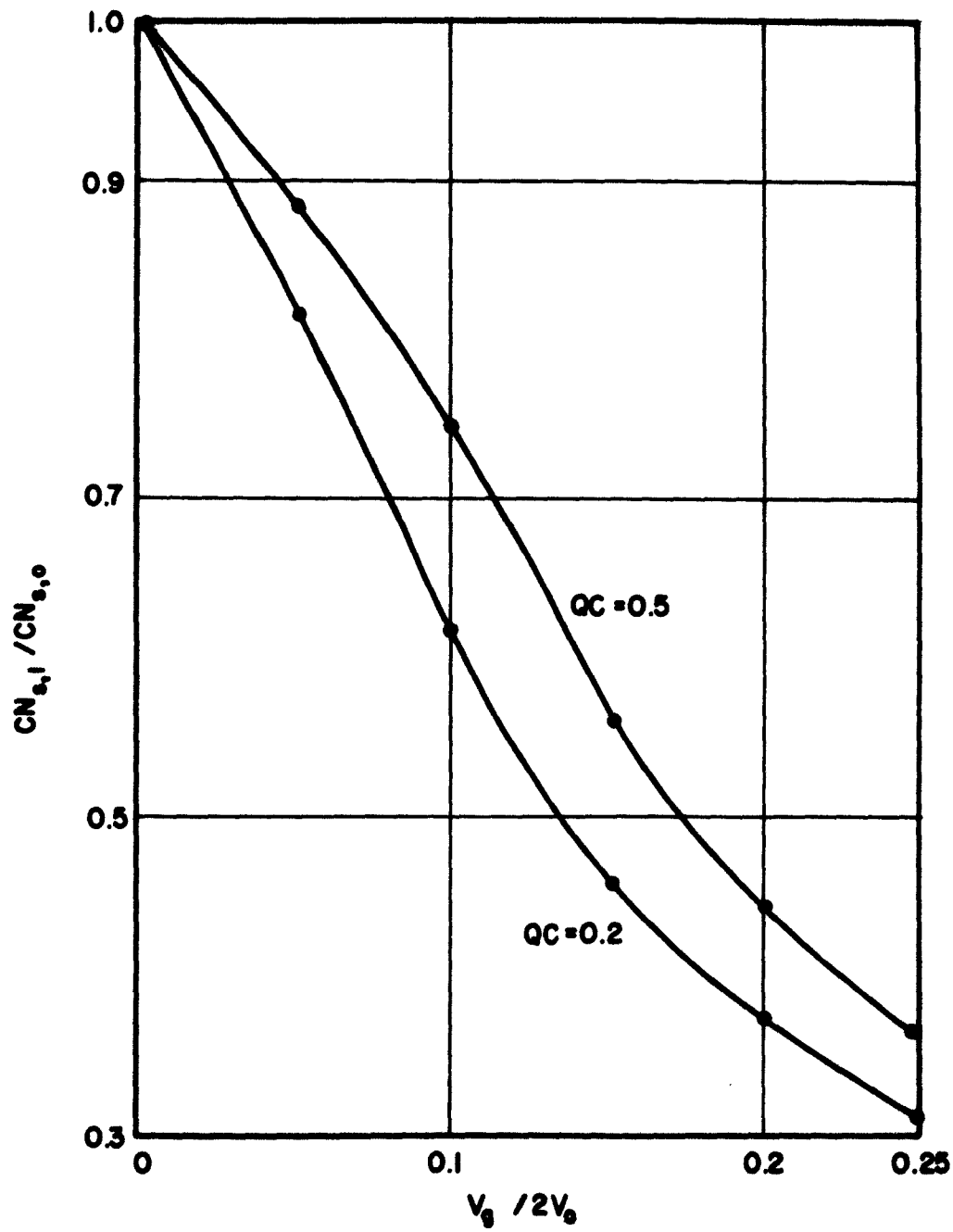

FIG. 6.3 THE RATIO OF THE NORMALIZED START-OSCILLATION LENGTH OF A VELOCITY PREMODULATED BWO TO THAT OF A REGULAR ONE VS. $V_g/2V_o$. ($\beta_q z = \pi/4$, C = 0.05)

is the synchronism parameter for the prebunched oscillator and b_o pertains to a regular one. The parameter b has already been defined in Chapter III and is also defined in the list of symbols at the end of this report.

In Fig. 6.3 the normalized start-oscillation length of a premodulated BWO ($CN_{s,1}$) is compared to that of a regular one ($CN_{s,o}$) as a function of $V_g/2V_o$. As explained in detail in Chapter III, the ratio of the actual physical length in the premodulated oscillator to that in a regular one can be expressed as,

$$\frac{z_1}{z_o} = \left(\frac{1 + Cb_1}{1 + Cb_o}\right)\left(\frac{CN_{s,1}}{CN_{s,o}}\right) \quad . \tag{6.36}$$

From the above results we can conclude that the start-oscillation length in a velocity premodulated BWO can be much lower than that of a regular one and the larger the modulation parameter $V_g/2V_o$ the greater the decrease in the start-oscillation length. For a premodulated and a regular BWO having the same slow-wave structure and oscillation frequency, the beam voltage in the premodulated one will be slightly higher. The ratio of the voltage in the premodulated one to that in the regular one can be expressed as

$$\frac{V_1}{V_o} = \left(\frac{1 + Cb_1}{1 + Cb_o}\right)^2 \quad . \tag{6.37}$$

6.5 Current Modulation of the Beam

For the case of current modulation of the stream where the current modulation at z = 0 is given by $g_m V_g e^{j\omega t}$, the following conditions must be satisfied,

$$u_{1s} + u_{1f} = 0 \tag{6.38}$$

and

$$i_{1s} = i_{1f} = \frac{g_m V_g}{2} \quad . \tag{6.39}$$

Following the same procedure employed in the velocity modulation case, the normalized current, velocity and space-charge density can be easily expressed as,

$$i_{1n} = \frac{i_1}{I_o} = \frac{g_m V_g}{I_o} \cos \beta_q z \quad , \tag{6.40}$$

$$u_{1n} = \frac{u_1}{u_o} = -j\left(\frac{\omega_q}{\omega}\right)\frac{g_m V_g}{I_o} \sin \beta_q z \quad , \tag{6.41}$$

$$\rho_{1n} = \frac{\rho_1}{\rho_o} = -\frac{g_m V_g}{I_o} \cos \beta_q z + j \frac{\omega_q}{\omega} \frac{g_m V_g}{I_o} \sin \beta_q z \quad . \tag{6.42}$$

It can be seen from the above equations that velocity modulation becomes current modulation after 90 degrees of drift. The start-oscillation conditions were then investigated for this case for a drift length $\beta_q z = 3\pi/4$. The results are given in Figs. 6.4 and 6.5.

Comparing these results to the velocity modulation case, it is seen that they are similar. The start-oscillation length decreases with current modulation and the greater the modulation the greater the decrease. In this case also the beam potential of a premodulated oscillator will be slightly greater than that of a regular one if both have the same slow-wave structure and operate at the same frequency.

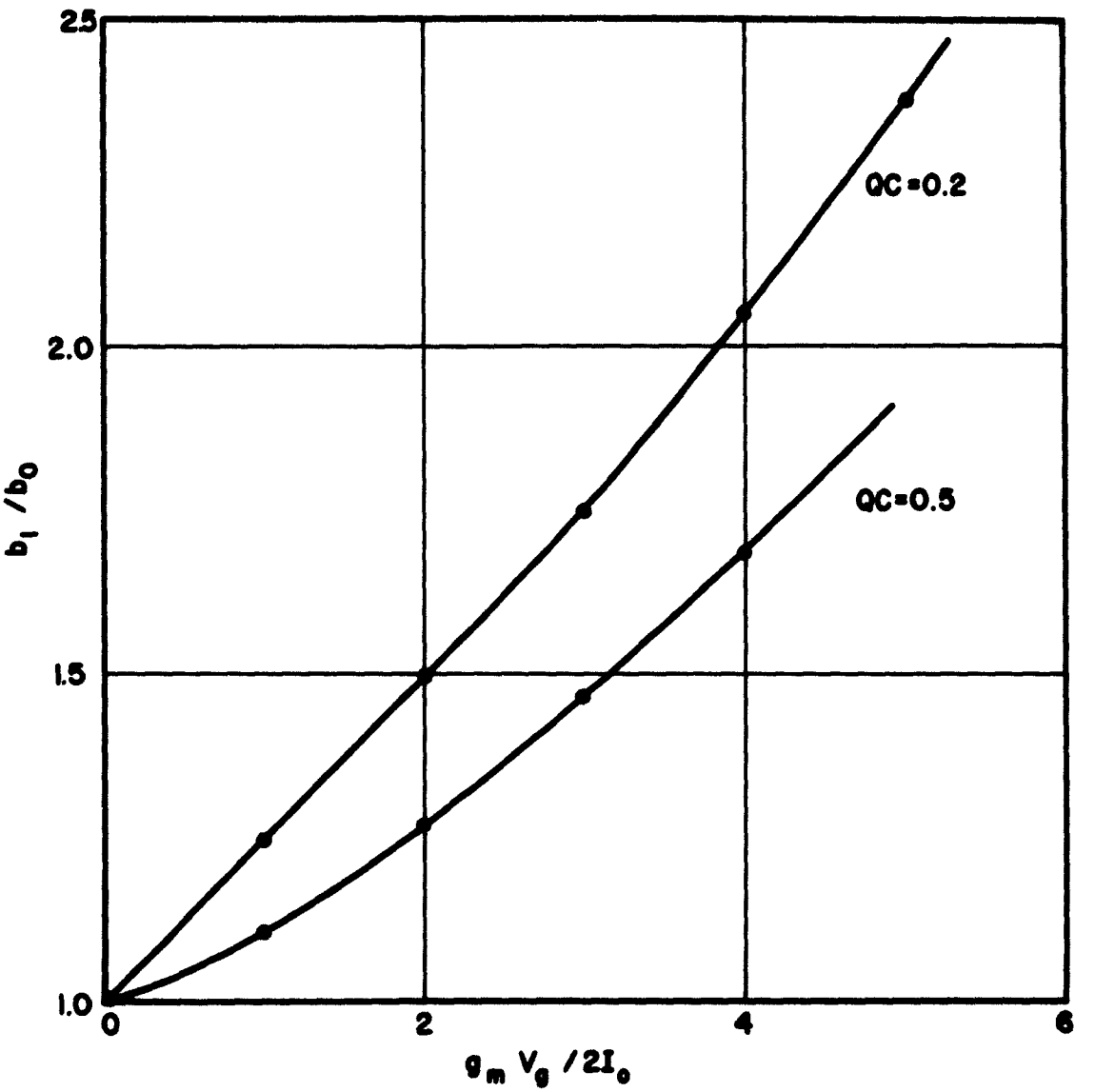

b_1 = the synchronism parameter for the premodulated BWO.

b_o = the synchronism parameter for the regular one.

FIG. 6.4 b_1/b_o VS. $g_m V_g/2I_o$ FOR A CURRENT PREMODULATED BWO.
($\beta_q z = 3\pi/4$, C = 0.05)

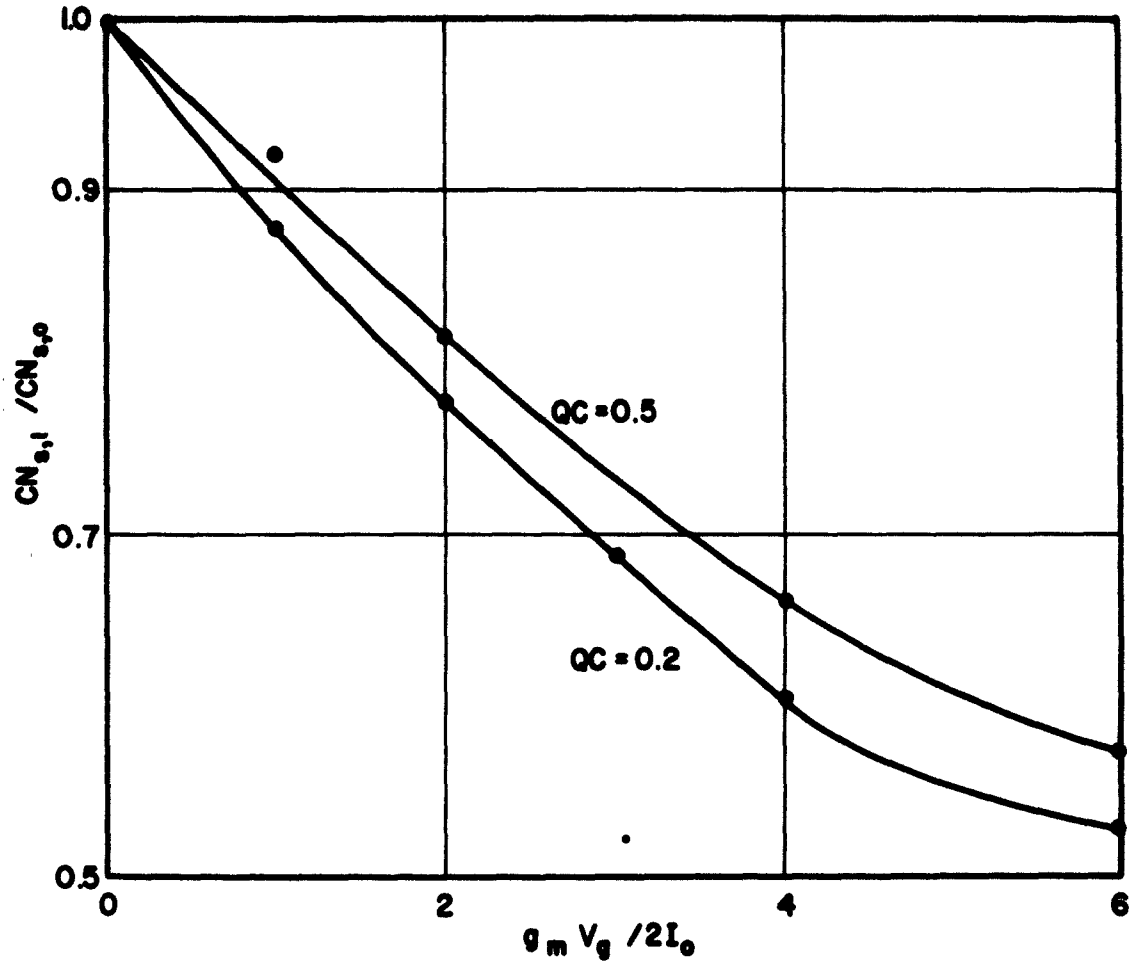

FIG. 6.5 THE RATIO OF THE NORMALIZED START-OSCILLATION LENGTH OF A CURRENT PREMODULATED BWO TO THAT OF A REGULAR ONE VS. $g_m V_g/2I_o$. ($\beta_q z = 3\pi/4$, C = 0.05)

CHAPTER VII. EFFICIENCY ENHANCEMENT OF BACKWARD-WAVE OSCILLATORS BY COLLECTOR DEPRESSION

7.1 Introduction

It is well known that the overall efficiency of beam-type devices such as traveling-wave amplifiers, klystrons, backward-wave oscillators and others, can be improved by employing so called "depressed collectors"[43,44,45]. This is achieved by operating the collector at a lower potential than the r-f structure thus conserving much of the power usually dissipated in it. The collector can be segmented into several sections and each section can be operated at an optimum potential.

In order to determine the optimum potentials for a specified set of segments, information about the energy state of the spent beam in a certain device is essential. The nonlinear calculations of Chapter IV were primarily concerned with the r-f interaction process, but they do give, however, information about the energy state of the spent beam in a backward-wave oscillator. This information can be used to determine the effect of collector depression on the overall efficiency of the device.

It is worthy to note here that even though a depressed collector can improve the overall efficiency of the device, it will not result in higher r-f power outputs. The improvement factor in efficiency due to collector depression will depend on the velocity spread of the spent beam, the greater the velocity spread the less the improvement factor will be for a fixed number of collector segments.

The velocity spread is generally greater in high interaction efficiency devices than that in low interaction efficiency ones. Since

the interaction efficiency of a backward-wave oscillator is very low, it is a good candidate for collector depression.

In this chapter the effect of collector depression on the efficiency of a backward-wave oscillator is investigated.

7.2 Theoretical Development

The evaluation of the effect of depressed collectors on the efficiency of a backward-wave oscillator is based on the theory developed by Rowe[46]. A brief presentation of the theoretical development is presented here.

The nonlinear calculations of beam-wave interaction in backward-wave oscillators were made for representative electron charge groups passing through the interaction region, where they are acted upon by both r-f circuit and space-charge fields. The total number of these charge groups constitutes the entering d-c beam charge. The velocity was defined in terms of the normalized Lagrangian variables as follows:

$$\frac{u_{tj}}{u_o} = \left[1 + 2\,Cu(y,\varphi_{o,j})\right] \tag{7.1}$$

where

$u_{tj} \triangleq$ the total velocity of the jth charge group,

$u(y,\varphi_{o,j}) \triangleq$ the normalized r-f velocity of the jth group.

From the principle of conservation of energy, the following relation can be written

$$\frac{mu_{tj}^2}{2} - qV_o = -qV_{qj} \tag{7.2}$$

where V_{qj} is the equivalent r-f potential for the jth group and is positive for kinetic energy given up (deceleration) by the group and negative when energy is absorbed by the charge group (acceleration). q is the charge of each of the groups.

For a group with average velocity u_o, Eq. 7.2 reduces to,

$$\frac{mu_o^2}{2} - qV_o = 0 \qquad (7.3)$$

which is simply the equivalence of the group's kinetic and potential energies.

Combining Eqs. 7.1, 7.2 and 7.3 results in,

$$\left(\frac{u_{tj}}{u_o}\right)^2 = [1 + 2\,Cu(y,\varphi_{o,j}]^2 = 1 - \frac{V_{qj}}{V_o} \quad . \qquad (7.4)$$

It is thus clear that a knowledge of $[1 + 2\,Cu_j]$ at the collector end of the device is essential for computing the plate-circuit efficiency for a multi-segment collector system. It will be assumed in this analysis that "m" electron charge groups are injected into the interaction region and that the beam transmission is 100 percent.

It is now convenient to define the following energies in joules associated with the device,

$\mathcal{E}_{d\text{-}c}$ = d-c beam input energy,

$\mathcal{E}_i$ = r-f input energy to the circuit, which is zero for a backward-wave oscillator,

$\mathcal{E}_d$ = r-f energy dissipated on the circuit,

$\mathcal{E}_c$ = d-c energy given to the collector,

$\mathcal{E}_o$ = r-f output energy.

Also characteristic efficiencies for the device can be defined as follows:

η_e = electronic conversion efficiency,

η_o = overall efficiency.

Assuming that "m" charge groups are injected into the interaction region, the electronic efficiency can then be written as,

$$\eta_e = \frac{\mathcal{E}_o - \mathcal{E}_i + \mathcal{E}_d}{\mathcal{E}_{d-c}} = 1 - \frac{\mathcal{E}_c}{\mathcal{E}_{d-c}} \tag{7.5}$$

and the overall efficiency as,

$$\eta_o = \frac{\mathcal{E}_o - \mathcal{E}_i}{\mathcal{E}_{d-c}} \quad . \tag{7.6}$$

It is obvious from Eqs. 7.5 and 7.6 that for a lossless structure, the electronic and overall efficiencies are equal.

The r-f energy given up by the beam is related to the electron group's r-f potentials as follows:

$$\mathcal{E}_o - \mathcal{E}_i + \mathcal{E}_d = \sum_{d=1}^{m} q\, V_{qj} \quad . \tag{7.7}$$

For a lossless backward-wave oscillator ($\mathcal{E}_i = \mathcal{E}_d = 0$).

In the case of a conventional BWO with the collector operated at the r-f structure potential the above defined energies and efficiencies are,

$$\mathcal{E}_{d-c} = m\, q\, V_o \quad , \tag{7.8a}$$

$$\mathcal{E}_c = \sum_{j=1}^{m} q(V_o - V_{qj}) \quad , \tag{7.8b}$$

$$\eta_e = 1 - \frac{\sum_{j=1}^{m} q(V_o - V_{qj})}{m\, q\, V_o} = \frac{1}{m} \sum_{j=1}^{m} \left(\frac{V_{qj}}{V_o} \right) \qquad (7.8c)$$

and

$$\eta_o = \frac{e_o}{q\, m\, V_o} \ . \qquad (7.8d)$$

The electronic efficiency given by Eq. 7.8c may also be written as,

$$\eta_e = \frac{1}{m} \sum_{j=1}^{m} \left\{ 1 - [1 + 2\, Cu(y, \varphi_{o,j}]^2 \right\} \ . \qquad (7.9)$$

The efficiency expressions for multi-segment collector backward-wave oscillators may be developed systematically from the above relations. It is assumed here that specific electron groups of the spent beam are collected at given potentials with one segment of the collector at the structure potential. Suppose then that the collector is segmented as shown in Fig. 7.1 where the d-c potentials are related as, $V_o > V_{c1} > V_{c2} > V_{c3} \ldots > V_{cr}$, i.e., r+1 segments are present. The total energy given up to the collector segments can then be expressed as,

$$e_{c,r+1} = \sum_{i=1}^{p_1} q(V_{c,r} - V_{qi}) + \sum_{j=1}^{p_2} q(V_{c,r-1} - V_{qj}) + \sum_{k=1}^{p_3} q(V_{c,r-2} - V_{qk})$$

$$+ \ \ldots \ + \sum_{\ell=1}^{p_{r+1}} q(V_o - V_{q\ell}) \qquad (7.10)$$

where

$$p_1 + p_2 + p_3 \ \ldots \ + p_{r-1} = m \ .$$

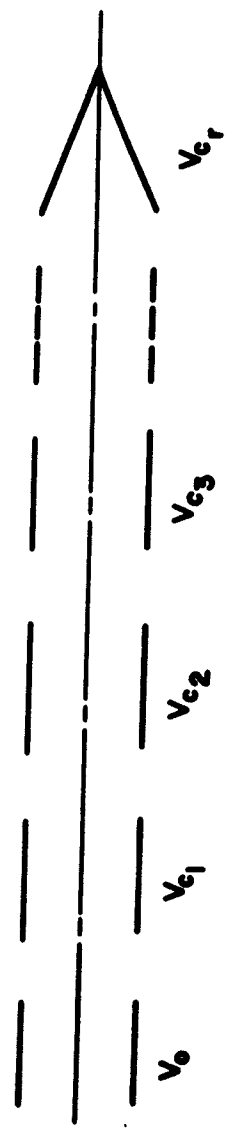

FIG. 7.1 SCHEMATIC DIAGRAM OF A SEGMENTED COLLECTOR.

The above equation can be simplified and expressed in terms of the charge group's velocities as follows:

$$\mathcal{E}_{c,r+1} = q\left\{ p_1 V_{c,r} + p_2 V_{c,r-1} + p_3 V_{c,r-2} + p_{r+1} V_o - V_o \sum_{j=1}^{m} 1 - [(1 + 2\,Cu(y,\varphi_{oj})]^2 \right\} . \quad (7.11)$$

Thus,

$$\mathcal{E}_{d-c,r+1} = \mathcal{E}_o + \mathcal{E}_d + \mathcal{E}_{c,r+1}$$

$$= q[p_1 V_{c,r} + p_2 V_{c,r-1} + p_3 V_{c,r-2} + \ldots + p_{r+1} V_o] . \quad (7.12)$$

The electronic efficiency for the (r+1) segment collector is then

$$\eta_{e,r+1} = \frac{\mathcal{E}_o + \mathcal{E}_d}{\mathcal{E}_{d-c,r+1}} \quad (7.13)$$

and the overall efficiency is

$$\eta_{o,r+1} = \frac{\mathcal{E}_o}{\mathcal{E}_{d-c,r+1}} . \quad (7.14)$$

It is convenient to compare the efficiencies for the device with r+1 collector segments to the efficiencies with a single collector at the r-f circuit potential. This can be expressed as,

$$\frac{\eta_{e,r+1}}{\eta_e} = \frac{\eta_{o,r+1}}{\eta_o} = \frac{e_{d-c}}{e_{d-c,r+1}}$$

$$= \frac{1}{\frac{p_1}{m}\left(\frac{V_{c,r}}{V_o}\right) + \frac{p_2}{m}\left(\frac{V_{c,r-1}}{V_o}\right) + \ldots + \frac{p_{r+1}}{m}} \quad . \tag{7.15}$$

The electronic efficiency for the (r+1) segment collector device may be written in terms of the electron group's velocities as,

$$\eta_{e,r+1} = \frac{\sum_{j=1}^{m} \left(1 - [1 + 2\,Cu(y,\Phi_{oj})]^2\right)}{p_1\left(\frac{V_{c,r}}{V_o}\right) + p_2\left(\frac{V_{c,r-1}}{V_o}\right) + \ldots + p_{r+1}} \quad . \tag{7.16}$$

The overall efficiency can be expressed as,

$$\eta_{o,r+1} = \frac{2C_o A_o^2 \frac{\left(1 - C_o \frac{d\theta}{dy}\right)}{(1+C_o b)}}{\frac{p_1}{m}\left(\frac{V_{c,r}}{V_o}\right) + \frac{p_2}{m}\left(\frac{V_{c,r-1}}{V_o}\right) + \ldots + \frac{p_{r+1}}{m}} \tag{7.17}$$

where A_o = the normalized r-f amplitude at the output of the BWO. For small values of C_o which is the case in most BWO's,

$$\frac{1 - C_o \frac{d\theta}{dy}}{1 + C_o b} \approx 1 \quad . \tag{7.18}$$

Equations 7.16 and 7.17 may now be used to calculate the electronic and overall efficiencies of a multi-segment depressed collector BWO. The

information needed in these equations has been obtained from the computations performed in Chapter IV.

7.3 Results of Calculations

The above theory has been employed to determine the efficiency improvement factors for several operating conditions in a backward-wave oscillator. The results are shown in Figs. 7.2 through 7.6. Figures 7.2 through 7.5 give the efficiency improvement factors for different numbers of collector stages and the degree of collector depression in each stage. It can be seen from these figures that for a specified number of stages, an optimum improvement factor is obtained for a certain combination of potentials on the different collector segments.

Figure 7.5 shows the optimum efficiencies obtainable by collector depression for different numbers of collector segments and for different operating conditions. It can be seen from this figure that the efficiency improvement factor is lower for tubes that were more efficient before collector depression. This is to be expected of course, since the more efficient a tube is before collector depression, the greater the velocity spread, and thus the lower the improvement factor becomes. The large improvement factors due to collector depression are mainly due to the very low interaction efficiencies of these devices.

A comparison of the efficiencies of uniform and tapered backward-wave oscillators can be obtained by reference to Fig. 7.6. In this comparison it is assumed that the uniform and tapered tubes both operate at the same voltage, current and frequency. This, as shown in detail in Chapter IV, results in a slightly longer tube in the tapered case. When tube No. 1 in Fig. 7.6 is tapered, the efficiency curve corresponding to tube No. 2 will be obtained. For this tube the taper starts at

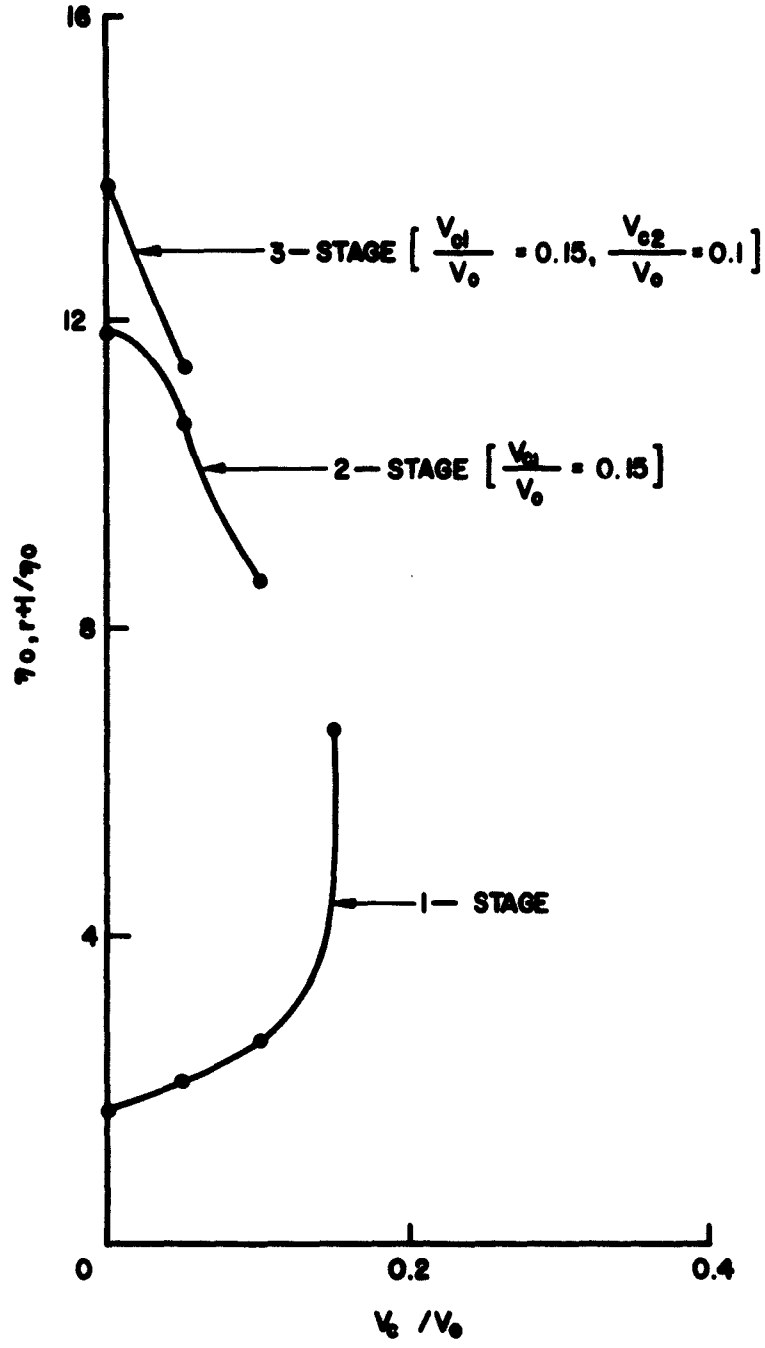

FIG. 7.2 EFFICIENCY IMPROVEMENT FACTOR AND OPTIMUM COLLECTOR SEGMENT VOLTAGES FOR A DEPRESSED-COLLECTOR UNIFORM BACKWARD-WAVE OSCILLATOR. ($C = 0.05$, $QC = 0$, $b_o = 1.625$, $d = 0$, $I/I_{s_o} \cong 1.15$, $2CA_o^2 = 0.025$)

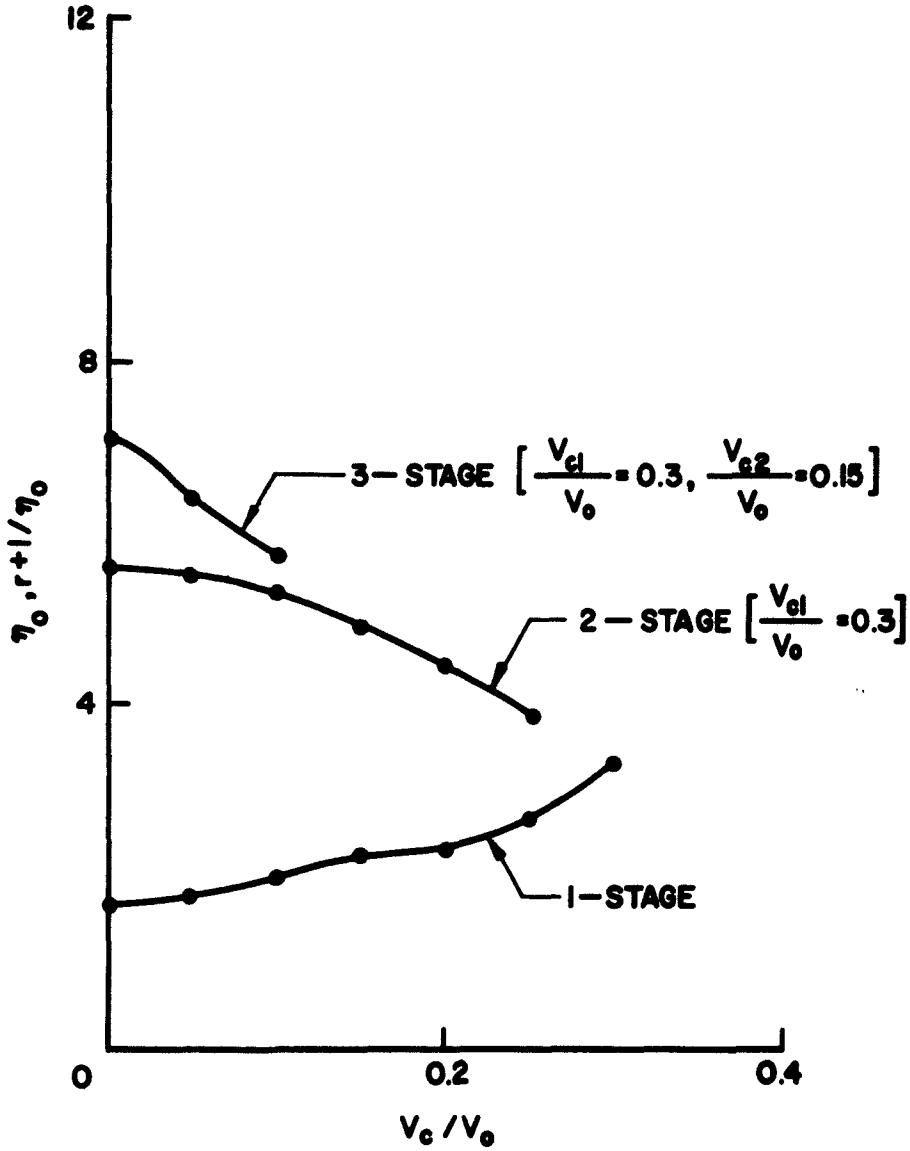

FIG. 7.3 EFFICIENCY IMPROVEMENT FACTOR AND OPTIMUM COLLECTOR SEGMENT VOLTAGES FOR A DEPRESSED-COLLECTOR UNIFORM BACKWARD-WAVE OSCILLATOR. ($C = 0.05$, $QC = 0$, $b_o = 1.825$, $d = 0$, $I/I_{s_o} \cong 1.5$, $2CA_o^2 = 0.072$)

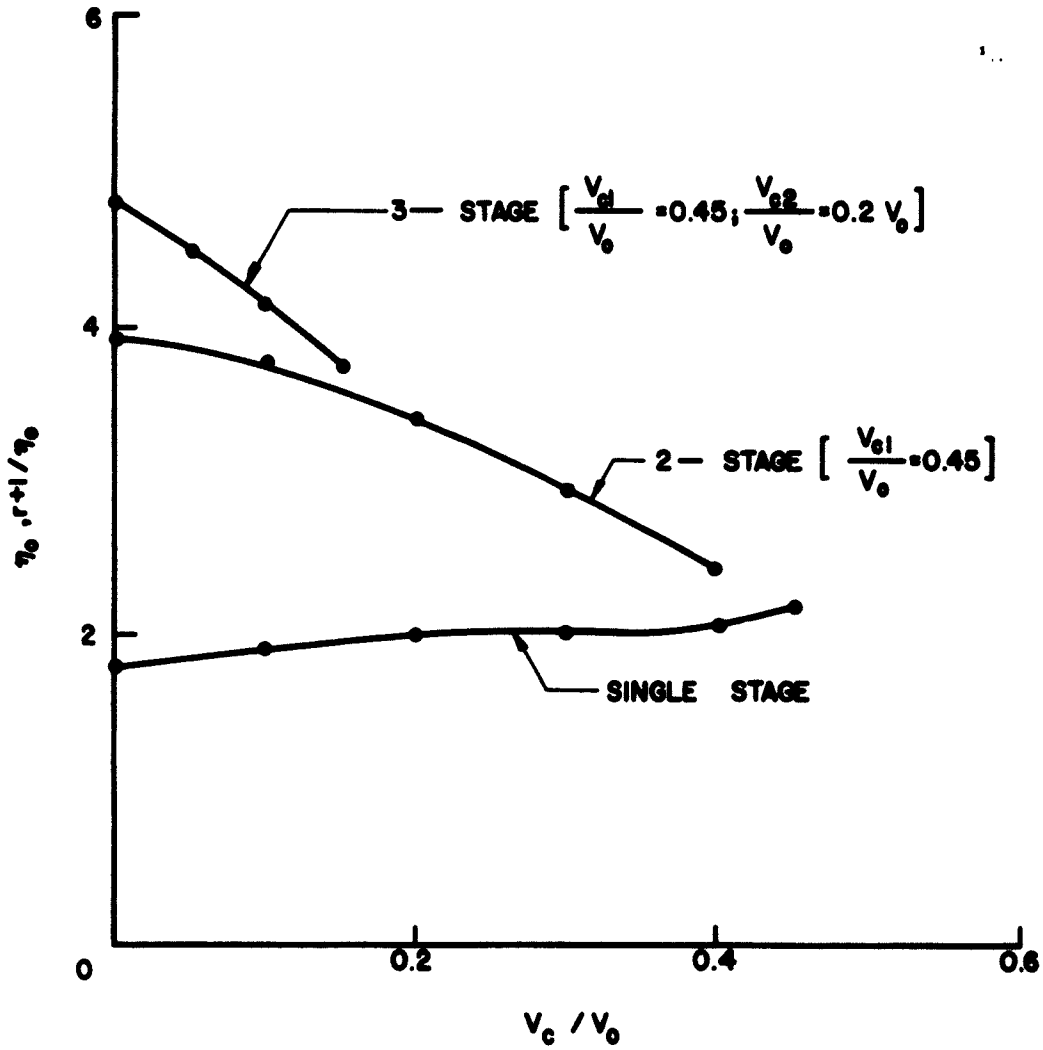

FIG. 7.4 EFFICIENCY IMPROVEMENT FACTOR AND OPTIMUM COLLECTOR SEGMENT VOLTAGES FOR A DEPRESSED-COLLECTOR UNIFORM BACKWARD-WAVE OSCILLATOR. ($C = 0.1$, $QC = 0$, $b_o = 1.925$, $d = 0$, $I/I_{s_o} \cong 1.2$, $2CA_o^2 = 0.096$)

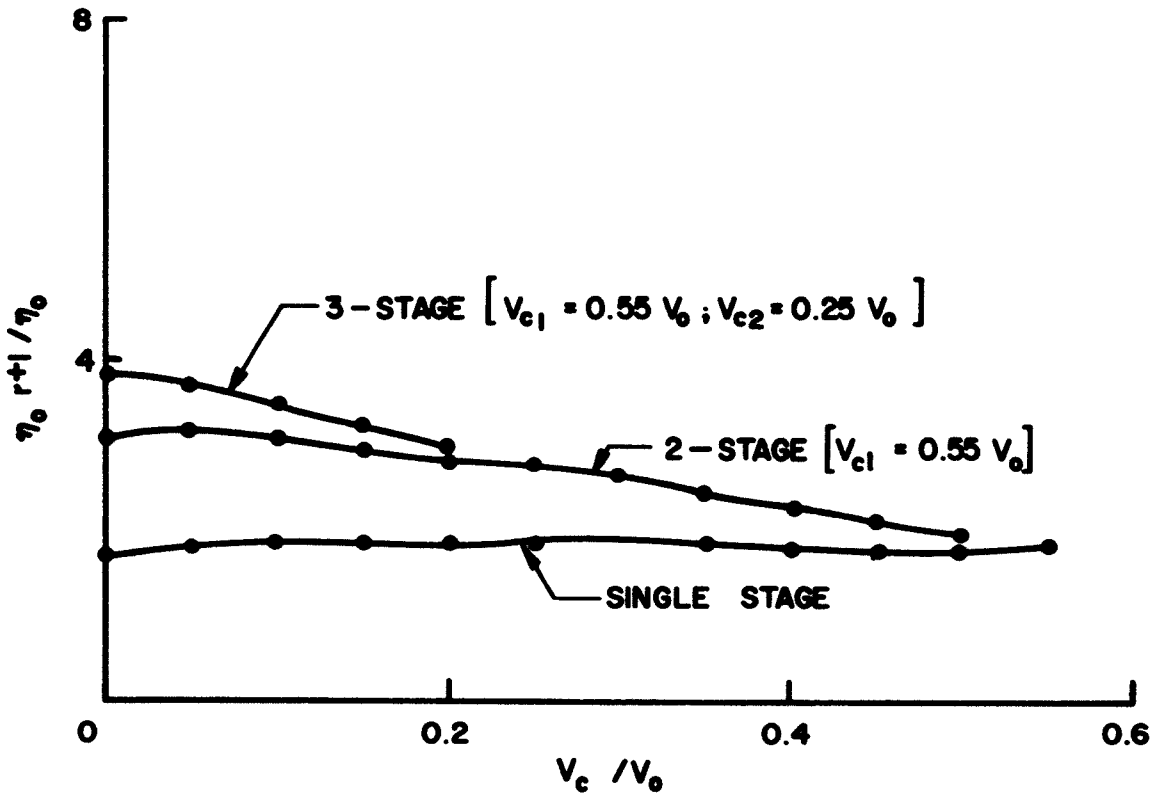

FIG. 7.5 EFFICIENCY IMPROVEMENT FACTOR AND OPTIMUM COLLECTOR SEGMENT VOLTAGES FOR A DEPRESSED-COLLECTOR UNIFORM BACKWARD-WAVE OSCILLATOR.
($C = 0.1$, $QC = 0$, $b_o = 2.06$, $d = 0$, $I/I_{s_o} \approx 1.5$, $2CA_o^2 = 0.136$)

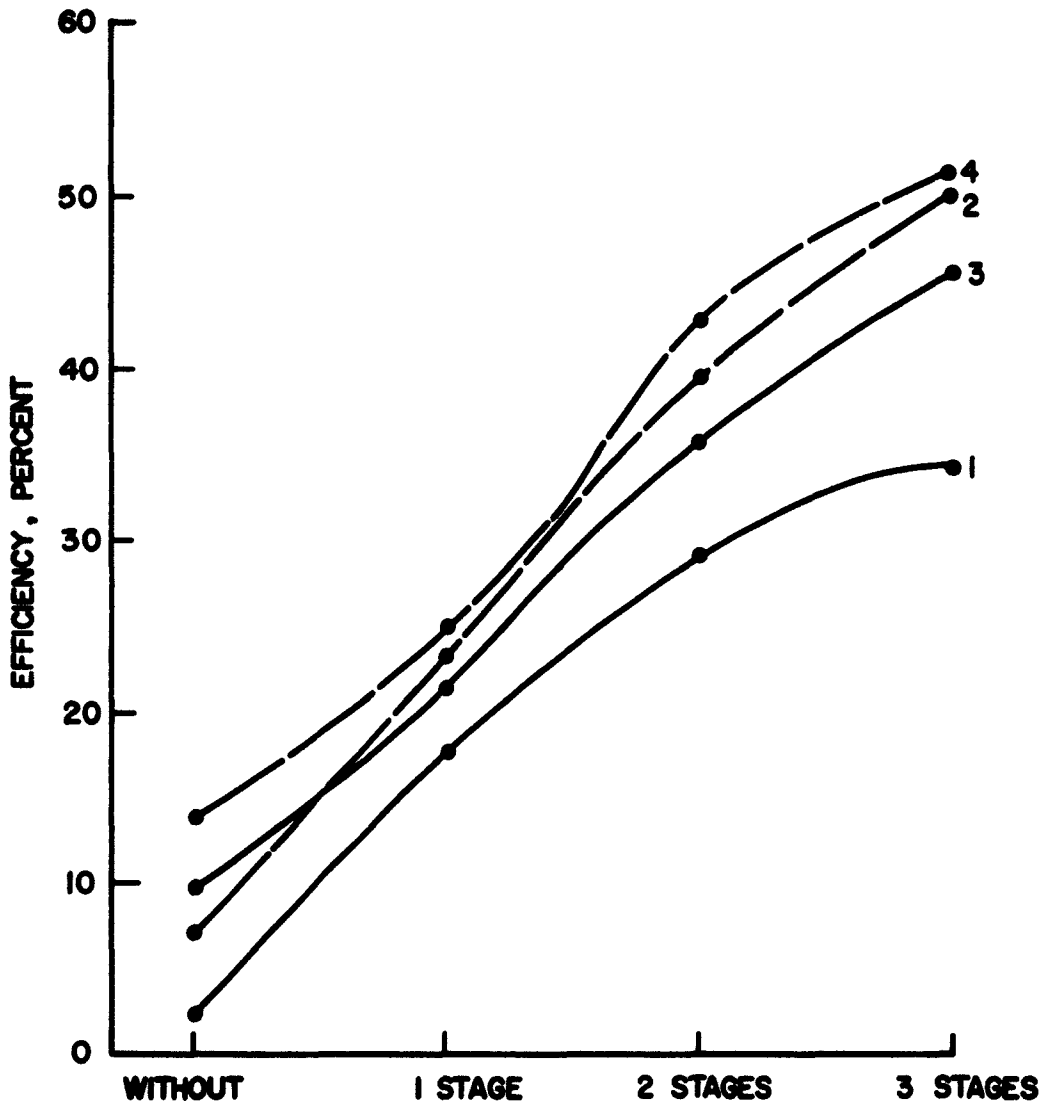

No. 1 corresponds to operating points of Fig. 7.2.

No. 2 corresponds to operating points of Fig. 7.3.

No. 3 corresponds to operating points of Fig. 7.4.

No. 4 corresponds to operating points of Fig. 7.5.

FIG. 7.6 OPTIMUM EFFICIENCY VS. NUMBER OF COLLECTOR STAGES IN A UNIFORM O-TYPE BACKWARD-WAVE OSCILLATOR.

approximately 70 percent of the length of the tube, and the overall length of the tapered tube is approximately 1.2 times that of the uniform one. When tube No. 3 is tapered the efficiencies shown for tube No. 4 result. For this tube the taper starts at approximately 70 percent of the tube length, and the overall length of the tapered tube is approximately 1.07 times that of the uniform one. It can be seen here also that the efficiency improvement factor is smaller for a tapered tube than that of a uniform one. This is due to the higher interaction efficiency in the tapered tube.

Concluding we can then say that depressed collectors can be effectively employed in backward-wave oscillators to enhance their efficiency. The improvement factor depends on how efficient a certain tube is before collector depression and the more efficient a tube before depression the lower the improvement factor.

CHAPTER VIII. SUMMARY, CONCLUSIONS AND SUGGESTIONS FOR FURTHER WORK

8.1 Start-Oscillation Conditions

A general set of small-signal equations describing the behavior of a backward-wave device up to start oscillation has been developed. Any kind of nonuniformity can be accommodated in the equations and its effect on the start-oscillation conditions can be determined. A method for solving these equations on an analog computer was discussed in detail and such a method proved to be very useful in this study. A coupled-mode approach was also employed where the coupled-mode equations were modified to accommodate a variable circuit phase velocity. For very weak tapers a WKBJ approximation was employed in order to obtain a closed-form solution through which the effect of the velocity taper on the start-oscillation conditions could be determined.

It was concluded from the coupled-mode theory results that a circuit phase velocity which increases with distance along the tube will always lead to higher start-oscillation currents. However, when the circuit phase velocity decreases with distance along the tube a decrease in the start-oscillation current may result under certain conditions. Several kinds of tapers in the circuit phase velocity where the velocity decreases with distance were investigated on the analog computer. These include linear, quadratic and exponential tapers. The results of the coupled-mode theory and those from the analog computer are in good agreement. It can be generally stated that if a uniform tube is weakly tapered in such a way that the phase velocity on the slow-wave structure

decreases with distance, and if the two tubes are to oscillate at the same frequency, then the voltage in the tapered tube will be lower and the start-oscillation current may be lower. The decrease in voltage and current depend on the amount of taper and the parameters of the uniform tube. However, when the strength of the taper exceeds a certain value, depending on the parameters of the tube, no oscillation can start. Similar results were obtained for a beam potential variation increasing with distance. A sinusoidal beam potential variation results in slightly higher start-oscillation currents. The increase in the current depends on the focusing lens strength and the number of d-c focusing periods.

8.2 Efficiency of Tapered Backward-Wave Oscillators

A nonlinear analysis using a Lagrangian formulation was employed to study the effect of velocity tapers. The equations were derived in a manner which allows the inclusion of any kind of nonuniformity in the circuit phase velocity or the d-c potential. Idealized circuit phase velocity tapers for phase focusing an ideal bunch in the interaction region were derived. The application of these tapers to actual situations in backward-wave oscillators resulted in higher efficiencies. The efficiency enhancement factors obtained by solving the equations on the digital computer should not be considered as optimum. Other more elaborate schemes can be devised and incorporated into the computer program which may result in better tapers and thus higher efficiencies. It is felt however that the cost in computer time would be prohibitive. The few cases that were investigated do show the applicability of the above easily derived tapers to actual situations.

An experimental backward-wave oscillator based on the idealized tapers resulted in efficiency improvement factors as high as two.

The effect of a sinusoidal beam potential variation on the efficiency was investigated. It was shown that for a certain lens strength and d-c focusing periods higher efficiencies are obtainable. However, for some values of lens strength and d-c focusing period no oscillation condition could be determined.

8.3 Prebunched-Beam Backward-Wave Oscillators

It was shown that a prebunched beam can be effectively employed in a backward-wave oscillator to obtain higher efficiencies and decrease the start-oscillation current. The applicability of a prebunched beam depends however on having a broadband prebuncher so that the advantageous voltage tunability of a backward-wave oscillator will not be negated.

8.4 Depressed Collectors

It has been determined that depressed collectors can enhance the efficiency considerably. The improvement factor depends on the operating conditions of the oscillator. Optimum collector segment voltages were obtained for different operating conditions. It should be remarked here that even though a depressed collector results in considerably higher efficiencies it does not result in higher r-f power output.

8.5 Suggestions for Further Work

In the coupled-mode theory analysis it was shown that analogous to a nonuniform transmission line where coupling between the forward and backward waves exists, coupling between the slow and fast space-charge waves exists in a beam with a nonuniform potential. This should be investigated further since this would seem to indicate that noise power in the slow space-charge wave may be transferred to the fast space-charge

wave and thus can then be removed. This, as is well known, is very desirable for low-noise devices.

Phase focusing and collector depression should be investigated further experimentally. It would be desirable to investigate the above schemes in a high power (high C) backward-wave oscillator. It is felt that in a high C oscillator the taper will show its effect more readily and will not be as critical as in a low C one.

The velocity taper can be designed to favor one part of the frequency band over the other. This is because the C value and thus the efficiency vary across the band. This will then lead to a lesser degree of r-f power variation across the band which is very desirable. It is felt that an experimental investigation of this will be worthwhile.

The increased efficiency in an oscillator whose beam potential varies sinusoidally along the length of the tube should be studied further so as to understand the specific reason for such an increase.

APPENDIX A. THE WKBJ SOLUTION TO THE COUPLED-MODE EQUATIONS OF A BACKWARD-WAVE OSCILLATOR WITH A WEAK CIRCUIT TAPER

The equations to be solved are Eqs. 2.89 and 2.90 and are repeated here for convenience,

$$\left[\frac{d}{dy} + j\beta_{c_n}(y) \right] a_c(y) = - k a_b(y) \quad , \tag{2.89}$$

$$\left[\frac{d}{dy} + j\beta_{b_n} \right] a_b(y) = - k a_c(y) \quad . \tag{2.90}$$

In order to obtain an equation in a_b alone, differentiate Eq. 2.90 and get

$$a_b'' + j\beta_{b_n} a_b' = - k a_c' \quad , \tag{A.1}$$

where the prime indicates the derivative with respect to y.

From Eq. 2.89 we have

$$a_c' = - k a_b - j\beta_{c_n}(y) a_c \tag{A.2}$$

and from Eq. 2.90

$$a_c = - \frac{a_b' + j\beta_{b_n} a_b}{k} \quad . \tag{A.3}$$

Substituting Eqs. A.3 and A.2 into Eq. A.1 gives

$$a_b'' + j \left[\beta_{b_n} + \beta_{c_n}(y) \right] a_b' + \left[|k|^2 - \beta_{c_n}(y) \beta_{b_n} \right] a_b = 0 \quad . \tag{A.4}$$

Let us now introduce a new variable f(y) which is related to $a_b(y)$ as follows,

$$a_b(y) = f(y)\, e^{-j \int_o^y \frac{\beta_{c_n}(y') + \beta_{b_n}}{2} dy'} \tag{A.5}$$

Substituting Eq. A.5 into Eq. A.4 yields

$$f'' + f\left[|k|^2 - j\frac{\beta'_{c_n}(y)}{2} + \left(\frac{\beta_{c_n}(y) - \beta_{b_n}}{2}\right)^2\right] = 0 \tag{A.6}$$

or

$$f''(y) + r^2(y)\, f(y) = 0 \ , \tag{A.7}$$

where

$$r^2(y) = \left[|k|^2 - j\frac{\beta'_{c_n}(y)}{2} + \left(\frac{\beta_{c_n}(y) - \beta_{b_n}}{2}\right)^2\right] . \tag{A.8}$$

If r(y) varies very slowly with y or, in other words, if $(r')^2/r^{5/2}$ and $r''/r^{3/2}$ are negligible, then one obtains the following solution.

$$f(y) = \frac{1}{\sqrt{r(y)}}\left[C_1\, e^{j \int_o^y r(y')dy'} + C_2\, e^{-j \int_o^y r(y')dy'}\right] \tag{A.9}$$

and

$$a_b(y) = \frac{1}{\sqrt{r(y)}}\left[C_1\, e^{j \int_o^y r(y')dy'} + C_2\, e^{-j \int_o^y r(y')dy'}\right]$$

$$\cdot\, e^{-j \int_o^y \frac{\beta_{c_n}(y') + \beta_{b_n}}{2} dy'} . \tag{A.10}$$

It is assumed that the beam enters the circuit unmodulated, and therefore $a_b(y) = 0$ at $y = 0$. Substituting this condition in Eq. A.10 we find $C_1 = -C_2$. Equation A.10 then becomes

$$a_b(y) = \frac{C_1}{\sqrt{r(y)}}\left[e^{j\int_0^y r(y')dy'} - e^{-j\int_0^y r(y')dy'}\right] \cdot e^{-j\int_0^y \frac{\beta_{c_n}(y') + \beta_{b_n}}{2} dy'} \quad . \quad (A.11)$$

From Eq. 2.90 the following is obtained

$$a_c(y) = -\frac{a_b'(y)}{k} - j\frac{\beta_{b_n}}{k} a_b \quad . \quad (A.12)$$

Substituting for a_b' and a_b from Eq. A.11 into Eq. A.12 and after some manipulation one obtains

$$a_c(y) = -\frac{C_1}{k}\left\{ j2r^{1/2}\cos\int_0^y r(y')dy' + \left[(\beta_{c_n} - \beta_{b_n})r^{-1/2} - jr^{-3/2}\, r'\right]\sin\int_0^y r(y')dy'\right\} e^{-j\int_0^y \frac{\beta_{c_n}(y') + \beta_{b_n}}{2} dy'} \quad . \quad (A.13)$$

Assume that the normalized oscillation length is $y = y_1$. Then at $y = y_1$, $a_c(y) = 0$. Substituting this in Eq. A.13 and dividing by

$$j2r^{1/2}\sin\int_0^{y_1} r(y')dy' \quad ,$$

gives

$$\cot \int_0^{y_1} r(y')dy' = j \frac{\beta_{c_n}(y_1) - \beta_{b_n}}{2r(y_1)} + \frac{1}{2} \frac{r'(y_1)}{r^2(y_1)} \qquad (A.14)$$

Now, assume a certain variation of $\beta_{c_n}(y)$. Consider a linear taper and take $\beta_{c_n}(y)$ to be

$$\beta_{c_n}(y) = \beta_{c_{on}}(1 + \alpha y) \quad , \qquad (A.15)$$

where $\beta_{c_{on}} = (1 + C_o b)/C_o$ is the normalized phase constant at $y = 0$, and α is a measure of the strength of the taper. With this choice of $\beta_{c_n}(y)$, $r(y_1)$ is then given by,

$$r(y_1) = \left[|k|^2 - \frac{j\alpha\beta_{c_{on}}}{2} + \left(\frac{\beta_{c_{on}}(1+\alpha y_1) - \beta_{b_n}}{2} \right)^2 \right]^{1/2} . \qquad (A.16)$$

Taking the derivative of Eq. A.16 and substituting into Eq. A.14 gives

$$\cot \int_0^{y_1} |k| \left\{ \left[1 - j \frac{\alpha\beta_{c_{on}}}{2|k|^2} + \left(\frac{1}{2|k|^2} \right)^2 \left(\beta_{c_{on}}(1 + \alpha y') - \beta_{b_n} \right)^2 \right\}^{1/2} dy'$$

$$= \frac{j \left[\beta_{c_{on}}(1 + \alpha y_1) - \beta_b \right]}{2|k| \left[1 - j \frac{\alpha\beta_{c_o}}{2|k|^2} + \left(\frac{1}{2|k|} \right)^2 \left(\beta_{c_{on}}(1 + \alpha y_1) - \beta_{b_n} \right)^2 \right]^{1/2}}$$

$$+ \frac{\alpha\beta_{c_{on}} \left[\beta_{c_{on}}(1 + \alpha y_1) - \beta_{b_n} \right]}{8|k|^3 \left\{ 1 - j \frac{\alpha\beta_{c_{on}}}{2|k|^2} + \left(\frac{1}{2|k|^2} \right)^2 \left[\beta_{c_{on}}(1 + \alpha y_1) - \beta_{b_n} \right]^2 \right\}^{3/2}} \qquad (A.17)$$

If we now assume a very weak taper such that

$$\left| \frac{\alpha\beta_{c_{on}}}{2|k|^2} \right| \ll 1 \tag{A.18}$$

and

$$\frac{1}{4|k|^2}\left[\beta_{c_{on}}(1+\alpha y) - \beta_{b_n}\right]^2 \ll 1 \ , \tag{A.19}$$

then Eq. A.17 reduces to

$$\cot \int_0^{y_1} |k| \left\{ \left[1 - j \frac{\alpha\beta_{c_{on}}}{4|k|^2} + \frac{1}{8|k|^2}\left(\beta_{c_{on}}(1+\alpha y') - \beta_{b_n}\right)^2 \right\} dy'$$

$$= \frac{j\left[\beta_{c_{on}}(1+\alpha y_1) - \beta_{b_n}\right]}{8|k|\left[1 - j\frac{\alpha\beta_{c_o}}{4|k|^2} + \frac{1}{8|k|^2}\left(\beta_{c_{on}}(1+\alpha y_1) - \beta_{b_n}\right)^2\right]}$$

$$+ \frac{(\alpha\beta_{c_{on}})\left[\beta_{c_{on}}(1+\alpha y_1) - \beta_{b_n}\right]}{8|k|^3\left[1 - j\frac{3\alpha\beta_{c_{on}}}{4|k|^2} + \frac{3}{8|k|^2}\left(\beta_{c_{on}}(1+\alpha y_1) - \beta_{b_n}\right)^2\right]} \ . \tag{A.20}$$

Again using assumptions A.18 and A.19 gives

$$\cot\left\{ |k|y_1 - j\frac{\alpha\beta_{c_{on}}}{4|k|}y_1 + \frac{1}{8|k|}\left[(\beta_{c_{on}} - \beta_{b_n})^2 y_1 + \alpha\beta_{c_{on}}(\beta_{c_{on}} - \beta_{b_n})\, y_1^2 \right.\right.$$

$$\left.\left. + \tfrac{1}{3}\alpha^2\beta_{c_{on}}^2\, y_1^2\right]\right\} = \frac{j\left[\beta_{c_{on}}(1+\alpha y_1) - \beta_{b_n}\right]}{2|k|}$$

$$\cdot\left[1 + j\frac{\alpha\beta_{c_o}}{4|k|^2} - \frac{1}{8|k|^2}\left(\beta_{c_{on}}(1+\alpha y_1) - \beta_{b_n}\right)^2\right] . \quad (A.21)$$

Following the same procedure as that of Bevensee's[19], write the left-hand side of Eq. A.21 as,

$$\cot(A+jB) = \frac{\sin A\cos A - j\sinh B\cosh B}{\sin^2 A\cosh^2 B + \cos^2 A\sinh^2 B} , \quad (A.22)$$

where,

$$A = |k|y_1 + \frac{1}{8|k|}\left[(\beta_{c_{on}} - \beta_{b_n})^2 y_1 + \alpha\beta_{c_{on}}(\beta_{c_{on}} - \beta_{b_n})\, y_1^2 \right.$$

$$\left. + \tfrac{1}{3}\alpha^2\beta_{c_{on}}^2\, y_1^3\right] = |k|y_1 + M \quad (A.23)$$

and

$$B = -\frac{\alpha\beta_{c_{on}}}{4|k|}y_1 . \quad (A.24)$$

For M very small and $|k|y_1 \cong \pi/2$

$$\sin A\cos A \cong \sin|k|y_1\left[\cos|k|y_1 - M\sin|k|y_1\right] \quad (A.25)$$

and for B very small

$$- j \sinh B \cosh B \cong - jB = j \frac{\alpha\beta_{c_{on}}}{4|k|} y_1 \qquad (A.26)$$

Also under the above assumptions,

$$\sin^2 A \cosh^2 B \cong 1 \ , \qquad (A.27)$$

$$\cos^2 A \sinh^2 B \ll 1 \ . \qquad (A.28)$$

Equation A.23 then becomes

$$\sin |k|y_1 \left[\cos |k|y_1 - M \sin |k|y_1\right] + j \frac{\alpha\beta_{c_{on}}}{4|k|} y_1$$

$$= j \left[\frac{\beta_{c_{on}}(1 + \alpha y_1) - \beta_{b_n}}{2|k|} \right] \left[1 + j \frac{\alpha\beta_{c_{on}}}{4|k|^2} \right.$$

$$\left. - \frac{1}{8|k|^2} \left(\beta_{c_{on}}(1 + \alpha y_1) - \beta_{b_n}\right)^2 \right] \ . \qquad (A.29)$$

It is then seen from Eq. A.29 that the start-oscillation conditions are now given approximately by

$$\frac{\alpha\beta_{c_{on}} y_1}{2} \cong \left[\beta_{c_{on}}(1 + \alpha y_1) - \beta_{b_n}\right] \qquad (A.30)$$

and

$$\cot |k|y_1 \cong \frac{\alpha^2\beta^2_{c_{on}}}{96|k|^4} \left[(|k|y_1)^2 - 6\right] |k|y_1 \ . \qquad (A.31)$$

These results are discussed in Chapter II.

APPENDIX B. SOLUTION OF THE NONUNIFORM BWO EQUATIONS ON THE ANALOG COMPUTER

The equations characterizing the behavior of a nonuniform backward-wave oscillator were presented in Section 3.2. The solution of these equations on an analog computer will now be discussed. The equations to be solved are,

$$\frac{d^2V_{cn}(y)}{dy^2} + \left(\frac{1 + C_o b}{C_o}\right)\frac{1}{\xi^2(y)}\,V_{cn}(y) + \frac{1}{\xi(y)}\,\frac{d\xi(y)}{dy}\,\frac{dV_{cn}(y)}{dy}$$

$$-j2\,\frac{d}{C_o}\,(1 + C_o b)^2\,\frac{1}{\xi^2(y)}\,V_{cn}(y)$$

$$= \frac{4C_o(1 + C_o b)}{\xi(y)}\,\rho_{1n} - j\,\frac{8C_o^2\,d(1 + C_o b)}{\xi(y)}\,\rho_{1n} \quad , \text{(B.1)}$$

$$\frac{1}{\zeta^{1/2}(y)}\,\frac{du_{1n}(y)}{dy} - \frac{1}{\zeta(y)}\,\frac{d\zeta^{1/2}(y)}{dy}\,u_{1n}(y) + \zeta^{1/2}(y)\,\frac{d\rho_{1n}(y)}{dy}$$

$$+\left[\frac{d\zeta^{1/2}(y)}{dy} + \frac{j}{C_o}\right]\rho_{1n}(y) = 0 \quad , \text{(B.2)}$$

$$\frac{1}{2}\,\frac{dV_{cn}(y)}{dy} + j\,\frac{4C_o\,QC}{[1 - 2C_o\sqrt{QC}]^2}\,\frac{1}{(1 + C_o b)}\,\xi(y)\,\rho_{1n}(y)$$

$$= \left[\frac{j}{C_o} + \frac{d\zeta^{1/2}(y)}{dy}\right]u_{1n}(y) + \zeta^{1/2}(y)\,\frac{du_{1n}(y)}{dy} \quad . \text{(B.3)}$$

These equations are a set of linear differential equations with variable coefficients. The solution to such a set of equations can be handled best on an analog computer. In order to program these equations on the analog computer they must be separated into real and imaginary parts. The dependent variable, V_{cn}, ρ_{1n}, u_{1n} are then split into real and imaginary components as follows:

$$V_{cn} = V_R + j\, V_I \ ,$$

$$u_{1n} = u_R + j\, u_I \ ,$$

$$\rho_{1n} = \rho_R + j\, \rho_I \ . \qquad \text{(B.4)}$$

Substituting Eq. B.4 into Eqs. B.1 through B.3 and separating the real and imaginary parts gives the following set of six differential equations.

$$\frac{d^2V_R}{dy^2} + \left(\frac{1 + C_o b}{C_o}\right)^2 \frac{1}{\xi^2(y)} V_R + \frac{1}{\xi(y)} \frac{d\xi(y)}{dy} \frac{dV_R}{dy}$$

$$+ 2 \frac{d}{C_o} (1 + C_o b)^2 \frac{1}{\xi^2(y)} V_I$$

$$= \frac{4C_o(1 + C_o b)}{\xi(y)} \rho_R + \frac{8C_o^2\, d(1 + C_o b)}{\xi(y)} \rho_I \ , \qquad \text{(B.5)}$$

$$\frac{d^2V_I}{dy^2} + \left(\frac{1 + C_o b}{C_o}\right)^2 \frac{1}{\xi^2(y)} V_I + \frac{1}{\xi(y)} \frac{d\xi(y)}{dy} \frac{dV_I}{dy}$$

$$- 2 \frac{d}{C_o} (1 + C_o b)^2 \frac{1}{\xi^2(y)} V_R$$

$$= \frac{4C_o(1 + C_o b)}{\xi(y)} \rho_I - \frac{8C_o^2\, d(1 + C_o b)}{\xi(y)} \rho_R \ , \qquad \text{(B.6)}$$

$$\frac{1}{\zeta^{1/2}(y)}\ \frac{du_R}{dy} - \frac{1}{\zeta(y)}\ \frac{d\zeta^{1/2}(y)}{dy}\ u_R + \zeta^{1/2}(y)\ \frac{d\rho_R}{dy}$$

$$+ \frac{d\zeta^{1/2}(y)}{dy}\ \rho_R - \frac{\rho_I}{C_o} = 0 \quad , \text{(B.7)}$$

$$\frac{1}{\zeta^{1/2}(y)}\ \frac{du_I}{dy} - \frac{1}{\zeta(y)}\ \frac{d\zeta^{1/2}(y)}{dy}\ u_I + \zeta^{1/2}(y)\ \frac{d\rho_I}{dy}$$

$$+ \frac{d\zeta^{1/2}(y)}{dy}\ \rho_R - \frac{\rho_R}{C_o} = 0 \quad , \text{(B.8)}$$

$$\frac{1}{2}\ \frac{dV_R}{dy} - \frac{4C_o\ QC}{[1 - 2C_o\sqrt{QC}]^2}\ \frac{1}{(1 + C_o b)}\ \xi(y)\ \rho_I$$

$$= -\frac{u_I}{C_o} + \frac{d\zeta^{1/2}(y)}{dy}\ u_R + \zeta^{1/2}(y)\ \frac{du_R}{dy} \quad , \text{(B.9)}$$

$$\frac{1}{2}\ \frac{dV_I}{dy} + \frac{4C_o\ QC}{[1 - 2C_o\sqrt{QC}]^2}\ \frac{1}{1 + C_o b}\ \xi(y)\ \rho_R$$

$$= \frac{u_R}{C_o} + \frac{d\zeta^{1/2}(y)}{dy}\ u_I + \zeta^{1/2}(y)\ \frac{du_I}{dy} \quad . \text{(B.10)}$$

The procedure for scaling the above equations is the same as that employed by Rowe and Sobol[1]. This is done by assuming an approximate voltage variation on the circuit of a uniform BWO. The start-oscillation y in a uniform oscillator is approximately

$$y_{s,o} \cong \frac{\pi^2}{5} \quad . \text{(B.11)}$$

The line voltage can then be approximately expressed as,

$$V_{cn}(y) = V_{cn}(0) \cos \frac{2y}{2\pi} \exp\left(- j \frac{y}{C_o}\right) . \qquad (B.12)$$

Assuming $V_{cn}(0)$ is unity and substituting in Eqs. B.1 through B.3 it can be shown that the maximum amplitudes of ρ_{in} and u_{in} are,

$$|\rho_{in}| \approx \frac{0.4}{C_o^2} , \qquad (B.13)$$

$$|u_{in}| \approx \frac{0.625}{C_o} . \qquad (B.14)$$

The time scale used is

$$\tau = \frac{y}{C_o} , \qquad (B.15)$$

where τ is the machine time. The derivatives with respect to the machine time then become

$$P \triangleq \frac{d}{d\tau} = C_o \frac{d}{dy} , \qquad (B.16)$$

$$P^2 \triangleq \frac{d^2}{dt^2} = C_o^2 \frac{d}{dy^2} . \qquad (B.17)$$

The tube analyzed in this study had a gain parameter $C_o = 0.05$. For a voltage maximum of 0.02 the scaling used is,

$$V = 0.02 \bar{V}$$

$$\rho = 5 \bar{\rho}$$

$$u = 0.2 \bar{u} , \qquad (B.18)$$

where the bar quantities represent machine variables. Equations B.16 and B.17 then become,

$$\frac{d}{dy} = 20\,P \quad , \tag{B.19}$$

$$\frac{d^2}{dy^2} = 400\,P^2 \quad . \tag{B.20}$$

We can now substitute the above quantities into Eqs. B.5 through B.10 and obtain a set of equations in machine variables which can then be programmed on the analog computer. This is done in two parts as follows:

B.1 Nonuniform Circuit Phase Velocity Equations

Here the beam potential is assumed to be constant but the circuit phase velocity varies with distance along the tube, i.e., $\zeta(y) = 1$ and $\xi(y)$ is arbitrary. Also d is assumed to be zero. Substituting the machine time and variables in Eqs. B.5 through B.10 and arranging, results in the following set of equations,

$$P^2\,\overline{V}_R = -\frac{(1 + 0.05\,b)^2}{\xi^2(\tau)}\,V_R + \frac{P\xi(\tau)}{\xi(\tau)}\,P\overline{V}_R + \frac{0.125(1 + 0.05\,b)}{\xi(\tau)}\,\overline{\rho}_R \quad , \tag{B.21}$$

$$P^2\,\overline{V}_I = -\frac{(1 + 0.05\,b)^2}{\xi^2(\tau)}\,\overline{V}_I + \frac{P\xi(\tau)}{\xi(\tau)}\,P\overline{V}_I + \frac{0.125(1 + 0.05\,b)}{\xi(\tau)}\,\overline{\rho}_I \quad , \tag{B.22}$$

$$P\,\overline{\rho}_R = -0.04\,P\,\overline{u}_R + \overline{\rho}_I \quad , \tag{B.23}$$

$$P\,\overline{\rho}_I = -0.04\,P\,\overline{u}_I - \overline{\rho}_R \quad , \tag{B.24}$$

$$P\,\overline{u}_R = 0.05\,P\,\overline{V}_R - \frac{0.250C}{[1 - 0.1\sqrt{QC}]^2}\,\frac{1}{(1 + 0.05\,b)}\,\xi(\tau)\,\overline{\rho}_I + \overline{u}_I \quad , \tag{B.25}$$

$$P\,\bar{u}_I = 0.05\,P\,\bar{V}_I + \frac{0.25QC}{[1 - 0.1\sqrt{QC}]^2}\,\frac{1}{(1 + 0.05\,b)}\,\xi(\tau)\,\bar{\rho}_R - \bar{u}_R \tag{B.26}$$

The initial conditions, Eqs. 3.45 through 3.48 now become,

$$\bar{u}_R(0) = \bar{u}_I(0) = \bar{\rho}_R(0) = \bar{\rho}_I(0) = 0\ , \tag{B.27}$$

$$\bar{V}_R(0) = \bar{V}_I(0) = \text{an arbitrary constant}, \tag{B.28}$$

$$P\,\bar{V}_R\Big|_o = (1 + 0.05\,b)\,\bar{V}_1(0) \tag{B.29}$$

and

$$P\,\bar{V}_I\Big|_o = -(1 + 0.05\,b)\,\bar{V}_R(0) \tag{B.30}$$

A "roadmap" showing the analog computer elements employed in solving the above set of differential equations is shown in Fig. B.1. The potentiometer settings are given in Table B.1. The elements involved in the function generator are shown in detail in Figs. B.2 through B.4 for the different tapers that were investigated.

Table B.1

Potentiometer Settings for Figure B.1

Potentiometer No.	Setting
6, 8	$(1 + 0.05\,b)^2$
7, 9	$0.125(1 + 0.05\,b)$
10, 11	0.04
12, 14	0.05

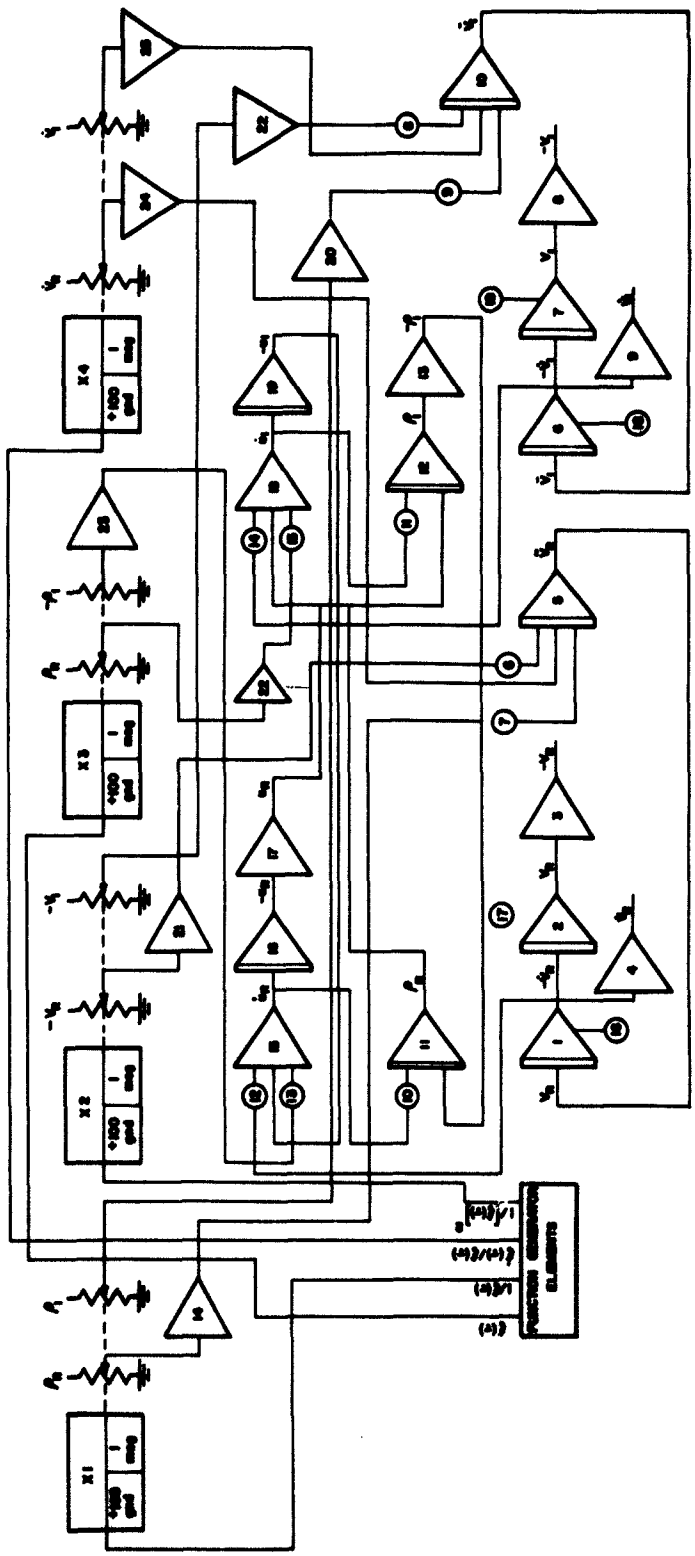

FIG. B.1 "ROADMAP" OF ANALOG COMPUTER ELEMENTS FOR FINDING START-OSCILLATION CONDITIONS OF A NONUNIFORM CIRCUIT PHASE VELOCITY BWO.

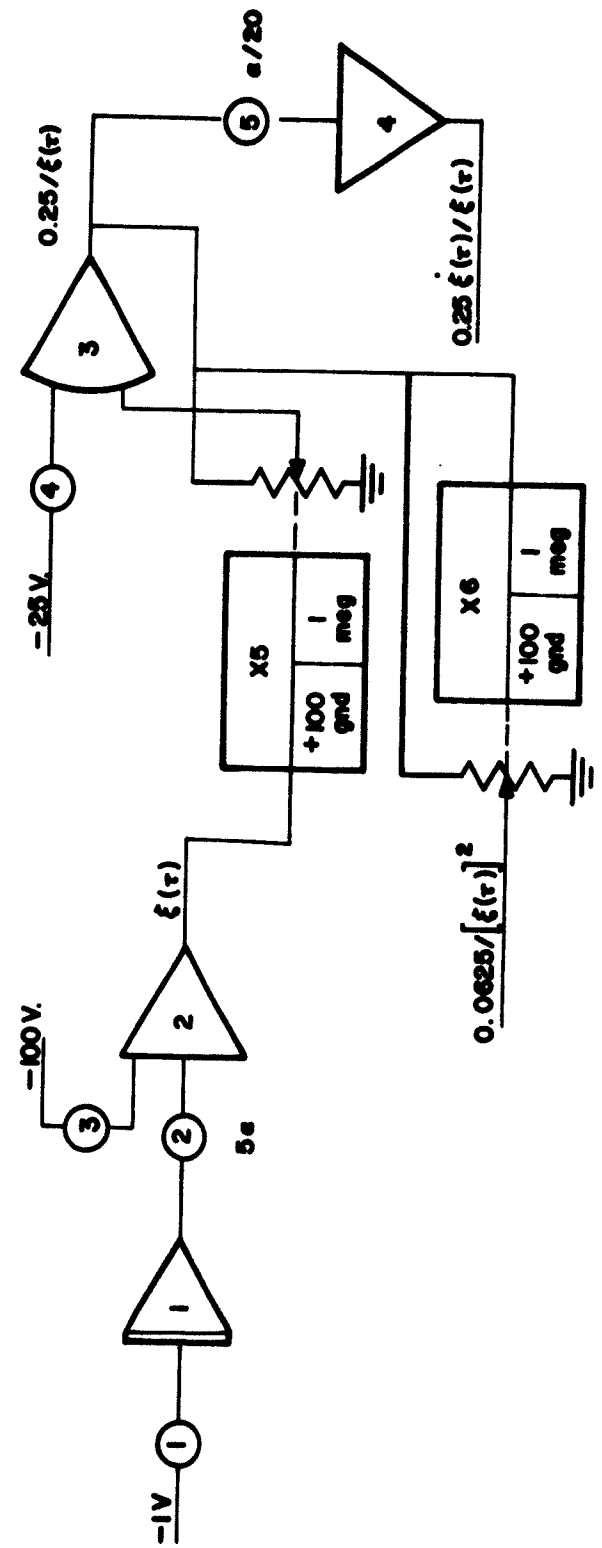

FIG. B.2 ELEMENTS OF FUNCTION GENERATOR FOR LINEAR CIRCUIT PHASE VELOCITY TAPER. $[\xi(\tau) = (1 - \alpha\tau/20)]$

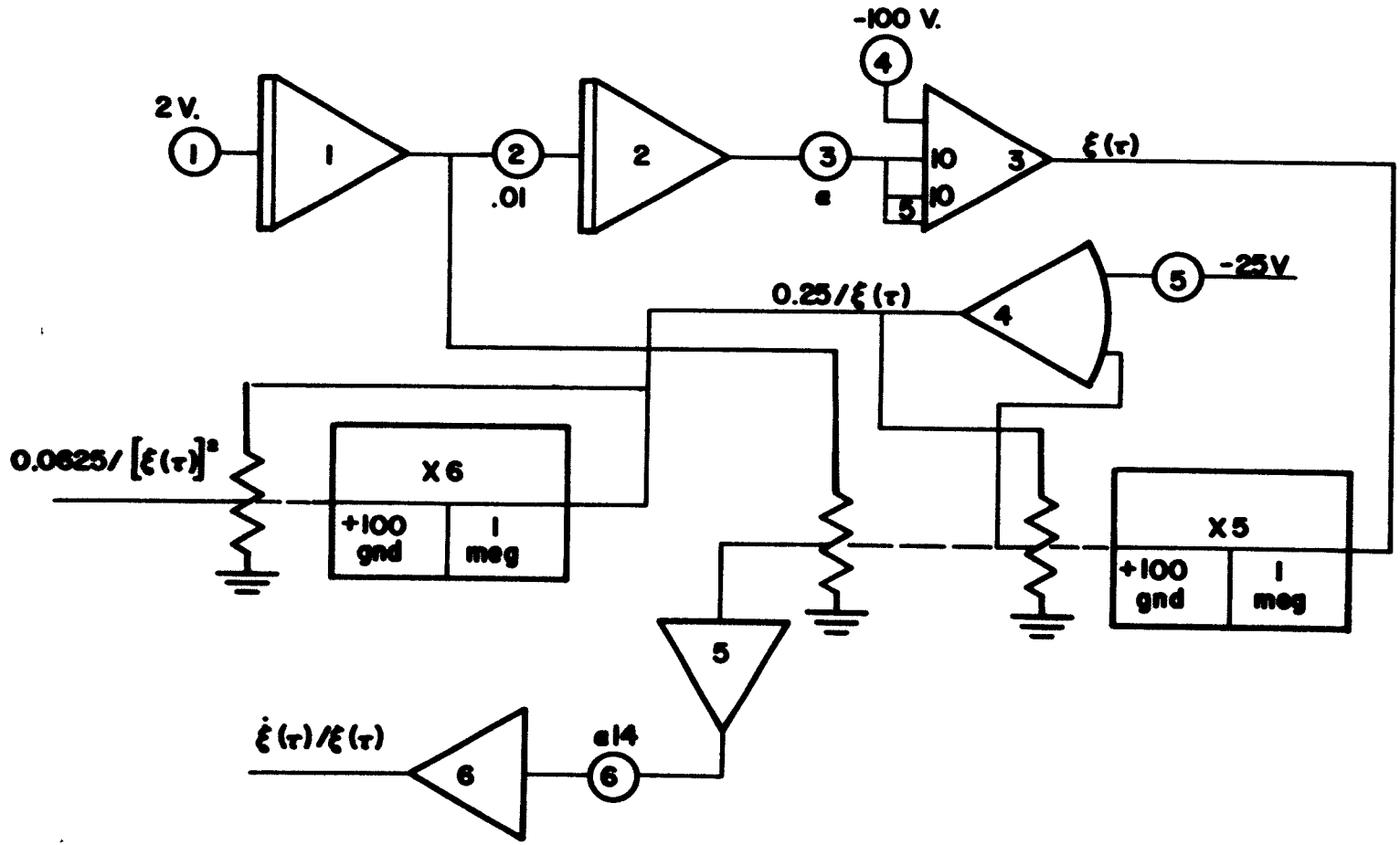

FIG. B.3 ELEMENTS OF FUNCTION GENERATOR TO QUADRATIC CIRCUIT PHASE VELOCITY TAPER. $[\xi(\tau) = (1 - \alpha\tau^2/400)]$

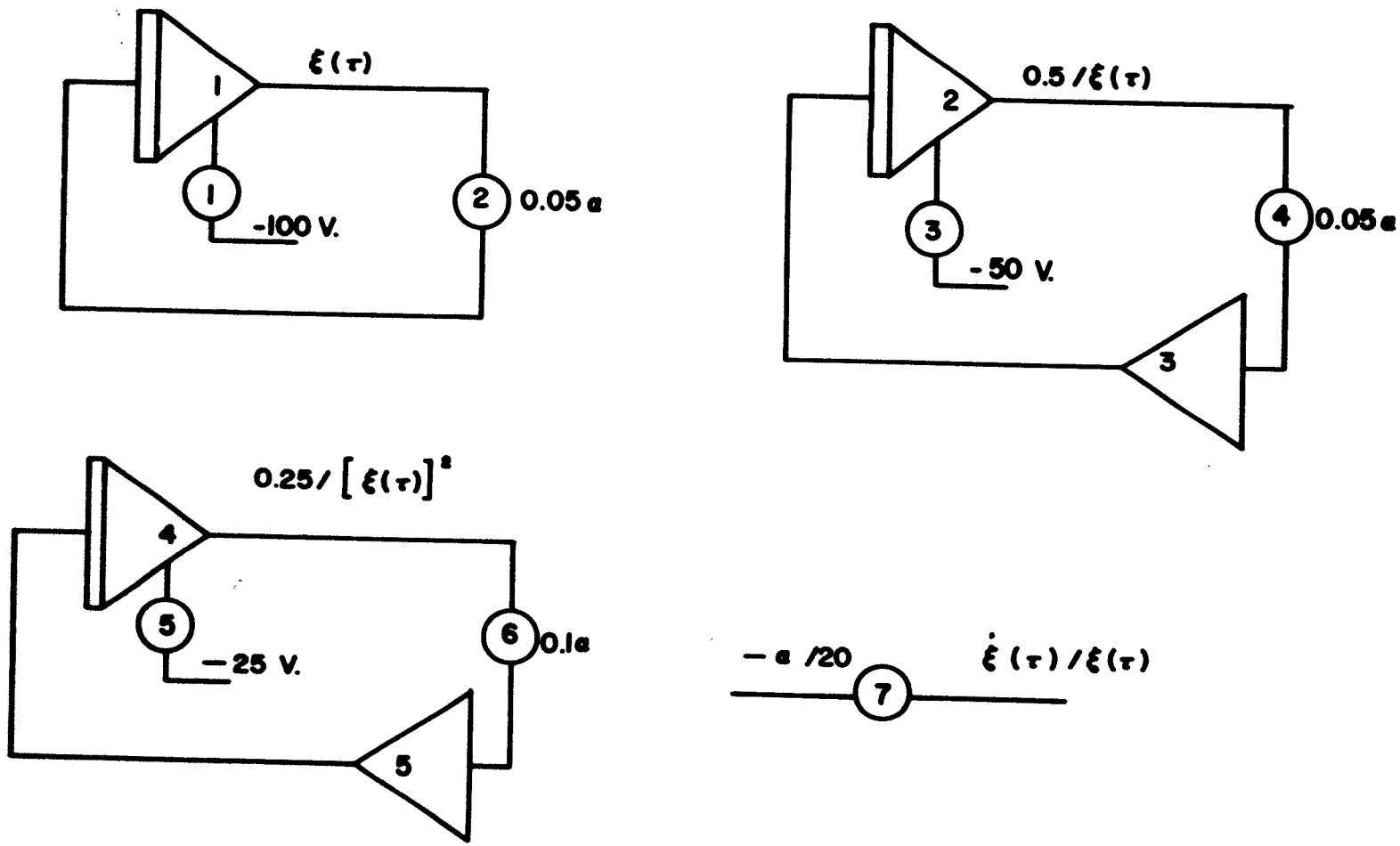

FIG. B.4 ELEMENTS OF FUNCTION GENERATOR FOR EXPONENTIAL CIRCUIT PHASE VELOCITY TAPER. $[\xi(\tau) = e^{-\alpha\tau/20}]$

Potentiometer No.	Setting
13, 15	$\dfrac{0.25\ QC}{[1 - 0.1\sqrt{QC}]^2\ (1 + 0.05\ b)}$
16	$0.5(1 + 0.05\ b)$
17, 19	$-\ 0.5$

B.2 Nonuniform Beam Potential Equations

Here the circuit phase velocity is assumed to be constant but the beam potential varies as a function of distance along the length of the tube, i.e., $\xi(y) = 1$ and $\zeta(y)$ is arbitrary. d is also assumed to be zero. Substituting the machine time and variables in Eqs. B.5 through B.10 results in the following set of equations:

$$P^2\,\overline{V}_R = -(1 + 0.05\ b)^2\,\overline{V}_R + 0.125(1 + 0.05\ b)\,\overline{\rho}_R \quad , \quad \text{(B.31)}$$

$$P^2\,\overline{V}_I = -(1 + 0.05\ b)^2\,\overline{V}_I + 0.125(1 + 0.05\ b)\,\overline{\rho}_I \quad , \quad \text{(B.32)}$$

$$P\,\overline{\rho}_R = -\frac{0.04P\,\overline{u}_R}{\zeta(\tau)} + \frac{0.04\ P[\zeta^{1/2}(\tau)]\,\overline{u}_R}{\zeta^{3/2}(\tau)} - \frac{P[\zeta^{1/2}(\tau)]}{\zeta^{1/2}(\tau)}\,\overline{\rho}_R + \frac{\overline{\rho}_I}{\zeta^{1/2}(\tau)} \quad , \quad \text{(B.33)}$$

$$P\,\overline{\rho}_I = -\frac{0.04\ P\,\overline{u}_I}{\zeta(\tau)} + \frac{0.04P[\zeta^{1/2}(\tau)]\,\overline{u}_I}{\zeta^{3/2}(\tau)} - \frac{P[\zeta^{1/2}(\tau)]}{\zeta^{1/2}(\tau)}\,\overline{\rho}_I - \frac{\overline{\rho}_R}{\zeta^{1/2}(\tau)} \quad , \quad \text{(B.34)}$$

$$P\,\bar{u}_R = \frac{0.05\bar{V}_R}{\zeta^{1/2}(\tau)} - \frac{0.25\,QC}{[1 - 0.1\sqrt{QC}]^2\,(1 + 0.05\,b)\,\zeta^{1/2}(\tau)}\,\bar{\rho}_I + \frac{\bar{u}_I}{\zeta^{1/2}(\tau)} - \frac{P[\zeta^{1/2}(\tau)]}{\zeta^{1/2}(\tau)}\,, \quad (B.35)$$

$$P\,\bar{u}_I = \frac{0.05\bar{V}_I}{\zeta^{1/2}(\tau)} + \frac{0.25\,QC}{[1 - 0.1\sqrt{QC}]^2\,(1 + 0.05\,b)\,\zeta^{1/2}(\tau)}\,\bar{\rho}_R - \frac{\bar{u}_R}{\zeta^{1/2}(\tau)} - \frac{P[\zeta^{1/2}(\tau)]}{\zeta^{1/2}(\tau)}\,\bar{u}_I\,. \quad (B.36)$$

The initial conditions are given by Eqs. B.27 through B.30.

For the sinusoidal beam potential variation where $\zeta(y) = 1\text{-}A\cos\alpha y$, the following approximations were made,

$$\frac{1}{\zeta(y)} \cong 1 + A\cos\alpha y\,,$$

$$\frac{1}{\zeta^2(y)} \cong 1 + 2A\cos\alpha y\,,$$

$$\frac{1}{\zeta^{1/2}(y)} = 1 + \frac{1}{2}A\cos\alpha y\,. \quad (B.37)$$

A "roadmap" showing the analog computer elements employed in solving the above set of equations is shown in Fig. B.5. The potentiometer settings are given in Table B.2. The elements involved in the function generator are shown in detail in Figs. B.6 through B.9 for the different nonuniformities that were investigated.

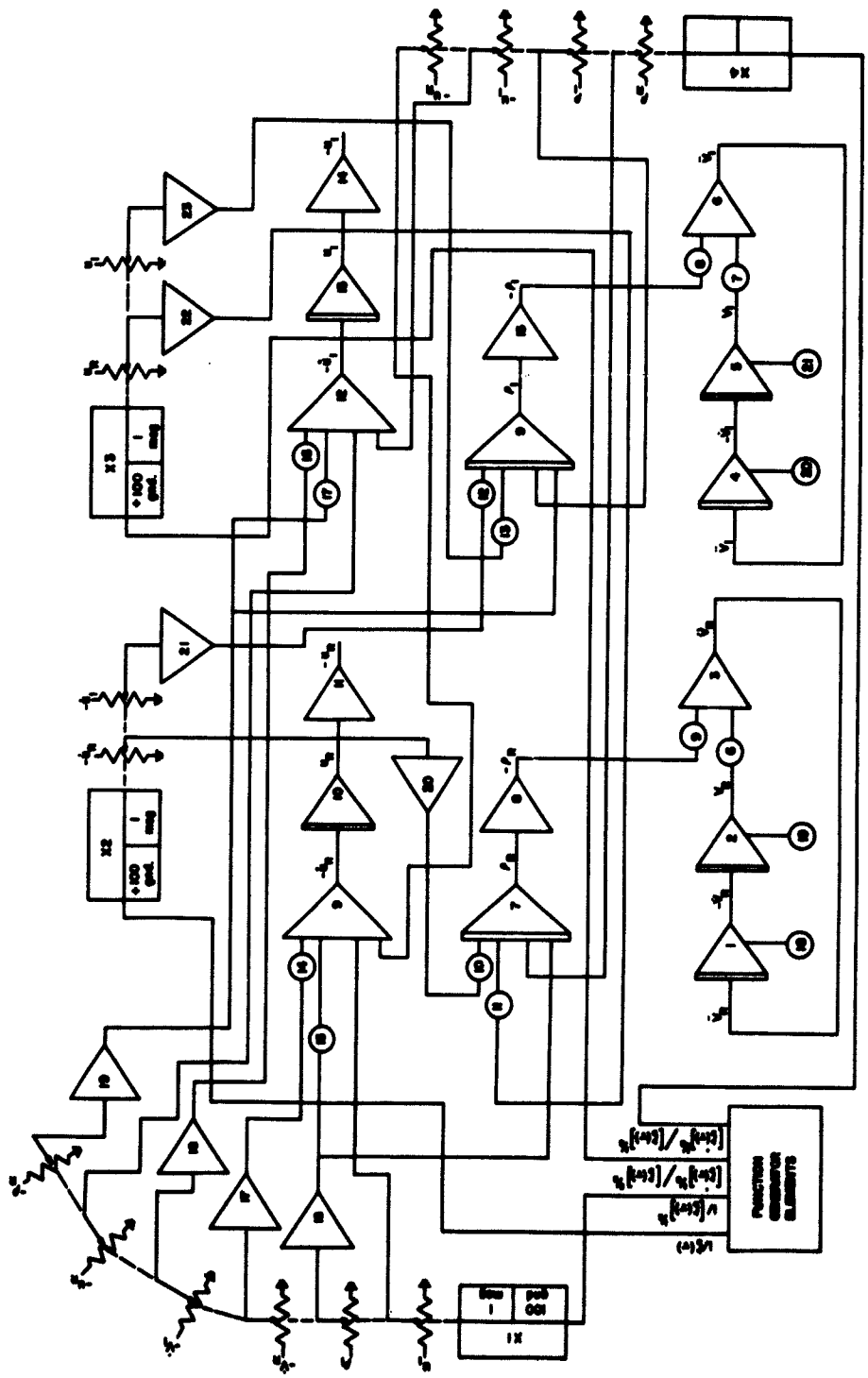

FIG. B.5 "ROADMAP" OF ANALOG COMPUTER ELEMENTS FOR FINDING START-OSCILLATION CONDITIONS OF A BWO WITH A NONUNIFORM BEAM POTENTIAL.

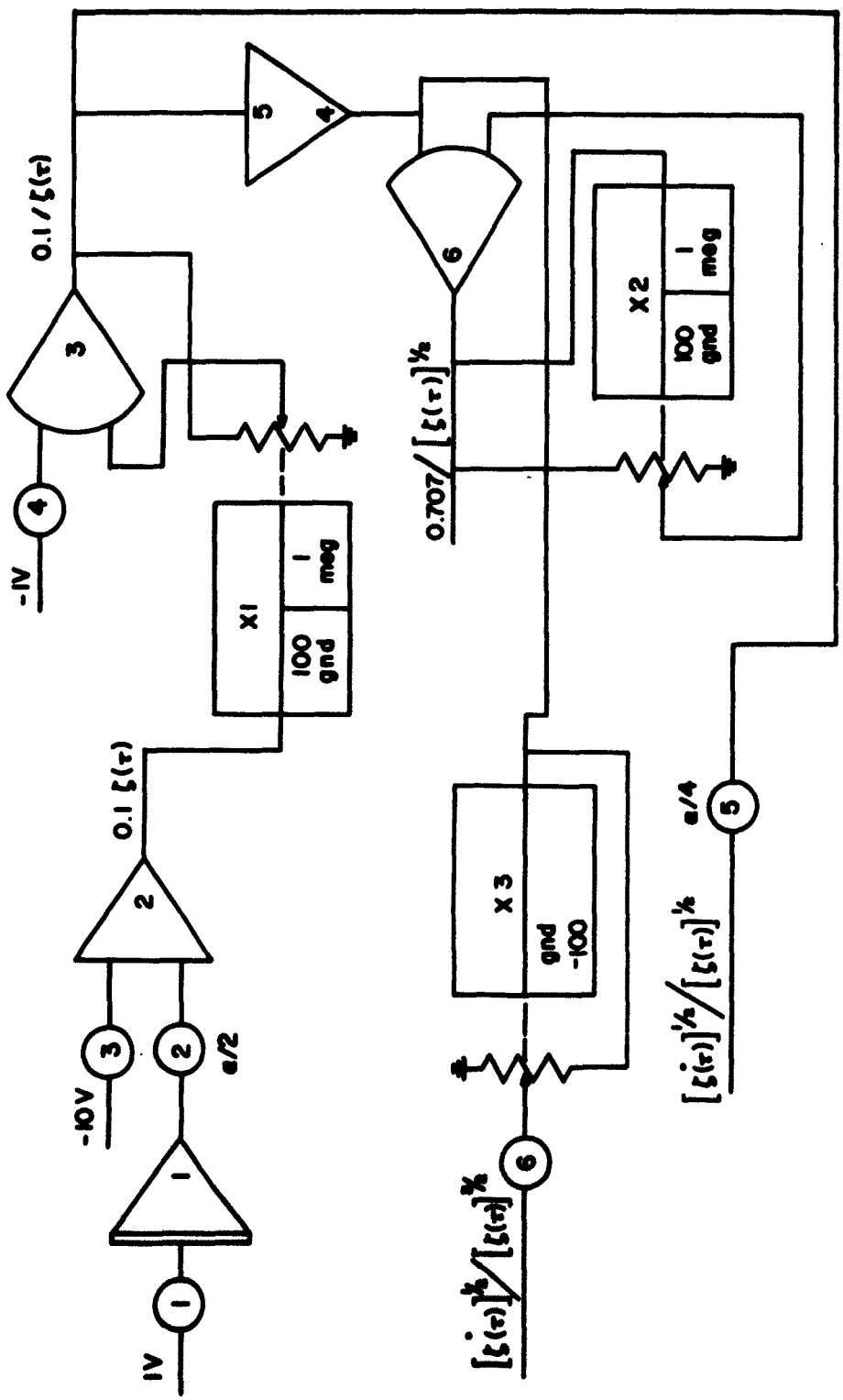

FIG. B.6 FUNCTION GENERATOR ELEMENTS FOR LINEAR POTENTIAL GRADIENT.

$[\zeta(\tau) = (1 + \alpha\tau/20)]$

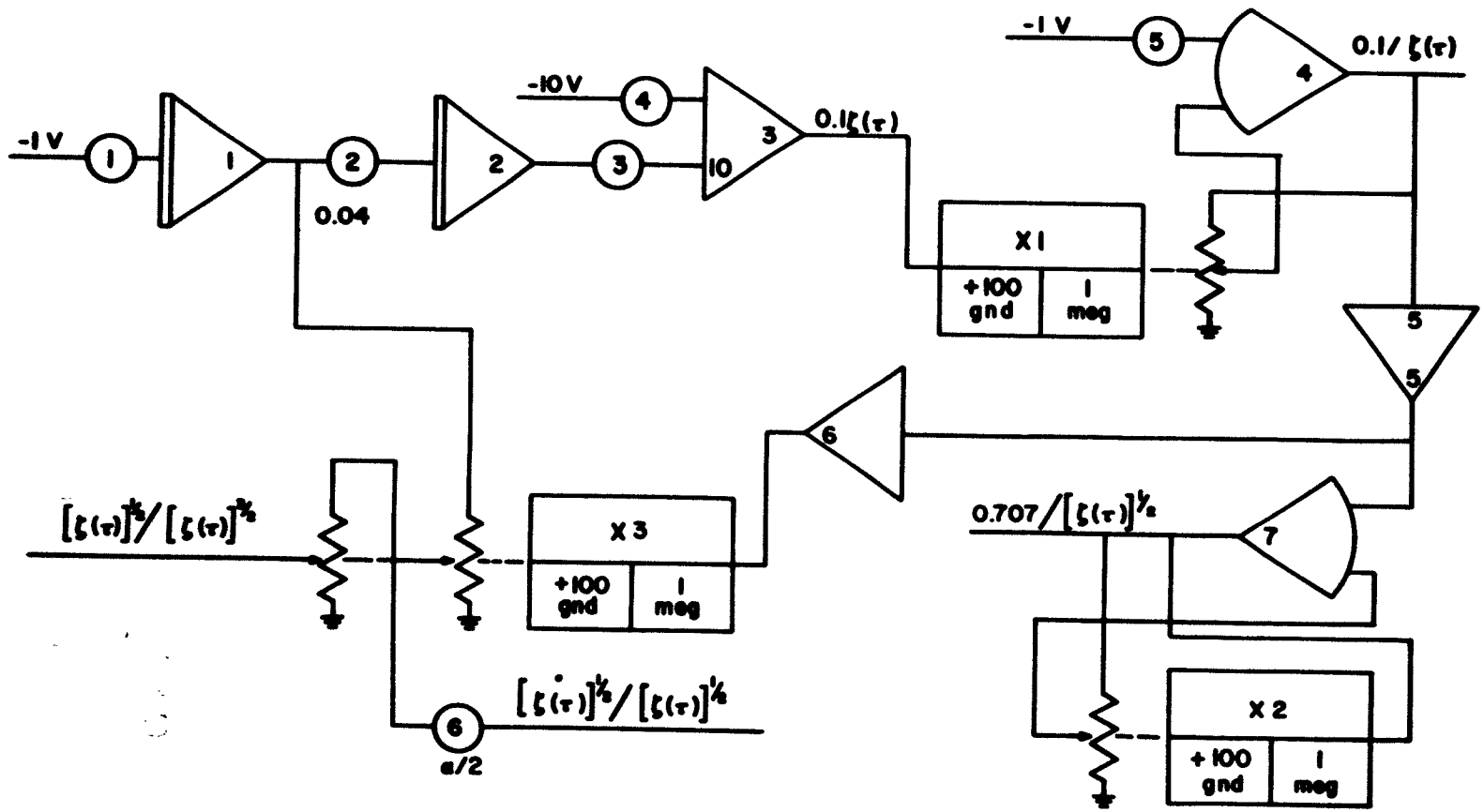

FIG. B.7 FUNCTION GENERATOR ELEMENTS FOR QUADRATIC POTENTIAL GRADIENT.

$[\zeta(\tau) = (1 + \alpha\tau^2/400)]$

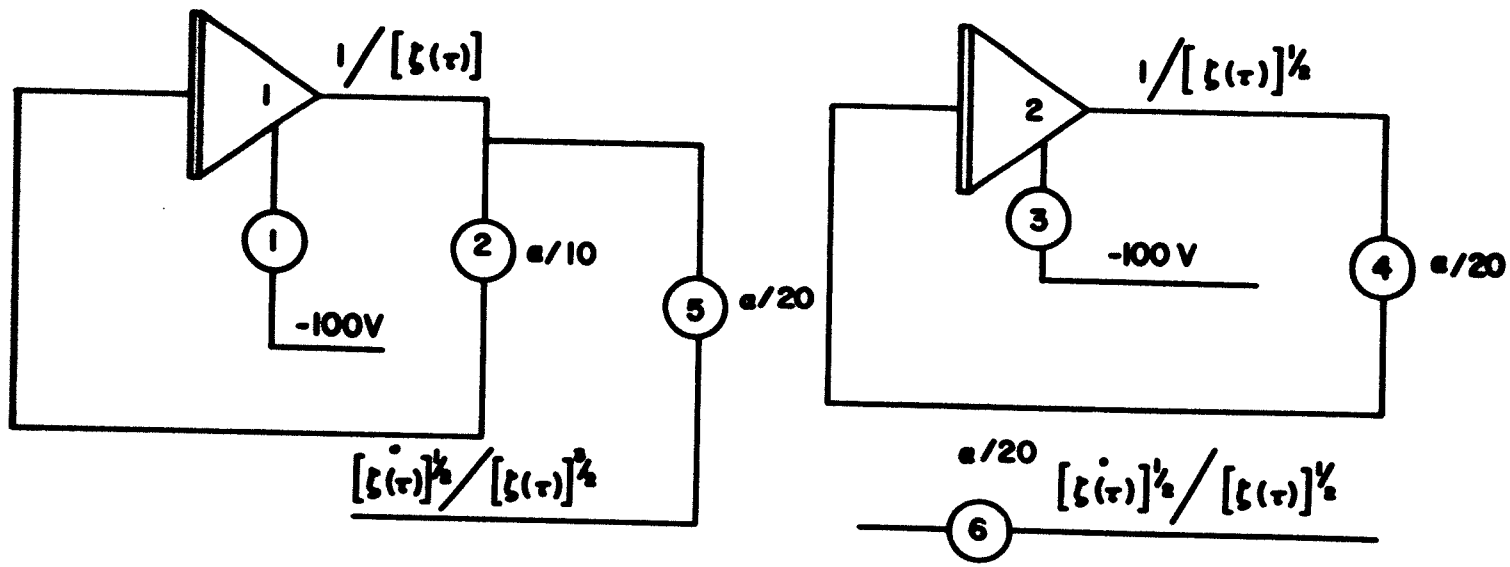

FIG. B.8 FUNCTION GENERATOR ELEMENTS FOR EXPONENTIAL POTENTIAL GRADIENT.

$[\zeta(\tau) = e^{2\alpha\tau/20}]$

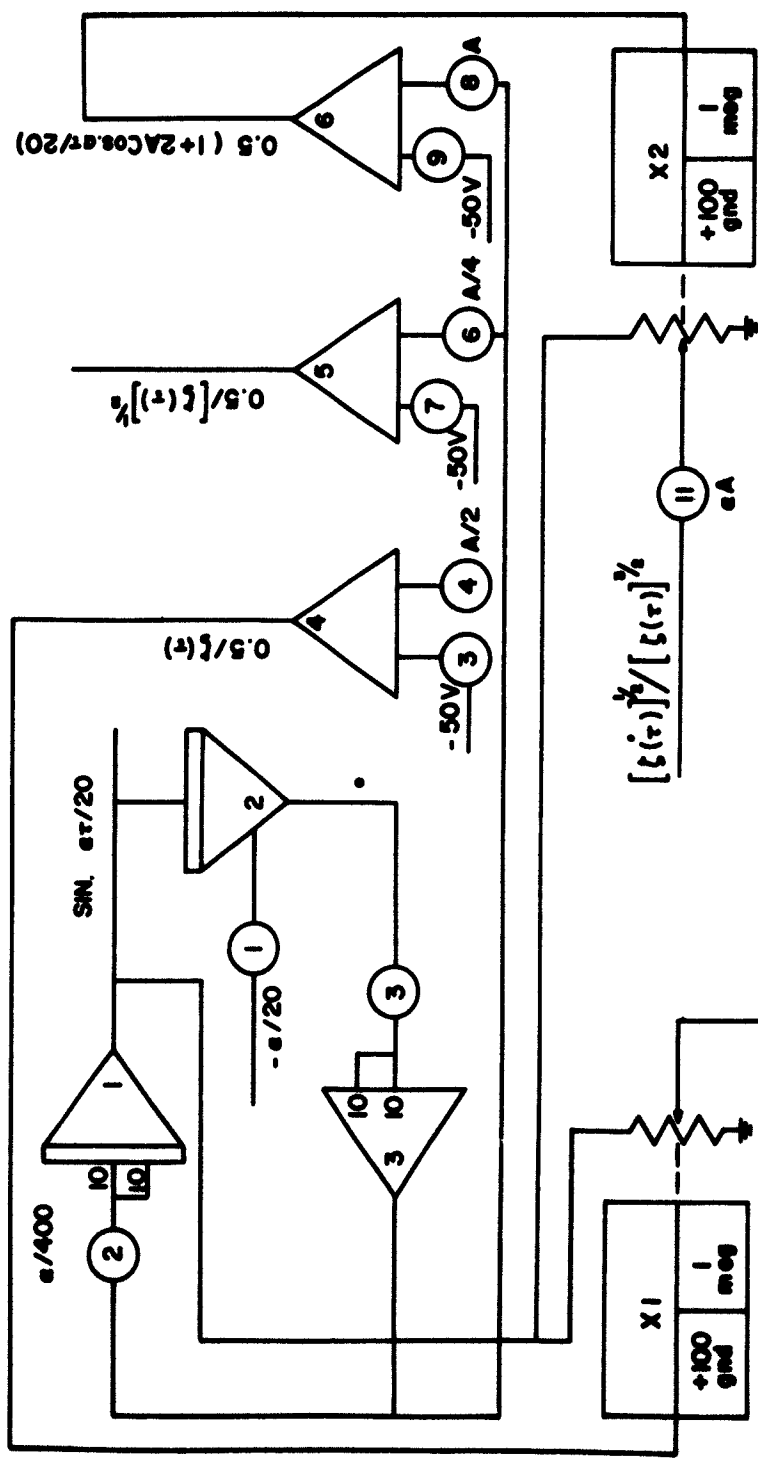

FIG. B.9 FUNCTION GENERATOR ELEMENTS FOR SINUSOIDAL BEAM POTENTIAL VARIATION.

$[\zeta(\tau) = 1 - A \cos \alpha\tau/20]$

Table B.2

Potentiometer Settings for Figure B.5

Potentiometer No.	Setting
6, 7	$(1 + 0.05\ b)^2$
8, 9	$0.125(1 + 0.05\ b)$
10, 11, 12, 13	0.04
14, 16	0.05
15, 17	$\dfrac{0.25QC}{[1 - 0.1\sqrt{QC}]^2\ (1 + 0.05\ b)}$
18	$0.5(1 + 0.05\ b)$
19, 21	- 0.5
20	$- 0.5(1 + 0.05\ b)$

BIBLIOGRAPHY

1. Kompfner, R. and Williams, N. T., "Backward-Wave Tubes", Proc. IRE, vol. 41, pp. 1602-1611; November, 1953.

2. Guenard, P., Doehler, O., Epsztein, B. and Warnecke, R., "New Uhf Oscillator Valves with Wide Electronic Tuning Band", Compt. Rend. Acad. Sci., Paris, vol. 235, pp. 236-238; 1952.

3. Pierce, J. R., Traveling-Wave Tubes, D. Van Nostrand Co., New York; 1950.

4. Heffner, H., "Analysis of the Backward-Wave Traveling-Wave Tube", Proc. IRE, vol. 42, pp. 930-937; June, 1954.

5. Johnson, H. R., "Backward-Wave Oscillators", Proc. IRE, vol. 43, pp. 684-697; June, 1955.

6. Goldberger, A. K., Palluel, P., "The O-Type Carcinotron", Proc. IRE, vol. 44, pp. 333-345; March, 1956.

7. Walker, L. R., "Starting Currents in the Backward-Wave Oscillator", Jour. Appl. Physics, vol. 24, pp. 854-860; July, 1953.

8. Harman, W. A., "Backward-Wave Interaction in Helix Type Tubes", Tech. Rpt. No. 13, Stanford University, Electronics Laboratory; April, 1954.

9. Grow, R. and Watkins, D. A., "Backward-Wave Oscillator Efficiency", Proc. IRE, vol. 43, pp. 848-856; July, 1955.

10. Muller, M., "Traveling-Wave Amplifiers and Backward-Wave Oscillators", Proc. IRE, vol. 42, pp. 1651-1658; November, 1954.

11. Currie, M. R. and Whinnery, J. R., "The Cascade Backward-Wave Amplifier: A High-Gain Voltage Tuned Filter for Microwaves", Proc. IRE, vol. 43, pp. 1617-1631; November, 1955.

12. Sedin, J., IRE Conference on Electron Devices, Denver, Colorado: June, 1956.

13. Gewartowski, J. W., "Velocity and Current Distribution in the Spent Beam of the Backward-Wave Oscillator", Trans. PGED-IRE, vol. ED-5, No. 4, pp. 215-223; October, 1958.

14. Meeker, J. G. and Rowe, J. E., "Phase Focusing in Linear Beam Devices", Trans. PGED-IRE, vol. 9, No. 3, pp. 257-266; May, 1962.

15. Cutler, C. C., "Increasing Traveling-Wave Tube Efficiency by Variation of Phase Velocity--Case 38543", Internal Memorandum, MM-53-1500-28, Bell Telephone Laboratories, Inc.; July 31, 1953.

16. Ruetz, J., Robinson, D. and Pavkovich, J., "The Effect of Tapered Circuits on Efficiency for High Power Traveling Wave Tubes", Paper Presented at Electron Devices Meeting, PGED-IRE, Washington, D. C.; October, 1960.

17. Hess, R. L., "Traveling-Wave Tube Large-Signal Theory, with Application to Amplifiers Having D-c Voltage Tapered with Distance", Ph.D. Dissertation, Electrical Engineering Department, University of California; July, 1960.

18. Geppert, D. V., "Analysis of Traveling-Wave Tubes with Tapered Velocity Parameter", Proc. IRE, vol. 46, No. 9, p. 1658; September, 1958.

19. Bevensee, R. M., "Beam Microwave Tubes with Tapered Structures", M. L. Report No. 855, Microwave Laboratory, Stanford University; October, 1961.

20. Rowe, J. E., "Analysis of Nonlinear O-Type Backward-Wave Oscillators", Proceedings of the Symposium on Electronic Waveguides, Microwave Research Inst. Symposia Series, vol. VIII, Polytechnic Press; 1958.

21. Pierce, J. R., "Coupling of Modes of Propagation", Jour. Appl. Physics, vol. 25, pp. 179-183; February, 1954.

22. Pierce, J. R., "The Wave Picture of Microwave Tubes", BSTJ, vol. 33, pp. 1343-1372; November, 1954.

23. Gould, R. W., "A Coupled Mode Description of the Backward-Wave Oscillator and Kompfner Dip Condition", Trans. PGED-IRE, vol. ED-2, No. 4, pp. 37-42; October, 1955.

24. Meeker, J. G., "Wave Picture of the Crestatron and Traveling-Wave Amplifier", University of Michigan, Electron Physics Laboratory, Technical Report No. 43; December, 1960.

25. Louisell, W. R., Coupled Mode and Parametric Electronics, John Wiley and Sons, New York; 1960.

26. Branch, G. M. and Mihran, T. G., "Plasma Reduction Factors in Electron Beams", Trans. PGED-IRE, vol. ED-2, No. 2, pp. 3-11; April, 1955.

27. Chu, L. J., "A Kinetic Power Theorem", Paper Presented at the Annual Conference on Electron Tube Research, Durham, N. H.; 1951.

28. Morse, P. M. and Feshback, H., Methods of Theoretical Physics, Part II, McGraw-Hill Book Co., New York, pp. 1092-1094; 1953.

29. Rowe, J. E. and Sobol, H., "Start-Oscillation Conditions in Modulated and Unmodulated O-Type Oscillators", Trans. PGED-IRE, vol. ED-8, No. 1, pp. 30-38; January, 1961.

30. Rowe, J. E., "A Large-Signal Analysis of the Traveling-Wave Amplifier: Theory and General Results", Trans. PGED-IRE, vol. ED-3, No. 1, pp. 39-57; January, 1956.

31. Dyott, R. B., Hogg, H. A. C., Hulley, M. A. and Kettlewell, E., "The Ophitron--An Electrostatically Focused Backward-Wave Oscillator", Record of the International Congress on Microwave Tubes, Munich, pp. 114-116; 1960.

32. Waters, W. E., "Electron Sheet Beam Focusing with Tape Ladder Lines", Jour. Appl. Physics, vol. 31, No. 10, pp. 1814-1820; October, 1960.

33. "Development of High Power Broad-Band Tubes and Related Studies", M. L. Report No. 773, Microwave Laboratory, Stanford University, pp. 37-44; January, 1961.

34. Rowe, J. E., "A Large-Signal Analysis of the Traveling-Wave Amplifier", Technical Report No. 19, University of Michigan, Electron Physics Laboratory; April, 1955.

35. Meeker, J. G., "Phase-Focusing in Linear Beam Devices", Technical Report No. 49, University of Michigan, Electron Physics Laboratory; August, 1961.

36. Tien, P. K., Walker, L. R. and Wolontis, V. M., "A Large-Signal Theory of Traveling-Wave Amplifiers", Proc. IRE, vol. 43, No. 3, pp. 260-277; March, 1955.

37. Rowe, J. E., "One-Dimensional Traveling-Wave Tube Analysis and the Effect of Radial Electric Field Variation", Trans. PGED-IRE, vol. ED-7, No. 1, pp. 16-21; January, 1960.

38. Ash, E. A. and Watkins, D. A., "The Helix as a Backward-Wave Structure", Jour. Appl. Physics, vol. 25, No. 6, pp. 782-790; June, 1954.

39. Rowe, J. E. and Meeker, J. G., "Interaction of Premodulated Electron Streams with Propagating Circuits", Jour. Elec. and Control, vol. 9, No. 6, pp. 439-466; December, 1960.

40. Hahn, W. C., "Small Signal Theory of Velocity Modulated Electron Beams", Gen. Elec. Rev., vol. 42, pp. 258-270; 1939.

41. Ramo, S., "Space-Charge and Field Waves in an Electron Beam", Phys. Rev., vol. 56, pp. 276-283; August, 1939.

42. Sterzer, F., "Improvement of Traveling-Wave Tube Efficiency Through Collector Potential Depression", Trans. PGED-IRE, vol. ED-5, No. 4, pp. 300-305; October, 1958.

43. Hansen, J. W., "Scheme for Improving Beam-Tube Performance by Depressing Collector Potential", Electronics Research Laboratory, University of California, Sci. Report No. 7, Issue 260, Series 60; December 15, 1959.

44. Wolkstein, H. J., "Effect of Collector Potential on the Efficiency of Traveling-Wave Tubes", RCA Review, vol. 19, pp. 259-282; June, 1958.

45. Rowe, J. E., "Efficiency Enhancement by Phase Focusing and Collector Depression", Fourth International Congress on Microwave Tubes, The Hague; September, 1962.

LIST OF SYMBOLS

A_o	Normalized amplitude of the output r-f wave.
$A(y)$	Normalized amplitude of the r-f wave along the tube.
$A_{d-c}(y)$	Normalized amplitude of the d-c gradient potential along the tube.
A_n	Fourier amplitude coefficient of cosine components in Fourier expansion for charge density.
$a_\pm$	The forward and backward modes on a transmission line, or the fast and slow space-charge modes on an electron beam.
a_c	The backward-wave mode on the circuit.
a_b	The slow space-charge mode on the electron beam.
a'	Mean radius of the transmission line, m.
B	Large-signal space-charge range parameter. $\omega b'(1 + C_o b_o)/u_o$.
B_n	Fourier amplitude coefficient of sine components in Fourier expansion for charge density.
b_o	Relative velocity parameter of the electrons and the cold circuit wave in the uniform section of the tube, $u_o - v_o/C_o v_o$.
$b(y)$	Relative velocity parameter at any point along the tube in normalized coordinate system, $u_o - v_o(y)/C_o v_o(y)$.
$b(z)$	Relative velocity parameter at any point along the tube in the (z,t) coordinate system, $u_o - v_o(z)/C_o v_o(z)$.
b'	Radius of the electron stream, m.
C_o	Interaction parameter, defined by $C_o^3 \triangleq Z_o I_o/4V_o$.
$C(z)$	Capacitance per unit length of a nonuniform transmission line, farads/m.
c	Velocity of light in free space.
d	Ohmic circuit-loss factor, $0.01836\ \ell/C_o$.
$\vec{E}$	The electric field intensity, volts/m.
$\vec{E}_c(z,t)$	The r-f electric field on the circuit, volts/m.

$\vec{E}_{sc_1}(z,t)$	The r-f space-charge field, volts/m.
$\vec{E}_{d-c}(z)$	The d-c electric field, volts/m.
$\mathcal{E}_d$	R-f energy dissipated on the circuit, joules.
$\mathcal{E}_{d-c}$	D-c beam input energy, joules.
$\mathcal{E}_c$	D-c energy given to the collector, joules.
$\mathcal{E}_i$	R-f input energy, joules.
$\mathcal{E}_o$	R-f output energy, joules.
e	The electronic charge, coulombs.
$F(\varphi-\varphi')$	Space-charge weighting function.
f	Frequency, cycles/sec.
Gc	Gigacycles = 10^9 cps.
$\vec{H}$	The magnetic field intensity, amperes/m.
I_m	Modified Bessel function of order m.
I_o	D-c beam current, amperes.
$I_c(z,t)$	The r-f current on the circuit, amperes.
i	The total beam current, amperes.
i_1	The r-f beam current, amperes.
$\vec{J}$	The convection current density, amperes/m^2.
L(z)	The inductance per unit length of a nonuniform transmission line, henrys/m.
$\ell(z)$	The series loss in db per wavelength on a nonuniform transmission line.
m	The mass of an electron, kg.
N	The number of stream wavelengths in a distance z.
N_{d-c}	The number of d-c focusing periods in an electrostatically focused tube.
n	The number of electron groups per r-f cycle.
n	An index of Fourier components of charge density.
P	The power flow along transmission line, watts.

p	Helix pitch, inches.
QC	Space-charge parameter.
$q(y)$	Normalized cold circuit phase velocity at any point along the tube, m/sec.
$R(z)$	Series resistance per unit length of a nonuniform transmission line.
R	Electron-plasma-frequency reduction factor.
t	Clock time, sec.
t_{oj}	Entrance time of jth electron group, sec.
u	The total beam velocity, m/sec.
u_o	Average electron velocity in the stream, m/sec.
u_1	The r-f beam velocity, m/sec.
$u(y,\varphi_{oj})$	When multiplied by $2C_o u_o$ represents the change in velocity of the jth electron from the average velocity u_o, in normalized coordinate system.
$u(z,t_{oj})$	When multiplied by $2C_o u_o$ represents the change in velocity of the jth electron from the average velocity u_o, in (z,t) coordinate system.
$u_t(y_i,\varphi_{oj})$	Total velocity of the jth electron at the y_ith level, equal to $u_o\,[1 + 2C_o u(y_i,\varphi_{oj})]$.
V_o	The d-c beam voltage, volts.
V_1	The beam kinetic potential, volts.
V_{ci}	The potential of the ith collector segment, volts.
$V_{d\text{-}c}(y)$	D-c voltage along the tube in normalized coordinate system, volts.
$V_{d\text{-}c}(z)$	D-c voltage along the tube in (z,t) coordinate system, volts.
$V_c(z,t)$	The r-f circuit voltage, volts.
V_g	The gap modulating voltage, volts.
V_{qj}	The equivalent r-f potential of the jth electron group, volts.
$V_{sc_1}(z,t)$	The space-charge potential, volts.

v_{oo}	The cold circuit phase velocity in the uniform section, m/sec.
$v_o(y)$	The cold circuit phase velocity at any point along the tube, in normalized coordinate system, m/sec.
$v_o(z)$	The cold circuit phase velocity at any point along the tube in the (z,t) coordinate system, m/sec.
$v(y)$	Actual r-f phase velocity along the circuit in the normalized coordinate system, m/sec.
$v(z)$	Actual r-f phase velocity along the circuit in the (z,t) coordinate system, m/sec.
v_{pf}	The phase velocity of the fast space-charge wave, m/sec.
v_{ps}	The phase velocity of the slow space-charge wave, m/sec.
$x(y)$	Normalized electron group velocity in the normalized coordinate system.
y	Normalized distance equal to $(\omega/u_o)\ C_o z$.
y_1	Normalized oscillation length of a tapered tube.
$y_{s,t}$	Normalized length at which taper starts.
$Z_o(z)$	The characteristic impedance of a nonuniform transmission line, ohms.
$Z_b(y)$	The impedance of an electron beam with a nonuniform potential, ohms.
z	Distance along the tube, m.
α	A taper parameter which designates the strength of the circuit phase velocity taper or the voltage gradient.
$\beta(z)$	Actual phase constant of transmission line, $\omega/v(z)$, radians/m.
$\beta_c(z)$	Undisturbed phase constant of nonuniform transmission line, $\omega/v_o(z)$, radians/m.
β_{e_o}	Phase constant of uniform electron beam, ω/u_o, radians/m.
$\beta_e(y)$	Phase constant of nonuniform electron beam, $\omega/u_o(y)$, in normalized coordinate system.
β_o	Free-space phase constant, ω/c, radians/m.
β_p	Plasma propagation constant, ω_p/u_o, radians/m.

β_q	Reduced plasma propagation constant, ω_q/u_o, radians/m.
γ	Radial propagation constant, equal to $\sqrt{\beta_c^2-\beta_o^2}$, radians/m.
ϵ_o	Permittivity of free space, farads/m.
$\zeta(y)$	Parameter designating the d-c voltage variation along the beam.
η	Ratio of charge to mass for an electron, e/m, kg/coul.
η	Interaction efficiency.
η_e	Electronic efficiency.
η_o	Overall efficiency.
$\theta(y)$	The phase lag of r-f wave relative to electron stream at any point along the tube in normalized coordinate system, radians.
$\theta(z)$	Phase lag of r-f wave relative to electron stream at any point along the tube in the (z,t) coordinate system, radians.
λ_o	Free space wavelength, c/f, m/sec.
λ_s	Wavelength along the electron beam, u_o/f, m/sec.
μ_o	Permeability of free space, henrys/m.
$\xi(y)$	Parameter representing the circuit phase velocity variation along the structure.
ρ_o	D-c space-charge density, coulombs/m.
ρ_1	R-f space-charge density, coulombs/m.
$\rho(y,\varphi)$	Instantaneous r-f space-charge density in the beam in the normalized coordinate system, coulombs/m.
$\rho(z,t)$	Instantaneous r-f space-charge density in the beam in the (z,t) coordinate system, coulombs/m.
φ_{oj}	Entrance phase of the jth electron group, radians.
$\varphi(y,\varphi_o)$	Phase of r-f wave at position y, relative to the reference position crest of a cosine wave which entered the tube at $y = 0$, $\varphi_o = 0$, radians.
$\varphi(y,\varphi_{oj})$	Phase of jth electron group at distance y, relative to the r-f wave, radians.

$\varphi(z,t_o)$ Phase of r-f wave at z relative to the reference positive crest of the wave at $z = 0$, $t_o = 0$; radians.

$\varphi(z,t_{oj})$ Phase of jth electron group at distance z, relative to the r-f wave, radians.

φ_f The phase angle at which a "hard-kernel-bunch" is focused, radians.

ω Angular frequency of r-f wave, radians/sec.

ω_p Electron plasma frequency, defined by $\omega_p^2 \triangleq \eta I_o/\pi\epsilon_o b'^2 u_o$, radians/sec.

ω_q Effective electron plasma frequency for a finite beam, equal to $\omega_p R$, radians/sec.

DISTRIBUTION LIST

No. Copies	Agency
1	Chief, Contract Branch, Harry Diamond Laboratories, Washington 25, D. C.
2	Technical Information Office, Branch 012, Harry Diamond Laboratories, Washington 25, D. C.
1	Chief of Laboratory 900, Harry Diamond Laboratories, Washington 25, D. C.
10	Mr. J. VanTrump, Chief, Electron Tube Branch, Harry Diamond Laboratories, Washington 25, D. C.
1	Electronic Technology Laboratory, Aeronautical Systems Division, Wright-Patterson Air Force Base, Ohio, ATTN: ASRNET-1, Mr. James Enright
10	Commander, Armed Services Technical Information Agency, Arlington Hall Station, Arlington 12, Virginia
1	Bureau of Ships, Code 691A4, Department of Navy, Washington 25, D. C., ATTN: Mr. W. J. Riegger
1	Electronics Engineer, Signal Corps Engineering Laboratory, Evans Signal Laboratories, Belmar, New Jersey, ATTN: Mr. Harold J. Hersh
1	Commander, Rome Air Development Center, Griffiss Air Force Base, Rome, New York, ATTN: Mr. H. Chiosa, RCIRR-3
1	Commander, Aeronautical Systems Division, Wright-Patterson Air Force Base, Ohio, ATTN: Mr. K. Hutchinson
1	Bendix Corporation, Systems Planning Division, Ann Arbor, Michigan, ATTN: Technical Library
1	Mr. A. G. Peifer, Bendix Corporation, Research Laboratories, Northwestern Hwy. & 10 1/2 Mile Road, Detroit 35, Michigan
1	The Electronics Research Laboratory, 427 Cory Hall, The University of California, Berkeley 4, California, ATTN: Mrs. Simmons
1	Professor Roy Gould, California Institute of Technology, Department of Electrical Engineering, Pasadena, California
1	Chalmers Institute of Technology, ATTN: Dr. O. E. H. Rydbeck, Research Laboratory of Electronics, Gibraltargarten 5 G, Gothenberg, Sweden

No. Copies	Agency
1	Professor W. G. Worcester, University of Colorado, Department of Electrical Engineering, Boulder, Colorado
1	Columbia Radiation Laboratory, Columbia University 538 West 120th Street, New York 27, New York
1	Professor L. Eastman, Cornell University, Department of Electrical Engineering, Ithaca, New York
1	University of Florida, Department of Electrical Engineering, Gainesville, Florida
1	Dr. E. D. McArthur, General Electric Company, Electron Tube Division of Research Laboratory, Schenectady, New York
1	Harvard University, Cruft Laboratory, Cambridge, Massachusetts, ATTN: Technical Library
1	Hughes Aircraft Company, Electron Tube Laboratory, Culver City, California, ATTN: Mr. John Mendel
1	University of Illinois, Department of Electrical Engineering, Electron Tube Section, Urbana, Illinois
1	Dr. Norman Moore, Litton Industries, 960 Industrial Road, San Carlos, California
1	Massachusetts Institute of Technology, Research Laboratory of Electronics, Cambridge 39, Massachusetts, ATTN: Documents Library
1	Microwave Electronics Corporation, 4061 Transport Street, Palo Alto, California, ATTN: Dr. S. F. Kaisel
1	Microwave Associates, ATTN: Dr. P. Chorney, Burlington, Massachusetts
1	Department of Electrical Engineering, University of Minnesota, Minneapolis, Minnesota, ATTN: Dr. W. G. Shepherd
1	Norwegian Defense Research Establishment, ATTN: Dr. Kjell Blotekjaer, Division for Radar, Bergen, Norway
1	Ohio State University, Department of Electrical Engineering, Columbus 10, Ohio, ATTN: Professor E. M. Boone
1	Polytechnic Institute of Brooklyn, Documents Library, Brooklyn, New York
1	Spencer Laboratory Library, Raytheon Company, Wayside Road, Burlington, Massachusetts, ATTN: Mr. W. W. Teich

No. Copies	Agency
1	Royal Institute of Technology, ATTN: Dr. Bertil Agdur, Microwave Department, Stockholm 70, Sweden
1	Sperry Corporation, Electronic Tube Division, Gainesville, Florida, ATTN: Mr. P. Bergman
1	Sperry Gyroscope Company, Great Neck, New York, ATTN: Engineering Library
1	Electronics Research Laboratory, Stanford University, Stanford, California, ATTN: Mr. David C. Bacon, Assistant Director
1	Librarian, Microwave Library, Stanford University, Stanford, California
1	Sylvania Electric Products, Inc., Mountain View, California, ATTN: Dr. Jules Needle
1	Varian Associates, 611 Hansen Way, Palo Alto, California, ATTN: Technical Library
1	Dr. D. A. Watkins, Watkins-Johnson Company, 3333 Hillview Avenue, Palo Alto, California
1	Mr. Gerald Klein, Manager, Microwave Tubes Section, Applied Research Department, Westinghouse Electric Corporation, Box 746, Baltimore 3, Maryland

AD_____

The University of Michigan, Electron Physics Laboratory, Ann Arbor, Michigan. EFFICIENCY AND START-OSCILLATION CONDITIONS IN NONUNIFORM BACKWARD-WAVE OSCILLATORS, by G. I. Haddad. March, 1965, 260 pp. incl. illus. (Contract No. DA-49-186-AMC-68(X), Project No. 96395)

The effect of several kinds of nonuniformities in the circuit phase velocity and beam potential on the start-oscillation conditions of an O-type BWO have been investigated. The nonuniformities include linear, quadratic and exponential circuit phase velocity tapers and linear quadratic, exponential and sinusoidal voltage gradients. It is shown that under certain conditions the taper may be employed to either reduce the start-oscillation current or to suppress backward-wave oscillations in forward-wave amplifiers.

Circuit phase velocity tapers for achieving phase-focusing and thus enhancing the efficiency of O-type BWO's are derived. Employing such a circuit taper in an experimental S-band BWO resulted in efficiency improvement factors of 1.2 to 2.0 to 1.0 over a frequency range of 2.0 to 4.0 Gc.

Efficiency enhancement through utilization of multisegment depressed collectors is investigated. Optimum collector segment voltages for achieving optimum efficiencies under typical operating conditions have been determined and are presented. The utilization of prebunched beams in BWO's is considered and the effect on the start-oscillation conditions and efficiency is determined.

UNCLASSIFIED

1. Coupled-Mode Description of the Interaction Between Nonuniform Circuits and Beams
2. Start-Oscillation Conditions of Nonuniform BWO's
3. Efficiency of Nonuniform BWO's
4. Experimental Tapered BWO
5. Prebunched Beam BWO
6. Efficiency Enhancement of BWO's by Collector Depression

I. Haddad, G. I.
II. Harry Diamond Laboratories

UNCLASSIFIED

AD_____

The University of Michigan, Electron Physics Laboratory, Ann Arbor, Michigan. EFFICIENCY AND START-OSCILLATION CONDITIONS IN NONUNIFORM BACKWARD-WAVE OSCILLATORS, by G. I. Haddad. March, 1965, 260 pp. incl. illus. (Contract No. DA-49-186-AMC-68(X), Project No. 96395)

The effect of several kinds of nonuniformities in the circuit phase velocity and beam potential on the start-oscillation conditions of an O-type BWO have been investigated. The nonuniformities include linear, quadratic and exponential circuit phase velocity tapers and linear, quadratic, exponential and sinusoidal voltage gradients. It is shown that under certain conditions the taper may be employed to either reduce the start-oscillation current or to suppress backward-wave oscillations in forward-wave amplifiers.

Circuit phase velocity tapers for achieving phase-focusing and thus enhancing the efficiency of O-type BWO's are derived. Employing such a circuit taper in an experimental S-band BWO resulted in efficiency improvement factors of 1.2 to 2.0 to 1.0 over a frequency range of 2.0 to 4.0 Gc.

Efficiency enhancement through utilization of multisegment depressed collectors is investigated. Optimum collector segment voltages for achieving optimum efficiencies under typical operating conditions have been determined and are presented. The utilization of prebunched beams in BWO's is considered and the effect on the start-oscillation conditions and efficiency is determined.

UNCLASSIFIED

1. Coupled-Mode Description of the Interaction Between Nonuniform Circuits and Beams
2. Start-Oscillation Conditions of Nonuniform BWO's
3. Efficiency of Nonuniform BWO's
4. Experimental Tapered BWO
5. Prebunched Beam BWO
6. Efficiency Enhancement of BWO's by Collector Depression

I. Haddad, G. I.
II. Harry Diamond Laboratories

UNCLASSIFIED